NONLINEAR DYNAMICS OF SIMPLE AND COMPOUND DROPS

by

JOHN ABRAHAM TSAMOPOULOS

Diploma National Technical University of Athens, 1979

M.S. Massachusetts Institute of Technology, 1981

Submitted to the Department of
Chemical Engineering
in Partial Fulfillment of the
Requirements of the Degree of

DOCTOR OF PHILOSOPHY

at the

MASSACHUSETTS INSTITUTE OF TECHNOLOGY

January 1985

Signature of Author Signature redacted
Department of Chemical Engineering

Certified by Signature redacted
Robert A. Brown
Thesis Supervisor

Accepted by Signature redacted
Chairman, Departmental
Committee on Graduate Students

NONLINEAR DYNAMICS OF SIMPLE AND COMPOUND DROPS

by

JOHN ABRAHAM TSAMOPOULOS

Submitted to the Department of Chemical Engineering
January, 1985 in partial fulfillment of the requirements
of the degree of Doctor of Philosophy

ABSTRACT

The objective of this thesis is to develop a rigorous mathematical framework for studying the nonlinear dynamics of simple and compound drops and bubbles and to apply this theory to several of the outstanding problems in drop dynamics. A combination of domain perturbation and multiple timescale methods are used to systematically compute the evolution of axisymmetric and inviscid simple and compound drops. The complexity of the nonlinear equations is reduced by using the symbolic manipulator MACSYMA.

The moderate-amplitude oscillations of incompressible drops and bubbles are first studied using a Poincaré-Lindstedt technique. The two cases are complimentary to each other which simplifies their treatment. It is shown that the increased inertia of the system slows down the motion by decreasing the frequency of the oscillation as the magnitude of the deformation increases. The corrections to the drop shape and velocity potential caused by mode coupling at second order in amplitude are predicted for two-, three-, and four-lobed motions. The two-lobed shape is named prolate when the axis of symmerty is the larger of the axes of the ellipsoid, whereas it is named oblate when the axis of symmetry is the smallest. The agreement of the analytic results with both experiments carried out at JPL and numerical solutions of Foote (1973), Alonso (1974) and Benner (1983) is very good.

Nuclear physics have contributed theoretical analysis and impetus for experimental study of liquid drops, since Bohr and Wheeler began modeling atomic nuclei as uniformly charged liquid drops with surface tension. The analysis is extended to the oscillations of a conducting charged drop. Again, a decrease in the oscillation frequency with increasing deformation is observed, but with a magnitude which depended on the total surface charge. The analysis also demonstrated the possibility of resonance between the fundamental mode of oscillation and one of its harmonics for particular values of the net charge on the drop. Both frequency and amplitude modulation of the oscillations are predicted for drop motions starting from general initial conditions. This effect cannot be anticipated from the linear analysis and proves that Rayleigh's solution (1882) for

small-amplitude oscillations can actually be unstable.

The dynamics of breakup of a charged drop is a long standing issue, although the neutrally stable shapes have been known since the early sixties. Rayleigh (1882) calculated the maximum charge that a spherical drop can carry before it becomes unstable due to electrostatic repulsion. The treatment shows that the first bifurcating family from the spherical shape evolves transcritically, so that the drop will be either unstable for elongated prolate shapes or stable for flat oblate shapes. The evolution of drop shape leading to breakup is also analyzed and the dependence of the amount of charge on the amplitude of the deformation is computed. The asymptotic analysis for the static shapes is in very good agreement with the finite element calculations for even large amplitude deformations of the drop.

Finally, the dynamics of a compound drop are examined in an effort to explain the observed motion of a bubble towards the center of the surrounding drop (Lee et al. 1981). This centering force is critical in the formation of hollow spherosymmetric shells that are made by centering a bubble inside a drop and solidifying the resulting shell. Metal and glass shells are currently being used as fuel targets for Inertial Confinement Fusion experiments and have great possibilities as a matrix material for load-bearing materials with extremely high strength to weight ratios. Physically, the centering must be due to the nonlinear dynamic coupling of the interfaces during oscillation, because all locations of a bubble inside a static drop are energetically equivalent. The analysis presented, reveals that a strong centering force is created by this dynamic mechanism when the compound drop oscillates in one of the two possible modes, the sloshing mode, in which the two interfaces are oscillating out of phase.

Thesis Supervisor: Robert A. Brown

Title: Professor of Chemical Engineering

ACKNOWLEDGEMENTS

I wish to express my sincere appreciation to my thesis advisor, Professor Robert Brown for his timely advice and for the stimulating discussions we had throughout the course of this research. I am also very thankful to the members of my thesis committee: Professors R. Armstrong, J. Brady, H. Greenspan and particularly T. Akylas for his many enlightening suggestions.

Many thanks to John Congalidis for his friendship and moral support even when he was away from MIT, to Antony Beris for his suggestions, to Peter Adornato for his numerical code and to Miguel Bibbo for his graphics routines.

Financial support for this work was provided by NSF, as well as by fellowships to the author by the Department of Chemical Engineering at MIT and by the Union Carbide and Halcon Companies. The use of the computer facilities at the Artificial Intelligence laboratory is greatfully acknowledged.

I dedicate this thesis to the memory of my beloved parents whose guidance, encouragement, understanding and sacrifices through my long education have been a source of inspiration.

In a letter to Karl Popper, Einstein once wrote:

"Theory cannot be fabricated out of the results of observation, it can only be invented."

Popper replied:

"Observation is always selective. It needs a chosen object, a definite task, an interest, a point of view, a problem.
Observations are always INTERPRETATIONS of the facts observed, ...they are interpretations in the light of theories."

TABLE OF CONTENTS

LIST OF FIGURES

LIST OF TABLES

I. OVERVIEW

The dynamics of liquid drops and bubbles held together by surface tension and vibrating because of induced perturbation have long been of interest to scientists and engineers in a variety of physical and biological applications, spaning areas as diverse as the length scales of the systems modeled by the fluid globes. Centimeter-sized drops and bubbles are important in chemical engineering separations, meteorology, and materials processing in space, where freely-suspended drops and liquid shells can be handled. Femtometer-sized (10^{-15} m) liquid drops with surface tension and electric charge have been used as models for predicting the dynamics of heavy nuclei (Bohr and Wheeler 1939), whereas celestrial-sized fluid bodies held together by self-gravitation and destabilized by centripetal acceleration are old, but still employed, models for the evolution of stars (Chandrasekhar 1969).

Each of these systems is described mathematically by a nonlinear moving-boundary problem for the shape of the fluid/fluid interface and the field variables, velocity, pressure, and electric potential, throughout the drop or in the surrounding fluid (for a bubble). These variables are calculated using conservation laws of momentum, mass and species in the bulk fluid and on the interface. The classical theories that form the basis for each of the applications of drop dynamics dealt with either the small-amplitude motions of the interface that can be analyzed by linear methods or with the nonlinear equilibrium or static shapes of bodies affected by the appropriate body forces and surface tension. These results are insufficient to explain a wide range of observations

of large-amplitude dynamic evolution.

The objective of this thesis is to develop a rigorous mathematical framework for studying the nonlinear dynamics of simple and compound drops and bubbles and to apply this theory to several of the outstanding problems in drop dynamics. As opposed to numerical solutions, our semi-analytical method is relatively inexpensive, yields an exhaustive mapping of the long-time response of the drop as a function of the initial deformation, and other appropriate parameters and uncovers the nonlinear effects of fluid inertia and capillarity. The analyses focus on the dynamics of freely oscillating, inviscid drops, bubbles and liquid shells, whereas the importance of the viscous forces are discussed elsewhere (Tsamopoulos and Brown 1983 & 1984).

The first area of interest is the nonlinear oscillations of single drops or bubbles in an infinite medium. The two cases are complimentary to each other which simplifies their treatment. It is shown that the increased inertia of the system slows down the motion by decreasing the frequency of the oscillation as the magnitude of the deformation increases. The experimentally observed first three modes of oscillation of a simple drop are shown in figure I.0.1, after Trinh et al. (1982). The two-lobed shape is named prolate when the axis of symmerty is the larger of the axes of the ellipsoid, whereas it is named oblate when the axis of symmetry is the smallest. The agreement of our analytic results with both experiments carried out at JPL and numerical solutions of Foote (1973), Alonso (1974) and Benner (1983) increased our confidence in the method we have followed.

Nuclear physics have contributed theoretical analysis and impetus

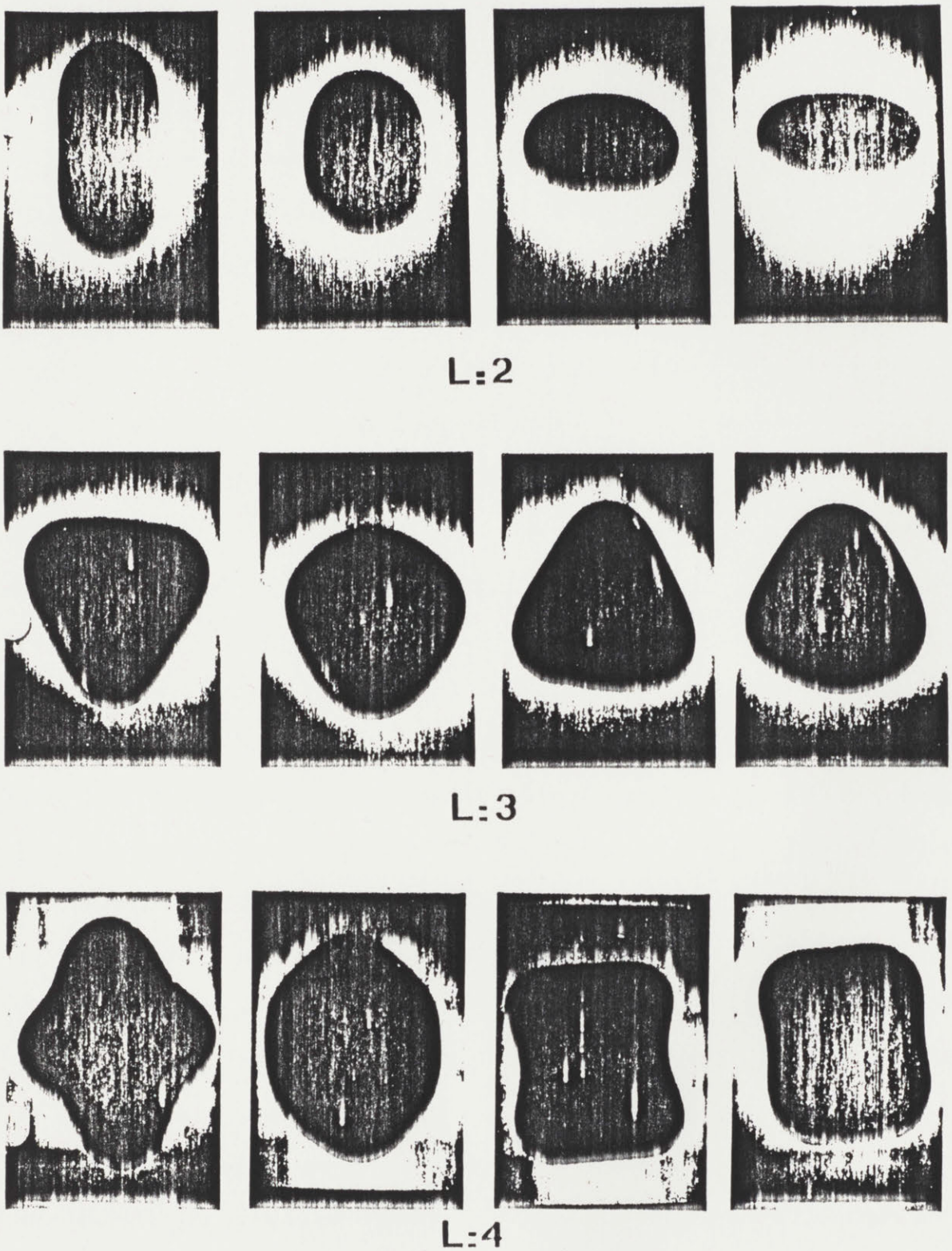

Figure I.0.1 Neutrally buoyant uncharged drop of silicone oil - CCl_4 immersed in distilled water and undergoing oscillation in the L=2,3,4 axisymmetric oscillation modes (Trinh et al. 1982).

for experimental study of liquid drops, since Bohr and Wheeler began modeling atomic nuclei as uniformly charged liquid drops with surface tension. We have extended this analysis to the oscillations of a conducting charged drop. Again a decrease in the oscillation frequency with increasing deformation is predicted, but with a magnitude which depended on the total surface charge. The analysis also demonstrated the possibility of resonance between the fundamental mode of oscillation and one of its harmonics for particular values of the net charge on the drop. This effect cannot be anticipated from the linear analysis and proves that Rayleigh's solution (1882) for small-amplitude oscillations can actually be unstable.

The dynamics of breakup of a charged drop is a long standing issue, although the neutrally stable shapes have been known since the early sixties. Rayleigh (1882) calculated the maximum charge that a spherical drop can carry before it becomes unstable due to electrostatic repulsion. Our treatment shows that the first bifurcating family from the spherical shape evolves transcritically, so that the drop will be either unstable for elongated prolate shapes or stable for flat oblate shapes. The evolution of drop shape leading to breakup is also analyzed and the dependence of the amount of charge on the amplitude of the deformation is computed.

Finally, the dynamics of a compound drop are examined in an effort to explain the observed motion of a bubble towards the center of the surrounding drop (Lee et al. 1981). This centering force is critical in the formation of hollow spherosymmetric shells that are made by centering a bubble inside a drop and solidifying the resulting shell. Metal and glass shells are currently being used as fuel targets for Inertial Confinement

Fusion experiments and have great possibilities as a matrix material for load-bearing materials with extremely high strength to weight ratios. Physically, the centering must be due to the nonlinear dynamic coupling of the interfaces during oscillation, because all locations of a bubble inside a static drop are energetically equivalent. The analysis presented in chapter VII reveals that a strong centering force is created by this dynamic mechanism.

II. PHYSICAL SYSTEMS DESCRIBED BY DROP DYNAMICS

Many studies have examined the equilibrium and stability of fluid globes in the presence of various internal and external fields of force. The classic investigations by Newton, Maclaurin, Jacobi, Riemann, Laplace, Lyttleton and Poincarè regarding the shape and stability of a homogeneous self-gravitating fluid in rigid body rotation and under the influence of surface tension have been summarized by Chandrasekhar (1969).

Swiatecki (1974) presented a survey of the equilibrium configurations of a rotating charged or gravitating liquid mass in a way that unifies the treatment of idealized rotating heavenly bodies, rotating drops in a weightless environment, and fluid mechanical equivalents of rotating nuclei. This unification was achieved by varying continuously two physical parameters in the equations. The first parameter, x, was the relative intensity of the inverse-distance (gravitational or electrostatic) energy to that of the surface energy. The second parameter, y, was a measure of the square of the angular momentum, and thus of the size of the disruptive centrifugal forces compared to the cohesive surface tension forces. Each system is described by a pair of x-y values as shown in figure II.0.1, after Swiatecki (1974). The y=0 axis implies no rotation, so the positive x-axis corresponds to nonrotating idealized nuclei, from light to heavy with increasing x. Self-gravitating globes exist for negative x. The classic case of astronomical masses without surface tension corresponds to $x \to -\infty$, as indicated in the left. Plateau's rotating globes, with no charge and negligible gravitation, correspond to the positive y-axis. Rotating nuclei and rotating gravitating masses with surface tension

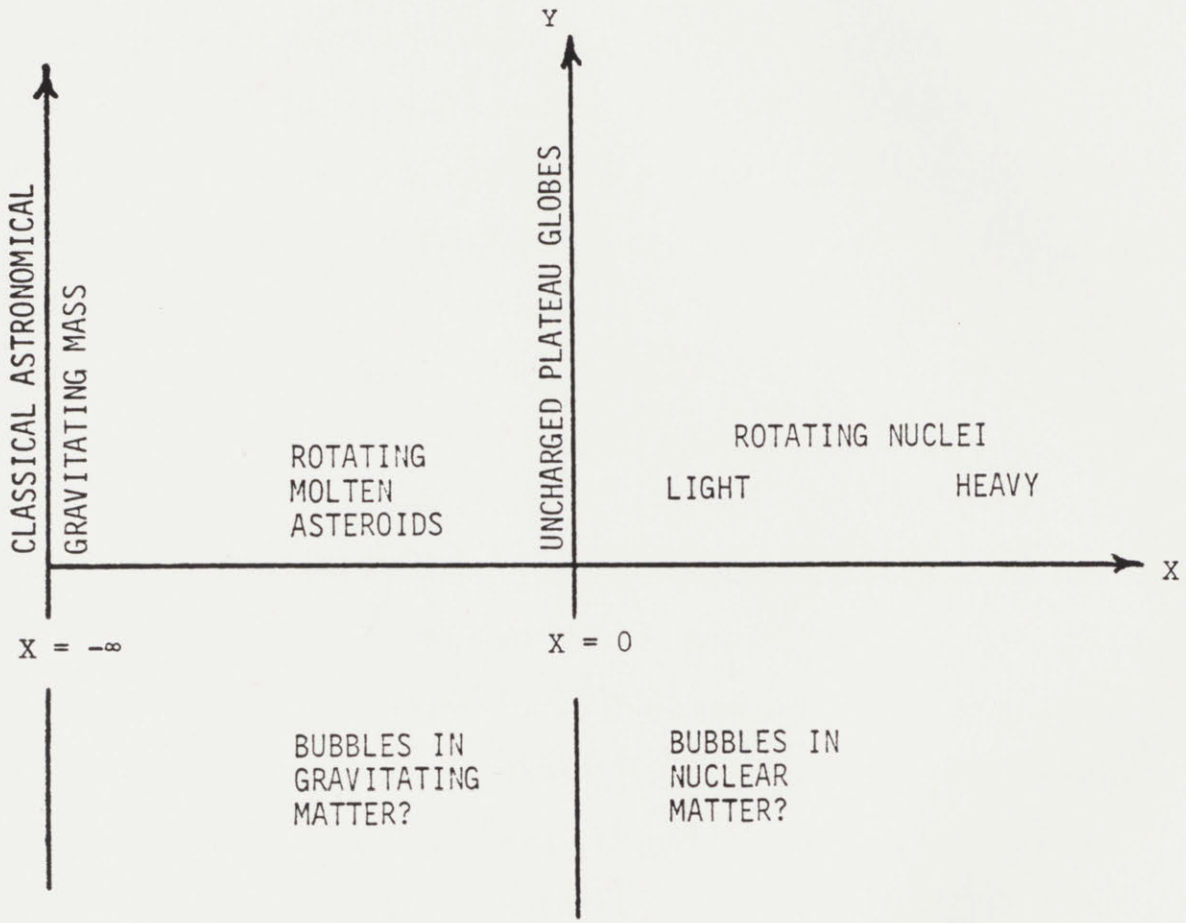

$$X \equiv \frac{(\text{charge})^2 - G(\text{Mass})^2}{10(\text{Volume})(\text{Surface Tension})}$$

$$Y \equiv \frac{5}{12} \frac{(\text{Angular Momentum})^2}{(\text{Volume})(\text{Mass})(\text{Surface Tension})}$$

Figure II.0.1 Physical systems arranged according to the intensities of inverse distance and rotational energies relative to the surface energy (Swiatecki 1974).

fill the upper half-plane. The negative y-plane corresponds to a bubble in a rotating container filled with a liquid (simple, gravitating, or uniformly charged). The bubble has negative inertial mass relative to the surrounding liquid, and experiences a negative centrifugal force which, instead of flattening the bubble, tends to elongate it along the axis of rotation.

Electrohydrodynamic phenomena in drops and bubbles are of interest in a wide variety of scientific and engineering applications and have long fascinated researchers starting with Lord Raleigh (1882). The dynamic response of liquid drops held together by surface tension, which carry electric charge and in the presence of an A.C. or D.C. electric field has been studied in physical systems ranging in size from milimeter raindrops (Sartor 1961; Brazier-Smith et al. 1971) to micron-sized spheres produced by fuel atomizers and ink jet delivery systems (Hendricks 1962; Williams 1973; Takamatsu et al. 1982). In particular, Brook and Latham (1968) have shown that size distributions of raindrops can be determined from a study of the fluctuations in the radar signal returned by falling raindrops, which in turn is caused by drop vibration. In this case, it is necessary to establish the relationship between the vibrational frequency and the charge carried by the drop, or the strength of the electric field in which it is situated and thereby to define conditions under which the electric forces may be important or may be neglected.

There is renewed interest in the shape and stability of charged drops as a mechanism of isolation and transport of small liquid masses. A conducting drop can be levitated statically in an insulating medium by accumulating a net charge Q on its interface and by applying a D.C. field

with a component E_0 in the direction of gravity. Such electrostatic levitators have been used to investigate physical properties and size distributions of aerosol particles (O' Konski and Thacker 1953; Davis and Ray 1980; Philip et al. 1983) and have been proposed for use in the containerless processing of ultra-pure or highly reactive materials such as semiconductor melts (Carruthers 1974).

A contribution of Fluid Mechanics to Biomedical research is to elucidate some of the general dynamical features that affect the disposition of an single cell, cell colonies and tissues (Greenspan 1981) and to effectively perform the biological separation between living and dead cells (Crane and Pohl 1968). Strong analogies exist between droplets (with or without charge) and cells, i.e. droplet - cell shape, encapsulated droplet - cell and cell membrane, adhesion and spread of a drop - cell mobility and adhesion.

Compound drops are considered in multiphase separations. The liquid in the shell acts as a liquid membrane which during settling causes a separation process to take place between the liquid inside it and the liquid outside. Such systems have been called double emulsions (Li 1971; Martin and Davies 1976).

Also, there are a variety of phenomena, both in nature and in industry, which involve drop or bubble formation and disappearance by mass transfer processes (Zwick and Plesset 1955). Other phenomena are related with their interactions with one another, or with other surfaces. Obvious natural examples are the growth of raindrops by the coalescence of drop pairs (Saunders 1974), the break up of large falling drops caused by their interaction with an air stream (Harper et al. 1972) and the splashing

and erosion produced by raindrops impacting on soil or by bubbles formed by cavitation near fast moving submerged surfaces (Van Winjgaarden 1976; Lauterborn and Bole 1975; Blake and Gibson 1981; Longuet-Higgins 1983). The coupled motion of two spherical drops submerged in an unbounded velocity field in the low Reynolds number regime has been studied by Hetsroni and Haber (1978) who computed the drag forces and the terminal settling velocities of the two drops.

The deformation and burst of a single drop in a shear field are of great importance. Depending on conditions, the drop may become a greatly elongated filament, or it may deform only moderately before bursting (Bathes-Biesel and Acrivos 1973; Torza et al. 1972; Rallison 1984).

All these cases involve the details of the deformation process and incorporate forces arising from surface tension, gravity, electric and magnetic fields, pressure, inertial and viscous action.

II.1 DYNAMICS OF CHARGED DROPS

II.1a Liquid drop model for the nucleus

The dynamics of a nucleus have been compared to those of a liquid drop which carries volumetrically distributed electric charge (Bohr and Wheeler 1939). In this case the molecules of the liquid correspond to the nucleons in the nucleus. When internal gravity and surface tension dominate in a drop, there is a close mathematical analogy with the case of volume charge and surface tension. The energy of self-gravitation shares the inverse-distance dependence of electrostatic energy. The density of a liquid is almost independent of its size so that the radius

of the drop is proportional to the cubic root of the number of molecules - a rule that closely applies to the nucleus. The energy necessary to evaporate the drop into well separated molecules is approximately proportional to their number which is analogous to the binding energy of a nucleus. On the other hand, in liquids, the motion of the constituents can be described in classical terms and their positions can be well defined, whereas in a nucleus the motion is necessarily of quantum character, since the uncertainty in the localization of the constituents is of the order of magnitude of their distance, 10^{-14} m. The transition point from the classical to the quantum mechanical regime is taken to be at the temperature where the De Broglie wavelength equals the inter-nucleon spacing (Alonso 1974).

In spite of these differences, attempts were made to describe nuclear dynamics and in particular, surface vibrations which arise from the excitation energy of the nucleus, in terms of the motion of a liquid drop under the influence of nuclear surface tension (Bersch 1983, A. Bohr and Mottelson 1975). If one includes the quantum effects for the giant vibrations the theory gives a quite simple and unexpected result, namely that the nucleus has a rigidity making it to respond like an elastic solid to sudden forces and like a viscous liquid to slow ones.

Swiatecki and Cohen (1956a, 1956b, 1962, 1963) in a series of papers have extensively studied the deformation energy of a charged drop with special reference to the fission process. Fission is a result of competition between the long-range electrostatic repulsion and the attractive short-range nuclear forces, idealized in this model as surface tension. A charged drop is stable against small deformations when the potential

energy is an increasing function of deformation (local minimum). The least energy necessary to divide the drop and the drop shape before break up are of importance in the discussion of fission thresholds and fission symmetry. The shapes of neutral equilibrium vary from a simple sphere and necked-in saddle-point shapes (Bohr and Wheeler family) to a cylinder like configuration with increasing equatorial waist and finally to two spheres (Frankel and Metropolis family) depending on the amount of net charge on the drop. The transition between these main families and some recently calculated ones was not believed to be continuous.

At low values of charge, fission, in the usual sense, does not exist. A sufficiently excited drop might split off fragments of various sizes in a way that may be termed spallation. Fission as a separate process would first appear for intermediate values of net charge and would follow the Frankel and Metropolis family of symmetric shapes. For still higher values of charge (close to the neutral stability limit for a spherical configuration) fission may lead to three or four fragments. Cohen and Swiatecki (1962) further suggest that the dynamical problem should change from an essentially two-body problem for low values of charge to a many-body problem for higher ones and thus introduce the idea of the formation of satelite drops during the fission.

Nevertheless, the stages between saddle points and scission present a problem of quite a different nature than the static equilibrium shapes. In particular, the dynamics of the process would be involved and the physical properties of the drop which determine the hydrodynamic behavior would have to be considered. Accurate and exhaustive experiments on many aspects of nucleus fisssion are available for a long time and further

information may be readily obtained owing to the ease of observing the fission of heavy elements. The real difficulties lie on the theoretical side, where the fundamental questions on the nature of the process have to be explored and settled.

II.1b Fluid Mechanics of a charged oscillating drop and dynamics of fission.

The analysis presented in the previous section is devoted to a study of the potential energy of deformation of a charged drop. The next step should be to calculate the kinetic energy and develop the solutions of the equations of motion of the system for different initial conditions. The large number of possible initial conditions will call for a discussion of the Statistical Mechanics of the problem in order to correlate average initial conditions with average end results of the division. On completion of the classical solution, the next step will be to replace the conjugate momenta in the Hamiltonian with quantum-mechanical operators and to study in an analogous way the quantummechanical and quantum-statistical properties of the resulting Schrödinger equation (Cohen and Swiatecki, 1963).

Tsang (1974) has investigated the similarities between volumetrically charged (nuclear) drops and conducting (rain) drops which were first considered by Rayleigh (1882). By an energy stability analysis applied to conducting drops immersed in an insulating medium, Rayleigh calculated the frequncies for small amplitude oscillations of an inviscid drop and established the amount of charge necessary to fission the drop. The modes of shape oscillation were described by Legendre polynomials and the levels of charge necessary to disrupt the n-th mode were given by

$$\tilde{Q}_c^{(n)} = 4\pi[\varepsilon_m \sigma R^3 (n+2)]^{1/2} , \quad n>1$$

where σ is the surface tension of the drop, ε_m is the permittivity of the medium and R is the radius of the spherical shape. The mode number n corresponds to the number of lobes on the deformed drop. At each critical value the spherical shape is neutrally stable with respect to the appropriate shape perturbation. Elementary bifurcation analysis applied to the modified Young-Laplace equation that governs the shape of the drop shows that new families of equilibrium shapes branch from these critical values and evolve transcritically in charge. The drop shapes in each family have the symmetry of the shape perturbation; for example, shapes in the first family have two lobes and the corresponding value $Q_c^{(2)}$ marks the absolute stability limit for spherical drops.

Oscillations of an inviscid liquid drop carrying surface charge can be altered by the Coulomb forces and by charge convection. Eliassen (1963) used the "pillbox" method to construct the general conservation equation on a moving and deforming surface that separates two immiscible fluids. The conservation principles are applied to an arbitrary cylinder-like volume element of fluid which contains a portion of the interface, and then the limit of the equation is taken as the height of the cylinder approaches zero. This method has also been used by Bupara (1965) to derive interfacial continuity, species, energy and momentum equations, (also see Aris 1962). We have derived the conservation equation for surface charge, and have shown that when the drop medium is a perfect conductor, the characteristic times for charge convection and conduction on the surface are much smaller than the characteristic time of drop motion. In this case the charge distribution on the surface assumes

the equilibrium value and the surface remains equipotential during the motion.

II.1c Effects of viscosity on drop dynamics

Initial oscillations of a deformed single or compound drop may be virtually irrotational if the ratio of the viscous boundary layer on the interface(s) - scaled as $(\nu/\omega)^{1/2}$ where ν is the dynamic viscosity and ω the natural frequency of the motion - is small compared to the characteristic length of the system. Viscosity generates vorticity near the interface(s) which diffuses eventually throughout the bulk fluid according to a transient conduction equation. A first order theory for viscous charged drop oscillations has been developed by Tang and Wong (1974).

The damping effects of viscosity can also be observed in Alonso's (1974) finite difference (see section III.2b) simulations of a dielectric charged drop. Figure II.1.1 reproduces her results and demonstrates the asymptotic decrease of both the kinematic and surface (dynamic) energy with time.

Miller and Scriven (1968) have carried out a normal mode analysis of the small amplitude oscillations of a viscous fluid droplet immersed in another viscous fluid. They derived a general dispersion relarion by which the frequency and the rate of damping can be calculated for arbitrary values of droplet size, physical properties of the fluids and interfacial viscosity and elasticity coefficients. When the viscosities of both fluids are low, but not zero, the primary contribution to the rate of damping of oscillations is generally the viscous dissipation

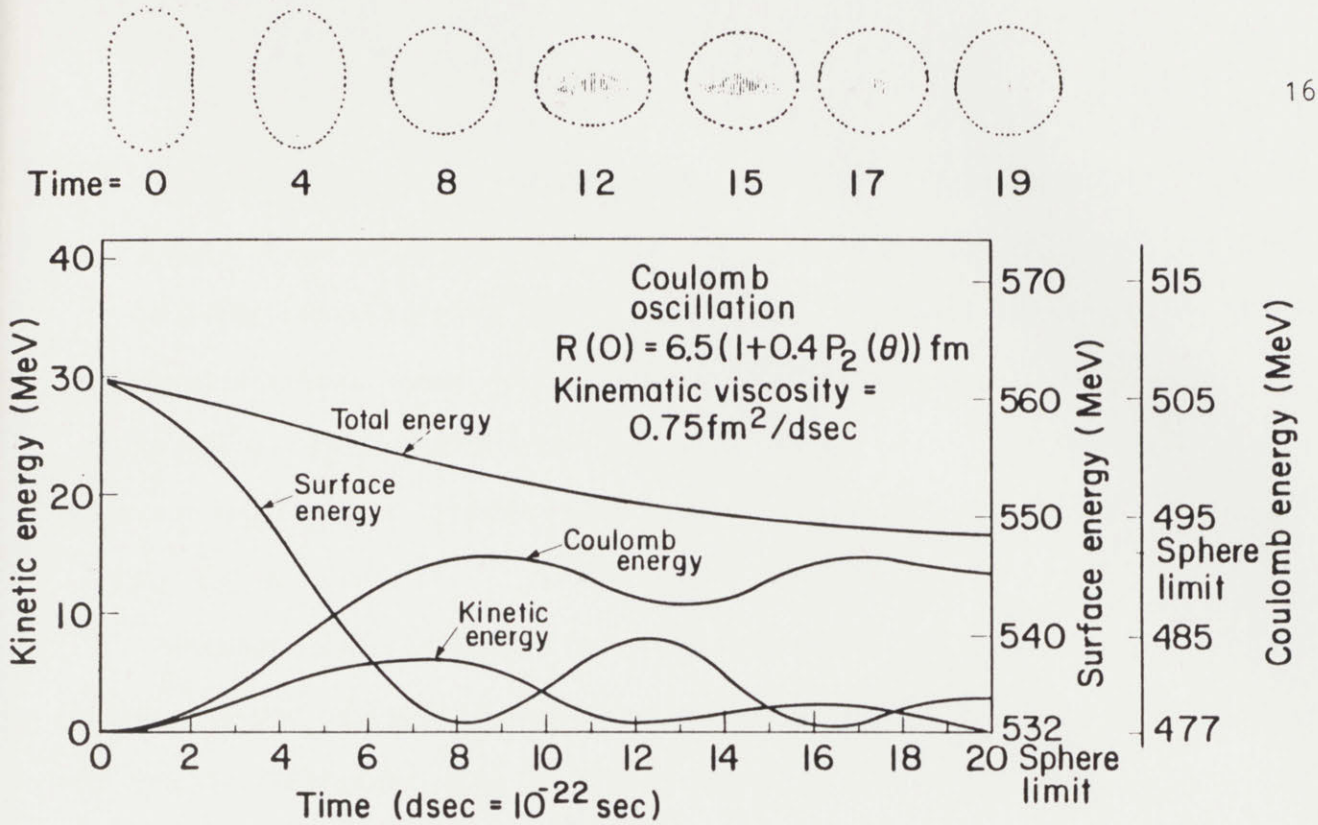

Figure II.1.1 Damped oscillations of volumetrically charged drops (Alonso 1974).

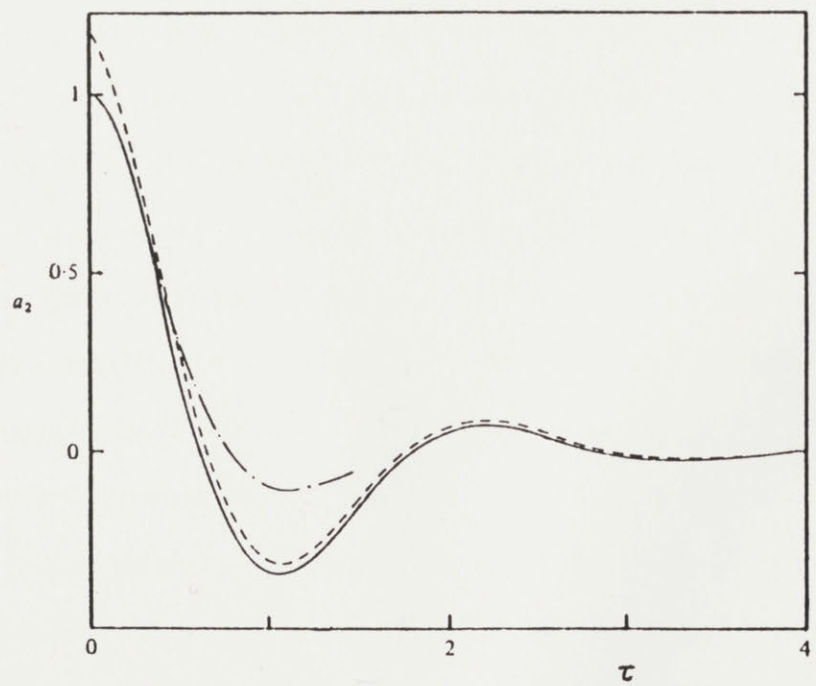

Figure II.1.2 Oscillation amplitude of a free drop $\alpha_2(0)=1$, $\dot{\alpha}_2(0)=0$. (——) Numerical inversion of Laplace Transform. (---) Least-damped normal mode. (-·-) Irrotational approximation (Prosperetti 1980a).

in a boundary layer near the interface. For this reason inviscid velocity profiles, which do not account for the boundary layer flow, do not lead to good approximations to the damping rate. The two exceptions in which the approximation based on inviscid profiles is adequate occur when the interface is free and either the interior or the exterior fluid is a gas of negligible density and viscosity, corresponding to the single bubble and drop case.

Prosperetti (1980a, 1980b) has examined the same linear viscous problem using Laplace transforms and has predicted the transient regime of the oscillations. The governing equation for the amplitude evolution is not a simple harmonic oscillator, but also includes an integral term of the interface velocity up to the time considered. This result is more general than the result of Miller and Scriven (1968). It reduces to the almost irrotational result for short times in the single fluid case, if its viscosity is low and the initial conditions do not introduce vorticity into the system (Lamb 1932). It also reduces to the normal mode analysis of Miller and Scriven for large times and any fluid properties, because then all past "memory" of the motion carried by the integral will have damped out and only the effects of the normal mode will prevail. In intermediate times this integral term acts as a forcing to the damped oscillator and changes its transition from the appropriate initial conditions to the expected final motion by modulating both its frequency and damping rate. Prosperetti's results are better understood using figure II.1.2 where the amplitude evolution of the 2-lobed mode is given with zero initial velocity according to the numerical inversion of an integro-differential equation (——). This is compared to the least-damped normal

mode (----) and the initial irrotational approximation (-•-•-).

Earlier Prosperetti (1974) showed that the damping factor of the system increases with time, in the early stages of the motion, and most unexpectedly that this increase is a function of $t^{3/2}$ instead of $t^{1/2}$ as is the case for transient diffusion in an infinite domain. This is the reason why the small-time irrotational solution is correct in practice for real fluids.

The nonlinear coupling of viscosity and free drop oscillations is still unresolved, except for the limited numerical simulations of Alonso (1974) and Foote (1973).

II.2 DYNAMICS OF COMPOUND DROPS

II.2a Inertial Confinement Fusion (ICF) target

Nuclear fusion reactors with inertial confinement and ignition systems are currently being developed for use as electricity generating units (Nuckolls et al. 1972, Kammash 1975, Yonas 1978). In these systems a fuel pellet containing an equimolar mixture of Deuterium and Tritium (DT) at 10-100 atm is exposed to a large pulse of energy from either laser- or electron-beam sources. The outer surface of the fuel pellet ablates and drives the remainder of the target into the intense compression needed to initiate a thermo-nuclear burning of the fuel. Hollow glass shells containing the fuel mixture are being produced for ICF targets (Hendricks 1976, 1977, 1981). Such a simple target is shown schematically in figure II.2.1 and is characterized by its outer radius R_1 and wall thickness, usually reported as aspect ratio $A=(R_1-R_2)/R_1$ where R_2 is

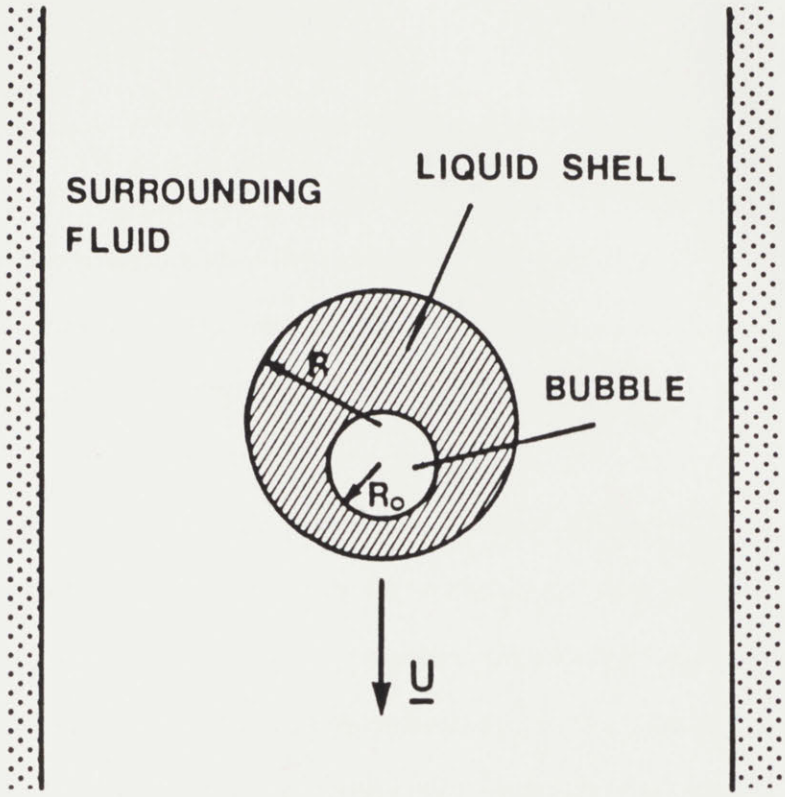

Figure II.2.1 Schematic diagram of Free-Falling Liquid Shell.

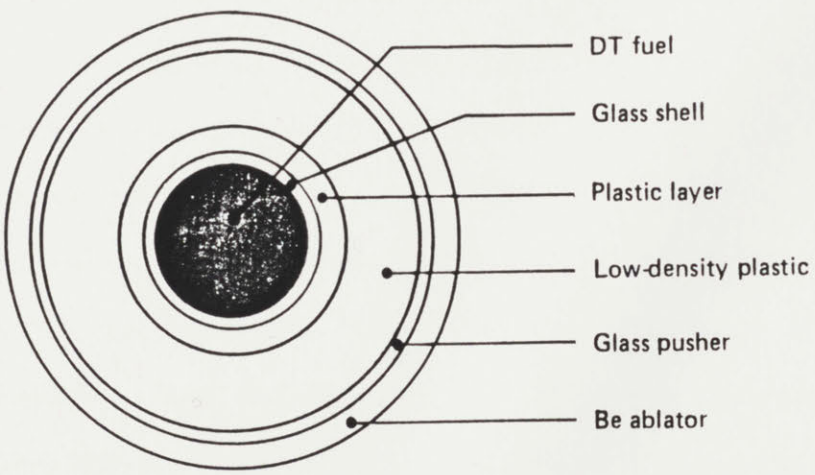

Figure II.2.2 Schematic diagram of a multilayer, multishell target design for high density, ablatively driven implosion (Hendricks 1977).

the inner radius of the shell. More complicated structures such as the multilayer assemblies shown in figure II.2.2 have become necessary to test and understand the laser-target interactions and may be fabricated at a later stage. The surrounding layers may be of glass, polymeric, cryogenic or other inorganic materials and metals.

The production and precise characterization of adequate targets require a combination of several technical and scientific disciplines, including glass technology, polymer chemistry and physics, optics and electron microscopy. For developmental work, fuel targets with outer radii of several hundred microns and aspect ratios of a few hundredths have been required. The economics of large-scale operation and the achievement of "breakeven" require targets of several millimeters in radius and aspect ratios of several hundredths.

The energy produced in any economical power production system must be worth more than the input power and investment costs to produce it. In addition, the cost must be competitive with other production sources. Simplistic arguments show that targets must be produced at rates of 5 to 10 per second and at cost of a few cents to a dollar each. The material cost of a shell is extremely small - as low as 1 microcent. The cost of the fuel is not as small (0.1 cents per 100 ng of Tritium). Thus, the total material cost in this simple, but often used target, is about 0.2 cents. It becomes then obvious, that the cost of a target in a finished state is essentially the cost of the manpower to handle, select, measure and assemble - items which will be greatly reduced, if the fabrication step meets the preset standards. For more details see Hendricks and

Johnson (1977).

Many of the most difficult production problems result from the stringent design requirements for surface finish, concentricity and target material composition. For example, the surface finish on a glass sphere used in a high-density implosion experiment may be no more than 100-300 A^0 peak to valley, the wall nonuniformity cannot exceed 1% and the microspheres must hold up to 100 atm of DT over a long period of time. It has been demonstrated (Nuckolls et al. 1972) that even a slight eccentricity of the shell leads to a large deviation from sphericity during the fuel implosion, which places severe limitations on the efficiency of the reaction by restricting the maximum pressure attainable inside the shell. Surfaces of such high quality are seldom found or studied in most materials research, development or use situations. Besides these surface requirements, one must achieve reproducibility of the ICF target, which translates into reproducing the initial droplets with the same mass of glass and injecting them under prespecified conditions in the furnace. For relatively simple targets of the exploding pusher type, the quality of the glass shell is not extremely critical. Variations in wall thickness, surface irregularities and some voids in the wall can be tolerated. However, even with such relaxed tolerances only a few in 10^6 to 10^9 of the commercially produced shells are acceptable, and even then, the only shells available have limited thicknesses (0.5 to 1.5 μm) and diameters (40 to 250 μm). As the requirements for higher quality and lower cost production were clarified, the need for a reliable source of spheres became obvious.

For these reasons it is imperative to develop the means of producing

high-quality hollow glass microspheres. In general, the melting point of the glass must ensure rapid and complete gel to glass fusion and its viscosity must be low enough to allow high sphericity and concentricity. Three distinctly different processes are currently being used for manufacturing hollow spheres.

LIQUID DROPLET TECHNIQUE. According to this method (Rosencwaig and Hendricks, 1977) an aqueous solution of glass forming chemicals (e.g. sodium silicate, boric acid, sodium and potassium hydroxide etc.) is forced through an orifice to form a cylindrical jet. A capillary wave launched onto the jet by means of a piezo-electric transducer, breaks up the jet into a series of uniform drops. These will attain an almost spherical shape in free fall as a result of surface tension in this low viscosity glass state. The solvent (water) is evaporated from the drops in a vertical column at about 350^0 C, leaving dry particles which continue into a higher temperature region of the furnace to form glass spheres. Water of hydration and gasses evolved from the chemical constituents expand in the molten glass spheres acting as an internal blowing agent and deform the glass into quite uniform hollow shells. These shells are then cooled, solidified - both during free-fall - and collected. The right temperature, solution composition, size of the orifice in the liquid-droplet generator and droplet transit time will produce hollow glass microspheres with specified diameter and wall thickness in a controlled fashion. For more details on the liquid droplet generator see Hendricks (1976), whereas a detailed description of the vertical furnace and the various Physical and Chemical processes that take place during the microshell fabrication is given by Hendricks (1977).

ANNULAR LIQUID JET METHOD. An axial flow of liquid surrounding a flow of gas at its core is extremely unstable (Calligher et al. 1977, Kendall 1980, 1981). Axisymmetric oscillations arise spontaneously, and grow so rapidly along the axial dimension that a pinch-off of the liquid and an encapsulation of the core gas occurs within as few as four jet diameters, whereas it required more than 500 diameters for the unperturbed regular liquid jet. The breakup in hollow drops is still driven by the surface tension instability, first described by Rayleigh (1879). Another advantage of the annular jet method is that, because of the external forcing, only a very short range of modes seem to become unstable, which yields a short range of drop sizes, whereas a wide range of wave numbers are unstable in the Rayleigh jet. The shells which result thereby may be described as thick wall bubbles, for which Van der Waals forces are unimportant. It has also been observed that altering the viscosities or densities of the fluids does not negatively affect the obtained shell.

DRIED GEL PROCESS. In this method dried granules of hydrated glass-forming oxides are dropped through a furnace (Hendricks et al. 1979, Woerner et al. 1980). The water of hydration is encapsulated and gases are evolved from the components forming small bubbles, whose walls become thin as expansion occurs. The internal bubble walls perforate and shortly one internal relatively large bubble is formed of all the smaller ones. This single bubble continues to expand and a hollow shell is formed. Preparation of the dry particles to be put into the furnace, requires that they are mixed into a slurry, dried, pulverized and sieved to gain high uniformity in size. Another method involved dissolving the chemicals in water and spray drying to form the dry particles which were then introduced

in the furnace. Unlike the two previous methods this one produces a distribution of shell sizes and thus considerable shorting must follow the primary fabrication. After the spheres have been collected from the furnace, they are washed, carefully examined (methods used include transmission interferometry, scanning electron microscopy etc.), filled with the DT mixture and coated with several layers of polymers or inorganic materials. Deuterium and Tritium diffuse rapidly through the wall when the spheres are at a temperature of about 350^{0}C and at appropriate pressures of that mixture.

II.2b The Fluid Mechanics of a bubble inside a drop

No matter which method for the fabrication of the ICF target is used, a bubble trapped inside a drop is ultimately produced. Any eccentricity of the liquid shell is transmitted to the shell used as ICF target upon solidification. The sphericity of the shell, and thus its value as a fusion target, depends on the ability of the forces acting on the bubble and drop, e.g. dynamic pressure, liquid inertia, viscosity and surface tension to counterbalance the net buoyancy of the bubble within the drop and the hydrodynamic drag on the outer surface of the drop; both of these forces if uncontrolled deform the spherosymmetric shell. For the initial stages of fusion experiments the quality requirements for the ICF targets were not as strict and the hollow glass shells could be very thin and have radii of the order of a few hundred microns. For these small and thin shells, surface tension forces dominate over all the others and the concentricity of the target is preserved. For targets with outer radii of several millimeters surface tension will not be sufficient and

the fluid mechanics of liquid shells will play an important role.

Only in the absence of gravity can a bubble inside a drop reach static equilibrium; gravity always causes the bubble to drift upwards (against the gravity field) through the drop. In this equilibrium state both the bubble and its surrounding liquid shell will be spherical, for surface tension drives both interfaces to the shapes with lowest surface energy or equivalently lowest surface area. When the liquid shell is static, all locations of the spherical bubble inside the drop are energetically equivalent and the relative position of the bubble is undetermined. Any tendency of the bubble to center inside the drop must be related either to fluid motions in the shell or bubble, or to forces other than surface tension that act on the static shell. In the more general case, the bubble will not stay at a certain position inside the shell but will move with an acceleration dictated by the net force acting on it.

For a static liquid shell one candidate for stabilizing the spherosymmetric configuration is an electrostatic force created between the two gas-liquid interfaces since it prohibits any tendency of the interfaces to move closer together. One possibility is the electrostatic force due to double layers at both interfaces that may be created by the collection of charged species on them. It has been shown by many authors (Vrij 1966, Vrij and Overbeck 1968 etc.) that these forces, which give rise to the so-called disjoining pressure at an interface, are appreciable only for films with thickness less than 1000 A^0 (this value depends on the ionic strength of the liquid) - much thinner than the shells of interest for ICF targets. These forces are important in preventing or promoting

the total collapse of the shell and Patzer and Homsy (1975) have obtained an expression for the critical thickness of the spherical fluid films at rupture.

The simplest induced fluid motion that could cause bubble centering - at least about one axis - is a rigid rotation of the entire shell. As Annamalai et al. (1980) have shown, a bubble in a more dense and rigidly rotating liquid migrates to the axis of rotation. Centripetal acceleration also causes the bubble to elongate along the axis of rotation and the outer shell surface to flaten at the poles (Brown and Scriven 1980, Chandrasekhar 1965, Princen et al. 1967) and hence leave the shell asymmetric.

The equilibrium size and thickness of a shell formed from given amounts of liquid and captured gas, depends only on the pressure in the gas surrounding the liquid. Sudden changes in the external pressure cause the diameter of the shell to contract, expand, or oscillate in time. Viscosity damps these motions and the shell finally settles into the new equilibrium shape dictated by a balance of bulk phase pressure differencies and capillary pressure.

Saffren et al. (1981) have developed an experimental procedure to study the effectiveness of the shell oscillations in centering the bubble. The heart of their apparatus is a neutral buoyancy tank which is a lucite box filled with silicon oil. Taking advantage of the fact that the density of the silicon oil is less than the water density, they created a vertical density gradient by adding a small amount of freon to the silicon oil, until the water droplet floated in the middle of the tank. A static compound drop was prepared so that the inner and outer boundary surfaces

were not concentric due to a slight density mismatch. However, as the shell was excited to oscillate in one of its normal mode frequencies (n=2), the two boundaries became concentric within the accuracy of their observation. This centering phenomenon took place within a few cycles of oscillation and the centering force seems to depend on the ocillation amplitude and the shell thickness. Also Lee et al. (1981) observed that by amplitude modulating the driving voltage of an acoustic levitating apparatus (Trinh et al. 1982), a strong centering force is generated in a submilimeter compound drop suspended by the radiation pressure in a gaseous medium. On the other hand, the force is much weaker when the drop radius is 5 mm or larger.

One mechanism proposed by Chi (1979) for this centering phenomenon relies on a dynamic pressure gradient, induced by the oscillations that makes the center position most favorable. The pressure fluctuations introduced by Saffren et al. (1981) and Lee et al. (1981) are not spherosymmetric, but take on the shape of the most dominant mode of the oscillation. The decomposition into normal modes of infinitesimal amplitude describes the decentering of the trapped bubble entirely by the first spherical harmonic $P_1(\cos\theta)$ (Morse and Feshbach 1953). These disturbances are calculated to be neutrally stable and induce no tendency for the bubble to move with respect of the drop, or equivalently, the linearization of the governing equations of fluid motion proves that the time constant associated with these disturbances is identically zero. As a result, it is necessary to consider the nonlinear effects to find the restoring forces responsible for the observed centering of the bubble inside the drop.

The normal mode analysis of Patzer and Homsy (1975) for small amplitude oscillations of a viscous liquid shell gives the same result for the decentering disturbance and makes it obvious that any tendency of the bubble to center must be described in terms of at least moderate amplitude motions, where fluid inertia and nonlinear interface curvature are accounted for.

Lee and Wang (1984) have attempted an analytical solution aimed at explaining the centering phenomenon. They have assumed that the displacement of the bubble from the center of the liquid drop is small compared with the bubble radius, but large compared with the amplitude of the wave on the shell surface. Thus, they have treated the linearized problem and included only some interaction terms. According to their results, the direction of the motion of the bubble center can be both towards or away from the liquid drop center, depending on the shell thickness and on the mode which was initially excited which is in contrast with the experiments.

III. METHODS OF SOLUTION FOR MOVING-BOUNDARY PROBLEMS

Physically motivated problems sometimes require the solution of a system of equations or the evaluation of an integral on a variable domain, not known a priori but determined as part of the problem. Depending on whether these boundaries are stationary or moving, such problems are usually referred to as free- or moving-boundary problems (Elliott and Ockendon 1982). Many fluid dynamical free- and moving-boundary problems are of this kind (wave motion, problems with phase change, coating flows etc.). In all these cases nonlinear partial differential equations are augmented by boundary conditions that apply on the "unknown" boundary and which further complicate the problem.

Traditionally, as a first step towards an understanding of the physical system, the governing equations are linearized, and thus infinitesimal disturbances (perturbations to the base solution of the linear problem) are considered. The study of the linearized problem is straightforward, in principle, although in practice the actual implementation of its solution may be involved, if more than one spatial dimension is considered or complicated boundary and initial conditions are imposed.

When one considers nonlinear problems the methods of solution are far more limited than those existing for linear problems. The intrinsic difficulty associated with the nonlinearity is essentially due to the fact that one cannot use superposition of elementary solutions to construct a more general solution of the governing equations. On the other hand, it is well known that the presence of a nonlinearity usually does not simply modify the results obtained by examining the linearized problem.

In fact, in some situations the most important and physically interesting phenomena (multiple steady states, time periodic phenomena etc.) are contained in the nonlinear terms. However, despite the progress made in the last few years in solving certain nonlinear equations exactly, the solutions of most systems remain unknown. Therefore, one is forced rather soon to look for meaningful approximations which could provide some understanding of nonlinear phenomena before, if necessary, proceeding to a numerical solution.

III.1 PERTURBATION METHODS

As mentioned before, nonlinear equations can be tackled by carrying out a perturbation expansion about a known solution. Furthermore, much of the interesting behavior occurs far from a known linear solution. This is unavoidable because we are looking at the behavior of highly nonlinear systems and hence cannot always utilize local linearizations around known solutions, since they are simple and typically symmetric and uniform.

One characteristic that distinguishes problems with spherical geometry from those in Cartesian or cylindrical geometry is the natural periodicity of the interface. This yields a discrete spectrum of the fundamental modes instead of a continuous one and allows us to disregard small variations in the spatial wavelength.

III.1a Domain Perturbation

Mathematically rigorous demonstrations of the existence of two dimension-

al progressive waves which are analytic in the amplitude of the wave can be found in Stoker's book (1957, Chapter 12). These demonstrations rely heavily on the theory of analytic functions of a complex variable and cannot be extended to three dimensional wave problems or to problems with more complicated boundary or initial conditions, like the one that is treated here.

The higher order theory of water waves uses a perturbation theory which represents solutions to problems as a power series in the amplitude of the wave. The procedure was familiar to applied mathematicians and Joseph in 1973 gave a systematic development which has now been applied to general elliptic and parabolic free- and moving-boundary problems. He named the method domain perturbation - a name that will be used hereafter.

This "Lagrangian" formulation does not rely on complex variables and applies to more general problems. A one parameter family of domains is used on which the field equations and boundary conditions are to be solved. The solution must be known in some reference (possibly static) domain onto which all higher order problems can be mapped. The solution in the perturbed domain is developed in a power series in the perturbation parameter, the coefficients of which are total derivatives of the field variables evaluated in the reference domain using the chain rule. The values of the coefficients on the boundary may be computed using the properties of the mapping on the boundary only, so that its nature in the interior need not be known. As a result the solution in the perturbed domain depends only on the boundary values of the perturbation method and can be computed solving a hierarchy of linear problems. In essence, by transforming the governing equations and the boundary conditions to

the undeformed domain we obtain a problem posed unambiguously there, whose solution implies that of the original problem on the perturbed domain.

More recently, Lebovitz (1982) proposed an "Euler-like" approach for the perturbation expansions which does not require transformation of the domain. He carries out the formal expansions of the dependent variables of the problem as if the domain were not perturbed, i.e., without making the coordinate transformation. If analytic continuation of the obtained solution is possible this method yields the correct result in the perturbed domain.

To date, all free-surface calculations involving surface tension are based on generalized Monge' surface representations (Brown et al. 1980) where the position vector identifying the free surface is expressed in a specific curvilinear coordinate system. The natural choice of system for a liquid shell is a radial representation in spherical polar coordinates. These representations are all limited to distortions of the interface that are not so severe that the menisci become multi-valued, although a perturbation solution may fail long before this has occured.

III.1b Nonlinear dynamics and stability

Some of the ideas used in studies of nonlinear waves (nonlinear periodic motion) have proved to be very useful in nonlinear stability problems as well. For small perturbations to a certain basic flow, the linearized governing equations provide the phase speed (eigenfrequency) of the perurbation as a function of the wave number (order of excited mode) and of certain dimensionless parameters, such as the Reynolds or

the Capillary number through the solution of an appropriate eigenvalue problem. The correspondence between dispersive water waves and nonlinear oscillations is indicated in parenthesis. For temporal instability, the wavenumber is taken to be real and, depending on the sign the imaginary part of the corresponding phase speed, perturbations either grow or decay exponentially, according to the linear theory. The locus of real wavenumbers would correspond to neutrally stable disturbances on a stability diagram. The exponential growth or decay rates predicted by linear theory will be modified when the neglected nonlinear terms are included and nonlinear hydrodynamic stability theories attempt to describe the evolution of disturbancies in the nonlinear regime.

The existing nonlinear stability theories are based on the ideas of Landau (1944) and the later work by Stuart (1971). The essential point is that a finite amplitude perturbation close to the stability curve can be described as a wave of slowly varying amplitude. Thus, for weakly nonlinear disturbances, evolution equations for the long time behavior of the amplitude can be derived by singular perturbation methods, such as the Linstedt-Poincarè technique, the multiple time scales etc., well described in standard texts (Bender and Orzag 1978; Nayfeh and Mook 1979).

In this sense, there is similarity between nonlinear dispersive waves and nonlinear stability theories. As expected both developments reduce to sinusoidal waves of constant amplitude in the linear limit. The modifications of the amplitude due to nonlinearity and away from neutral conditions are described by the evolution equations.

Among the nonlinear mechanisms through which energy can be transfered from one mode to another is the harmonic resonance, which has been a

subject of much interest in the last twenty years (Phillips 1981). This phenomenon takes place whenever the harmonic eigenfrequency of a conservative system is an integral multiple of the fundamental. It is called second harmonic resonance when this occurs between the fundamental and its second harmonic. Harmonic resonance occurs in the oscillating charged drop for various values of the net charge on the drop surface and is analyzed in Chapter V.

Another possibility which in certain situations can initiate quite dramatic effects is provided by physical systems in which two frequencies can assume almost equal values. In this case there exist solutions of the linearized equations which have linearly growing amplitudes. This secular behavior of the amplitude, which is somewhat similar to resonance in an externally forced, simple harmonic oscillator, has been called direct resonance, (see Akylas and Benney 1980). In the nonlinear regime, the linear growth of a disturbance at direct resonance will be modified, but nevertheless, the amplitude of such a disturbance must be larger than expected. Also the nonlinear interactions must be stronger due to the presence of secularly growing terms in the linear level. A drop can be brought into a neutrally stable situation when the charge it carries creates a repulsive force which is almost equal to the surface tension force that keeps it together. In this case the eigenfrequencies of the motion, which are imaginary and of opposite sign, simultaneously approach zero.

III.2 NUMERICAL METHODS

It is widely believed that exact analytic solutions are superior to numerical solutions in that they are valid for arbitrary parameter values and often give more insight into the behavior of the system. Unfortunately there are cases where the nonlinear perturbation solution cannot be reached either because the algebra is very involved or a systematic and consistent way cannot be developed. Furthermore, given the fairly complicated equations we are dealing with, even when a formal analytical solution can be found, it is often of limited utility.

In these cases but also to verify approximate results computer-aided methods can be used to reveal the full nonlinear behavior. Numerical and analytical methods for solving nonlinear problems are closely related, both relying heavily on local expansions. Indeed, similar expansions are often used in both cases, the difference arising from the necessary use of discretized equations and specific parameter values in the computer-aided analysis. Numerical methods also allow the use of important iterative techniques which give rapid convergence to solutions which are infeasible to obtain otherwise.

III.2a Finite Element methods

Finite element methods are systematic techniques for constructing approximations to functions which are themselves solutions to partial differential equations. To formulate these approximations, the domain of the function is divided into subdomains or elements and in each element the unknown functions are approximated by low-order polynomials. The

coefficients of the polynomials are chosen so that the function has a specified degree of inter-element continuity and so that the weighted residuals of the equation governing the behavior of the function are zeroed. In this way the original problem defined for continuous variables is reduced to a system of algebraic equations for the coefficients of the polynomials - a discrete problem. The so-called finite element basis functions (Strang and Fix 1973) are combinations of element polynomials that automatically satisfy the continuity constraints and which are more convenient than the element polynomials for computer-aided calculation.

Finite element techniques are the preferred method for solving steady free-surface viscous flow problems where one phase is tenuous. The methods that have been developed differ in the technique used to determine the location of the free-surface, and in the numerical iteration scheme used to solve the resulting set of nonlinear algebraic equations.

Ettouney and Brown (1983) and Beris et al. (1984) transformed the domain with a free-boundary to a fixed domain before discretizing the problem with a fixed finite-element mesh. This transformation has the advantage of making explicit the nonlinearities inherent in the problem. They exploited this by using Newton's method to solve the nonlinear equation set that resulted from the finite element formulation. Newton's method converges quadratically to the solution, a marked improvement over the linearly convergent schemes of successive substitutions, and also forms the basis for modern methods for studying numerically the multiplicity and existence of steady flow fields (Ungar and Brown 1982). Saito and Scriven (1981) and Chang and Brown (1984) have solved similar problems in the original domain also using Newton's method. Instead of the global

mapping of Ettouney and Brown they took advantage of the isoparametric mapping for each quadrilateral element onto a square element where the dependence of the basis functions on the moving surface is expressed explicitly.

Numerical techniques for solving free-surface problems also differ in the algorithm used to locate the meniscus. Two schemes are in use, the so-called kinematic and normal stress iteration methods (Silliman and Scriven 1980). The kinematic scheme locates the interface so that the fluid velocity evaluated at the interface agrees with the value extrapolated from the bulk flow. Since the balance of normal stress on the interface, which includes the action of the surface tension, is satisfied only approximately the kinematic iteration is most applicable in the absence of surface tension (high Weber or Capillary numbers). Free-surface location based on the balance of normal stresses across the interface is most applicable when surface tension is important.

In a time-dependent calculation the finite element discretization results in a system of ordinary differential equations. Explicit methods of solution are possible when the finite element mass matrix is diagonalized and include the classical Runge-Kutta and Adams-Bashforth methods (Gear 1971). These will circumvent the problem of solving a large system of nonlinear equations at each time step, but may be limited by numerical stability constaints to severly small time steps. Implicit methods such as the Euler-predictor/Newton-corrector formulation employed by Gresho et al. (1978) have the advantage of increased stability but require the solution of algebraic equation sets.

Patzek et al. (1982) and Basaran et al. (1982) have calculated the

inviscid axisymmetric oscillations of the free liquid conducting drops with or without electrical charge. They solved Bernoulli's equation for the surface shape and Laplace's equation for the velocity potential. Galerkin's weighted residual method was used and the velocity potential was represented by biquadratic finite element basis functions on a tessellation that deforms in proportion to the free surface. The integral equation for the surface charge was solved by the boundary element method. The trapezoidal rule with variable step size was used for the time integration. The accuracy of the results was tested by the constancy of drop volume and smallness of mass and momentum fluxes across the the drop interface.

III.2b Finite Difference and Spectral methods

Finite difference schemes have been developed for free-surface flows using either Lagrangian techniques (particle based coordinates) or Eulerian techniques (fixed coordinates). The Marker-and-Cell method (MAC) developed at Los Alamos (Harlow and Welsch, 1965) solves the full Navier-Stokes equations for an incompressible, viscous fluid with free- or moving-surface. Velocity components and pressure are defined over a staggered Eulerian mesh. A Langrangian system of marker particles is defined and these markers are moved through the grid at interpolated local fluid speeds, behaving like dye particles in actual experiments. As time progresses, the position of these marker particles serves to specify the location of the fluid surface, and hence, can define in which computing "cells" the surface boundary conditions should be applied. The forces and pressures are calculated at the centers of the cells, and velocities are evaluated at the cell boundaries. The code first calculates a set of velocities

over the cells by solving the bulk equations in the finite-difference form. Then it adjusts the velocities to conserve volume, and satisfy the boundary conditions and vorticity requirements. When a unique solution has been reached, the particles move according to the local velocities for a small time step, new forces are calculated and the processes is repeated. The MAC method is well documented elsewhere (Welch et al., 1966) and some of the necessary modifications will be mentioned in the following.

In the original MAC calculations, the surface is specified as being a region of surface "cells", and is only resolved by the fixed Eulerian mesh. Daly (1969) improved this crude evaluation of curvatures by using the Lagrangian marker particles whose spacing is important. He then determined the actual surface curvature from the orientation of an interpolation curve which passed through the surface particle array. He employed a cubic spline which not only ensures smooth variation but also permits the evaluation of necessary derivatives on the surface. Since, in general, the spline curve will not go through the center of a given cell, where the pressure is defined, it is necessary to specify where the surface curvature is actually evaluated, and several methods have been tested. Others have proposed to evaluate the boundary condition on the cell surface rather than on the center.

If Lagrangian particles are too far apart the surface is not well resolved, if the spacing is too close, small fluctuations in particle position will generate faulty curvatures which in turn requires "smoothing" of the surface. Also one has the option to add or delete particles from the surface to keep their spacing within proper bounds. The last limitation in this method is that it applies to axially symmetric geometries.

Foote (1973) has used this MAC code and Alonso (1974) has used a modified version called SQUISH in problems related to drop dynamics. Their results will be compared with our analysis in the Chapter IV.

Longuet-Higgins and Cokelet (1976) have developed a different finite difference method to treat water waves of finite depth. They used boundary particles and by exploiting the irrotationality throughout the flow field reduced the problem to one of solving a linear integral equation on the free-surface as part of the time-stepping procedure.

Most of the numerical schemes depend on the use of point values to represent continuous variation and use finite-difference methods for differentiation and integration. If the flow region is large, or the boundary radii of curvature small, then the numerical approximations through finite differences may be rather poor. It has been shown by Fornberg and Whitham (1978) that spectral and pseudospectral methods, using Fourier series to represent horizontal variation, were particularly accurate and effective in solving the Korteweg de Vries equation of shallow-water waves. They preferred these spectral methods over finite difference techniques. For irrotational motion the governing equations (described in Chapter IV) are linear, the nonlinearity arises from the boundary conditions which apply on the unknown moving surface. Also, only the boundary conditions contain first order time derivatives, so that, if an initial solution is known, advancing this solution in time should be a relative simple linear process. The most severe problem is that of approximating accurately the dependent variables and their derivatives on the surface.

Fenton and Rienecker (1982) assumed that all dependent variables

can be represented at any instant in time by a finite Fourier series in x, throughout the region of interest, which is a direct result of the normal mode analysis of the linearized water wave problem. At the same time this requires that the motion is periodic in x, with some finite period L, the wavelength, a true limitation in the cartesian geometry but a natural condition on the spherical one. Substituting the finite Fourier series form for the velocity potential into the kinematic and dynamic free-surface conditions yielded a coupled set of ordinary differential equations which they solved numerically to obtain the time evolution of the Fourier components. Advancing the interface shape function in time is straight forward but the field variables are more complicated, and computationally expensive. This is because advancing the field variables at points on the surface, gives information about them on the updated boundary surface from which it is not possible to simply obtain the space derivatives needed for the next time step, which have to be evaluated independently and prior to the time integration.

Multer (1973) also used Fourier methods in an attempt to solve the full nonlinear equations numerically. The free-surface was defined by discretely spaced boundary particles, as used in several of the finite difference methods described earlier. While this is an advantage for finite difference methods because the computational particles tend to congregate where the curvature is high, it is not an advantage for Fourier approximations, as observed by Rienecker and Fenton (1981). In addition if the particles are free to move, then one of the advantages of the Fourier approximation is lost, namely that the trapezoidal rule can be used for integrations with the same accuracy as the Fourier approximation.

In summary, a spectral method would have definite advantages in treating this problem because it can resolve easier the discrete spectrum of the eigenmodes which is, for all practical purposes, finite, as the analytic results show, even when the nonlinear coupling is included (see Chapter IV).

IV. NONLINEAR OSCILLATIONS OF INVISCID DROPS AND BUBBLES

In order to understand the mechanics of coupling of spherical modes, the problem of single drop or bubble oscillations in an infinite medium was undertaken - a problem which has interest of its own as described in chapter II. This study will reveal which is the appropriate action towards enhancing the centering motion of the bubble inside an oscillating drop and will improve the undestanding of breakup dynamics.

The free oscillations of drops and bubbles have been studied since the original reports by Savart (1833) and Plateau (1873) of pulsating motions caused by the breakup of a liquid jet. The small-amplitude oscillations of an inviscid globe held together by interfacial tension were first analysed by Rayleigh (1879, see also Lamb 1932), who identified the fundamental modes of motion in terms of Legendre polynomials and calculated the corresponding frequencies. These linear results have been extended to include viscosity, first for a drop surrounded by a low-density gas (Reid 1960), and then for a drop in a viscous outer medium by Miller and Scriven (1968) and more recently by Marston (1980) and Prosperetti (1980a,b). Experiments (Marston & Apfel 1979, 1980; Trinh et al. 1982) performed on drops suspended in a neutrally buoyant and immiscible liquid have confirmed the oscillation frequencies of the linear theory for small amplitude deformations, but have shown a marked decrease in frequency with increasing amplitude (Trinh & Wang 1982). This decrease was anticipated by Rayleigh (1879), but has not been explained by either analysis or full numerical simulation of drop oscillations. The only computer simulations for slightly viscous drops have been carried out

by Foote (1973) and Alonso (1974). Both authors used the marker-and-cell finite-difference technique for solving time-depended free-surface flows with viscosity, an extremely difficult numerical problem. The small number of calculations available in these works makes difficult the quantitative prediction of the sensitivity of the frequency and the evolution of the drop shape on the amplitude and mode of oscillation. More recently Benner (1983; see also Basaran et al. 1982) has approached the problem of inviscid drop oscillations using the method of finite elements, but these results have not been extensively published, yet.

In this chapter we present the asymptotic analysis for moderate-amplitude axisymmetric oscillations of inviscid and incompressible liquid globes. As pointed out by Miller & Scriven (1968), the analysis of the motion of an interface separating two inviscid liquids leads to a discontinuity between the components of fluid velocity tangential to and on either side of the interface. The slip is a result of neglecting a viscous boundary layer that develops on both sides of the interface and removes the singularity in tangential velocity. We avoid the physically unacceptable results associated with inviscid liquid/liquid systems by limiting our study to cases where one phase is either a vacuum or a tenuous gas, so that its hydrodynamical effects can be neglected. The two limits of liquid internal and external to the closed interface are denoted as drops and bubbles, respectively. In these single-fluid flows no boundary layers develop as the viscosity of the liquid is taken to be zero.

The analysis is based on the method of Lindstedt & Poincaré (see Nayfeh & Mook 1979) for approximating the time-periodic solutions of nonlinear differential equations. This method is simpler and less powerful

than the multiple-scale method since it is applicable to phenomena that do not exhibit amplitude variation. Our approach to the problem of an oscillating drop parallels previous applications of this perturbation scheme to inviscid standing waves (Tadjbakhsh & Keller 1960; Concus 1962).

IV.1 FORMULATION

IV.1a Drops

We consider the time-periodic, irrotational and incompressible motion of an inviscid drop with volume $\tilde{V}=4\pi R^3/3$, density ρ and interfacial tension σ. It is assumed that the ratio $gR^2\rho/\sigma$ is sufficiently small, so that gravitational forces are negligible. The surface of the drop during axisymmetric oscillations is described by $RF(\theta,t)$, where $F(\theta,t)$ is the dimensionless shape function of the drop and θ is the meridional angle in spherical coordinates. Scales based on the results of the linear theory are used to define the dimensional velocity potential $(\sigma R/\rho)^{1/2}\phi(r,\theta,t)$, pressure $(2\sigma/R)P(r,\theta,t)$, angular frequency $(\sigma/\rho R^3)^{1/2}\omega$, and time $(\rho R^3/\sigma)^{1/2}t/\omega$, each in terms of its dimensionless counterpart. The dimensionless radial coordinate is scaled with the static radius R of the drop. In terms of these variables the equations governing the inviscid time-periodic motion are

$$\nabla^2\phi = 0 \qquad (0\leq r\leq F(\theta,t),\ 0\leq\theta\leq\pi), \qquad \text{(IV.1.1)}$$

$$\frac{\partial\phi}{\partial r} = 0 \qquad (r = 0,\ 0\leq\theta\leq\pi), \qquad \text{(IV.1.2)}$$

$$2P + \omega\frac{\partial\phi}{\partial t} + \frac{1}{2}\left[\left(\frac{\partial\phi}{\partial r}\right)^2 + \left(\frac{1}{r}\frac{\partial\phi}{\partial\theta}\right)^2\right] = G(t) \qquad (0\leq r\leq F(\theta,t),\ 0\leq\theta\leq\pi), \qquad \text{(IV.1.3)}$$

$$\frac{\partial \phi}{\partial r} = \omega \frac{\partial F}{\partial t} + \frac{1}{r^2} \frac{\partial \phi}{\partial \theta} \frac{\partial F}{\partial \theta} \qquad (r=F(\theta,t)), \tag{IV.1.4}$$

$$\Delta P_0 + 2P = \{- \frac{F_{\theta\theta}}{F} - \cot(\theta) \frac{F_\theta}{F} [1+(\frac{F_\theta}{F})^2] + 2 + 3(\frac{F_\theta}{F})^2 \}/\{ F [1+(\frac{F_\theta}{F})^2]^{3/2} \}$$

$$(r=F(\theta,t)), \tag{IV.1.5}$$

$$\nabla\phi(r,\theta,t+2\pi) = \nabla\phi(r,\theta,t), \tag{IV.1.6}$$

$$\int_0^\pi F^3(\theta,t) \sin(\theta)\, d\theta = 2, \tag{IV.1.7}$$

$$\int_0^\pi \int_0^{2\pi} F(\theta,t)\, P_n(\theta) \sin(\theta) \cos(t)\, dt\, d\theta = \frac{2\pi\varepsilon}{2n+1} \quad (n = 2,3,..), \tag{IV.1.8}$$

$$\int_0^\pi \int_0^{2\pi} F(\theta,t)\, P_n(\theta) \sin(\theta) \sin(t)\, dt\, d\theta = 0 \qquad (n = 2,3,..). \tag{IV.1.9}$$

Equation (IV.1.1) is the Laplace equation governing irrotational flow; (IV.1.2) is the condition for zero radial velocity at the center of the drop; (IV.1.3) is Bernoulli's equation for the pressure everywhere in the drop; (IV.1.4) is the kinematic condition relating the surface velocity to the velocity field of the material there, so that fluid does not penetrate the interface. Equation (IV.1.5) is the balance of dynamic and capillary pressure across the interface, where the right-hand side of this equation is the negative of the local mean curvature 2**H** of the interface; (IV.1.6) is the condition for the periodicity in time of the velocity field; (IV.1.7) is the constraint for constant volume of the drop. The static pressure difference across the interface is ΔP_0; the function G(t) is introduced into (IV.1.3) by integration. With the choice of the mean value of F, it is clear that the mean value of ϕ_t cannot be zero and the potential must at least have a term proportional to t in its expansion, which is circumvented by absorbing the constant of

integration G(t) in ϕ_t (see Lamb 1932). Since only space derivatives of the potential occur in physical quantities, terms proportional to t are still acceptable in ϕ. Equations (IV.1.8) and (IV.1.9) define the amplitude and phase of the oscillatory motion, respectively. If the shape function $F(\theta,t)$ is represented as a series of Legendre polynomials, the constraint (IV.1.8) dictates that only the term proportional to $P_n(\theta)\cos(t)$ contributes to the amplitude ε. Equation (IV.1.9) requires the shape function to be always orthogonal to $P_n(\theta)\sin(t)$ and hence sets the phase of the oscillation to be given by cos(t) alone.

IV.1b Bubbles

The equation set governing the dynamics of bubbles is identical with (IV.1.1) - (IV.1.9) except that the velocity potential is defined external to the interface $F(\theta,t)$ and the boundary condition (IV.1.2) is replaced by an appropriate far-field condition (IV.1.11)

$$\nabla^2\phi = 0 \qquad (F(\theta,t)\leq r\leq\infty,\ 0\leq\theta\leq\pi), \tag{IV.1.10}$$

$$\frac{\partial\phi}{\partial r} \to 0 \qquad (r\to\infty,\ 0\leq\theta\leq\pi), \tag{IV.1.11}$$

Also the sign on the pressure contribution in the Young-Laplace equation (IV.1.5) is changed.

IV.2 PERTURBATION SOLUTION

IV.2a Drops

The solutions of the problem (IV.1.1) - (IV.1.9) are composed of the shape function $F(\theta,t)$, the velocity potential $\phi(r,\theta,t)$ and the frequency

ω. We calculate these variables as the terms in expansions of the amplitude of the motion by the now classical Poincaré-Linstedt method. This application is complicated by the dependence of the velocity potential $\phi(r,\theta,t)$ on the shape of the mathematical domain as given by the moving boundary $r=F(\theta,t)$. We account for changes in this boundary shape by combining the normal Poincaré-Linstedt expansion with the domain perturbation technique as detailed by Joseph (1973). To do this, the boundary shape is immobilized as a sphere by introducing the change of coordinates $r\equiv\eta F(\theta,t)$. The expansions of the dependent variables in terms of ε are

$$\begin{bmatrix} F(\theta,t;\varepsilon) \\ \phi(r,\theta,t;\varepsilon) \\ \omega(\varepsilon) \end{bmatrix} = \sum_{k=0}^{\infty} \frac{\varepsilon^k}{k!} \begin{bmatrix} F^{(k)}(\theta,t) \\ \phi^{[k]}(\eta,\theta,t) \\ \omega^{(k)} \end{bmatrix}, \qquad \text{(IV.2.1)}$$

where

$$F^{(k)}(\theta,t) \equiv \frac{d^k F(\theta,t;0)}{d\varepsilon^k}, \quad \omega^{(k)} \equiv \frac{d^k \omega(0)}{d\varepsilon^k}, \quad \phi^{[k]}(\eta,\theta,t) \equiv \frac{d^k \phi(\eta,\theta,t;0)}{d\varepsilon^k} \qquad \text{(IV.2.2)}$$

The static spherical drop is recovered as the zeroth-order solution of the equation set, i.e. $F^{(0)}(\theta,t) = 1$ and $\phi^{(0)}(\eta,\theta,t) = 0$, where the arbitrary reference potential inside the drop has been set to zero. Using the chain rule for differentiation, each term $\phi^{[k]}(\eta,\theta,t)$ in the expansion for the potential can be written as a sum of a contribution evaluated on the spherical domain ($0\leq\eta\leq1$, $0\leq\theta\leq\pi$) and terms that account for the deformation of the domain at each order of ε. The first three relationships are

$$\phi^{[0]}(\eta,\theta,t;0) \equiv \phi^{(0)}(\eta,\theta,t;0), \qquad \text{(IV.2.3a)}$$

$$\phi^{[0]}(\eta,\theta,t;0) \equiv \frac{\partial\phi}{\partial\varepsilon}(\eta,\theta,t;0) + F^{(1)}(\theta,t)\,\frac{\partial\phi}{\partial\eta}(\eta,\theta,t;0)$$

$$\equiv \phi^{(1)}(\eta,\theta,t) + F^{(1)}(\theta,t)\,\frac{\partial\phi^{(0)}}{\partial\eta}, \qquad \text{(IV.2.3b)}$$

$$\phi^{[2]}(\eta,\theta,t;0) \equiv \phi^{(2)}(\eta,\theta,t) + F^{(2)}(\theta,t)\,\frac{\partial\phi^{(0)}}{\partial\eta} + F^{(1)2}\,\frac{\partial^2\phi^{(0)}}{\partial\eta^2} + 2F^{(1)}\,\frac{\partial\phi^{(1)}}{\partial\eta} \qquad \text{(IV.2.3c)}$$

where $\phi^{(k)}(\eta,\theta,t) \equiv \partial^k\phi/\partial\varepsilon^k$ are always defined in the spherical coordinate system. As outlined by Joseph (1973), the equation sets governing the terms $\phi^{(k)}(\eta,\theta,t)$ account for changes in the domain shape only through corrections to the boundary conditions on the meniscous at each order of ε. These equation sets are presented below.

The expansion of the mean curvature in (IV.1.5) is greatly facilitated if the corrections to the shape function are represented at each order as a series of Legendre polynomials

$$F^{(k)}(\theta,t) = \sum_{m=0}^{\infty} F_m^{(k)}(\theta,t) = \sum_{m=0}^{\infty} \delta_m^{(k)}(t)P_m(\theta) \qquad \text{(IV.2.4)}$$

Then the mean curvature is expanded in terms of the amplitude as

$$-2\mathbf{H} = 2 + \varepsilon \sum_{i=2}^{\infty} (i-1)(i+2)F_i^{(1)}(\theta,t) + \frac{\varepsilon^2}{2}\Big\{ \sum_{j=0}^{\infty} (j-1)(j+2)F_j^{(2)}(\theta,t)$$

$$- 4 \sum_{k=2}^{\infty} (k^2+k-1)(F_k^{(1)}(\theta,t))^2\Big\} + \mathbf{O}(\varepsilon^3). \qquad \text{(IV.2.5)}$$

The equations governing the terms $(F^{(1)}, \phi^{(1)}, \omega^{(0)})$ are

$$\nabla^2\phi^{(1)} = 0 \qquad (0\leq\eta\leq 1,\ 0\leq\theta\leq\pi), \qquad \text{(IV.2.6)}$$

$$\frac{\partial\phi^{(1)}}{\partial\eta} = 0 \qquad (\eta=0,\ 0\leq\theta\leq\pi), \qquad \text{(IV.2.7)}$$

$$\frac{\partial \phi^{(1)}}{\partial \eta} = \omega^{(0)} \frac{\partial F^{(1)}}{\partial t} \qquad (\eta=1,\ 0 \leq \theta \leq \pi), \tag{IV.2.8}$$

$$\omega^{(0)} \frac{\partial \phi^{(1)}}{\partial t} + \sum_{n=2}^{\infty} (n-1)(n+2) F_n^{(1)}(\theta,t) = 0 \qquad (\eta=1), \tag{IV.2.9}$$

$$\nabla \phi^{(1)}(\eta,\theta,t+2\pi) = \nabla \phi^{(1)}(\eta,\theta,t), \tag{IV.2.10}$$

$$\int_0^{\pi} F^{(1)}(\theta,t) \sin(\theta)\, d\theta = 0, \tag{IV.2.11}$$

$$\int_0^{\pi} \int_0^{2\pi} F^{(1)} P_n(\theta) \sin(\theta) \cos(t)\, dt\, d\theta = \frac{2\pi}{2n+1} \quad (n=2,3,..), \tag{IV.2.12}$$

$$\int_0^{\pi} \int_0^{2\pi} F^{(1)} P_n(\theta) \sin(\theta) \sin(t)\, dt\, d\theta = 0 \qquad (n=2,3,..). \tag{IV.2.13}$$

The pressure has been eliminated from (IV.2.9) by substitution from the first-order form of Bernoulli's equation (IV.1.3).

The equation set (IV.2.6) - (IV.2.13) has an infinite number of solutions, each of the form

$$\begin{aligned} F^{(1)}(\theta,t) &\equiv F_n^{(1)}(\theta,t) = \cos(t)\, P_n(\theta), \\ \phi^{(1)}(\eta,\theta,t) &\equiv \phi_n^{(1)}(\eta,\theta,t) = \frac{-(n-1)(n+2)}{\omega^{(0)}} \eta^n \sin(t)\, P_n(\theta), \\ \omega^{(0)} &\equiv \omega_n^{(0)} = (n(n-1)(n+2))^{1/2} \quad (n = 2,3,..), \end{aligned} \tag{IV.2.14}$$

which corresponds to the linear modes of the oscillation analysed by Rayleigh (1879). The mode n=1 describes a rigid translation of the drop and has been omitted so that the centre of mass of the drop is fixed with respect to the coordinate system.

The equations governing the terms ($F^{(2)}$, $\phi^{(2)}$, $\omega^{(1)}$) are

$$\nabla^2 \phi^{(2)} = 0 \qquad (0 \leq \eta \leq 1,\ 0 \leq \theta \leq \pi), \tag{IV.2.15}$$

$$\frac{\partial \phi^{(2)}}{\partial \eta} = 0 \qquad (\eta=0,\ 0\leq\theta\leq\pi), \tag{IV.2.16}$$

$$\frac{\partial \phi^{(2)}}{\partial \eta} - \omega_m^{(0)}\frac{\partial F^{(2)}}{\partial t} = 2\omega_n^{(1)}\frac{\partial F_n^{(1)}}{\partial t} + 2\frac{\partial F_n^{(1)}}{\partial \theta}\frac{\partial \phi_n^{(1)}}{\partial \theta} - 2F_n^{(1)}\frac{\partial^2 \phi_n^{(1)}}{\partial \eta^2}(\eta=1), \tag{IV.2.17}$$

$$\omega_m^{(0)}\frac{\partial \phi^{(2)}}{\partial t} + \sum_{m=2}^{\infty}(m-1)(m+2)F_m^{(2)}(\theta,t) = -2\omega_n^{(1)}\frac{\partial \phi_n^{(1)}}{\partial t} - 2\omega_n^{(0)}F_n^{(1)}\frac{\partial^2 \phi_n^{(1)}}{\partial \eta \partial t}$$

$$- \left[\left(\frac{\partial \phi_n^{(1)}}{\partial \eta}\right)^2 + \left(\frac{1}{\eta}\frac{\partial \phi_n^{(1)}}{\partial \eta}\right)^2\right] + 4(n^2+n-1)F_n^{(1)2} \qquad (\eta=1), \tag{IV.2.18}$$

$$\nabla\phi^{(2)}(\eta,\theta,t+2\pi) = \nabla\phi^{(2)}(\eta,\theta,t), \tag{IV.2.19}$$

$$\int_0^{\pi}\{2F_n^{(1)2} + F^{(2)}\}\sin(\theta)\,d\theta = 0, \tag{IV.2.20}$$

$$\int_0^{\pi}\int_0^{2\pi} F^{(2)}\,P_n(\theta)\sin(\theta)\cos(t)\,dt\,d\theta = 0 \qquad (n=2,3,..), \tag{IV.2.21}$$

$$\int_0^{\pi}\int_0^{2\pi} F^{(2)}\,P_n(\theta)\sin(\theta)\sin(t)\,dt\,d\theta = 0 \qquad (n=2,3,..), \tag{IV.2.22}$$

where the subscripts n denote the particular linear solution (IV.2.14) for which the solutions of (IV.2.15) - (IV.2.22) hold. The velocity potential $\phi^{(2)}$ is expanded in a Legendre series that satisfies (IV.2.15) and (IV.2.16),

$$\phi^{(2)}(\eta,\theta,t) = \sum_{m=0}^{\infty}\gamma_m(t)\,\eta^m\,P_m(\theta), \tag{IV.2.23}$$

and the shape function $F^{(2)}$ is assumed to be given by (IV.2.4). Equations (IV.2.17) and (IV.2.18) are reduced to a sequence of non-homogeneous second-order equations for the coefficients $\{\gamma_m(t)\}$ and the correction to the frequency $\omega^{(1)}$ by forming successively the integrals of (IV.2.17) and (IV.2.18) with each of the set $\{\sin(\theta)P_m(\theta)\}$. Applying the orthogonality

property of Legendre polynomials and eliminating the coefficients $\{\delta_m^{(2)}(t)\}$ between the two equations yields

$$\frac{d^2\gamma_m}{dt^2} + \frac{m(m-1)(m+2)}{\omega(0)^2}\gamma_m = \frac{(2m+1)(m-1)(m+2)}{2\omega(0)^2} \{ - 4\omega^{(1)} \sin(t) \langle P_n , P_m \rangle$$

$$- \frac{(n-1)(n+2)}{\omega^{(0)}} \sin(2t) \langle P_n'^2 - (n-1)nP_n^2 , P_m \rangle$$

$$+ \frac{\omega(0)}{(m-1)(m+2)} \sin(2t) [- 2(n^3+3n^2-2) \langle P_n^2 , P_m \rangle$$

$$- \frac{(n-1)^2(n+2)^2}{\omega(0)^2} \langle n^2P_n^2+P_n'^2 , P_m \rangle] \} \qquad \text{(IV.2.24)}$$

where the notation $\langle h(\theta),g(\theta) \rangle$ stands for the inner product

$$\langle h(\theta),g(\theta) \rangle \equiv \int_0^\pi h(\theta)\, g(\theta)\, \sin(\theta)\, d\theta \qquad \text{(IV.2.25)}$$

The integrals in the non-homogeneous terms in the set (IV.2.24) are expressed in terms of the well-known 3j and 6j symbols for spherical harmonics (Rotenberg et al. 1959) which extend the orthogonality properties of integrals of two Legendre polynomials to integrals involving products of three or four polynomials and their derivatives. In other words, these so called Clebsch-Gordan relations, provide rules by which the transformation of products of Legendre polynomials or their derivatives to a finite sum of Legendre polynomials is carried out. These rules are equivalent to the well-known transformations of products of trigonometric functions into sums, which are useful when the geometry of the problem is cartesian. A graphic example of the mode coupling at higher orders in the perturbation expansion is given in figure IV.2.1, where the most common normal modes are excited by the initial deformation. Only a few of the integrals on the right-side of (IV.2.24) are non-zero for each choice of the first-order solution (IV.2.14), and these dictate the coupling

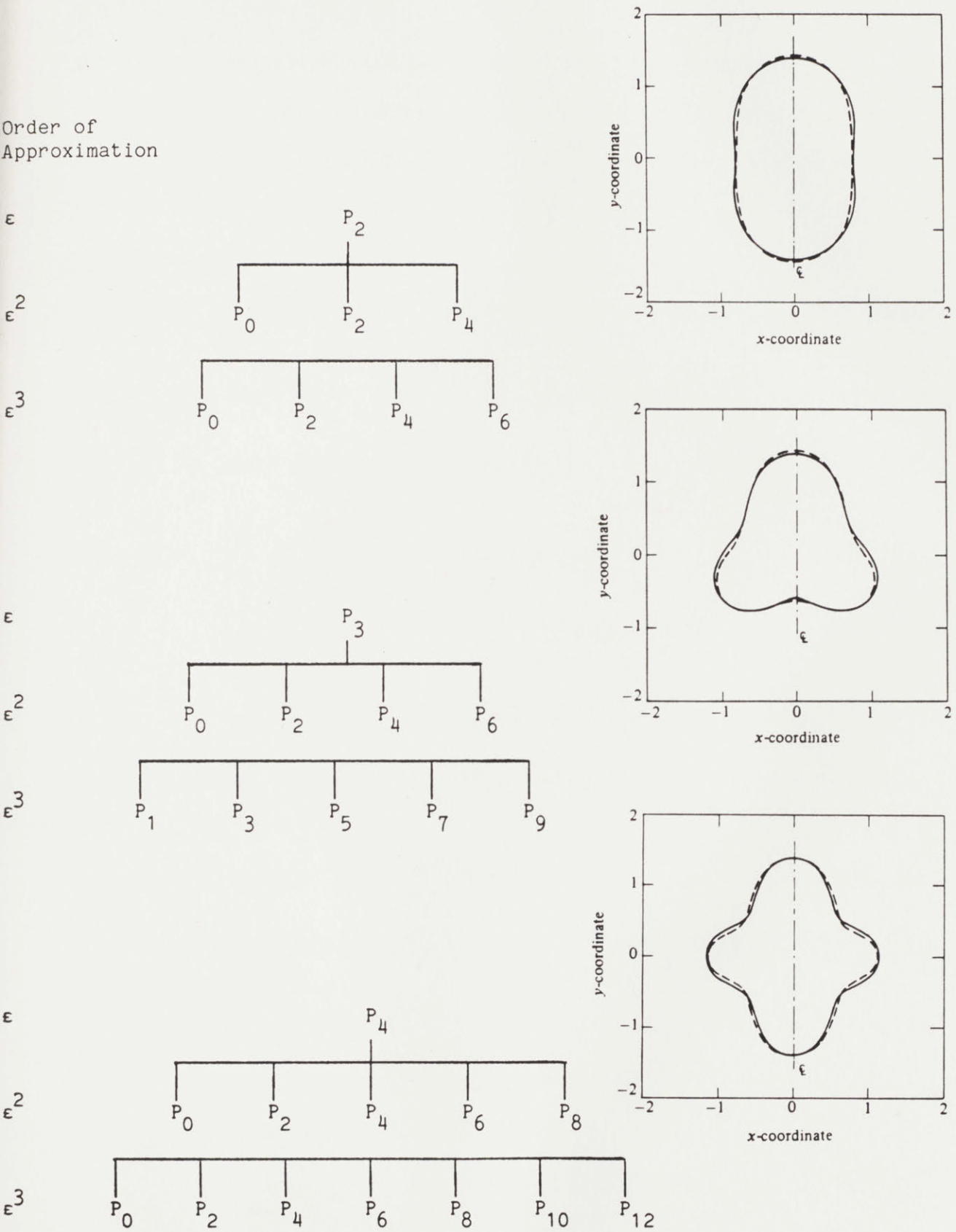

Figure IV.2.1 Mode coupling for the first three spherical harmonics.

of modes of oscillation that arise at second order. The algebra in this and subsequent manipulations is tedious, and the reduction of the formulas has been greatly expedited by the use of the symbolic manipulator MACSYMA (MACSYMA 1977; Pavelle et al. 1981) available on the M.I.T. computer system.

The non-trivial equations that result from (IV.2.24) are as follows:

for n = 2,
$$L_{22}(\gamma_2(t)) = -2\omega^{(1)}\sin(t) - \frac{104}{7\omega^{(0)}}\sin(2t), \qquad \text{(IV.2.26a)}$$
$$L_{24}(\gamma_4(t)) = \frac{324}{35\omega^{(0)}}\sin(2t), \qquad \text{(IV.2.26b)}$$

for n = 3,
$$L_{32}(\gamma_2(t)) = -\frac{32}{\omega^{(0)}}\sin(2t), \qquad \text{(IV.2.27a)}$$
$$L_{33}(\gamma_3(t)) = -\frac{4}{3}\omega^{(1)}\sin(t), \qquad \text{(IV.2.27b)}$$
$$L_{34}(\gamma_4(t)) = -\frac{300}{11\omega^{(0)}}\sin(2t), \qquad \text{(IV.2.27c)}$$
$$L_{36}(\gamma_6(t)) = \frac{3200}{77\omega^{(0)}}\sin(2t), \qquad \text{(IV.2.27d)}$$

for n = 4,
$$L_{42}(\gamma_2(t)) = -\frac{4150}{77\omega^{(0)}}\sin(2t), \qquad \text{(IV.2.28a)}$$
$$L_{44}(\gamma_4(t)) = -\omega^{(1)}\sin(t) - \frac{53136}{1001\omega^{(0)}}\sin(2t), \qquad \text{(IV.2.28b)}$$
$$L_{46}(\gamma_6(t)) = -\frac{350}{11\omega^{(0)}}\sin(2t), \qquad \text{(IV.2.28c)}$$
$$L_{48}(\gamma_8(t)) = \frac{124950}{143\omega^{(0)}}\sin(2t), \qquad \text{(IV.2.28d)}$$

where
$$L_{nm}(\gamma_m(t)) \equiv \left[\frac{d^2()}{dt^2} + \frac{m(m-1)(m+2)}{\omega_n^{(0)2}}\right]\gamma_m(t)$$

In forming these equation sets it has been assumed that the contribution

of any purely homogeneous equation is zero. This is formally true only if m is constainted to satisfy

$$\frac{m(m-1)(m+2)}{\omega_n^{(0)2}} \neq (\text{integer})^2, \qquad \text{(IV.2.29)}$$

for $m \neq n$. Equation (IV.2.29) excludes values of m for which the linear theory yields a time frequency that is an integral multiple of a fundamental frequency.

In each set the frequency correction $\omega^{(1)}$ is determined so that secular terms in the solution vanish, which leads to

$$\omega^{(1)} = 0 \quad (n = 2,3,..) \qquad \text{(IV.2.30)}$$

The solutions of (IV.2.26) - (IV.2.28) are then determined so that the constraints (IV.2.20) - (IV.2.22) are satisfied. The final forms for the corrections $(F^{(2)}, \phi^{(2)})$ are as follows

$$\text{for } n = 2, \quad F^{(2)}(\theta,t) = -\frac{2}{5}\cos^2(t) + \frac{11}{14}\left(1 - \frac{29}{33}\cos(2t)\right) P_2(\theta) + \frac{18}{35}\left(1 + \frac{3}{5}\cos(2t)\right) P_4(\theta), \qquad \text{(IV.2.31)}$$

$$\phi^{(2)}(\eta,\theta,t) = \frac{\sin(2t)}{\omega_2^{(0)}}\left[\frac{13}{5} + \frac{104}{21} P_2(\theta)\,\eta^2 + \frac{324}{175} P_4(\theta)\,\eta^4\right]; \qquad \text{(IV.2.32)}$$

$$\text{for } n = 3, \quad F^{(2)}(\theta,t) = -\frac{2}{7}\cos^2(t) + \frac{22}{21}\left(1 - \frac{4}{11}\cos(2t)\right) P_2(\theta) + \frac{101}{231}\left(1 - \frac{453}{202}\cos(2t)\right) P_4(\theta) + \frac{130}{231}\left(1 + \frac{1}{13}\cos(2t)\right) P_6(\theta), \qquad \text{(IV.2.33)}$$

$$\phi^{(2)}(\eta,\theta,t) = \frac{\sin(2t)}{\omega_3^{(0)}}\left[\frac{85}{14} + \frac{60}{7} P_2(\theta)\,\eta^2 + \frac{375}{22} P_4(\theta)\,\eta^4 + \frac{800}{77} P_6(\theta)\,\eta^6\right]; \qquad \text{(IV.2.34)}$$

$$\text{for } n = 4, \quad F^{(2)}(\theta,t) = -\frac{2}{9}\cos^2(t) + \frac{3575}{2772}\left(1 - \frac{1097}{5005}\cos(2t)\right) P_2(\theta) +$$

$$\frac{927}{2002}\left(1 - \frac{301}{309}\cos(2t)\right) P_4(\theta) + \frac{305}{792}\left(1 - \frac{263}{61}\cos(2t)\right) P_6(\theta)$$

$$+ \frac{70}{117}\left(1 - \frac{2744}{9163}\cos(2t)\right) P_8(\theta), \qquad \text{(IV.2.35)}$$

$$\phi^{(2)}(\eta,\theta,t) = \frac{\sin(2t)}{\omega_4^{(0)}}\left[\frac{21}{2} + \frac{7470}{539} P_2(\theta)\,\eta^2 + \frac{17712}{1001} P_4(\theta)\,\eta^4 + \frac{525}{11} P_6(\theta)\,\eta^6\right.$$

$$\left. + \frac{66150}{2431} P_8(\theta)\,\eta^8\right]. \qquad \text{(IV.2.36)}$$

The corrections then to the velocity potential in the physical coordinate system (r,θ) are reconstructed by substituting the expressions for $\phi^{(1)}(\eta,\theta,t)$ and $\phi^{(2)}(\eta,\theta,t)$ into (IV.2.1) and using the definition of the coordinate $\eta = r/F(\theta,t;\varepsilon)$ to order ε^2.

The analysis is extended to third order in order to calculate the first non-zero correction to the frequency $\omega^{(2)}$. The corrections to the velocity potential and the shape function $(\phi^{(3)}, F^{(3)})$ are written as expansions analogous to (IV.2.23) and (IV.2.4), and the kinematic and dynamic equations are reduced to a sequence of decoupled second-order equations in time by the same procedure used to calculate the sets (IV.2.26) - (IV.2.28). The correction $\omega^{(2)}$ is determined so that the solutions to these equations contain no secular terms. The details of this derivation are given in the Appendix B, here we list only the frequency corrections

$$\text{for } n = 2, \qquad \omega^{(2)} = -\frac{34409}{29400}\,\omega^{(0)} \cong -1.17037\,\omega^{(0)}, \qquad \text{(IV.2.37)}$$

$$\text{for } n = 3, \qquad \omega^{(2)} = -\frac{783899}{396396}\,\omega^{(0)} \cong -1.97757\,\omega^{(0)}, \qquad \text{(IV.2.38)}$$

$$\text{for } n = 4, \qquad \omega^{(2)} = -\frac{181430960793}{64865536736}\,\omega^{(0)} \cong -2.79703\,\omega^{(0)}. \qquad \text{(IV.2.39)}$$

Since the correction $\omega^{(3)}$ will be identically zero, the terms (IV.2.37 - 39) give predictions for the frequency that are valid up to the fourth order in the amplitude, (see Tsamopoulos and Brown 1983).

The kinetic **K** and surface **P** energies of the drop are given by the expressions

$$\mathbf{K} \equiv \frac{1}{2}\int_v \nabla\phi\cdot\nabla\phi \, dv, \qquad \mathbf{P} \equiv \int_0^{\pi} (F^2 + F_\theta^2)^{1/2} F \sin(\theta) \, d\theta, \quad \text{(IV.2.40)}$$

where v is the volume of the drop. These quantities are approximated as follows

$$\text{for } n=2, \ \mathbf{K} = \frac{4}{5}\varepsilon^2 \sin^2(t) + O(\varepsilon^3), \quad \mathbf{P} = 2 + \frac{4}{5}\varepsilon^2 \cos^2(t) + O(\varepsilon^3); \quad \text{(IV.2.41)}$$

$$\text{for } n=3, \ \mathbf{K} = \frac{10}{7}\varepsilon^2 \sin^2(t) + O(\varepsilon 3), \ \mathbf{P} = 2 + \frac{10}{7}\varepsilon^2 \cos^2(t) + O(\varepsilon^3); \quad \text{(IV.2.42)}$$

$$\text{for } n=4, \ \mathbf{K} = 2\varepsilon^2 \sin^2(t) + O(\varepsilon^3), \quad \mathbf{P} = 2 + 2\varepsilon^2 \cos^2(t) + O(\varepsilon^3); \quad \text{(IV.2.43)}$$

The lowest-order terms in both the kinetic and potential energies are due to ε-order corrections in the shape and velocity potential, and thus do not represent the finite-amplitude behaviour of the oscillations.

IV.2b Bubbles

The procedure for calculating the first- and second-order corrections to the frequency, shape and velocity potential for a bubble follows directly from that outlined in IV.2a. The results are given here in the form of the series (IV.2.1). The solutions to the first order problem are

$$F^{(1)}(\theta,t) \equiv F_n^{(1)}(\theta,t) = \cos(t) \, P_n(\theta)$$

$$\phi^{(1)}(\eta,\theta,t) \equiv \phi_n^{(1)}(\eta,\theta,t) = \frac{(n-1)(n+2)}{\omega^{(0)}\ \eta^{n+1}} \sin(t)\ P_n(\theta) \qquad \text{(IV.2.44)}$$

$$\omega^{(0)} \equiv \omega_n^{(0)} = ((n^2-1)(n+2))^{1/2} \quad (n = 2,3,..)$$

The second order corrections ($F^{(2)}$, $\phi^{(2)}$, $\omega^{(1)}$) are as follows

for n = 2, $$F^{(2)}(\theta,t) = -\frac{2}{5}\cos^2(t) + \frac{3}{7}\left(1 - \frac{7}{9}\cos(2t)\right) P_2(\theta) +$$

$$+ \frac{4}{105}\left(1 + \frac{228}{7}\cos(2t)\right) P_4(\theta), \qquad \text{(IV.2.45a)}$$

$$\phi^{(2)}(\eta,\theta,t) = \frac{\sin(2t)}{\omega_2^{(0)}}\left[-\frac{7}{5} + \frac{16}{21} P_2(\theta)\ \eta^{-3} + \frac{3072}{245} P_4(\theta)\ \eta^{-5}\right], \qquad \text{(IV.2.45b)}$$

$$\omega^{(1)} = 0; \qquad \text{(IV.2.45c)}$$

for n = 3, $$F^{(2)}(\theta,t) = -\frac{2}{7}\cos^2(t) + \frac{53}{84}\left(1 - \frac{289}{1961}\cos(2t)\right) P_2(\theta) +$$

$$\frac{9}{154}\left(1 - 9\cos(2t)\right) P_4(\theta) - \frac{185}{1848}\left(1 - \frac{1571}{111}\cos(2t)\right) P_6(\theta), \qquad \text{(IV.2.46a)}$$

$$\phi^{(2)}(\eta,\theta,t) = \frac{\sin(2t)}{\omega_3^{(0)}}\left[-\frac{55}{14} + \frac{500}{111} P_2(\theta)\ \eta^{-3} + \frac{2150}{63} P_6(\theta)\ \eta^{-7}\right], \qquad \text{(IV.2.46b)}$$

$$\omega^{(1)} = 0; \qquad \text{(IV.2.46c)}$$

for n = 4, $$F^{(2)}(\theta,t) = -\frac{2}{9}\cos^2(t) + \frac{590}{693}\left(1 - \frac{71}{1711}\cos(2t)\right) P_2(\theta) +$$

$$\frac{9}{91}\left(1 - \frac{29}{33}\cos(2t)\right) P_4(\theta) - \frac{2}{45}\left(1 + \frac{281}{11}\cos(2t)\right) P_6(\theta)$$

$$- \frac{1253}{6435}\left(1 - \frac{1351}{179}\cos(2t)\right) P_8(\theta), \qquad \text{(IV.2.47a)}$$

$$\phi^{(2)}(\eta,\theta,t) = \frac{\sin(2t)}{\omega_4^{(0)}}\left[-\frac{15}{2} + \frac{20400}{2233} P_2(\theta)\ \eta^{-3} + \frac{8532}{1001} P_4(\theta)\ \eta^{-5} +\right.$$

$$- \frac{144}{11} P_6(\theta)\, \eta^{-7} + \frac{9212}{143} P_8(\theta)\, \eta^{-9}], \qquad \text{(IV.2.47b)}$$

$$\omega^{(1)} = 0. \qquad \text{(IV.2.47c)}$$

The first non-zero corrections to the oscillation frequency appear at second order in the amplitude and are as follows

for n = 2, $$\omega^{(2)} = - \frac{23549}{15435}\, \omega^{(0)} \cong - 1.52569\, \omega^{(0)} ; \qquad \text{(IV.2.48)}$$

for n = 3, $$\omega^{(2)} = - \frac{5672825}{2461536}\, \omega^{(0)} \cong -2.30459\, \omega^{(0)} ; \qquad \text{(IV.2.49)}$$

for n = 4, $$\omega^{(2)} = - \frac{14775015009}{4939864930}\, \omega^{(0)} \cong -2.99098\, \omega^{(0)} . \qquad \text{(IV.2.50)}$$

And in general, the frequency decreases proportionally to the square of the amplitude, result which should be expected on physical grounds since the introduction of the nonlinear terms in Bernoulli's equation increases the inertia of the system.

IV.3 RESULTS AND COMPARISONS

Representative shapes of drops and bubbles through a half-period of oscillation are shown on figures IV.3.1 and IV.3.2 for the lowest three fundamental modes of deformation, n = 2, 3, 4. In both figures, the continuous curves represent the shapes predicted by the first-order results and the dashed curves are the shapes corrected to second order in amplitude. In each case, the amplitude has been set to ε=0.4, which for n=2 corresponded to a pure prolate-to-oblate oscillation of $\alpha \equiv L/W \cong 1.81$. This value of ε has been chosen so that the correction to the

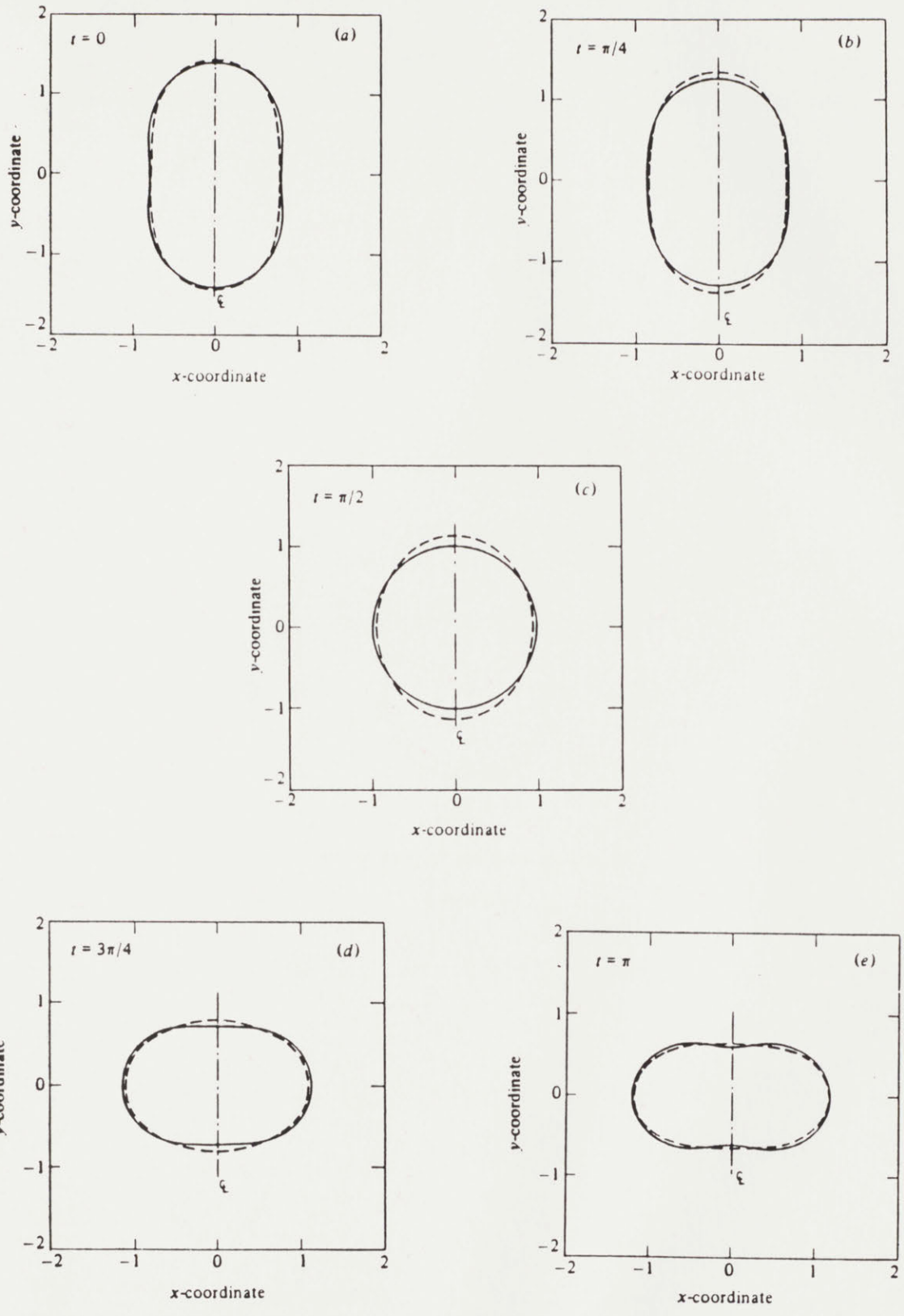

Figure IV.3.1 Shapes of drops oscillating in the n=2 (a-e), n=3 (f-j), and n=4 (k-o) modes for the amplitude ε=0.4. The solid (——) and dashed (---) curves are respectively the first- and second-order approximations to the drop shapes.

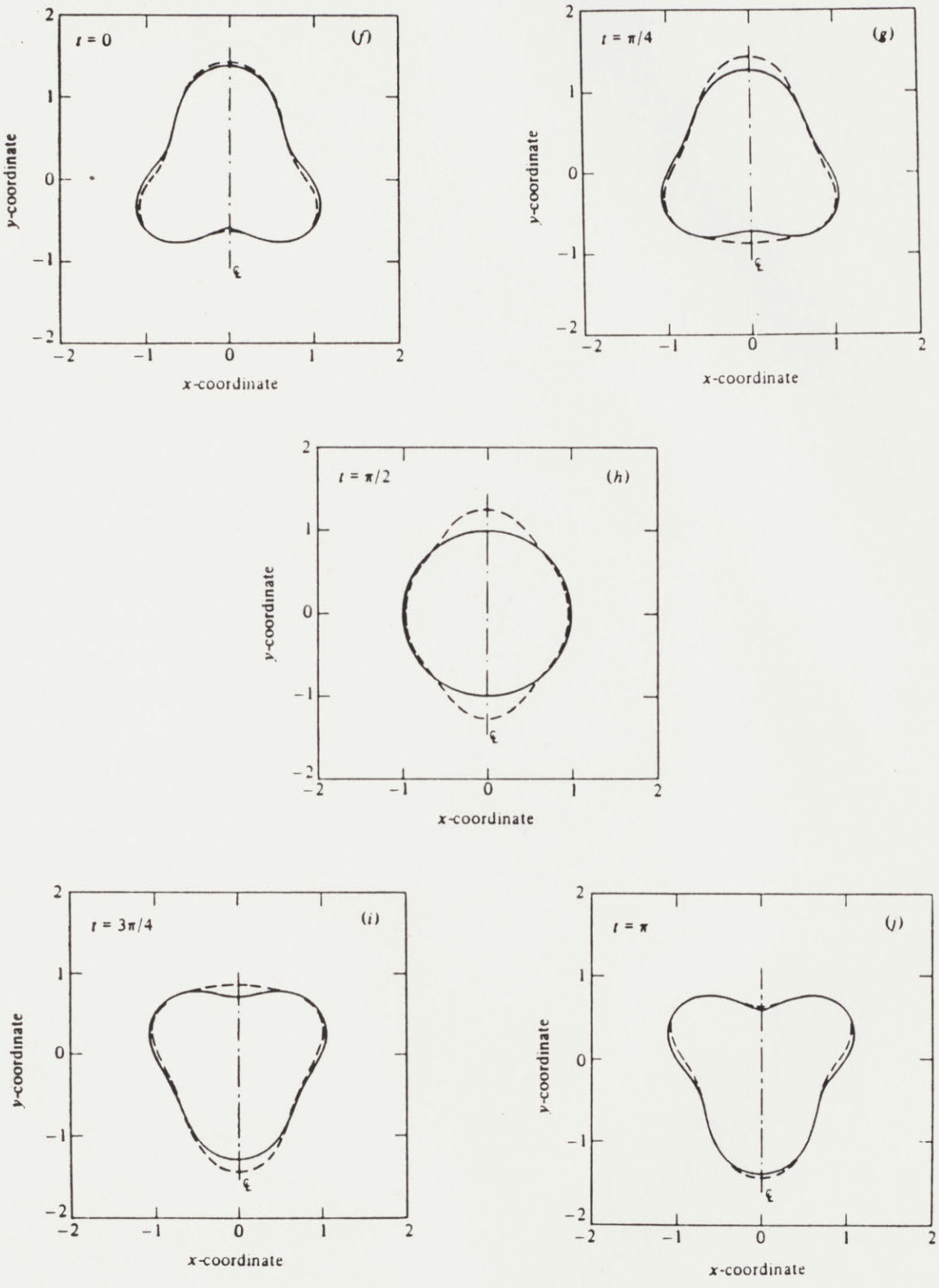

Figure IV.3.1 (Continued)

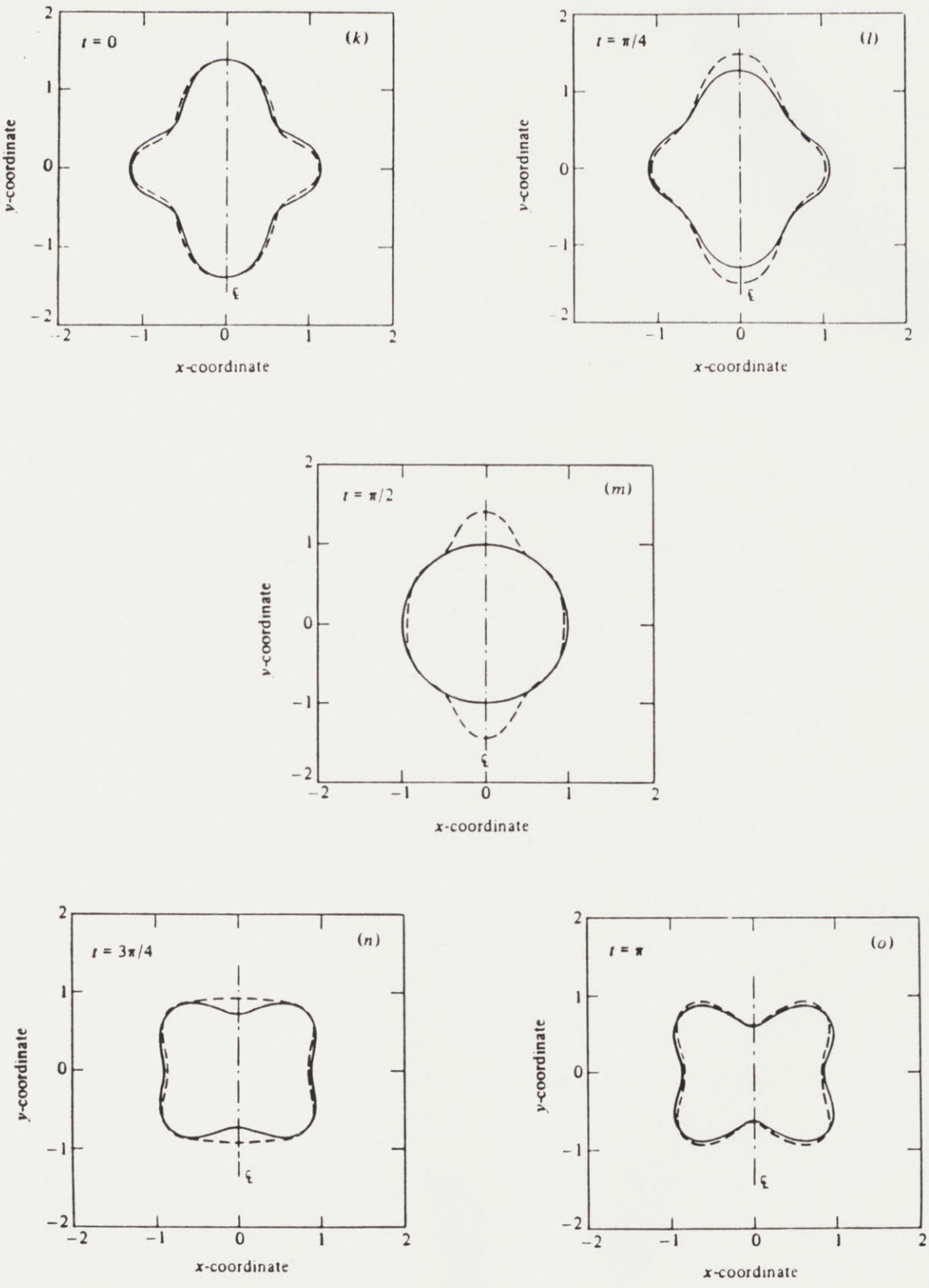

Figure IV.3.1 (Continued)

shape at order ε^3 will be $O(10^{-2})$ of the deformation (assuming $F^{(3)}(\theta,t) = O(1)$) and so that the shapes in figures IV.3.1 and IV.3.2 show the same magnitude of deformation as the numerical calculations of Foote (1973) and Alonso (1974).

For the shapes in figure IV.3.1, the drop had its largest distortion at t=0 when it had no velocity. The linear theory predicted a perfectly spherical shape after a quarter of a period ($t=\pi/2$). The second-order corrections deformed this sphere into a prolate shape for the fundamental (n=2) mode of oscillation and into multilobed forms for the n=3 and n=4 modes. At $t=\pi$ the distortion of the shape was again maximum and the velocity zero. For times between π and 2π the drop retraced the shapes in its evolution between t=0 and π.

The differences between the contributions of inertia in drops and bubbles are seen by comparing the second-order approximations shown in figures IV.3.1 and IV.3.2. Two-, three- and four-lobed drop oscillations were much more elongated along the axis of symmetry for $\pi/4 \leq t \leq 3\pi/4$ than corresponding oscillating bubbles. For n=2 mode oscillation, the coefficient for the term $P_2(\theta)$ in (IV.2.31) was largest in the second-order correction for the drop shape, whereas the term proportional to $P_4(\theta)$ dominated the correction (IV.2.45a) for the bubble. For the n=4 oscillation mode, the shapes of the drop and bubble became qualitatively different for $\pi/4 \leq t \leq 3\pi/4$. For t near $\pi/2$, the bubble had an eight-lobed shape, while the drop had a four-lobed form at the same times; compare figures (IV.3.1m) and (IV.3.2m).

A number of asymptotic results for oscillating drops can be compared directly with the numerical calculations of Foote (1973) and Alonso (1974)

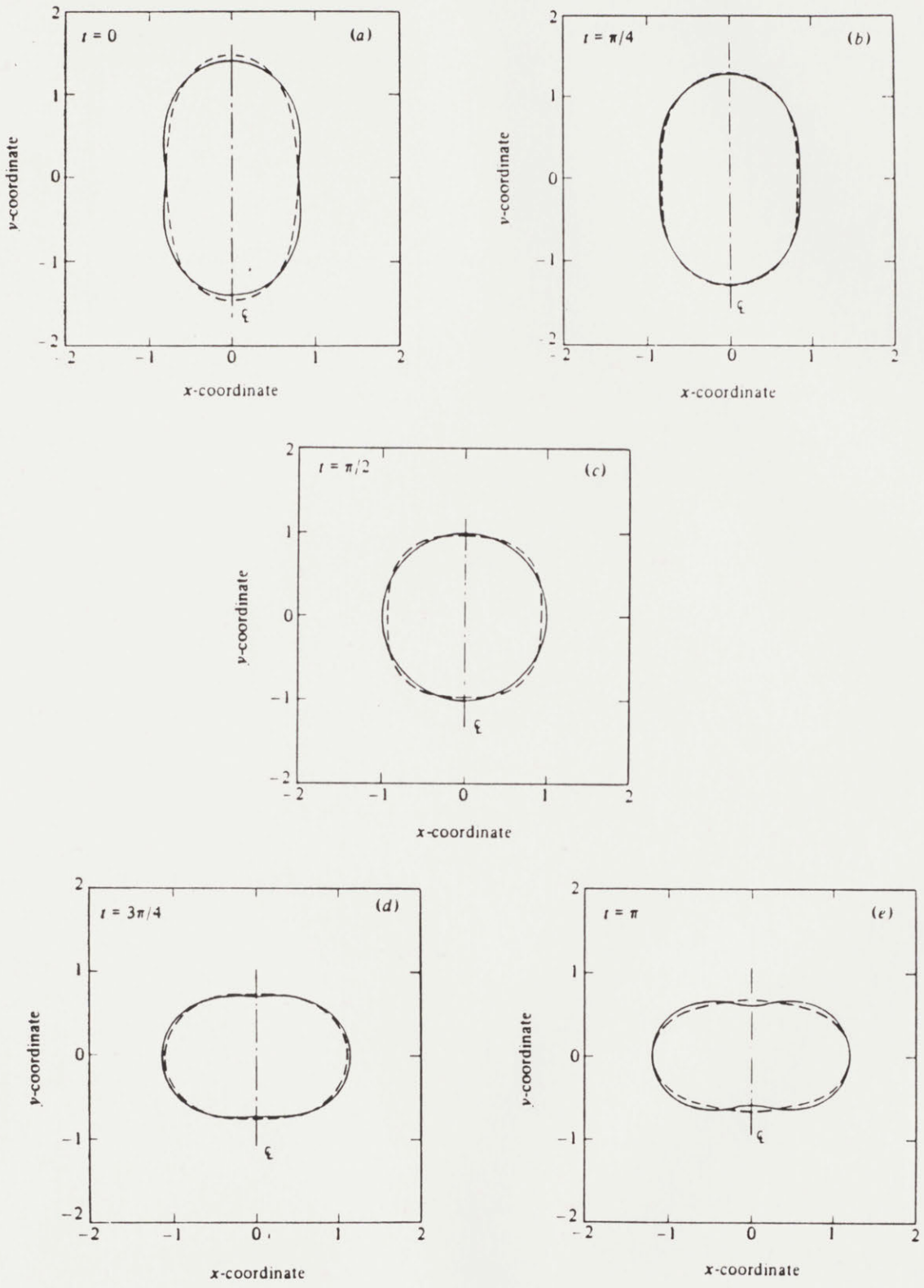

Figure IV.3.2 Shapes of bubbles oscillating in the n=2 (a-e), n=3 (f-j), and n=4 (k-o) modes for the amplitude ε=0.4. The solid (——) and dashed (---) curves are respectively the first- and second-order approximations to the bubble shapes.

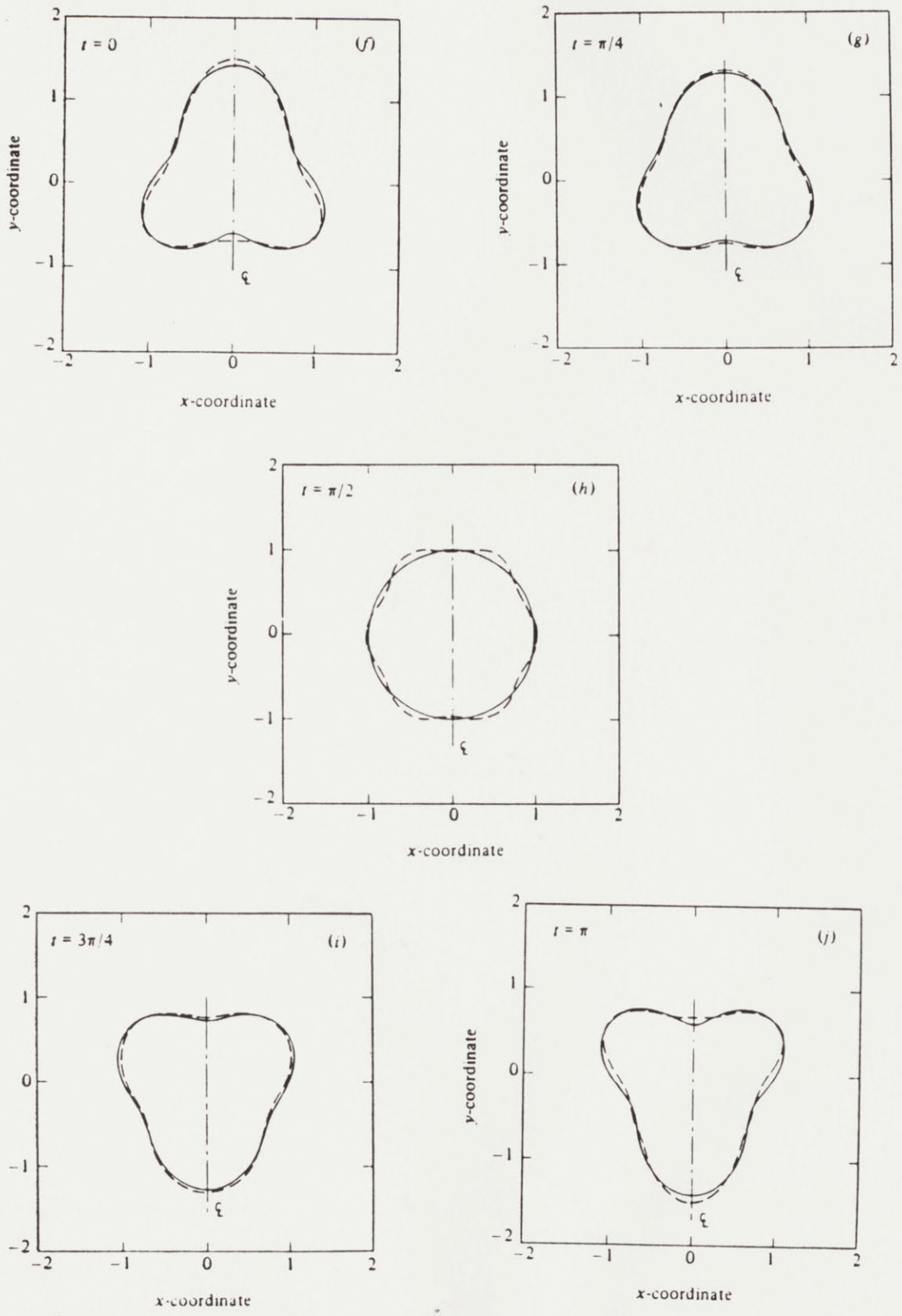

Figure IV.3.2 (Continued)

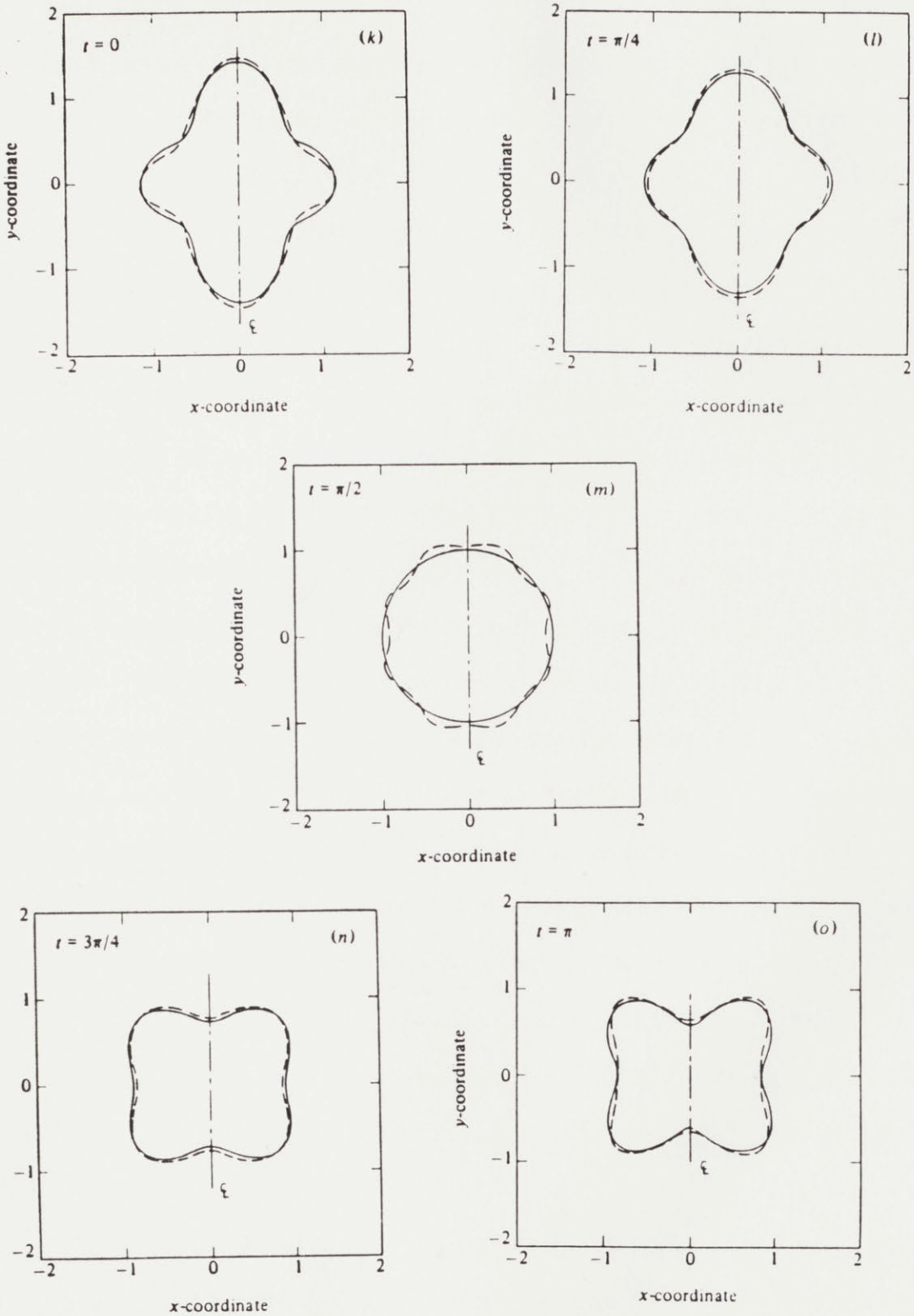

Figure IV.3.2 (Continued)

for viscous drops oscillating in the fundamental mode. The effect of viscosity on the frequency of oscillation and on the shape of the drop is small when the product $(\sigma R/\rho\nu^2)^{1/2}$ is large, where ν is the kinematic viscosity (see Chandrasekhar 1961). In the calculations of Foote ($R = 0.06$ cm, $\nu = 0.06$ cm^2/s, $\sigma = 75$ dyn/cm, $\rho = 1$ g/cm^3, $\alpha = 1.7$) and Alonso ($R = 0.66*10^{-12}$ cm, $\nu = 0.75*10^{-4}$ cm^2/s, $\sigma = 1.6*10^{20}$ dyn/cm, $\rho = 1.66*10^{15}$ g/cm^3, $\alpha = 1.8$ and 2.5) this ratio was 35.4 and 3.3 respectively. Thus the comparison of Foote's calculations with our inviscid theory is reasonable, while Alonso's results may deviate substantially solely because of viscosity.

The drop shapes shown in figure IV.3.1 are in qualitative agreement with those calculated by both Foote and Alonso. Several other points of agreement are worth mentioning. As noted by Foote, the linear theory predicted shapes that were slightly re-entrant when t=0. This feature was not apparent in either our asymptotic results correct to second order (see figure IV.3.1a) or in Foote's numerical results. Alonso used least-squares techniques to fit her numerically calculated shapes with a sequence of Legendre polynomials and discovered that the shapes were well represented by sums of the $P_2(\theta)$ and $P_4(\theta)$ functions alone, as predicted by (IV.2.14) and (IV.2.31). Also, the sine-squared time dependence of the kinetic and potential energies predicted in equation (IV.2.41) agreed with the calculations of both Foote and Alonso.

A drop undergoing n=2 oscillations spent a considerably longer part of each period in a prolate form than in an oblate one. The percentage excess time is shown in figure IV.3.3 as a function of the amplitude of the oscillation, as measured by $\alpha \equiv L/W$. Also shown in this figure are the results of Foote (1973) that have been extrapolated from the

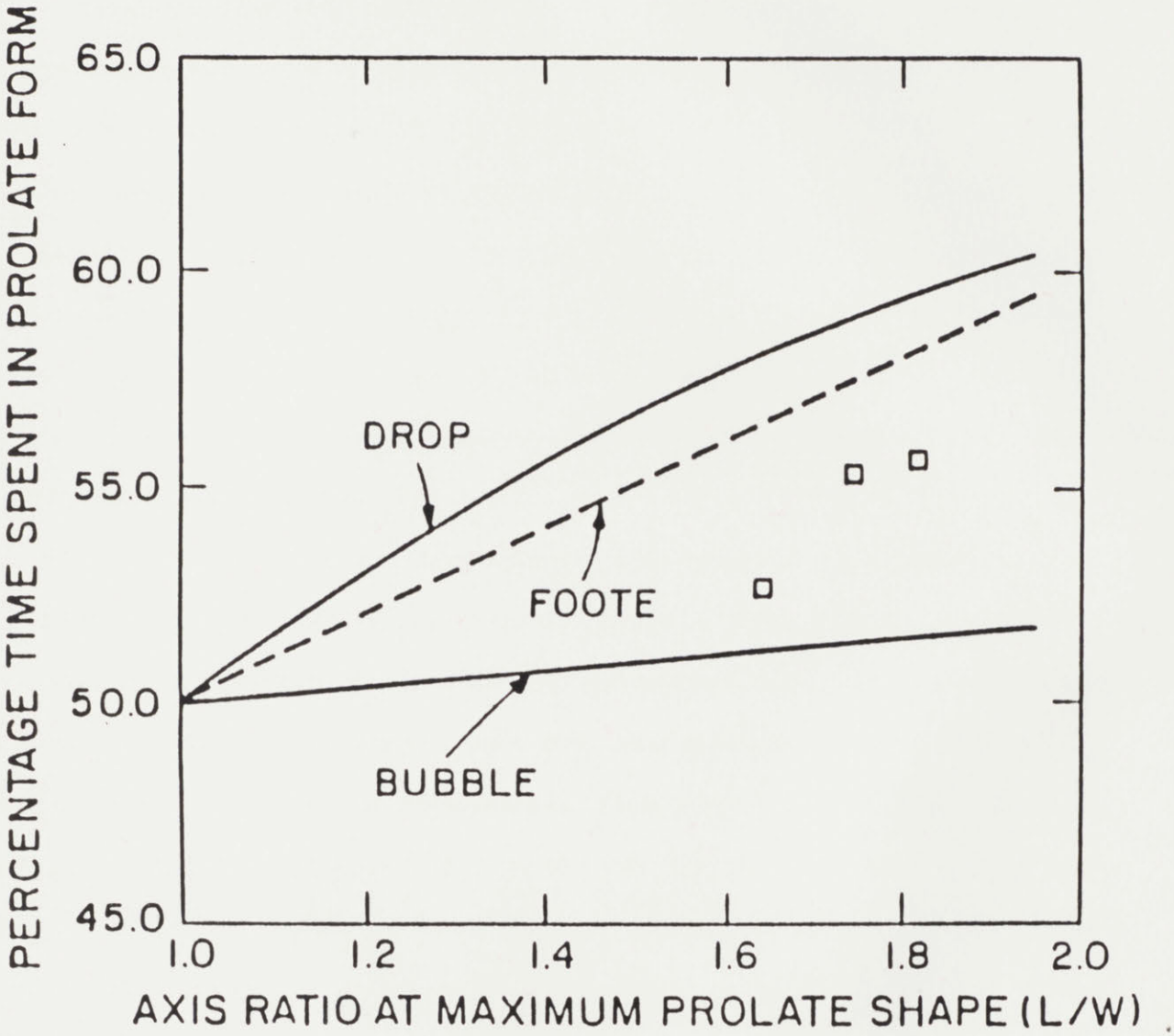

Figure IV.3.3 The percentage of each period that the drop in n=2 oscillation spends in a prolate form as a function of the amplitude of the oscillation measured by the maximum ratio of the major to minor axis L/W. Asymptotic results (——), numerical calculations of Foote (---) and experimental results (□) of Trinh and Wang are shown.

data point (α=1.7, excess time=14%) and his comment that the excess time varied linearly with oscillation amplitude. The agreement is reasonable. Bubbles exhibited only a slight tendency to stay in prolate forms, as shown by the line on figure IV.3.3.

The quadratic decrease in frequency with amplitude predicted here is compared on figure IV.3.4 to the numerical results of Foote and Alonso. The asymptotic results are within four per cent of Foote's viscous calculations over the entire range of amplitude $0 \leqq \alpha \leqq 1.8$ presented by that author. The single value calculated from Alonso's report differed more significantly from our results.

Finally, the inviscid predictions are compared on figures IV.3.3 and IV.3.4 to experimental results of Trinh & Wang (1982) for almost neutrally buoyant drops of silicone oil and carbon tetrachloride suspended in distilled water. The shapes were set into oscillation by acoustically driving the drop near its fundamental frequency. The driver was then turned off and the drop motion evolved into free oscillation. In the limit of moderate-amplitude oscillations and large drops ($R \cong 1$ cm), the oscillation frequencies measured this way were expected to be near those of an inviscid liquid/liquid system. This conclusion was reached by calculating the viscous correction to the inviscid frequency derived by Prosperetti (1980b, see figure 14) using the physical parameters from the experiments of Trinh & Wang. [1]

Trinh & Wang's measurements for the percentage of time spent in prolate shapes by the neutrally buoyant drop are shown on figure IV.3.3,

---

[1]We have assumed σ = 40 dyn/cm as a reasonable interfacial tension for a clean oil/water interface.

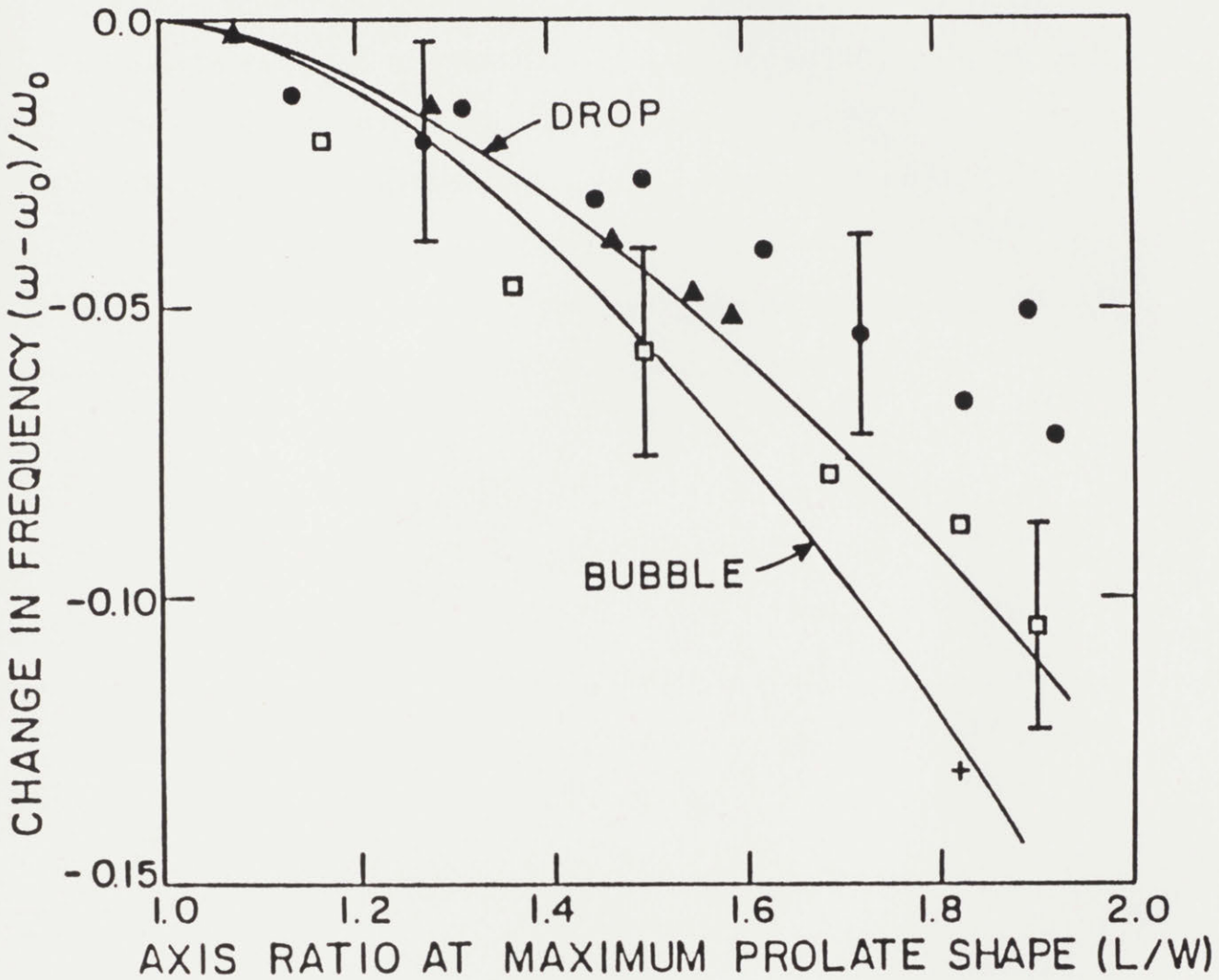

Figure IV.3.4 The change in n=2 oscillation frequency with increasing amplitude of oscillation as measured by L/W. Asymptotic results (——), numerical calculations of Foote (▲) and Alonso (+), and experimental results of Trinh and Wang (●, R=0.49 cm; □, R=0.62 cm) are shown.

and, as expected, are bracketed by the inviscid calculations for drops and bubbles. Experimental data for the dependence of frequency on amplitude for drops with radii of 0.62 cm (□) and 0.49 cm (●) are shown on figure IV.3.4. The data for the larger drop are again described by an asymptotic result intermediate to the calculations for drops and bubbles for α less than 1.7. The experimental measurements for the smaller drop differ systematically from the inviscid results; this difference may represent the coupling between viscosity and the finite-amplitude motion.

V. RESONANT OSCILLATIONS OF INVISCID CHARGED DROPS

The dynamic response of liquid drops held together by surface tension and carrying electrical charge is important in a great variety of applications. The motion of such drops has been studied in physical systems ranging in size from milimeter raindrops (Brazier-Smith et al. 1971; Tsang 1974) and micron-sized spheres produced by fuel atomizers and ink-jet delivery systems (Williams 1973) to the femtometer drops used as models for nuclear fission (Cohen & Swiatecki 1962, 1963; Nix 1972). Rayleigh (1982; also see Hendricks & Schneider 1963) was the first to treat the effect of electrical charge on nearly spherical drops. By an energy stability analysis applied to conducting drops immersed in an insulating medium, Rayleigh calculated the frequencies for small-amplitude oscillations of an inviscid drop and established the amount of charge necessary to fission the drop. The modes of shape oscillation were described by single Legendre polynomials and the levels of charge necessary to disrupt the nth mode were given as

$$\tilde{Q}_c^{(n)} = 4\pi\{\varepsilon_m \sigma R^3 (n+2)\}^{1/2}$$

where σ is the surface tension of the drop, ε_m the permittivity of the medium and R is the radius of the spherical shape. The mode number n corresponds to the number of lobes on the deformed shape. The two-lobed form becomes unstable at the lowest value $\tilde{Q}=\tilde{Q}_c^{(2)}$, which marks the absolute stability limit for nearly spherical drops.

Rayleigh's pioneering work has been the basis for other analyses of drop dynamics which generalize the calculations to include viscosity

(Tang & Wong 1974; Hasse 1975) and charge relaxation due to a dielectric drop and external medium (Saville 1974). These studies considered only small-amplitude oscillations and values of charge below the Rayleigh limit. The finite-difference calculations of Alonso (1974) for a slightly viscous drop with volumetrically distributed charge and the finite-element calculations of Basaran et al. (1982) for inviscid drops with surface charge are the only studies of nonlinear dynamics for charged drops. Such computations are relatively expensive, so that an exhaustive mapping of drop response as a function of the initial drop shape and the net electrical charge has not been undertaken. Experiments aboard the Space Shuttle are also planned, but must be even more limited in scope because of time restrictions. The use of perturbation analysis to guide both the experiments and further calculations is in order.

It is anticipated that the oscillation frequency of a charged drop will be less than that for an uncharged one. The physical reason behind it is that the restoring capillary force is now weakened, being opposed by the electrostatic repulsion.

In this chapter the asymptotic analysis is presented of the moderate-amplitude axisymmetric oscillations of an inviscid conducting drop with electrical charge suspended in a tenuous insulating medium. The calculations are focused on describing the effect of the amplitude of deformation on the form of the oscillation and on describing the harmonic resonance between the fundamental motion and secondary modes induced by nonlinear interactions. The present analysis is based on the method of multiple timescales as applied to approximating the time-periodic solutions of nonlinear conservative differential equations. This method is a general-

ization of the Poincaré-Linstedt technique since it allows for both frequency and amplitude modulations on timescales that differ from the associated with fundamental motion. As shown in section V.2, the two approaches are identical for regular oscillations. The multiple-timescale approach affords systematic treatment of the cases of harmonic resonance.

Harmonic resonance has long been known for two- and three-dimensional inviscid waves. Wilton (1915) first demonstrated secondary harmonic resonance in capillary-gravity waves and computed the special case of waves of permanent form with a phase shift relative to the fundamental frequency. Bretherton (1964) was the first to solve the general equations derived from a multiple-scale expansion which included slow amplitude modulation of the waveform. In a series of papers McGoldrick (1965, 1970b, 1972) and his collaborators have thoroughly analysed second- and third-order resonance in water waves including both surface tension and gravity. Both phenomena have been confirmed experimentally (McGoldrick et al. 1966; McGoldrick 1970a). In general the higher order corrections to a weakly nonlinear oscillator can be considered as a response of the system of oscillators described by the linear part of the equations to the forcing terms due to the nonlinear part. This response is normally constant and small, but an exception occurs when the frequency of the forced oscillation is equal to the frequency of the free oscillations that can serve as its harmonics, then resonance occurs and the harmonic can draw energy from the fundamental. Phillips (1981) has recently reviewed the rapid developments in the theory of wave interactions.

The analysis of nonlinear oscillations and resonance of an isolated drop has advantages over the parallel studies of initially planar waves.

The natural periodicity of the drop's surface results in a discrete spectrum of the fundamental modes as described by Rayleigh. For planar water waves the spectrum is continuous in the spatial wavenumber and detuning of resonant interactions caused by variation of this wavenumber from the critical value for resonance, must be considered in both experiments and calculations. Also, the formulation of the planar-wave problem requires consideration of the variation of this spatial wavelength with the amplitude of the oscillation. The general problem of combined wavelength, amplitude and frequency modulation for two-dimensional waves is, as yet, unsolved. Again, the periodicity of the drop removes the need for incorporating wavelength variation and makes the formulation in section V.1 the most general for this problem. The major disadvantage of calculations for an oscillating drop over the analysis for planar waves is the more complex algebra generated by the velocity and electrostatic potentials expressed in terms of Legendre polynomials. We have again, carried out these calculations using the symbolic manipulator MACSYMA.

V.1 FORMULATION

We consider the irrotational and incompressible motion of an electrically conducting inviscid drop with volume $\tilde{V}=4\pi R^3/3$, density ρ, surface tension σ and net electrical charge Q. The motion of the drop in a tenuous surrounding medium is caused by initially introducing a small axisymmetric deformation. As in chapter IV, the surface of the drop is described by $RF(\theta,t)$, where $F(\theta,t)$ is the dimensionless shape function of the drop and θ is the meridional angle in spherical coordinates. The same scales

employed in chapter IV are used to define the dimensional velocity potential $(\sigma R/\rho)^{1/2}\phi(r,\theta,t)$, pressure $(2\sigma/R)P(r,\theta,t)$ and time $(\rho R^3/\sigma)^{1/2}t$ in terms of their dimensionless counterparts. The inviscid equations of motion and boundary conditions are

$$\nabla^2\phi = 0 \qquad (0\leq r\leq F(\theta,t),\ 0\leq\theta\leq\pi), \tag{V.1.1}$$

$$\frac{\partial\phi}{\partial r} = 0 \qquad (r = 0,\ 0\leq\theta\leq\pi), \tag{V.1.2}$$

$$2P + \frac{\partial\phi}{\partial t} + \frac{1}{2}\left[\left(\frac{\partial\phi}{\partial r}\right)^2 + \left(\frac{1}{r}\frac{\partial\phi}{\partial\theta}\right)^2\right] = G(t) \qquad (0\leq r\leq F(\theta,t),\ 0\leq\theta\leq\pi), \tag{V.1.3}$$

$$\frac{\partial\phi}{\partial r} = \frac{\partial F}{\partial t} + \frac{1}{r^2}\frac{\partial\phi}{\partial\theta}\frac{\partial F}{\partial\theta} \qquad (r=F(\theta,t)), \tag{V.1.4}$$

$$\Delta P_0 + 2P + \frac{1}{2\pi}\left(T^e_{n2} - T^e_{n1}\right) = -2H \qquad (r=F(\theta,t),\ 0\leq\theta\leq\pi), \tag{V.1.5}$$

$$\int_0^\pi F^3(\theta,t)\sin(\theta)\,d\theta = 2, \tag{V.1.6}$$

The above mentioned equations are the same as in chapter IV except the normal-stress balance (V.1.5) that equates the pressure differences caused by capillarity and drop motion to the contributions of the normal electric stress from inside T^e_{n1} and outside T^e_{n2} the drop. The reference pressure difference ΔP_0 is determined by the constraint of constant drop volume (V.1.6). We absorb the constant of integration G(t) into the time derivative $\partial\phi/\partial t$. As explained by Lamb (1932, section 227), including this integration constant in (V.1.3) leads to terms constant in space and proportional to t in the velocity potential, but has no other effect on the solution to (V.1.1) - (V.1.6) because only space derivatives of ϕ appear in these equations.

The medium surrounding the drop is assumed to be electrically insulating,

and the dimensionless electrostatic potential $V(r,\theta,t)$ and the uniform potential in the drop V_0 are both scaled with $(4\pi\varepsilon_m/\sigma R)^{-1/2}$, where ε_m is the permittivity of the medium. The electric field is related to the potential as $\mathbf{E}=-\nabla V$ and is scaled with $(4\pi\varepsilon_m R/\sigma)^{-1/2}$; the dimensionless net charge Q is scaled with $(4\pi\sigma\varepsilon_m R^3)^{-1/2}$. The equations and boundary conditions governing the electrostatic potentials are

$$\nabla^2 V = 0 \qquad (F(\theta,t)\leq r\leq\infty,\ 0\leq\theta\leq\pi), \tag{V.1.7}$$

$$V \to 0 \qquad (r \to \infty,\ 0\leq\theta\leq\pi), \tag{V.1.8}$$

$$\mathbf{n}\cdot\nabla V = -4\pi q(\theta,t) \qquad (r=F(\theta,t),\ 0\leq\theta\leq\pi), \tag{V.1.9}$$

$$\mathbf{t}\cdot\nabla V = 0 \qquad (r=F(\theta,t),\ 0\leq\theta\leq\pi), \tag{V.1.10}$$

$$2\pi\int_0^\pi qF(F^2 + F_\theta^2)^{1/2}\sin(\theta)\,d\theta = Q\ . \tag{V.1.11}$$

in which $q(\theta,t)$ is the local surface charge density and $\mathbf{n}$ and $\mathbf{t}$ are the unit vectors normal and tangential to the drop surface and are defined as

$$\mathbf{n} \equiv \frac{F\mathbf{e}_r - F_\theta\mathbf{e}_\theta}{(F^2 + F_\theta^2)^{1/2}}, \qquad \mathbf{t} \equiv \frac{F\mathbf{e}_\theta + F_\theta\mathbf{e}_r}{(F^2 + F_\theta^2)^{1/2}}\ . \tag{V.1.12}$$

In these equations $F_\theta \equiv \partial F/\partial\theta$, and $(\mathbf{e}_r,\mathbf{e}_\theta)$ are the unit vectors in spherical coordinates. In formulating (V.1.7) - (V.1.12) we have assumed that charge is confined to the interface and equilibrates in a time much shorter than the characteristic time of the fluid motion. With these assumptions, (V.1.11) is the charge balance on the interface. Equation (V.1.11) follows from the general conservation equation for a species on a deforming surface first derived by Bupara (1965; see also Moeckel 1974) when bulk and surface

convection are negligible compared to conduction. Then the assumption of electrostatic equilibrium follows if the characteristic time for the conduction is much smaller than the time for a typical drop oscillation, or

$$\left(\frac{\rho R^3}{\sigma} \right)^{1/2} >> \frac{\chi_0}{4\pi\epsilon_m R^2} \quad ,$$

where χ_0 is the resistivity of the drop. For the case of even distilled water ($\chi_0 = 10^4$ Ωm, $\rho = 1$ g/cm^3, $\sigma = 75$ dyn/cm) in air ($\epsilon_m = 8.8*10^{-2}$ F/m) this inequality is satisfied by several orders of magnitude when $R = 0.1$ cm. Equation (V.1.10) guarantees that the tangential component of the electric field is continuous across the interface. This is equivalent to the requirement that the potential be continuous across $F(\theta,t)$, and sets the constant potential V_0.

The electric stress caused by the external electric field is defined as (Stratton 1941)

$$\mathbf{T}_2^e \equiv \mathbf{EE} - \frac{1}{2} |\mathbf{E}|^2 \mathbf{I} \qquad \text{(V.1.13)}$$

where $\mathbf{I}$ is the identity tensor and $|\mathbf{E}|$ is the magnitude of $\mathbf{E}$. The component of this stress normal to the surface of the drop,

$$T_{n2}^e \equiv \mathbf{nn} : \mathbf{T}_2^e = \frac{1}{2} (\mathbf{n} \cdot \mathbf{E})^2 \quad , \qquad \text{(V.1.14)}$$

appears in the normal-stress balance (V.1.5) and couples together the fluid flow and electrostatic problems. The spatially uniform potential inside the conducting drop forces $\mathbf{T}_1^e$ to be zero, hence $T_{n1}^e \equiv 0$.

The dynamical problem for the velocity and electrostatic potentials and the drop shape are solved for motions originating with an initial

deformation of the drop. We describe initial deformations which satisfy conservation of mass (V.1.6) and which have no initial velocity, i.e.

$$\frac{\partial F}{\partial t}(\theta,0) = 0. \qquad \text{(V.1.15)}$$

We define the amplitude of the oscillation ε in terms of this initial deformation as

$$F(\theta,0) = 1 + \varepsilon P_n(\theta) + O(\varepsilon^2). \qquad \text{(V.1.16)}$$

where $P_n(\theta)$ is the Legendre polynomial of nth order. The forms of the initial condition (V.1.16) that satisfy the volume integral (V.1.6) up to $O(\varepsilon^3)$ are

$$F(\theta,t) = 1 + \varepsilon P_2(\theta) - \frac{1}{5}\varepsilon^2 - \frac{2}{105}\varepsilon^3 + \ldots \quad \text{for } n=2, \qquad \text{(V.1.16a)}$$

$$F(\theta,t) = 1 + \varepsilon P_3(\theta) - \frac{1}{7}\varepsilon^2 - 0\varepsilon^3 + \ldots \quad \text{for } n=3, \qquad \text{(V.1.16b)}$$

$$F(\theta,t) = 1 + \varepsilon P_4(\theta) - \frac{1}{9}\varepsilon^2 - \frac{6}{1001}\varepsilon^3 + \ldots \quad \text{for } n=4. \qquad \text{(V.1.16c)}$$

The amplitude ε is taken to be a small parameter in the analysis that follows.

V.2 PERTURBATION SOLUTION AWAY FROM RESONANCE

We determine the potential fields ($\phi(r,\theta,t)$, $V(r,\theta,t)$) and drop shape $F(\theta,t)$ for moderate-amplitude motions by constructing expansions in the initial amplitude of the deformation ε. The asymptotic methods couple together the method of multiple timescales for freely oscillating non-dissipative systems and the domain perturbation technique outlined

by Joseph (1973) and used also in Chapter IV. Formally, we assume that the dependent variables are functions of three timescales related to the actual time as $T_0=t$, $T_1=\varepsilon t$ and $T_2=\varepsilon^2 t/2$. The different timescales are introduced into the field equations by expanding the partial derivative $\partial/\partial t$ as

$$\frac{\partial}{\partial t} \equiv \frac{\partial}{\partial T_0} + \varepsilon \frac{\partial}{\partial T_1} + \frac{\varepsilon^2}{2}\frac{\partial}{\partial T_2} + O(\varepsilon^3). \qquad (V.2.1)$$

The expansion for the domain shape is implemented by transforming the drop shape to the unit sphere using the change of coordinates $r\equiv\eta F(\theta,t)$ and expanding each dependent variable in a Taylor series

$$\begin{bmatrix} F(\theta,t;\varepsilon) \\ \phi(r,\theta,t;\varepsilon) \\ V(r,\theta,t;\varepsilon) \end{bmatrix} = \sum_{k=0}^{\infty} \frac{\varepsilon^k}{k!} \begin{bmatrix} F^{(k)}(\theta,T_0,T_1,T_2) \\ \phi^{[k]}(\eta,\theta,T_0,T_1,T_2) \\ V^{[k]}(\eta,\theta,T_0,T_1,T_2) \end{bmatrix}, \qquad (V.2.2)$$

where the superscript [k] denotes the kth total derivative of the quantity with respect to ε. As in chapter IV, each term in these expansions for the potentials can be written as a sum of a contribution based on the spherical domain ($0\leq\eta\leq1$, $0\leq\theta\leq\pi$) and terms that account for the deformation of the domain at each order of ε. The derivatives evaluated on the spherical domain are denoted by $\phi^{(k)}(\eta,\theta,T_0,T_1,T_2)\equiv\partial^{(k)}\phi/\partial\varepsilon^{(k)}$. Because the drop shape $F(\theta,t)$ is independent of the radial coordinate, $F^{[k]}(\theta,T_0,T_1,T_2)=F^{(k)}(\theta,T_0,T_1,T_2)$. Expressions for the total derivatives of a potential up to $\phi^{[2]}$ are given by equation (IV.2.3) of chapter IV. We anticipate the form of the solution to the drop shape and expand $F^{(k)}$ at each order as a series of Legendre polynomials

$$F^{(k)}(\theta,T_0,T_1,T_2) = \sum_{m=0}^{\infty} F_m^{(k)}(\theta,T_0,T_1,T_2) = \sum_{m=0}^{\infty} \delta_m^{(k)}(T_0,T_1,T_2)\, P_m(\theta). \quad (V.2.3)$$

Using these forms for the corrections to $F(\theta,t)$, the mean curvature of the drop and the unit normal and tangent vectors are conveniently expanded in ε; the results valid up to $O(\varepsilon^3)$ are given in Appendix A.

The equations governing the zeroth-order contributions from the set (V.1.1) - (V.1.16) describe a static charged drop and have the solution

$$\begin{bmatrix} F^{(0)}(\theta,T_0) \\ \phi^{(0)}(\eta,\theta,T_0) \\ V^{(0)}(\eta,\theta,T_0) \end{bmatrix} = \begin{bmatrix} 1 \\ 0 \\ Q/\eta \end{bmatrix}. \quad (V.2.4)$$

The arbitrary reference potential V_0 inside the drop has been set equal to Q.

The equation set that governs the first-order corrections ($F^{(1)}$, $\phi^{(1)}$, $V^{(1)}$) is

$$\nabla^2\phi^{(1)} = 0 \qquad (0\leq\eta\leq 1,\ 0\leq\theta\leq\pi), \quad (V.2.5)$$

$$\frac{\partial\phi^{(1)}}{\partial\eta} = 0 \qquad (\eta=0,\ 0\leq\theta\leq\pi), \quad (V.2.6)$$

$$\frac{\partial\phi^{(1)}}{\partial\eta} = \frac{\partial F^{(1)}}{\partial T_0} \qquad (\eta=1,\ 0\leq\theta\leq\pi), \quad (V.2.7)$$

$$\frac{\partial\phi^{(1)}}{\partial T_0} - \frac{1}{4\pi}\frac{\partial V^{(0)}}{\partial\eta}\left[\frac{\partial V^{(1)}}{\partial\eta} + F^{(1)}\frac{\partial^2 V^{(0)}}{\partial\eta^2}\right] = -\sum_{n=2}^{\infty}(n-1)(n+2)F_n^{(1)}(\theta,t)(\eta=1), \quad (V.2.8)$$

$$\int_0^{\pi} F^{(1)}(\theta,t)\sin(\theta)\,d\theta = 0, \quad (V.2.9)$$

$$\nabla^2 V^{(1)} = 0 \qquad (1\leq\eta\leq\infty,\ 0\leq\theta\leq\pi), \quad (V.2.10)$$

$$V^{(1)} \to 0 \qquad (\eta\to\infty,\ 0\leqq\theta\leqq\pi), \tag{V.2.11}$$

$$\int_0^{\pi} \left[\frac{\partial V^{(1)}}{\partial \eta} + F^{(1)} \frac{\partial^2 V^{(0)}}{\partial \eta^2} \right] \sin(\theta)\, d\theta = 0 \quad (\eta=1), \tag{V.2.12}$$

$$\frac{\partial V^{(1)}}{\partial \theta} + \frac{\partial F^{(1)}}{\partial \theta} \frac{\partial V^{(0)}}{\partial \eta} = 0 \quad (\eta=1,\ 0\leqq\theta\leqq\pi), \tag{V.2.13}$$

$$F^{(1)}(\theta,0,0,0) = P_n(\theta), \tag{V.2.14}$$

$$\frac{\partial F^{(1)}}{\partial T_0}(\theta,0,0,0) = 0. \tag{V.2.15}$$

The pressure and normal electric stress have been eliminated from (V.2.8) by substituting from the first-order forms of Bernoulli's equation and the definition of the electric stress tensor. Also, (V.2.12) is a combination of the conditions for the jump in the normal component of the electric field at the interface and the condition for conservation of total charge.

The solutions to (V.2.5) - (V.2.15) have the form of the linear oscillation modes described by Rayleigh (1882) cast in the framework of the multiple-scale expansion

$$F^{(1)}(\theta,T_0,T_1,T_2) = c_n(T_1,T_2) \cos(\Psi_n)\, P_n(\theta), \tag{V.2.16a}$$

$$\phi^{(1)}(\eta,\theta,T_0,T_1,T_2) = - c_n(T_1,T_2) \frac{\eta\, \omega_n^{(0)}}{n} \sin(\Psi_n)\, P_n(\theta), \tag{V.2.16b}$$

$$V^{(1)}(\eta,\theta,T_0,T_1,T_2) = c_n(T_1,T_2) \frac{Q}{\eta^{n+1}} \cos(\Psi_n)\, P_n(\theta). \tag{V.2.16c}$$

where $\Psi_n \equiv \omega_n T_0 + h_n(T_1,T_2)$, $\omega_n \equiv \left[n(n-1)(n+2 - \frac{Q^2}{4\pi}) \right]^{1/2}$. (V.2.16d)

and $\{c_n(T_1,T_2),\ h_n(T_1,T_2)\}$ are functions of the slower timescales which

are to be determined as part of the second-order problem subject to the initial conditions

$$c_n(0,0) = 1, \quad h_n(0,0) = 0. \tag{V.2.17}$$

The functions $\{c_n(T_1,T_2)\}$ and $\{h_n(T_1,T_2)\}$ represent the modulation in the slow timescales of the amplitude and frequency of the oscillations, respectively. As noted by Rayleigh, drops with net charge less than $Q_c^{(n)} = [4\pi(n+2)]^{1/2}$ oscillate with stable standing waves, whereas drops with greater charge are unstable and fission. The lowest value of $Q_c^{(n)}$ that sets the maximum admissible charge on the drop, corresponds to n=2 and is the Rayleigh stability limit $Q_c^{(2)}=4\pi^{1/2}$. In this chapter, we consider only drops with net charge below this limit.

The equation set for the second-order terms $(\phi^{(2)}, V^{(2)}, F^{(2)})$ is cumbersome because of the multitude of non-homogeneous terms that are generated by the domain perturbation, but is listed in Appendix B. These equations are solved by expanding the two potentials $(\phi^{(2)}, V^{(2)})$ in series of Legendre polynomials and powers of η

$$\begin{bmatrix} \phi^{(2)}(\eta,\theta,T_0,T_1,T_2) \\ V^{(2)}(\eta,\theta,T_0,T_1,T_2) \end{bmatrix} = \sum_{m=0}^{\infty} P_m(\theta) \begin{bmatrix} \gamma_m(T_0,T_1,T_2)\eta^m \\ \beta_m(Q,T_0,T_1,T_2)\eta^{-m-1} \end{bmatrix} \tag{V.2.18}$$

which satisfy the field equations and boundary conditions, except those on the drop surface. The correction to the drop shape is given by (V.2.3). The displacement condition (B9) can be integrated directly with respect to θ to give $V^{(2)}$ in terms of $F^{(2)}$ and lower-order quantities. Substituting this result into (B3) and (B4) and forming the integrals with $\{\sin(\theta)P_m(\theta)\}$ yields a sequence of second-order non-homogeneous equations for the co-

efficients $\{\gamma_m(T_0,T_1,T_2)\}$. These are

$$\frac{\partial^2\gamma_m}{\partial T_0^2} + \omega_m \gamma_m = 2(\frac{\omega_m^2}{m} + \frac{\omega_n^2}{n})[\frac{\partial c_n}{\partial T_1}\cos(\Psi_n) - c_n \sin(\Psi_n)\frac{\partial h_n}{\partial T_1}] \langle P_n, P_m\rangle$$

$$- c_n^2 \omega_n \sin(2\Psi_n)[3\omega_n^2 + 4(n^2 + n - 1) - \frac{Q^2}{4\pi}(n^2 + 8n - 3)$$

$$+ \frac{Q^2}{4\pi}(m + 1)(2n) - (n - 1)\frac{\omega_m^2}{m}] \langle P_n^2, P_m\rangle$$

$$+ c_n^2\omega_n \sin(2\Psi_n)[\frac{Q^2}{4\pi} + \frac{\omega_n^2}{n^2} + \frac{\omega_m^2}{nm}] \langle P_n'^2, P_m\rangle + \frac{Q}{4\pi}(m+1)\frac{\partial K_m}{\partial T_0}\langle 0, P_m\rangle. \quad (V.2.19)$$

where $\langle f(\theta),g(\theta)\rangle$ is the inner product of these functions weighted with $\sin(\theta)$ on the interval $[0,\pi]$, and K_m is an integration constant from (B9).

The solvability condition for the equations (V.2.19) eliminates the secular terms and leads to the result

$$\frac{\partial c_n}{\partial T_1} = \frac{\partial h_n}{\partial T_1} = 0. \quad (V.2.20)$$

or that the modulation functions depend only on T_2. The solutions of (V.2.19), determined so that the initial conditions (B10), (B11) and the integral constraints (B5), (B8) are satisfied, are written in the form

$$F_k^{(2)}(\theta,T_0,T_1,T_2) = \sum_{j=0}^{8} L_{2kj}(T_0,T_2)\, P_j(\theta). \quad (V.2.21)$$

where the numerical values for the coefficients are tabulated in Appendix B. The corrections for $\phi^{(2)}$ and $V^{(2)}$ can be expressed in a matrix form similar to (V.2.21) with the elements $\{\eta^j M_{2kj}(T_0,T_2)\}$ and $\{N_{2kj}(T_0,T_2)/\eta^{j+1}\}$ respectively, replacing $\{L_{2kj}(T_0,T_2)\}$. The exact forms of these coefficients are also given in Appendix B (see equations (B13) and (B14).

The dependence of the frequency and amplitude modulations on the slow timescale T_2 is computed from the solvability conditions of the third-order problem, which is listed in Appendix C. The corrections to the shape and the potentials ($F^{(3)}$, $\phi^{(3)}$, $V^{(3)}$) are again expanded in Legendre series, and a set of second-order ordinary differential equations is derived by the same procedure used to solve the second-order problem. The solvability condition for this set dictates that

$$\frac{\partial c_n}{\partial T_2} = 0, \tag{V.2.22}$$

so that the amplitude of the oscillation is not modulated up to $O(\varepsilon^2)$; the $\{c_n\}$ are taken to be unity to satisfy the initial condition (V.2.17). Solvability also requires that the frequency modulation takes the form

$$h_2(T_2) = -\frac{8}{245}\frac{T_2 \sum_{j=0}^{4} A_{2j}\,\hat{Q}^j}{\omega_2^3\,\omega_4^2\,(\omega_4^2 - 4\omega_2^2)} \quad \text{for } n=2, \tag{V.2.23a}$$

$$h_3(T_2) = -\frac{288}{11011}\frac{T_2 \sum_{j=0}^{6} A_{3j}\,\hat{Q}^j}{\omega_3\,\omega_2^2\,\omega_4^2\,\omega_6^2\,(\omega_2^2 - 4\omega_3^2)(\omega_6^2 - 4\omega_3^2)} \quad \text{for } n=3, \tag{V.2.23b}$$

$$h_4(T_2) = -\frac{2488320}{2433431}\frac{T_2 \sum_{j=0}^{8} A_{4j}\,\hat{Q}^j}{\omega_2^2\,\omega_4^3\,\omega_6^2\,\omega_8^2\,(\omega_2^2 - 4\omega_4^2)(\omega_6^2 - 4\omega_4^2)(\omega_8^2 - 4\omega_4^2)} \quad \text{for } n=4, \tag{V.2.23c}$$

where $\hat{Q} \equiv Q^2/4\pi$, and the coefficients $\{A_{ij}\}$ are listed in Table V.2.1. Because there can be no dependence of the frequency modulation on any odd powers of the amplitude, the results (V.2.23) are accurate up to $O(\varepsilon^4)$. For values of $\hat{Q}$ in the range of $0 \leq \hat{Q} < 4$, the drop oscillates stably and both

Table V.2.1 Coefficients in the frequency corrections in equation (V.2.23)

	L=2	L=3	L=4
A_{10}	6606528	4214241024000	55735591155609600
A_{11}	-4961440	-4128178176000	-77949491906388480
A_{12}	1419804	1682216124000	45351373912349312
A_{13}	-177168	-362825358328	-14555386948486656
A_{14}	7945	43303979512	2840187292166640
A_{15}	-	-2679419780	-345863703031648
A_{16}	-	66094721	25619763735024
A_{17}	-	-	-1049270108016
A_{18}	-	-	18006768899

$h_2(T_2)$ and $h_3(T_2)$ remain negative. The frequency modulation $h_4(T_2)$ for the four-lobed oscillation is positive in the region $2.3 \leq \hat{Q} < 8/3$ and is infinite at $\hat{Q}=8/3$. At this value of the net charge the four-lobed motion resonates with six-lobed oscillations and the scalings for the modulation functions derived in this section are no longer valid. The proper analysis close to this resonant point is described in section V.3. The above mentioned frequency modulations reduce to the results of the previous analysis (chapter IV) for $Q=0$.

V.3 SECOND HARMONIC RESONANCE

The regular forms of the weakly nonlinear oscillations described in V.2 are not valid when the frequencies of the higher harmonics of the fundamental mode are close to integral multiples of its frequency. This does not occur for uncharged drops up to second order in amplitude, but happens for charged drops that satisfy the condition

$$\frac{m(m-1)(m+2 - Q^2/4\pi)}{\omega_n^2} = (\text{integer})^2, \quad m \neq n. \tag{V.3.1}$$

For the two- and three-lobed modes of oscillation, the values of Q required for resonance are above the Rayleigh limit for electrostatic bursting. Resonance is detectable for four-lobed oscillations when the net charge is near $Q_r=(32\pi/3)^{1/2}<Q_c$, where $\omega_6^2=4\omega_4^2$. Then the four-lobed fundamental resonates with the six-lobed form, and the two modes exchange energy in a periodic or aperiodic fashion, depending on the initial deformation of the drop.

In the remainder of this section we analyse this second harmonic

resonance. The analysis used here parallels the work of McGoldrick (1972) for capillary-gravity waves. We consider drops with net charge slightly different from $Q_r \equiv Q^{(0)}$, or

$$Q = Q_r + Q^{(1)}\varepsilon \equiv Q_r + (\frac{3\pi}{8})^{1/2}\ \lambda\varepsilon, \tag{V.3.2}$$

where $\lambda=O(1)$. The linear oscillation frequencies at these values of Q are given by

$$\omega_4 = 2\sqrt{10}\ (1 - \frac{3}{20}\ \lambda\varepsilon), \tag{V.3.3}$$

$$\omega_6 = 4\sqrt{10}\ (1 - \frac{3}{32}\ \lambda\varepsilon), \tag{V.3.4}$$

The formulation of the linear problem (V.2.5) - (V.2.15) for n=4 is unaffected by the possibility of resonance, and, for convenience in subsequent manipulations, its solution is written in complex form as

$$F^{(1)}(\theta,T_0,\ T_1) = \{A(T_1)e^{-i\omega_4 T_0} + c.c.\}\ P_4(\theta), \tag{V.3.5a}$$

$$\phi^{(1)}(\eta,\theta,T_0,\ T_1) = \{-\frac{1}{4}i\omega A(T_1)e^{-i\omega_4 T_0} + c.c.\}\ P_4(\theta)\ \eta^4, \tag{V.3.5b}$$

$$V^{(1)}(\eta,\theta,T_0,\ T_1) = \{A(T_1)e^{-i\omega_4 T_0} + c.c.\}\ P_4(\theta)\ Q^{(0)}/\eta^5, \tag{V.3.5c}$$

where {c.c.} stands for the complex conjugate of the immediately preceding term. We carry our analysis of resonance only to terms $O(\varepsilon)$; so to this order of approximation the term $A(T_1)$ will depend on only the single slow timescale T_1, (see Tsamopoulos and Brown 1984).

The form of the singularities of the second-order coefficients in the regular perturbation when Q is near Q_r (e.g. see the coefficients I_{61} and I_{62} in (B13)) suggests that the first-order solution be modified

to include a second harmonic constituent (n=6). This new mode may not be present initially (t=0), but will be excited through the resonance with the exciting fundamental (n=4). We write the more general $\mathbf{O}(\varepsilon)$ solution as

$$F^{(1)}(\theta,T_0,T_1) = \{A(T_1)e^{-i\omega_4 T_0} + c.c.\}\, P_4(\theta) + \{B(T_1)e^{-i\omega_6 T_0} + c.c.\}\, P_6(\theta)\,, \qquad (V.3.6a)$$

$$\phi^{(1)}(\eta,\theta,T_0,T_1) = \{-\tfrac{1}{4}i\omega_4 A(T_1)e^{-i\omega_4 T_0} + c.c.\}\, P_4(\theta)\, \eta^4 + \{-\tfrac{1}{6}i\omega_6 B(T_1)e^{-i\omega_6 T_0} + c.c.\}\, P_6(\theta)\, \eta^6, \qquad (V.3.6b)$$

$$V^{(1)}(\eta,\theta,T_0,T_1) = \{A(T_1)e^{-i\omega_4 T_0} + c.c.\}\, P_4(\theta)\, Q^{(0)}/\eta^5 + \{B(T_1)e^{-i\omega_6 T_0} + c.c.\}\, P_6(\theta)\, Q^{(0)}/\eta^7\,. \qquad (V.3.6c)$$

The dependence of the net charge on the amplitude through (V.3.2) introduces new terms into the non-homogeneous parts of (B4) and (B9). These terms are, for (B4)

$$-\frac{Q^{(0)}Q^{(1)}F^{(1)}}{2\pi} \qquad (V.3.7)$$

and, for (B9),

$$-2Q^{(1)}\frac{\partial F^{(1)}}{\partial\theta}\,. \qquad (V.3.8)$$

Introducing the generalized solutions (V.3.6) into the modified form of the second-order problem and following the same procedure outlined in section V.2 leads to a second-order differential equation like (V.2.19).

Eliminating secular terms from this equation requires setting to zero the coefficients multiplying not only the terms $\exp(\pm i\omega_4 T_0)$ and $\exp(\pm i\omega_6 T_0)$ that resonate exactly, but also those coefficients multiplied by $\exp(\pm 2i\omega_4 T_0)$ and $\exp[\pm i(\omega_6-\omega_4)T_0]$ that nearly resonate because

$$2\omega_4 T_0 \equiv (\omega_6 - N\varepsilon) T_0 = \omega_6 T_0 - NT_1 , \qquad (V.3.9a)$$

$$(\omega_6 - \omega_4) T_0 \equiv (\omega_4 + N\varepsilon) T_0 = \omega_4 T_0 + NT_1 . \qquad (V.3.9b)$$

where $N \equiv 9\lambda\sqrt{10}/40$. Thus the differences between these two frequencies and the fundamental n=4 and n=6 modes are only in the slow timescale T_1. The solvability conditions that result from equating to zero these secular terms are

$$\alpha_1 \left(\frac{dA}{dT_1} - \alpha_3 iA\right) = iA^* B e^{-iNT_1} , \qquad (V.3.10a)$$

$$\alpha_2 \left(\frac{dB}{dT_1} - \alpha_4 iB\right) = iA^2 e^{iNT_1} , \qquad (V.3.10b)$$

where $\alpha_1 \equiv \frac{143}{267\sqrt{10}}$, $\alpha_2 \equiv \frac{88}{89\sqrt{10}}$, $\alpha_3 \equiv \frac{\lambda}{\sqrt{10}}$ and $\alpha_4 \equiv \frac{9\lambda}{4\sqrt{10}}$.

Equations similar to (V.3.10) were first derived by Bretherton (1964) for planar water waves. In sections V.3a and V.3b we consider separately the cases of exact resonance ($\lambda=0$) and the detuning caused by a slight variation in Q from Q_r ($\lambda\neq 0$).

V.3a Exact Resonance

Introducing the substitutions $A(T_1) \equiv r_1(T_1)e^{i\theta_1(T_1)}$ and $B(T_1) \equiv r_2(T_1)$ $e^{i\theta_2(T_1)}$, where the $\{r_i,\theta_i\}$ are real functions of the slow timescale, reduces (V.3.10) to

$$\alpha_1 \frac{dr_1}{dT_1} = - r_1 r_2 \sin(\hat{\theta}), \qquad \alpha_2 \frac{dr_2}{dT_1} = r_1^2 \sin(\hat{\theta}), \tag{V.3.11a,b}$$

$$\alpha_1 r_1 \frac{d\theta_1}{dT_1} = r_1 r_2 \cos(\hat{\theta}), \qquad \alpha_2 r_2 \frac{d\theta_2}{dT_1} = r_1^2 \cos(\hat{\theta}). \tag{V.3.11c,d}$$

where $\hat{\theta} \equiv \theta_2 - 2\theta_1$. Just as for the modulation equations arising for planar water waves (Benney 1962), the first two relations (V.3.11a,b) have an energy-like integral

$$\alpha_1 r_1^2 + \alpha_2 r_2^2 \equiv E, \tag{V.3.12}$$

where E is proportional to the $O(\varepsilon)$ energy carried in the system. The functions $r_1(T_1)$, $r_2(T_1)$ and the relative phase $\hat{\theta}(T_1)$ are, from (V.3.11), related by

$$r_1^2 r_2 \cos(\hat{\theta}) \equiv L, \tag{V.3.13}$$

where L is a constant. Using (V.3.12) and (V.3.13), the set (V.3.11) is decoupled into the form

$$\frac{\alpha_1}{2} \frac{dr_1^2}{dT_1} = - \frac{1}{\sqrt{\alpha_2}} (\alpha_1 r_1^6 + E r_1^4 - \alpha_2 L^2)^{1/2} , \tag{V.3.14a}$$

$$\frac{\alpha_2}{2} \frac{dr_2^2}{dT_1} = \frac{1}{\alpha_1} (\alpha_2^2 r_2^6 - 2E\alpha_2 r_2^4 + E^2 r_2^2 - \alpha_1^2 L^2)^{1/2}, \tag{V.3.14b}$$

$$\alpha_1 r_1^2 \frac{d\theta_1}{dT_1} = \alpha_2 r_2^2 \frac{d\theta_2}{dT_1} = L . \tag{V.3.14c}$$

The third-order polynomial in r_1^2 on the right-hand side of (V.3.14a) has three real roots $\{\rho_i\}$ which satisfy the inequalities

$$-E/3\alpha_1 \leq \rho_1 \leq 0 \leq \rho_2 \leq 2E/3\alpha_1 \leq \rho_3 \leq E/\alpha_1 .$$

The solutions of (V.3.14) are expressed as

$$r_1^2(T_1) = \rho_3 + (\rho_2 - \rho_3)\, sn^2(\tau;k), \tag{V.3.15a}$$

$$r_2^2(T_1) = \frac{\alpha_1}{\alpha_2}(\rho_1 + \rho_2 - (\rho_2 - \rho_3)\, sn^2(\tau;k)), \tag{V.3.15b}$$

$$\theta_1(T_1) = \theta_1(0) + \frac{(\alpha_2/\alpha_1)^{1/2}\, L}{\rho_3\,(\rho_3 - \rho_1)^{1/2}}\, \Pi(1 - \frac{\rho_2}{\rho_3}\ ;\ \tau|k), \tag{V.3.15c}$$

$$\theta_2(T_1) = \theta_2(0) + \frac{(\alpha_2/\alpha_1)^{1/2}\, L}{(\rho_1 + \rho_2)(\rho_3 - \rho_1)^{1/2}}\, \Pi(\frac{\rho_2 + \rho_3}{\rho_1 + \rho_2}\ ;\ \tau|k), \tag{V.3.15d}$$

where sn is Jacobi's elliptic function and Π is the incomplete elliptic integral of the third kind (Abramowitz & Stegun 1964) with $\tau \equiv [(\rho_3-\rho_1)/(\alpha_1\alpha_2)]^{1/2}T_1$ and $k \equiv (\rho_3-\rho_2)/(\rho_3-\rho_1)$. The first-order solution (V.3.6) then consists of periodic amplitude modulations between the two largest roots (ρ_2,ρ_3) together with periodic phase modulations of the same period superimposed on a slow linear frequency shift on the slow timescale, which is similar to the $O(\varepsilon^2)$ Poincaré correction to the frequency for regular oscillations.

Phase-plane plots for the amplitudes of the two modes are readily constructed using (V.3.14) and are shown in figure V.3.1. For initial conditions such that L=0, the individual phases of the two interacting modes are constant and the modal amplitudes follow the outermost trajectory in figure V.3.1. Then the initial condition corresponds to purely four-lobed deformation ($r_1(0)=R_1$, $r_2(0)=0$), and the general solution (V.3.15) simplifies to

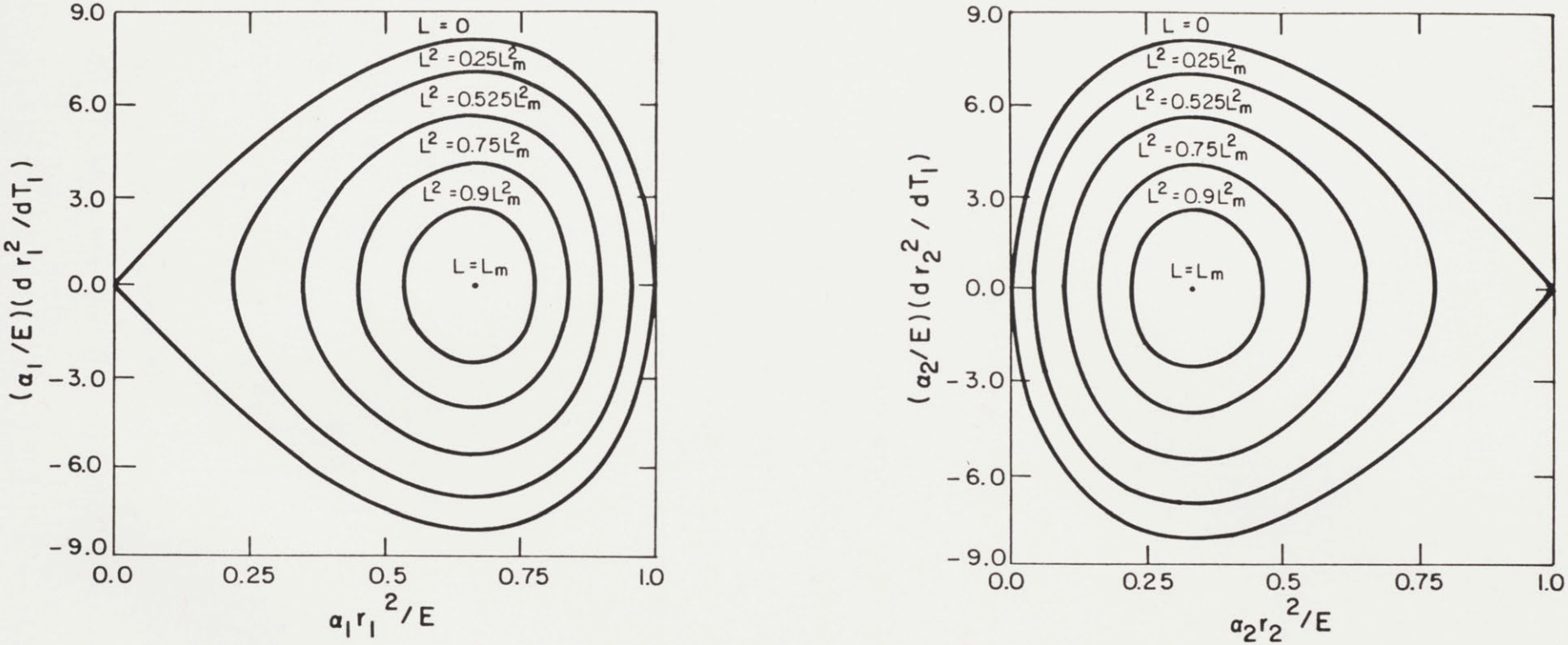

Figure V.3.1 Phase-plane plots of the fundamental (a) and the resonating mode harmonic (b) with $Q=\sqrt{(32\pi/3)}$.

$$r_1(T_1) = R_1 \operatorname{sech} \frac{R_1 T_1}{(\alpha_1 \alpha_2)^{1/2}} , \qquad \text{(V.3.16a)}$$

$$r_2(T_1) = R_1 \left(\frac{\alpha_1}{\alpha_2}\right)^{1/2} \tanh \frac{R_1 T_1}{(\alpha_1 \alpha_2)^{1/2}} , \qquad \text{(V.3.16b)}$$

$$\theta_2 - 2\theta_1 = \pm \frac{\pi}{2} . \qquad \text{(V.3.16c)}$$

At exact resonance a purely four-lobed oscillation of any amplitude cannot persist, but transforms into a six-lobed oscillation within less than three periods of the initially excited mode. Drop shapes for this case are shown in figure V.3.2 for the initial phase conditions $\theta_1(0)=0$ and $\theta_2(0)=\pi/2$ with $\varepsilon=0.2$.

The amplitudes of the interacting four- and six-lobed modes are given in figure V.3.3 as functions of time for the same conditions used to calculate the drop shapes in figure V.3.2. When $\varepsilon=0.2$ the n=4 mode has decreased to 71.6% of its maximum value and the n=6 mode has reached 69.8% of its maximum value within one oscillation cycle. The corresponding percentages after three cycles are 14.9% and 98.9% for the n=4 and n=6 modes respectively. Because of this transient in the $O(\varepsilon)$ solution, the complete solution of the second-order problem will initially have terms proportional to the n=2,4,6 and 8 Legendre modes, but after about three cycles the shape will have significant components from the n=10 and n=12 modes.

The inner trajectories in figure V.3.1 correspond to initial conditions such that $0 < L^2 < 4E^3/27\alpha_1^2\alpha_2 \equiv L_m^2$ for which the disturbances are combinations of four- and six-lobed shapes with continuous modulations of both magnitude and phase. These modes continuously exchange energy during oscillations

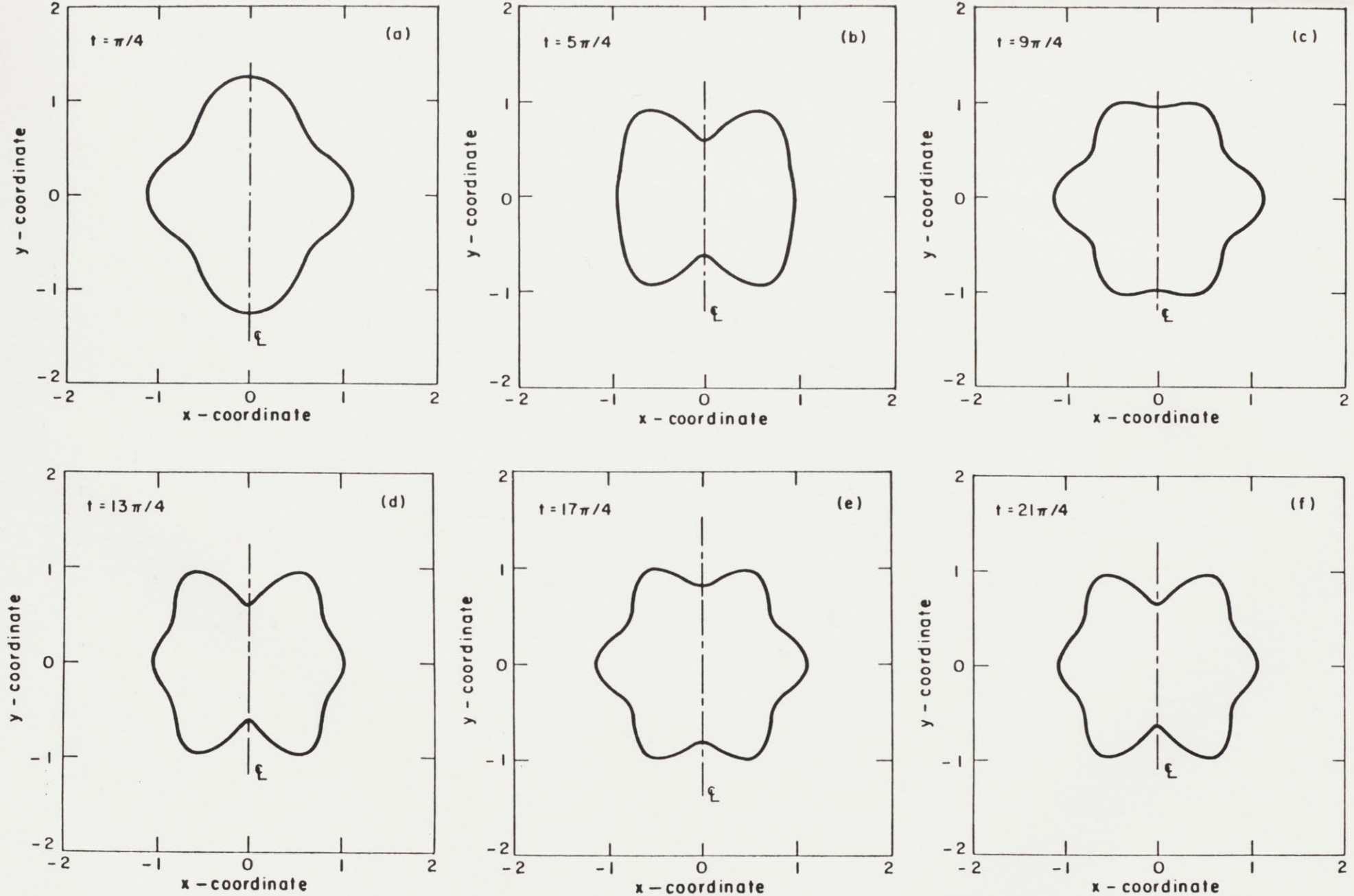

Figure V.3.2 Shapes of drops initially perturbed by an n=4 mode with $Q=\sqrt{(32\pi/3)}$ and $\varepsilon=0.2$.

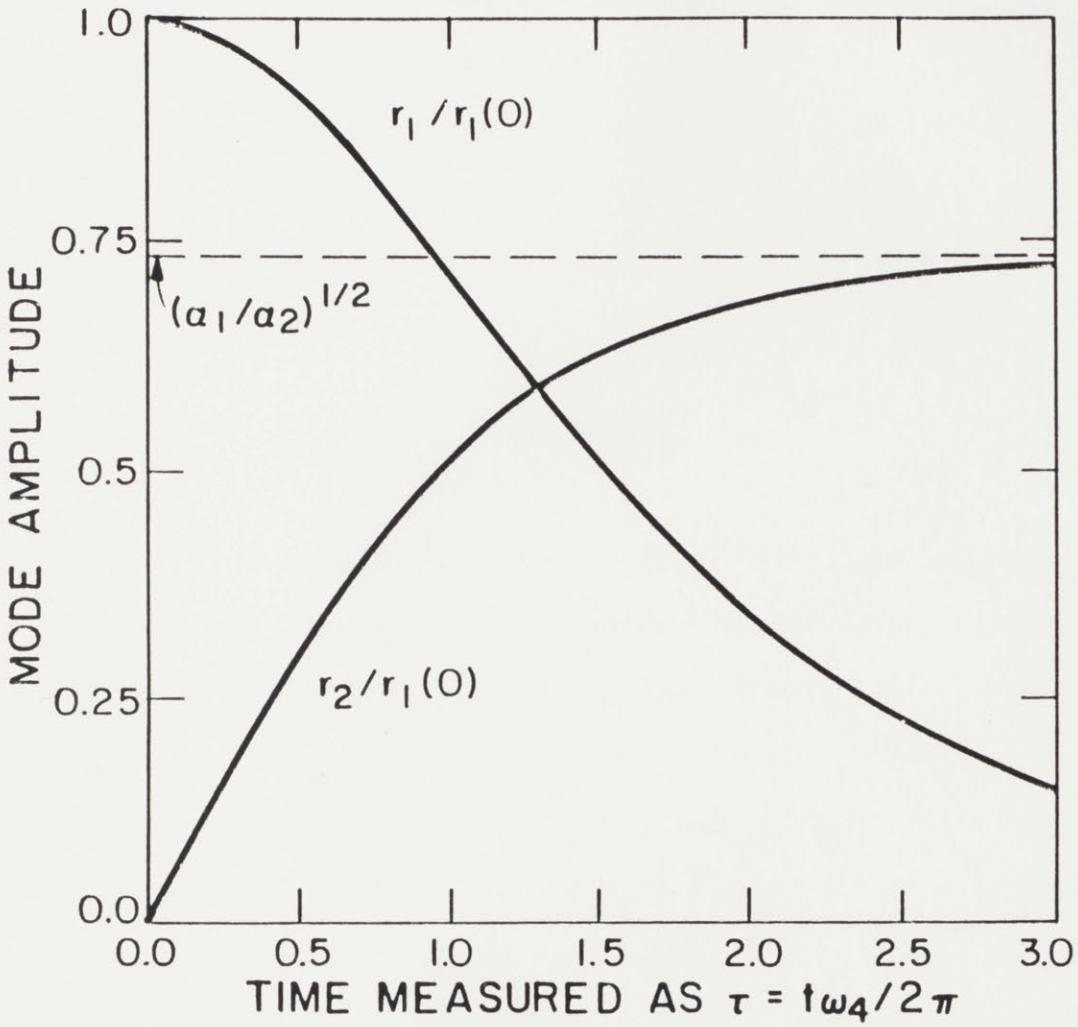

Figure V.3.3 Aperiodic modulation of the amplitude of the fundamental and the resonating mode with $Q=\sqrt{(32\pi/3)}$ and $\varepsilon=0.2$.

at a frequency which is slightly modulated about the mean value. The relative phase $\hat{\theta}$ between these modes always falls between $-\pi/2 < -\hat{\theta}_m \leq \hat{\theta} \leq \hat{\theta}_m < \pi/2$, where $\hat{\theta}_m = \cos^{-1}(L/L_m)$. This phase is maximum when the amplitudes are undergoing maximum growth ($\alpha_1 r_1^2 = 2\alpha_2 r_2^2$), and is zero when the rate of change of the amplitudes is zero.

The timescale for these resonant oscillations is better understood by considering the case $L^2 = L_{max}^2/2$. If the initial amplitude of the deformation is taken as $\varepsilon = 0.2$ one full cycle of the energy exchange between the four- and six-lobed modes occurs in

$$\frac{\omega_4}{\varepsilon\pi}\left[\frac{\alpha_1\ \alpha_2}{\rho_3 - \rho_1}\right]^{1/2} \cong \frac{0.8256}{E^{1/2}}$$

cycles for the $n=4$ fundamental oscillation. This implies that the time for the resonant interaction is inversely proportional to the square root of the total energy input E or the initial amplitude, ε, of the oscillations.

For initial conditions such that $L = L_{max}$, both the amplitude and the phase modulations present for $0 < L < L_{max}$ vanish entirely and the timescale of the resonant interaction between the $n=4$ and $n=6$ modes has dropped to zero. The trajectories for this initial condition are represented by the single point on each of the phase-plane plots shown in figure V.3.1. The general solution of the modulation equations (V.3.15) reduces in this case to

$$\frac{1}{2}\alpha_1 r_1^2 = \alpha_2 r_2^2 = \frac{1}{3} E\ , \qquad \text{(V.3.17a)}$$

$$2\theta_1 = \theta_2 = \pm\left(\frac{2}{\alpha_1\alpha_2}\right)^{1/2} r_1\ T_1\ , \qquad \text{(V.3.17b)}$$

where we have assumed $\theta_1(0)=0$.

V.3b Oscillations near resonance

Variations in the oscillation frequencies of the four- and six-lobed motions caused by the dependence of these frequencies on the small amplitude and small differences between the true net charge and the value Q_r will detune the resonance. The effect of this detuning on the drop motion is considered by analysing (V.3.10) with $\lambda \neq 0$. With the substitution

$$W(T_1) \equiv iA^{*2}Be^{-iNT_1} \tag{V.3.18}$$

(V.3.10) are reduced to

$$\alpha_1 \frac{d}{dT_1}(AA^*) = -\alpha_2 \frac{d}{dT_1}(BB^*) = 2Re(W), \tag{V.3.19}$$

so that an integral quantity analogous to E in (V.3.12) is defined as

$$E = \alpha_1 AA^* + \alpha_2 BB^* , \tag{V.3.20}$$

and is independed of the detuning parameter λ, which appears only in the coefficients α_3 and α_4. To derive a condition equivalent to (V.3.13) we introduce a real-valued function

$$Z(T_1) \equiv \alpha_1 (R_1^2 - AA^*) \equiv \alpha_2 (BB^* - R_2^2), \tag{V.3.21}$$

where R_1 and R_2 are the moduli of the initial amplitudes of the n=4 and n=6 modes respectively. Substituting (V.3.18) and (V.3.21) into the set (V.3.10) leads to the second integral

$$(2\alpha_3 - \alpha_4 + N)Z - 2L = 2Im(W) . \tag{V.3.22}$$

Combining (V.3.18) - (V.3.22) gives the general equation

$$\left(\frac{dZ}{dT_1}\right)^2 = 4\{ \left(R_1^2 - \frac{Z}{\alpha_1}\right)\left(R_2^2 + \frac{Z}{\alpha_2}\right) - [L - (2\alpha_3 - \alpha_4 + N)Z/2]^2 \}, \qquad (V.3.23)$$

which can be integrated in terms of elliptic integrals.

We consider the solution of (V.3.23) only in the case when the initial condition is composed of only the fundamental mode ($R_2=0$). For this situation it is readily shown that $W(0)=Z(0)=L=0$, $E=\alpha_2 R_1^2$, and (V.3.23) reduces to

$$\left(\frac{dZ}{dT_1}\right)^2 = 4Z\{\frac{1}{\alpha_1^2\alpha_2}(E - Z)^2 - \hat{N}^2 Z\} \quad , \qquad (V.3.24)$$

where $\hat{N}=(2\alpha_3-\alpha_4+N)/2$; this constant is somewhat different from the one derived for planar waves by McGoldrick (1972) because of the existence of the linear terms in (V.3.10). The quadratic polynomial in Z in (V.3.24) has two distinct positive roots, $0 \leq \rho_1 \leq E \leq \rho_2$, if $\hat{N}\neq 0$ or two roots equal to E if $\hat{N}=0$. This later case corresponds to the situation at exact resonance ($\lambda=0$) and (V.3.24) can be easily integrated to yield

$$Z(T_1) = E \tanh^2 \left[\frac{2T_1}{\alpha_1} \left(\frac{E}{\alpha_2}\right)^{1/2} \right] \quad . \qquad (V.3.25)$$

which when combined with the definition (V.3.21) can be reduced to a form similar to (V.3.16). The initial value Z(0) is equal to E and is the maximum value of the four-lobed component of the oscillation.

When detuning occurs $\hat{N}$ is not zero and the general solution of (V.3.24) is an oscillation of finite period with value between the smaller root of (V.3.24)

$$\rho_1 = \frac{\alpha_1^2 \alpha_2 \hat{N}^2}{2} \left\{1 + \frac{2E}{\alpha_1^2 \alpha_2 \hat{N}^2} - \left(1 + \frac{4E}{\alpha_1^2 \alpha_2 \hat{N}^2} \right)^{1/2} \right\} \qquad (V.3.26)$$

and zero. The root ρ_1 is the largest value of Z obtained during the detuned oscillations. The effect of detuning on the energy transfer between the initial fundamental (n=4) and the second harmonic (n=6) is shown in figure V.3.4 by a plot of the maximum amplitude of the six-lobed component as a function of $\hat{N}$ which measures the variation of Q from Q_r. The amplitude of the n=6 component is scaled with its asymptotic value $(E/\alpha_2)^{1/2}$ for exact resonance. The ability of the resonance mechanism to transfer energy between the fundamental its second harmonic decreases as $\hat{N}^{-1}$ or λ^{-1}. As this plot indicates there is a band of frequencies and therefore electric charges near Q_r for which the resonant interaction is most effective.

V.4 THIRD HARMONIC RESONANCE

Resonance between, the fundamental mode and one of its third-order harmonics occurs for charged drops at particular values of $Q<Q_c^{(2)}$. In particular, the fundamental two-lobed motion resonates with its four-lobed harmonic for Q=0, i.e. for uncharged inviscid drops. Also, the n=3 fundamental and its n=5 harmonic resonate at $Q=\sqrt{(260\pi/17)}$ and the n=4 fundamental and its n=8 harmonic resonate at $Q=\sqrt{(88\pi/13)}$. In each case the $O(\varepsilon)$ solution $F^{(1)}(\theta,T_0,T_1,T_2)$ must be taken to be a combination of the fundamental and resonant harmonic modes and the amplitude modulations (corresponding to $A(T_1,T_2)$ and $B(T_1,T_2)$ in (V.3.6)) are determined from the solvability of the second- and third-order problems. The solvability condition at $O(\varepsilon^2)$ will guarantee that the amplitude modulations are only functions of the slowest timescale T_2, and the conditions at $O(\varepsilon 3)$ give equations

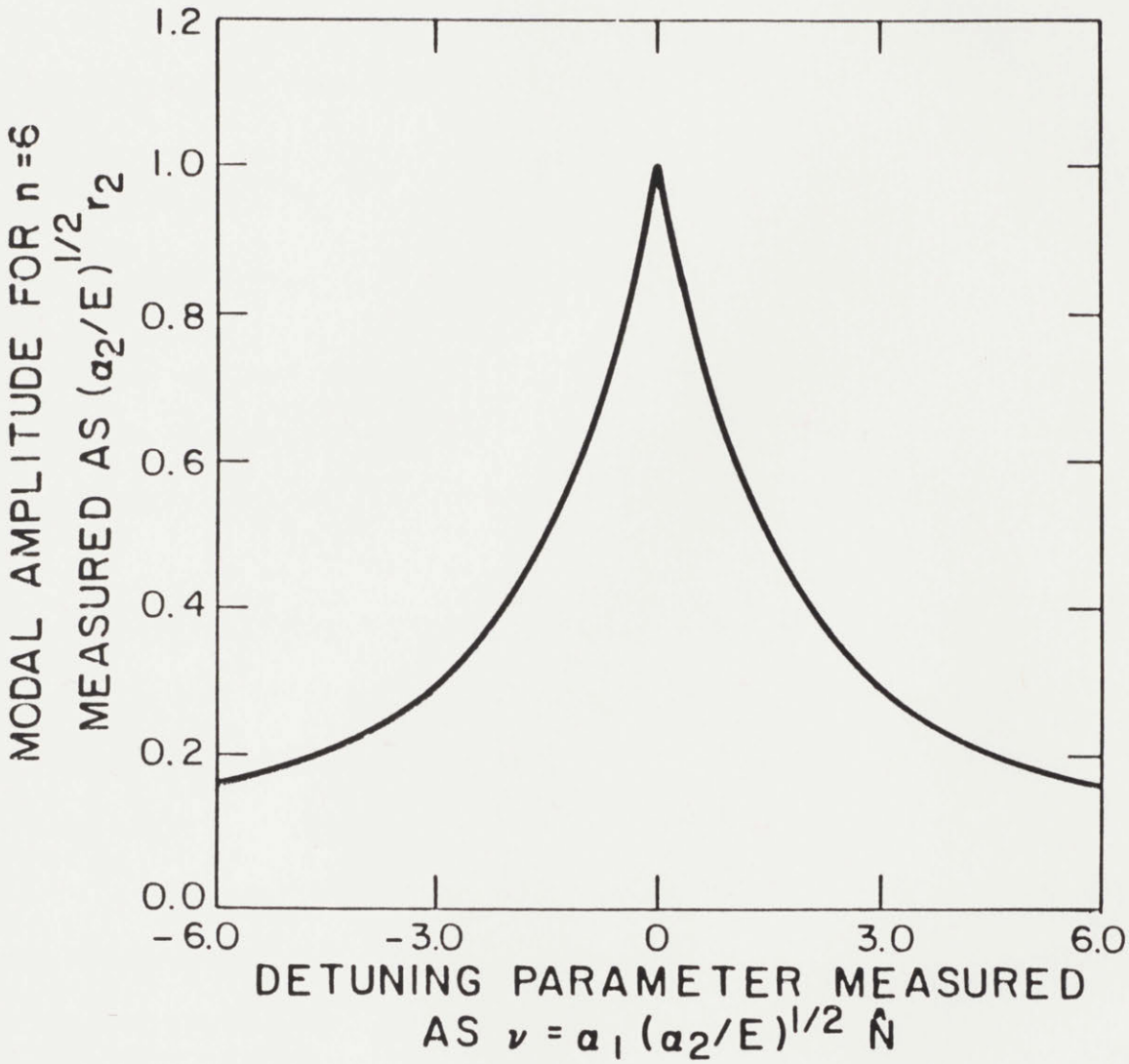

Figure V.3.4 Response of the amplitude of the second harmonic near resonance as a function of the detuning parameter $\hat{N}$.

which govern the amplitude modulations $A(T_2)$ and $B(T_2)$ as a function of T_2 and the Poincaré correction to the frequency. The derivation of these equations and their solution will be tedious, as suggested by the form of the third-order problem far from resonance given in Appendix C. Qualitatively these equations will be of the form

$$\frac{d}{dT_2} A = c_{11} A^2 A^* + c_{12} A^{*2} B + c_{13} BB^* A + c_1 A \qquad \text{(V.4.1a)}$$

$$\frac{d}{dT_2} B = c_{21} B^2 B^* + c_{22} AA^* B + c_{23} A^3 + c_2 B \qquad \text{(V.4.1b)}$$

We have not pursued this work in detail; see McGoldrick (1972) and Nayfeh (1971) for the parallel analysis for capillary-gravity waves. McGoldrick et al. (1966) have also observed these third-order interactions experimentally.

The third harmonic resonance for an uncharged drop set into motion from an initial deformation with components of both the n=2 fundamental and the n=4 harmonic modes will appear as a continuous and periodic modulation of amplitude for these modes in time with a frequency which modulates with ε^2. For the case of ε=0.2 discussed earlier, this scaling implies that **O**(10) oscillation cycles of the fundamental frequency will be needed to observe the resonant energy exchange.

V.5 DISCUSSION

Moderate-amplitude oscillations of inviscid charged drops display an array of nonlinear dynamic phenomena as varied as those that have been observed for planar water waves. Besides a decrease in oscillation frequency with amplitude caused by interactions between the fluid inertia

and drop shape, resonant interactions between the fundamental mode and secondary and tertiary harmonics can completely change the pattern of the oscillation. In terms of the classifications used by McGoldrick (1972), these resonances are selective and weak. They are selective in that only particular combinations of the fundamental and its harmonic can resonate at particular values of the electrical charge Q. They are weak because the timescale for the resonant interaction is long when compared with a typical period for the fundamental oscillation.

In general, since the oscillating inviscid drop is a conservative system a single mode can rarely persist in steady state, instead it will share its energy with those of its harmonics that resonate with it. On the other hand steady-state can be reached in a non-conservative system when the energy input to the higher harmonics by the fundamental is balanced by their own viscous energy loss.

The analysis presented in section V.3 for the second harmonic resonance of a four-lobed oscillation for $Q=Q_r$ shows three particular forms for this long timescale response, depending on the initial deformation of the drop. An aperiodic drop motion is only possible when the initial deformation is composed of the fundamental n=4 mode alone. Small changes in frequency caused by variation in Q from Q_r and oscillation amplitude detune the resonance so that the actual motion described a time-periodic exchange of energy between the n=4 mode and its n=6 harmonic. This type of periodic exchange occurs for more general initial deformations which include both modes and are accompanied by small frequency modulations about the mean.

For either of these periodic or aperiodic motions the oscillation

pattern is distinct from the form valid far from resonance. In both cases, the amplitude of the harmonic mode has magnitude similar to the fundamental for the initial part of the motion. This change in pattern should be observable in calculations and experiments so long as data is collected for a period comparable to the long timescale. We feel that the second-harmonic resonance described in V.3 will be easily observed, but that some of the cases of tertiary resonance described in V.4 will be more difficult. The third type of resonant oscillation is strictly periodic with constant amplitude and phase, but is the most unlikely to be observed because of the precise ratio of initial amplitudes required.

Predictions of experimental observation of these three types of resonance must take into account the effects of the omnipresent viscosity of real drops, which will detune the interactions and cause damping. The quantitative effects of this detuning are difficult to calculate rigorously; however, its qualitative significance can be estimated from simple approximate calculations. As mentioned in section II.1c, Prosperetti (1980a) has shown that the damping of small-amplitude oscillations of a viscous drop is governed by an integrodifferential equation which reduces to Lamb's (1932, section 305) theory for a drop with small viscosity at short times when the initial disturbance is irrotational. For the resonant interactions predicted by the inviscid analysis to be observed in slightly viscous drops, the timescale for viscous dissipation, or equivalently for vorticity diffusion from the interface, must be much longer than the characteristic time for the inviscid motion

$$\tau_n \equiv \frac{1}{(n-1)(2n+1)} \frac{R^2 \rho}{\mu} \gg \left[\frac{\rho R^3}{\sigma} \right]^{1/2} , \qquad (V.5.1)$$

where n is the primary mode of oscillation. This condition is satisfied for water drops with n up to eight.

When there are a number of small-amplitude modes of the form given by (V.3.6), the orthogonality between each component guarantees that, within the order of the approximation, each mode decays independently of the others. When the rate of energy transfer between resonantly coupled modes is independet of the viscosity, the amplitude equations for exact second-order resonance are modified to account for viscous damping and give

$$\alpha_1 \frac{dA}{dT_1} = iA^*B - i\frac{\alpha_1}{\tau_4}A, \qquad \alpha_2 \frac{dB}{dT_1} = iA^2 - i\frac{\alpha_2}{\tau_6}B. \qquad \text{(V.5.2a,b)}$$

The effects of viscosity on the resonant interactions of internal waves (Davis & Acrivos 1967) and capillary waves (McGoldrick 1970) have been derived using similar arguments. McGoldrick analysed the equivalent set of spatial equations in the (A,B) phase plane as a function of initial conditions.

Comparing (V.5.2) with (V.3.10) shows that the principal effect of a slight viscosity is to attenuate the two interacting modes at the same decay rates present in the absence of their interaction. Because the timescale for third-order resonance (uncharged drops) is an order of magnitude greater than the one discussed above, it is more favourably comparable to the viscous timescale. As a result, these interactions will be more difficult to observe experimentally.

The experimental systems presently in use rely on acoustic pressure (Jacobi et al. 1981) or electric fields (Davis & Ray 1980) to position the drop. The acoustic field forces the drop to oscillate, and opens

the possibility of parametrically excited oscillations. Levitation of a charged drop in a d.c. electric field allows the determination of the net charge, but deforms the drop and changes the oscillation frequencies. These deformations have recently been calculated for a static drop (Adornato & Brown 1983), and are small for the full range of values for the field strength and charge accessible before breakup. This suggests that the oscillation frequencies computed for small values of the field by Sample, Raghupathy & Hendricks (1970) are good approximations. Resonant oscillations are detuned even for small changes in these frequencies.

All the calculations presented in this chapter are restricted to charge values below the Rayleigh limit for breakup of the spherical form. Introducing oscillation will interact with this limit, thus causing the drop to become unstable at lower values of the charge. This effect is considered in the next chapter.

VI. DYNAMICS OF CHARGED DROP BREAKUP

The prediction of the shape and stability of fluid globes in the presence of various internal and external force fields has been a long standing problem of interest in a variety of applications, ranging from theories for the formation of heavenly bodies (Chandrasekhar 1969) to calculations of nuclear fission based on liquid drop models of nuclear cohesion (Bohr and Wheeler 1939). Cohen et al. (1974) brought together all the calculations of static equilibrium and energy stability analysis for liquid masses ranging from nuclear to astrophysical dimension, when the forces present are rigid-body rotation and a volumetrically distributed charge or gravitational attraction. Surface tension forces, which are present in ordinary liquid drops, are not included in models of heavenly masses, but are included in calculations for the nucleus as an approximation to short-range attractive forces between the nucleons. The calculations summarized by Cohen et al. are all based on determining static shapes as the stationary points for an appropriate potential energy function and ascertaining stability by calculating whether the shape is a local minimum to all small deformations. The energy input necessary to divide the drop and the drop shape before breakup are important in discussions of fission thresholds and fission symmetry; however, these questions involve consideration of fission dynamics and have only been addressed by a few investigators (Bohr and Mottelson 1975; Bersch 1983). The goal of this chapter is to present a complete view of the dynamics near drop breakup for one important limit of the force fields present in Cohen et al.'s summary.

We consider an electrically charged liquid drop of millimeter size or larger held together by surface tension. The drop is electrically conducting with a net surface charge $\tilde{Q}$ and is immersed in an insulating medium. Lord Rayleigh (1882) considered the stability of such spherical drops to infinitesimal shape disturbances described by Legendre polynomials and determined that the critical amount of charge just necessary to disrupt the nth mode axisymmetric disturbance was

$$\tilde{Q}_c^{(n)} = 4\pi\{\varepsilon_m \sigma R^3 (n+2)\}^{1/2} \qquad n \geq 2,$$

where R is the radius of the spherical drop, σ is the interfacial tension between the drop and the medium and ε_m is the electrical permittivity of the medium. The mode number n indicates the number of lobes on the deformed drop that is neutrally stable at the value of charge given by $\tilde{Q} = \tilde{Q}_c^{(n)}$. The two-lobed shape perturbation becomes unstable at the lowest value of $\tilde{Q} = \tilde{Q}_c^{(2)}$ and corresponds to the limit of stability for the spherical shape computed by Rayleigh. Tsang (1974) has shown the similarities between the linear stability theory for non-conducting drops with volumetrically distributed charge and the results of Rayleigh.

The evolution of the drop close to the critical value $\tilde{Q} = \tilde{Q}_c^{(n)}$ is not predicted by these linear analyses. Experiments with charged liquid drops (Hendricks 1962; Pfeifer and Hendricks 1967) suggest that the Rayleigh limit marks the end of stable, static configurations for a whole drop. Basaran and Scriven (1981) and Adornato and Brown (1983) used partial results of finite element calculations of the shapes of static charged drops to surmise that the Rayleigh limit corresponds to

a subcritical bifurcation in terms of charge between the families of spheres and two-lobed (both prolate and oblate) forms. Only the approximate solutions of Hill and Wheeler (1953) for a volumetrically charged drop and those of Taylor (1964) for a drop with surface charge disagree with this assertion. Hill and Wheeler used series of Legendre polynomials to approximate the axisymmetric shapes originating from the value of charge for neutral stability of a sphere and show that this point marks a transcritical bifurcation near which the family of two-lobed forms exists at both higher and lower values of charge. The same feature is contained in G.I. Taylor's calculations for the conducting drop, but has gone unnoticed by either the author or other researchers. This point is critical to unraveling the dynamics of drop breakup. Hill and Wheeler's calculations and the more accurate calculations of Cohen and Swiatecki (1963) predicted that prolate shapes exist for $\tilde{Q}$ less than the Rayleigh limit and hence should be unstable to small amplitude axisymmetric disturbances from elementary arguments linking bifurcation to linear stability. The oblate forms evolved to higher values of charge and should be stable. The solution structure predicted by this analysis is shown schematically in figure VI.0.1.

Bohr and Wheeler (1939) first recognized the importance of the prolate axisymmetric forms in the theory of nuclear fission, as estimates for the energy barrier separating stable spherical forms from fission. They predicted the evolution of these forms to low values of Q and conjectured that the shape family ends at Q=0 with the static form of two equal spheres with the same total volume just touching each other. Cohen and Swiatecki (1962 and 1963) used better approximations to drop shape to verify this

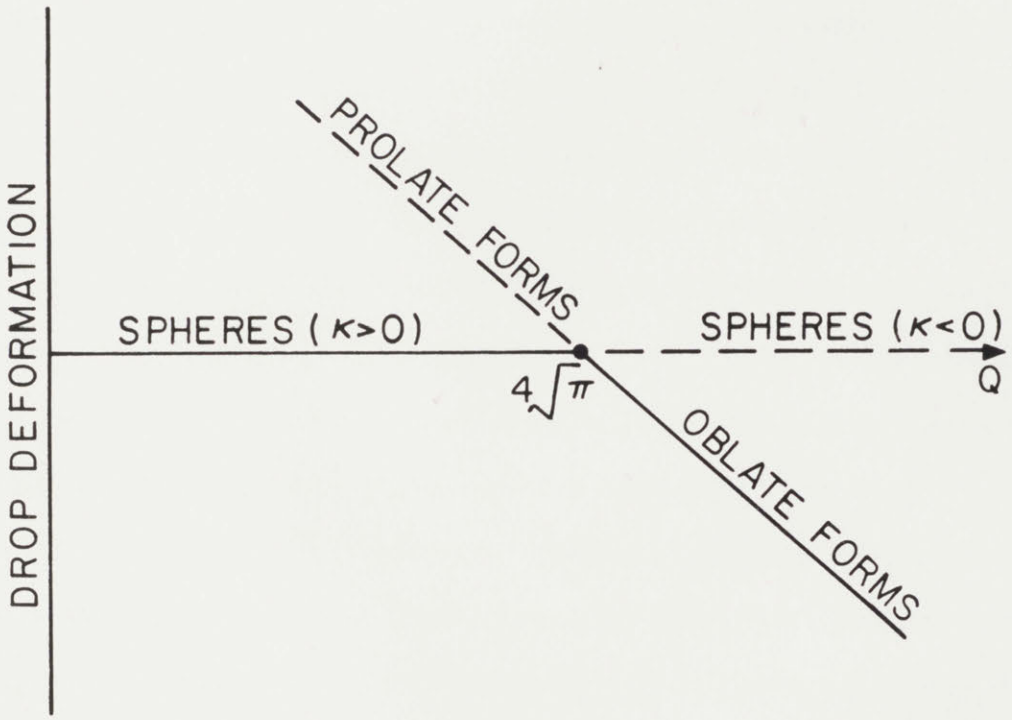

Figure VI.0.1 Families of static drop shapes, as represented by Taylor's asymptotic calculations.

evolution of the family of axisymmetric prolate shapes. Cohen et al. (1974) have expanded on this approach to include rigid rotation of the drop and have linked these axisymmetric forms with the stable, tri-axial rigidly rotating shapes known for uncharged drops (Plateau 1863; Brown and Scriven 1980a and 1980b). The stability to non-axisymmetric disturbances of the oblate forms predicted to exist beyond the Rayleigh limit does not seem to have been rigorously examined, although Businaro and Galone (1955) state without proof that oblate shapes are unstable.

We use a combination of nonlinear asymptotic methods for drop dynamics and finite element calculations of static forms to determine the evolution of axisymmetric, charged inviscid drops near the Rayleigh limit. The asymptotic methods follow in the spirit of the nonlinear stability theories of Landau (1944) and Stuart (1971) in that a finite amplitude perturbation to a static form, close to the point of neutral stability, is described as a wave of slowly varying amplitude. Thus, for weakly nonlinear disturbances, the evolution equations for the long time behavior can be described by singular perturbation methods, such as the multiple time-scale technique used here. The dynamical analysis used here expands on the previous stability predictions for static charged drops by providing information about drop breakup.

Analysis of the nonlinear dynamics of an inviscid charged drop near the Rayleigh limit presents a particularly interesting problem because two fundamental frequencies of its motion coalesce as $\tilde{Q}$ approaches $\tilde{Q}_c^{(2)}$ and because the nonlinear couplings of surface tension and inertial forces in the spherical geometry are different than in the planar or cylindrical configurations. The approach of two frequencies to almost equal values

has been shown to initiate solutions to the linearized equations with linearly growing amplitudes in time. This secular behavior of the amplitude is somewhat similar to resonance in an externally forced, harmonic oscillator and has been called direct resonance by Akylas and Benney (1980). It leads to stronger nonlinear interactions and relatively larger deformations of the drop near the Rayleigh limit.

The strength of the nonlinear interactions described below depend simultaneously on the magnitude of the deformation of the drop and on the distance of $\tilde{Q}$ from the Rayleigh limit. Accordingly, the small parameter ε used in the expansions must scale both effects. Similar analyses have been presented by Nayfeh (1970), Kiang (1969), and others for determination of the cutoff wavenumber for the breakup of a liquid jet and of an accelerating planar interface separating two fluids, the Rayleigh-Taylor problem. The critical points in both these problems correspond to subcritical bifurcations between the families of either cylindrical (liquid jet; Brown and Scriven 1980c) or planar (Rayleigh-Taylor; Pimbley 1976) interfaces and deformed static shapes. The different nonlinear couplings described by Legendre polynomials in the spherical geometry make the bifurcation transcritical for the charged drop problem.

In the previous chapter we presented the nonlinear dynamics of charged drops for $\tilde{Q}$ away from $\tilde{Q}_c^{(2)}$ and showed that the regular perturbation equations and their solutions are singular at the Rayleigh limit. In this chapter, we give a rescaled equation set that alleviates this singularity. Thus, the analysis in chapter V can be viewed as the mathematical outer expansion to the inner expansion presented here. Many of the perturbation equations derived in the inner analysis have similar form to equations presented

in chapter V and the details of the new results are presented as extensions of equations given there.

The multiple timescale expansions appropriate for studying the dynamics of inviscid drops near the Rayleigh limit are presented in Section VI.2. These results confirm the prediction of the transcritical bifurcation of Taylor's theory, but show the oblate forms to be unstable to moderate amplitude, axisymmetric shape disturbances. The evolution of these instabilites is charted. The axisymmetric equilibrium shapes in the two-, three- and four-lobed families are computed by the same finite-element analysis used by Adornato and Brown (1983) to study levitated drops. The numerical calculations of the prolate and oblate forms are described in section VI.3 and demonstrate that the validity of the asymptotic analysis extends well into the nonlinear regime. The stability of the oblate forms to non-axisymmetric disturbances in discussed briefly in Section VI.4.

VI.1 GOVERNING EQUATIONS

We consider the irrotational and incompressible motion of an electrically conducting inviscid drop with volume $\tilde{V} \equiv 4\pi R^3/3$ and density ρ. The motion of the drop in a tenuous surrounding medium is caused by introducing initially either a small axisymmetric deformation or a finite velocity of vibration. The evolution of the surface of the drop is described in spherical coordinates by the radial position $\tilde{r} = RF(\theta,t)$, where $F(\theta,t)$ is the dimensionless shape function for the drop and θ is the meridional angle in spherical coordinates. The dimensionless equations of motion

and boundary conditions for the fluid in the drop and its surface are written in terms of the velocity potential $\phi(r,\theta,t)$ as

$$\nabla^2\phi = 0 \qquad (0\leq r\leq F(\theta,t),\ 0\leq\theta\leq\pi), \tag{VI.1.1}$$

$$\frac{\partial\phi}{\partial r} = 0 \qquad (r = 0,\ 0\leq\theta\leq\pi), \tag{VI.1.2}$$

$$2P + \frac{\partial\phi}{\partial t} + \frac{1}{2}\left[\left(\frac{\partial\phi}{\partial r}\right)^2 + \left(\frac{1}{r}\frac{\partial\phi}{\partial\theta}\right)^2\right] = G(t) \qquad (0\leq r\leq F(\theta,t),\ 0\leq\theta\leq\pi), \tag{VI.1.3}$$

$$\frac{\partial\phi}{\partial r} = \frac{\partial F}{\partial t} + \frac{1}{r^2}\frac{\partial\phi}{\partial\theta}\frac{\partial F}{\partial\theta} \qquad (r=F(\theta,t)), \tag{VI.1.4}$$

$$\Delta P_0 + 2P + \frac{1}{2\pi}\left(T^e_{n2} - T^e_{n1}\right) = -2H \qquad (r=F(\theta,t),\ 0\leq\theta\leq\pi), \tag{VI.1.5}$$

$$\int_0^\pi F^3(\theta,t)\sin(\theta)\,d\theta = 2, \tag{VI.1.6}$$

The normal-stress balance (VI.1.5) equates the pressure differences caused by capillarity and drop motion to the contributions of the normal electric stress from inside T^e_{n1} and outside T^e_{n2} the drop. The expression for the mean curvature **H** written in terms of $F(\theta,t)$ and its expansion in terms of the amplitude of deformation about a sphere are given in Appendix A. The equations and boundary conditions governing the electrostatic potential $V(\eta,\theta,t)$ are

$$\nabla^2 V = 0 \qquad (F(\theta,t)\leq r\leq\infty,\ 0\leq\theta\leq\pi), \tag{VI.1.7}$$

$$V \to 0 \qquad (r\to\infty,\ 0\leq\theta\leq\pi), \tag{VI.1.8}$$

$$\mathbf{n}\cdot\nabla V = -4\pi q(\theta,t) \qquad (r=F(\theta,t),\ 0\leq\theta\leq\pi), \tag{VI.1.9}$$

$$\mathbf{t}\cdot\nabla V = 0 \qquad (r=F(\theta,t),\ 0\leq\theta\leq\pi), \tag{VI.1.10}$$

$$2\pi\int_0^\pi qF\left(F^2 + F_\theta^2\right)^{1/2}\sin(\theta)\,d\theta = Q\ . \tag{VI.1.11}$$

where $q(\theta,t)$ is the local surface charge density, $\mathbf{n}$ and $\mathbf{t}$ are the unit vectors normal and tangential to the drop surface, and $Q \equiv \tilde{Q}\ (\sigma 4\pi\varepsilon_m R^3)^{1/2}$ is the dimensionless net charge on the drop. The expansions of the unit vectors $\mathbf{n}$ and $\mathbf{t}$ about a spherical shape are presented Appendix A. The electric stress is defined in terms of the of the electric field $\mathbf{E} = -\nabla V$ as (Stratton 1941)

$$T_2^e \equiv \mathbf{EE} - \frac{1}{2}\,|\mathbf{E}|^2\mathbf{I} \qquad \text{(VI.1.13)}$$

where $\mathbf{I}$ is the identity tensor and $|\mathbf{E}|$ is the magnitude of $\mathbf{E}$. The component of this stress normal to the surface of the drop T_{n2}^e appears in the normal stress balance (VI.1.5) and couples together the flow field and electrostatic problems. The spatially uniform potential inside the conducting drop forces the electric stress T_1^e to be zero there.

The dynamical problem for the velocity and electrostatic potentials and the drop shape is solved for two types of initial conditions. First, we consider the case when drop motion due to the initial deformation satisfies conservation of mass and zero initial velocity

$$\frac{\partial F}{\partial t}\,(\theta,0) = 0, \qquad \text{(VI.1.14a)}$$

$$F(\theta,0) = 1 \pm \varepsilon\, P_2(\theta) - \frac{1}{5}\,\varepsilon^2 + \ldots\,, \qquad \text{(VI.1.14b)}$$

where prolate and oblate disturbances correspond to the positive and negative signs in the last equation. The second set of initial conditions studied are motions due to non-zero, but irrotational velocity fields and deformed drop shape

$$\frac{\partial F}{\partial t}\,(\theta,0) = g_1(\theta;\varepsilon) \neq 0, \qquad \text{(VI.1.15a)}$$

$$F(\theta,0) = g_2(\theta;\varepsilon). \qquad \text{(VI.1.15b)}$$

The scaling near the Rayleigh limit necessary to handle these two initial conditions is different.

VI.2 PERTURBATION SOLUTIONS NEAR RAYLEIGH LIMIT

The potential fields ($\phi(r,\theta,t)$, $V(r,\theta,t)$) and the drop shape $F(\theta,t)$ for moderate-amplitude motions are determined by constructing expansions in the amplitude of the deformation ε, as defined by the boundary conditions, for $\varepsilon<<1$. The solution procedure involves a combination of domain perturbations (Joseph 1973) and the method of multiple timescale expansions, as outlined in the previous chapter for the dynamics away from $Q = Q_c^{(2)}$. The singularity of the asymptotic equations, as this value of charge is approached, is readily seen from the results of the regular perturbation analysis in chapter V. First, as Q approaches $Q_c^{(2)}$ the linear frequency of the inviscid two-lobed oscillation $\omega_2 \equiv (4 - Q^2/4\pi)^{1/2}$ approaches zero. In this same limit, the asymptotic approximations for the second- and higher-order terms of the solution in a formal power series in ε become singular (for example see equations B3, B4 and B12, as well as expressions for G_{21}, G_{22}, and G_2 in Appendix B). This singularity is a manifestation of the multiplicity of solutions near $Q_c^{(2)}$ caused by the bifurcation to other static shape families. The local analysis must account for this multiplicity.

To remove this singularity we rescale the variables in ε so that this parameter also determines the relationship between the distance,

in terms of net charge from the Rayleigh limit, and the deformation of the drop. Then the new perturbation expansion will yield an explicit expression between Q and ε for constructing the bifurcating solution families. The proper scaling for each of the two initial conditions (VI.1.14) and (VI.1.15) and the analysis of these cases is outlined below.

VI.2a Dynamics of Drops with Zero Initial Velocity

When the net charge Q approaches the Rayleigh limit ($\omega_2 \to 0$) the dominant terms in the regular perturbation expansions described in chapter V behave as

$$F(\theta) \sim \sum_{n=1}^{\infty} H_n \varepsilon^n P_2(\theta) , \qquad \text{(VI.2.1a)}$$

$$\phi(\eta,\theta) \sim \sum_{n=1}^{\infty} G_n \varepsilon^n \eta^2 \omega_2 P_2(\theta), \qquad \text{(VI.2.1b)}$$

where the coefficients $\{H_n\}$ and $\{G_n\}$ are both $O(\omega_2^{2-2n})$ and the transformed radial coordinate η is defined below. The form of the series suggests that the appropriate scaling between the amplitude of the motion and the frequency is $\omega_2 \sim \varepsilon^{1/2}$, or $\omega_2 = (\kappa\varepsilon)^{1/2}$ where $\kappa = O(1)$ when the drop starts from rest with the initial conditions (VI.1.14).

This dependence of frequency on amplitude is valid only for a range of values for Q close to the Rayleigh limit given by

$$Q = 4\sqrt{\pi}\left(1 - \frac{\kappa}{16}\varepsilon - \ldots\right) \equiv Q^{(0)} + \varepsilon Q^{(1)} + \varepsilon^2 Q^{(2)} + \ldots \qquad \text{(VI.2.2)}$$

The method of multiple timescales is applied by assuming that the dependent variables are functions of two scales related to the actual time by $T_0 = t$ and $T_{1/2} = \varepsilon^{1/2} t$, and $\partial/\partial t$ is expressed as

$$\frac{\partial}{\partial t} = \frac{\partial}{\partial T_0} + \varepsilon^{1/2} \frac{\partial}{\partial T_{1/2}} \qquad \text{(VI.2.3)}$$

The expansion of the domain shape about a sphere is implemented by transforming the drop shape by $r \equiv \eta\, F(\theta,t)$ and expanding each variable in the form

$$\begin{bmatrix} F(\theta,t;\varepsilon) \\ \phi(r,\theta,t;\varepsilon) \\ V(r,\theta,t;\varepsilon) \end{bmatrix} = \sum_{k=0}^{\infty} \varepsilon^k \begin{bmatrix} F^{(k/2)}(\theta,T_0,T_{1/2}) \\ \phi^{[k/2]}(\eta,\theta,T_0,T_{1/2}) \\ V^{[k/2]}(\eta,\theta,T_0,T_{1/2}) \end{bmatrix}, \qquad \text{(VI.2.4)}$$

As in chapter V, each term in these expansions for the potentials is written as a sum of a contribution based on the spherical domain ($0 \leq \eta \leq 1$, $0 \leq \theta \leq \pi$) and terms that account for the deformation of the domain at each order of ε. The terms evaluated on the spherical domain are denoted by $\phi^{(k/2)}(\eta,\theta,T_0,T_{1/2})$ and calculated by the formulas given in chapter IV (see equation IV.2.3). Because of the appearance of the fractional powers of ε in the expansions (VI.2.4), the factorial term used in chapter V has been omitted so that perturbation equations of second or higher order given in Appendix B must be modified appropriately. The shape function $F(\theta,t)$ is independent of the radial coordinate, and its derivatives are simplified as $F^{[k/2]}(\theta,T_0,T_{1/2}) \equiv F^{(k/2)}(\theta,T_0,T_{1/2})$. We anticipate the form of the drop shape at each order in the expansion as a series of Legendre polynomials

$$F^{(k/2)}(\theta,T_0,T_{1/2}) = \sum_{m=0}^{\infty} \delta_m^{(k/2)}(T_0,T_{1/2})\, P_m(\theta) \quad . \qquad \text{(VI.2.5)}$$

Expressions for the mean curvature of the drop and the unit normal and

tangent vectors expanded in terms of ε are given in the Appendix of B with the drop shape at each order represented by equation (VI.2.5).

The static spherical drop is recovered as the leading order solution in the expansion (VI.2.4):

$$\begin{bmatrix} F^{(0)}(\theta,T_0) \\ \phi^{(0)}(\eta,\theta,T_0) \\ V^{(0)}(\eta,\theta,T_0) \end{bmatrix} = \begin{bmatrix} 1 \\ 0 \\ Q^{(0)}/\eta \end{bmatrix}, \qquad \text{(VI.2.6)}$$

where the arbitrary reference potentials inside the drop have been set to zero for the velocity and to $Q^{(0)}$ for the electric field.

The next non-trivial problem appears at $O(\varepsilon)$ and is given by equations (V.2.5) -(V.2.11) and (V.2.13)-(V.2.15) in the previous chapter, where only the expression for the conservation of charge (V.2.12) must be modified to account for the dependence of the net charge on the amplitude through equation (VI.2.2) above. This equation becomes

$$\int_0^{\pi} \left[\frac{\partial V^{(1)}}{\partial \eta} + F^{(1)} \frac{\partial^2 V^{(0)}}{\partial \eta^2} \right] \sin(\theta)\, d\theta = -2Q^{(1)} \quad (\eta=1). \qquad \text{(VI.2.7)}$$

The solution of this equation set as Q approaches $4\sqrt{\pi}$ from below is

$$\begin{bmatrix} F^{(1)}(\theta,T_0,T_{1/2}) \\ \phi^{(1)}(\eta,\theta,T_0,T_{1/2}) \\ V^{(1)}(\eta,\theta,T_0,T_{1/2}) \end{bmatrix} = \begin{bmatrix} A(T_{1/2})\, P_2(\theta) \\ 0 \\ Q^{(1)}/\eta + A(T_{1/2})P_2(\theta)Q^{(0)}/\eta^3 \end{bmatrix}, \qquad \text{(VI.2.8)}$$

where $A(T_{1/2})$ is the slowly varying amplitude of the motion which is determined along with $Q^{(1)}$ as part of the higher-order problem using the initial condition

$$A(0) = \pm 1 \quad , \tag{VI.2.9}$$

derived from equation (VI.1.14b). Here the positive sign gives a prolate perturbation and the negative sign an oblate one. The form of the solution (VI.2.8) can also be computed by taking the limit $\omega_2 \to 0$ of the result (V.2.16) of chapter V, but then the correct timescale is not recovered. It can also be predicted in advance that the correction to the velocity potential vanishes to first order, because the characteristic timescale for the motion approaches infinity in this limit.

The variables defining the correction at $O(\varepsilon^{3/2})$ are governed by the equation set

$$\nabla^2 \phi^{(3/2)} = 0 \qquad (0 \leqq \eta \leqq 1,\ 0 \leqq \theta \leqq \pi), \tag{VI.2.10}$$

$$\frac{\partial \phi^{(3/2)}}{\partial \eta} = 0 \qquad (\eta = 0,\ 0 \leqq \theta \leqq \pi), \tag{VI.2.11}$$

$$\frac{\partial \phi^{(3/2)}}{\partial \eta} = \frac{\partial F^{(3/2)}}{\partial T_0} + \frac{\partial F^{(1)}}{\partial T_{1/2}} \qquad (\eta = 1,\ 0 \leqq \theta \leqq \pi), \tag{VI.2.12}$$

$$\frac{\partial \phi^{(3/2)}}{\partial T_0} - \frac{1}{4\pi} \frac{\partial V^{(0)}}{\partial \eta} \left[\frac{\partial V^{(3/2)}}{\partial \eta} + F^{(3/2)} \frac{\partial^2 V^{(0)}}{\partial \eta^2} \right] = -4F^{(3/2)} \qquad (\eta = 1,\ 0 \leqq \theta \leqq \pi), \tag{VI.2.13}$$

$$\int_0^{\pi} F^{(3/2)}(\theta, t) \sin(\theta)\, d\theta = 0, \tag{VI.2.14}$$

$$\nabla^2 V^{(3/2)} = 0 \qquad (1 \leqq \eta \leqq \infty,\ 0 \leqq \theta \leqq \pi), \tag{VI.2.15}$$

$$V^{(3/2)} \to 0 \qquad (\eta \to \infty,\ 0 \leqq \theta \leqq \pi), \tag{VI.2.16}$$

$$\int_0^{\pi} \left[\frac{\partial V^{(3/2)}}{\partial \eta} + F^{(3/2)} \frac{\partial^2 V^{(0)}}{\partial \eta^2} \right]_{\eta=1} \sin(\theta)\, d\theta = -2Q^{(3/2)} \quad , \tag{VI.2.17}$$

$$\frac{\partial V^{(3/2)}}{\partial \theta} + \frac{\partial F^{(3/2)}}{\partial \theta} \frac{\partial V^{(0)}}{\partial \eta} = 0 \qquad (\eta = 1,\ 0 \leqq \theta \leqq \pi), \tag{VI.2.18}$$

$$F^{(3/2)}(\theta,0,0) = 0 \qquad (0\leqq\theta\leqq\pi), \tag{VI.2.19}$$

$$\frac{\partial F^{(3/2)}}{\partial T_0}(\theta,0,0) + \frac{\partial F^{(1)}}{\partial T_{1/2}}(\theta,0,0) = 0 \qquad (0\leqq\theta\leqq\pi). \tag{VI.2.20}$$

The solution to equations (VI.2.10)-(VI.2.20) is calculated as

$$\begin{bmatrix} F^{(3/2)}(\theta,T_0,T_{1/2}) \\ \phi^{(3/2)}(\eta,\theta,T_0,T_{1/2}) \\ V^{(3/2)}(\eta,\theta,T_0,T_{1/2}) \end{bmatrix} = \begin{bmatrix} 0 \\ B(T_{1/2}) + \frac{1}{2}\frac{dA}{dT_{1/2}} P_2(\theta)\ \eta^2 \\ 0 \end{bmatrix}, \tag{VI.2.21}$$

where $B(T_{1/2})$ is unknown and is determined from the solution of the next non-trivial problem. Equation (VI.2.20) gives the second initial condition on the function $A(T_{1/2})$ as

$$\frac{dA}{dT_{1/2}}(0) = 0. \tag{VI.2.22}$$

The appearance of the first nonzero correction to the velocity potential at this order of approximation, as well as the form of solution in (VI.2.21), can be anticipated from the $O(\varepsilon)$ solution valid away from the Rayleigh limit and from the correct timescale valid in the inner region where $Q \to Q_c^{(2)}$.

The equation set that governs the variables at $O(\varepsilon^2)$ is lengthy because of the many non-homogenous terms generated by the domain perturbation at this order. These equations are given in a somewhat different form in Appendix B. The differences are due to (a) the 2! used in the definition of the series expansion used in chapter V is not included here, (b) the different scaling on time arising near the Rayleigh limit which introduces the additional terms $\partial F^{(3/2)}/\partial T_{1/2}$ in equation (B3) and $\partial\phi^{(3/2)}/\partial T_{1/2}$

in (B4), and (c) the dependence of the net charge on ε which leads to the terms $-Q^{(0)}Q^{(1)}F^{(1)}/2\pi$ in (B4), $-2Q^{(1)}(\partial F^{(1)}/\partial\theta)$ in (B9), and $-2Q^{(2)}$ in the right-hand side of (B8). The solution to this equation set is found by expanding the potentials $(\phi^{(2)}, V^{(2)})$ in Legendre polynomials and powers of η as

$$\begin{bmatrix} \phi^{(2)}(\eta,\theta,T_0,T_{1/2}) \\ V^{(2)}(\eta,\theta,T_0,T_{1/2}) \end{bmatrix} = \sum_{m=0}^{\infty} P_m(\theta) \begin{bmatrix} \gamma_m(T_0,T_{1/2})\eta^m \\ \beta_m(Q,T_0,T_{1/2})\eta^{-m-1} \end{bmatrix}, \quad \text{(VI.2.23)}$$

which satisfy the field equations and boundary conditions everywhere except on the drop surface. Substituting the forms (VI.2.23) and (VI.2.5) into the normal stress and kinematic conditions for the $O(\varepsilon^2)$ problem yields differential equations for the coefficients in the corrections to the velocity potential and drop shape, $\{\gamma_m\}$ and $\{\delta_m\}$, respectively, as

$$\sum_{m=0}^{\infty} \left[\frac{d\gamma_m}{dT_0} + (m-1)(m+2 - \frac{Q^{(0)2}}{4\pi}) \gamma_m \right] = -\frac{dB}{dT_{1/2}}$$

$$+ \frac{Q^{(1)2}}{8\pi} + c\frac{Q^{(0)}}{4\pi} - \frac{1}{2}\frac{d^2A}{dT_{1/2}^2} P_2(\theta)$$

$$+ 2\frac{Q^{(0)}Q^{(1)}}{4\pi} A(T_{1/2}) P_2(\theta)$$

$$+ A(T_{1/2})^2 \left[-\frac{4}{5} + \frac{12}{7} P_2(\theta) + \frac{144}{35} P_4(\theta) \right], \quad \text{(VI.2.24)}$$

and

$$\sum_{m=0}^{\infty} \left(m\gamma_m - \frac{d\delta_m}{dT_0} \right) P_m(\theta) = 0, \quad \text{(VI.2.25)}$$

where c is an integration constant. The solvability conditions for this

differential equation set yields the evolution equation for the slowly varying amplitude $A(T_{1/2})$

$$\frac{d^2A}{dT_{1/2}^2} + \kappa A - \frac{24}{7} A^2 = 0 \quad , \qquad \text{(VI.2.26)}$$

with the initial conditions (VI.2.9) and (VI.2.22). This amplitude equation differs from the result of the standard nonlinear stability analyses valid in the vicinity of the critical wavelength in the liquid jet and Rayleigh-Taylor problems (Kiang 1969; Nayfeh 1970). The A^2 term arises from the spherical geometry instead of the term A^2A^*, where A^* is the complex conjugate of A, which appears in the other studies. The second derivative of the modulating amplitude in equation (VI.2.26) is expected because of the direct resonance between the $P_2(\theta)$ terms at different orders of ε (Akylas and Benney 1980).

Equation (VI.2.26) is integrated once to give

$$\left(\frac{dA}{dT_{1/2}} \right)^2 = - (A \pm 1) \left[-\kappa (A \pm 1) + \frac{16}{7} (A^2 \pm A + 1) \right]. \qquad \text{(VI.2.27)}$$

Static drop shapes are given by the roots of the polynomial on the right-hand side of the expression, depending on whether Q is less than ($\kappa>0$) or greater than ($\kappa<0$) the Rayleigh limit. The family of spherical shapes corresponds to the stationary point A = 0 for all values of κ (charge). As predicted by Taylor's analysis and shown schematically in figure VI.0.1, prolate static forms exist for $A = 7\kappa/24$ and $\kappa > 0$ or values of $Q < 4\sqrt{\pi}$. Oblate forms are possible for $\kappa < 0$ and are given by the root $A = 7\kappa/24$.

The stability of the static shapes follows from a phase-plane analysis of equation (VI.2.27); plots of $A'(T_{1/2})$ versus $A(T_{1/2})$ are shown in figure VI.2.1 for fixed values of κ greater than (figure VI.2.1A) and

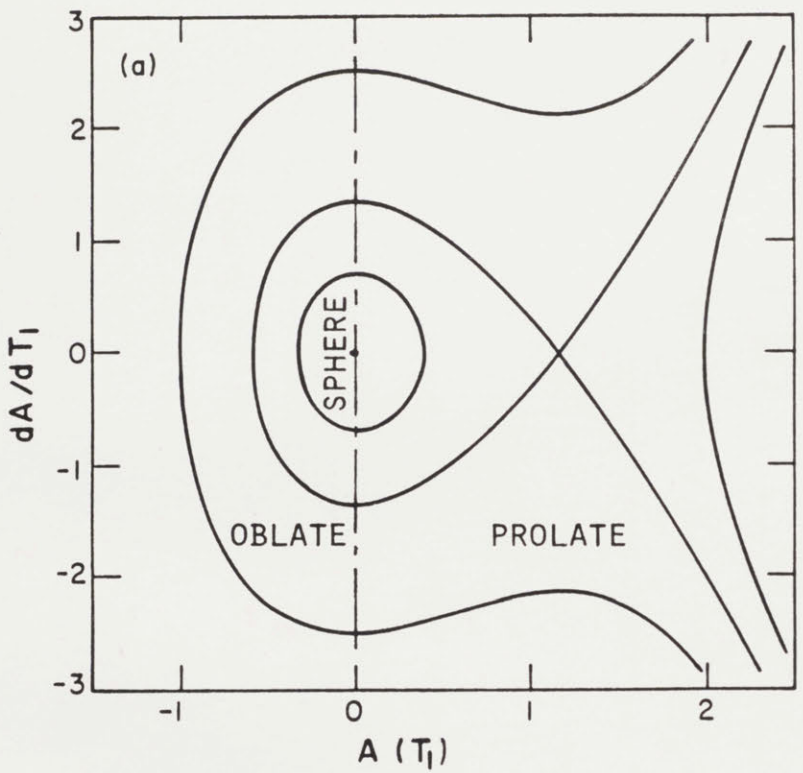

$\kappa = 4.0$

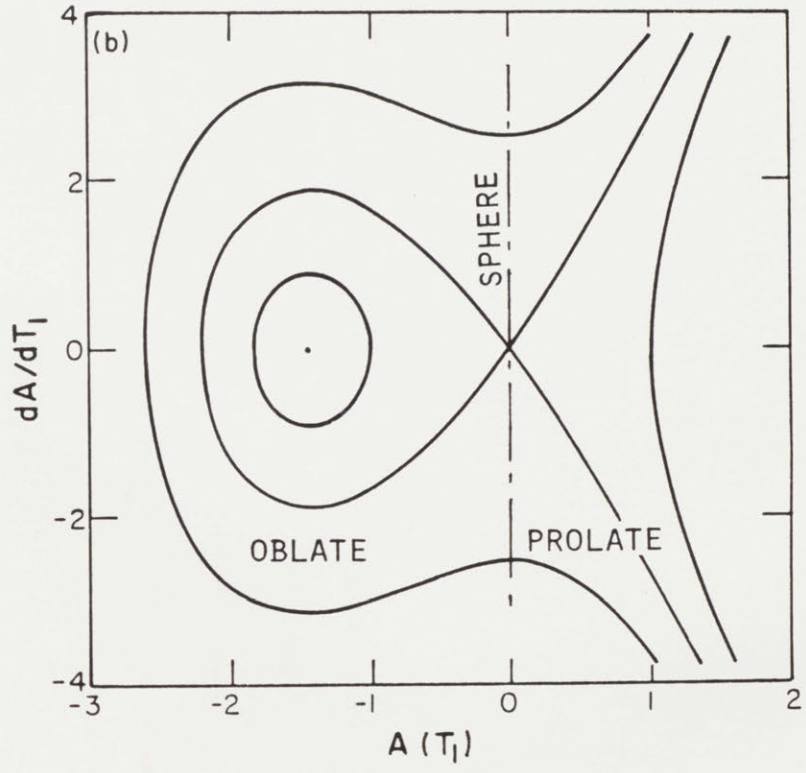

$\kappa = -5.0$

Figure VI.2.1 Phase-plane diagrams for the amplitude modulation function $A(T_{1/2})$ for (a) $\kappa>0$ and (b) $\kappa<0$.

less than (figure VI.2.1B) zero. For small amplitude perturbations, the spherical form $(A,A') = (0,0)$ is a stable center for $\kappa > 0$ and a saddle point for $\kappa < 0$. The oblate static shapes $(A,A') = (7\kappa/24,0)$, $\kappa < 0$, are stable centers and the prolate forms $(A,A') = (7\kappa/24,0)$, $\kappa > 0$, are saddle points. These results agree with bifurcation analysis of only the static forms.

The nonlinear dynamic analysis predicts the stability of the spherical forms to moderate amplitude perturbations. It follows from equation (VI.2.27) that spherical shapes with initial disturbances of magnitude $-7\kappa/48 < A(0) < 7\kappa/24$ evolve along orbits inside the separatrix for this particular positive value of κ and are stable. The drop oscillates between prolate and oblate forms during each period of oscillation. Initial disturbances outside the separatrix lead eventually to drop breakup through a succession of prolate configurations. The oblate shapes are predicted to be stable for $\kappa < 0$ for initial shape perturbations satisfying $7\kappa/16 < A(0) < 0$, where the resulting oscillations are restricted to oblate forms. Shape perturbations leading to either slightly prolate or highly deformed oblate drop shapes cause instability through a sequence of elongating prolate forms, (see Tsamopoulos et al. 1984).

The form of the amplitude modulation caused by the direct resonance near the Rayleigh limit for the stable motions about the sphere is calculated exactly as the solution of equation (VI.2.27). For $\kappa \geq 24/7$ and $A(0) = +1$, the third-order polynomial in A on the right hand side of equation (VI.2.27) has three real roots ρ_i which satisfy the inequalities

$$-1 < \rho_1 \leq -1/2 < \rho_2 \leq 7\kappa/24 \leq \rho_3 \leq 7\kappa/16 \quad ,$$

where $\rho_2 = 1$. Then the stable solution of (VI.2.27) is

$$A(T_{1/2}) = \rho_1 + (\rho_2 - \rho_1)\, sn^2(\tau\ ;\ k), \qquad \text{(VI.2.28)}$$

$$\tau \equiv 2[(\rho_3 - \rho_1)/7]^{1/2}\, T_{1/2}\ , \quad k \equiv (\rho_2 - \rho_1)/(\rho_3 - \rho_1), \qquad \text{(VI.2.29)}$$

where sn is the Jacobi elliptic function (Abramowitz and Stegun 1964). According to equation (VI.2.28), amplitude modulation occurs between the two smaller roots ρ_1 and ρ_2. Equation (VI.2.28) also holds when $\kappa \geqq 48/7$ and $A(0) = -1$, but the roots follow the inequalities

$$-1 = \rho_1 < 1 < \rho_2 \leqq 2 \leqq 7\kappa/24 \leqq \rho_3 \leqq 7\kappa/16\ .$$

These two cases for the roots of the polynomial correspond to the same physical picture of drop oscillation.

The last case arises when $\kappa < -24/7$ and $A(0) = -1$ and leads to quite different results. The roots of the polynomial obey the inequalities

$$7\kappa/16 < \rho_1 < 7\kappa/24 \leqq \rho_2 < 1/2 \leqq -7\kappa/48 < \rho_3 < 1,$$

where $\rho_2 = -1$. The initial amplitude $A(0) = -1$ is exactly stationary for $\kappa = -24/7 \cong -3.4286$ and the stable oscillations of $A(T_{1/2})$ are described by equation (VI.2.28) for κ less than this value. This stationary point corresponds to a static oblate shape existing for $Q > 4\sqrt{\pi}$. The stable oscillations of the amplitude $A(T_{1/2})$ with time is shown in figure VI.2.2 for $A(0) = +1$ and values of $\kappa > \kappa_c \equiv +24/7$. Away from κ_c the motion resembles the simple sinusoidal oscillation between prolate and oblate forms expected from the regular perturbation analysis of the previous chapter. The period of the motion increases as κ approaches κ_c and the drop spends more time in the prolate form. The evolution of an initially

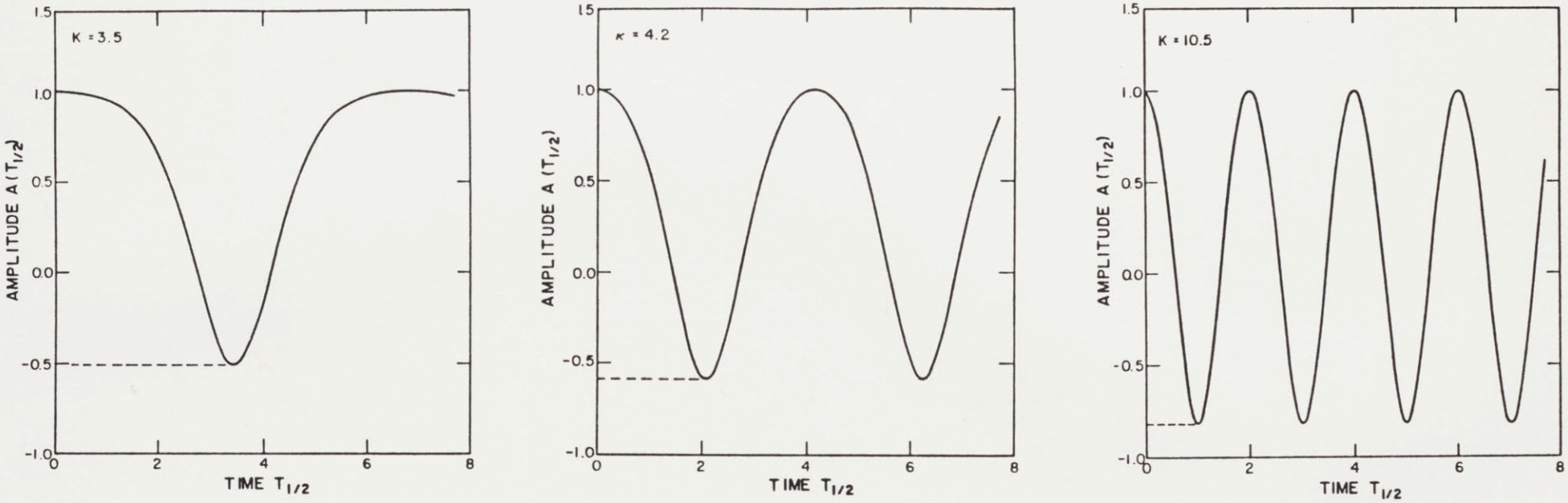

Figure VI.2.2 Evolution of amplitude function A for stable drop oscillation plotted as a function of the slow time scale $T_{1/2}$ for three values of κ.

prolate perturbation (A(0) = +1) for drops with $\kappa < \kappa_c$ is shown in figure VI.2.3. The deformation of the drop grows slowly until a point where it suddenly increases almost exponentially in time. The perturbation analysis ceases to be valid when the deformation becomes large. The pause before the exponential increase is larger for κ closer to κ_c.

The bounds given by equation (VI.2.27) on the amplitude of the initial perturbation for stable oscillation about a spherical drop for Q close to $Q_c^{(2)}$ can be rewritten in terms of equation (VI.2.2) as a correction to the Rayleigh limit for loss-of-stability of a spherical form. Then

$$Q^{(1)} = -\frac{6\sqrt{\pi}}{7} , \qquad \text{(VI.2.30)}$$

indicating that finite amplitude prolate disturbances destabilize the drop, whereas the drop is more stable to oblate perturbations. The nonzero coefficient at $O(\varepsilon)$ in equation (VI.2.2) also confirms the transcritical bifurcation. The increased stability of the oblate forms is caused by two effects. First, the surface area for the oblate shapes is larger than that for a prolate form with the same amount of deformation, so that the effective surface charge density is lower. Also, the Coulomb forces associated with surface charge along the equator of an oblate spheroid are smaller than those produced at the poles of a prolate form by a similar net charge density.

The complete solution of the $O(\varepsilon^2)$ problem includes terms introduced through the nonlinear coupling to lower orders in ε and is computed by the procedure outlined in chapter V. These results are

$$F^{(2)}(\theta, T_0, T_{1/2}) = -\frac{1}{5} A(T_{1/2}) + \frac{24}{35} [\, A(T_{1/2})^2 - \cos(2T_0\sqrt{6})\,] P_4(\theta),$$

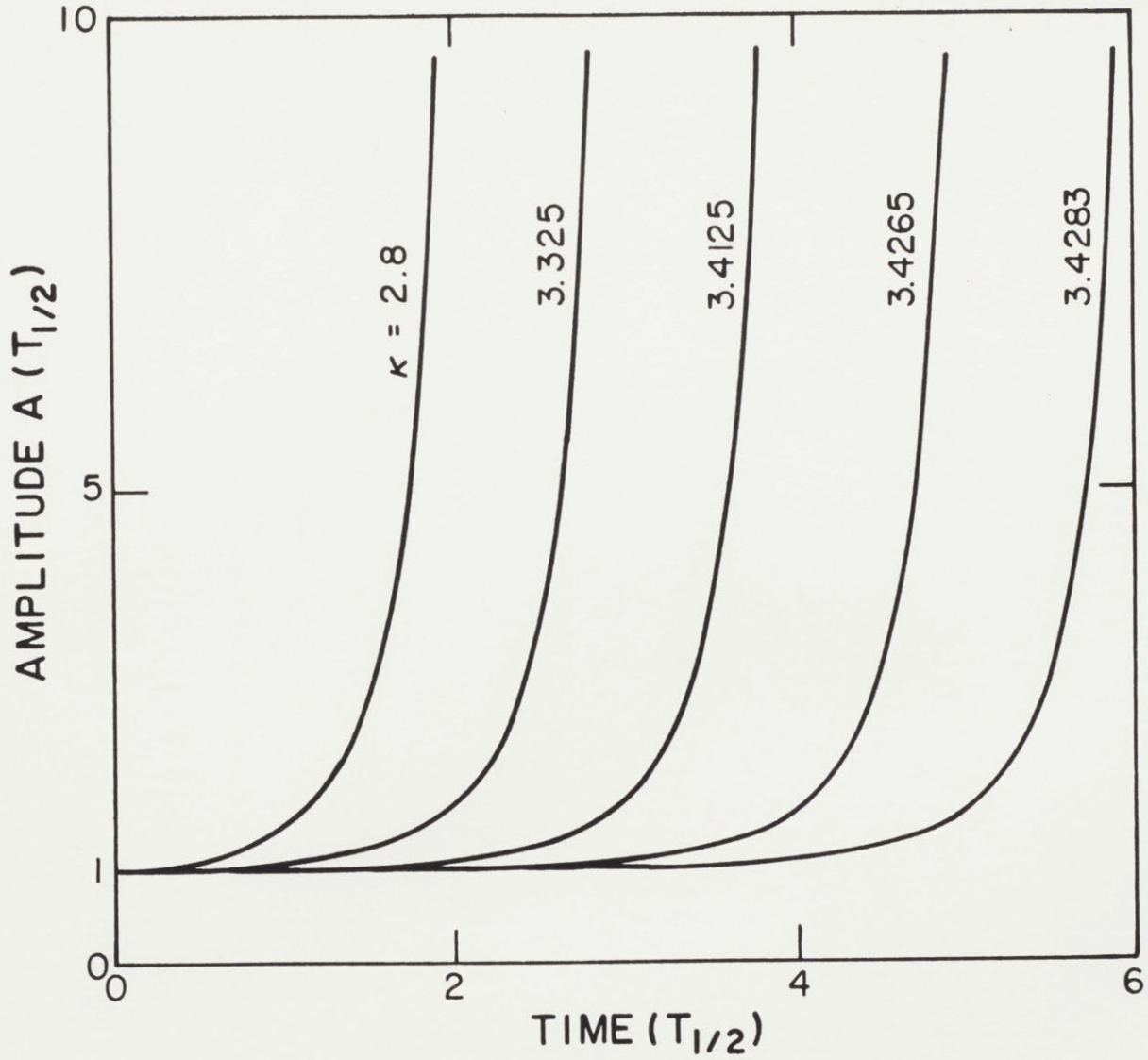

Figure VI.2.3 Evolution of amplitude function A for unstable drop motion plotted as a function of the slow time scale $T_{1/2}$ for several values of κ.

$$\phi^{(2)}(\eta,\theta,T_0,T_{1/2}) = \frac{12}{35}\sqrt{6}\,\sin(2T_0\sqrt{6})\,\eta^4\,P_4(\theta)\,, \qquad \text{(VI.2.31)}$$

$$V^{(2)}(\eta,\theta,T_0,T_{1/2}) = \frac{Q^{(2)}}{\eta} + \left[\frac{4}{7}Q^{(0)}A(T_{1/2}) + Q^{(1)}\right]A(T_{1/2})\,\eta^{-3}\,P_2(\theta)$$

$$+ \frac{12}{7}Q^{(0)}\left[A(T_{1/2})^2 - \frac{2}{5}\cos(2T_0\sqrt{6})\right]\eta^{-5}\,P_4(\theta),$$

where $Q^{(2)}$ must be computed from the solvability condition at $O(\varepsilon^3)$. The solution at $O(\varepsilon^2)$ is completed by calculating the constant $B(T_{1/2})$ in the velocity potential (see equation (VI.2.21)) from the equation

$$\frac{\partial B}{\partial T_{1/2}} = \frac{Q^{(2)}}{\sqrt{\pi}} + \frac{Q^{(1)^2}}{8\pi} - \frac{6}{5}A(T_{1/2})^2\,. \qquad \text{(VI.2.32)}$$

The calculation of $Q^{(2)}$ from the third order dynamical problem is very involved because the $O(\varepsilon^{5/2})$ and $O(\varepsilon^3)$ problems must be computed. This constant can also be computed from a straight forward bifurcation analysis (e.g. see Brown and Scriven 1980a and Ungar and Brown 1982) of only the static forms carried out to $O(\varepsilon^3)$. The equation set for the static forms is simply equations (VI.1.1)-(VI.1.13) without the time dependence for either the field variables or drop shape. Then the perturbation method is completely regular in powers of the amplitude ε of the drop deformation and the forms valid to $O(\varepsilon^2)$ for the prolate and oblate shapes are computed as

$$F(\theta;\varepsilon) = 1 + \varepsilon\,P_2(\theta) + \varepsilon^2\left[-\frac{1}{5} + \frac{24}{35}P_4(\theta)\right] + O(\varepsilon^3)\,, \qquad \text{(VI.2.33a)}$$

$$V(\eta,\theta;\varepsilon) = \frac{Q^{(0)}}{\eta} + \varepsilon\left[\frac{Q^{(1)}}{\eta} + \frac{Q^{(0)}}{\eta^3}P_2(\theta)\right] + \varepsilon^2\left\{\frac{Q^{(2)}}{\eta} + \right.$$

$$\left.\frac{1}{\eta^3}\left[\frac{4}{7}Q^{(0)} + Q^{(1)}\right]P_2(\theta) + \frac{12Q^{(0)}}{7\eta^5}P_4(\theta)\right\} + O(\varepsilon^3), \qquad \text{(VI.2.33b)}$$

$$Q(\varepsilon) = 4\sqrt{\pi} - \varepsilon \frac{6\sqrt{\pi}}{7} + \varepsilon^2 \frac{363}{490}\sqrt{\pi} + O(\varepsilon^3) , \qquad \text{(VI.2.33c)}$$

where $Q^{(2)} = (363\sqrt{\pi})/490$ in equations (VI.2.31) and (VI.2.32).

The drop shapes predicted by the $O(\varepsilon^2)$ solution for the breakup of a sphere perturbed by a prolate deformation with $\varepsilon = 0.3$ are shown in figure VI.2.4 for $\kappa = 3.4125 < \kappa_c$. The shape slowly elongates, developing a neck, before it breaks into two drops with one or more satelite drops. This evolution is independent of whether the initial perturbation is prolate or oblate. For unstable oblate forms at $T_0 = 0$, the drop first evolves to a prolate form before following this path. The actual prediction of the number and size of the fission products formed by Rayleigh breakup involves understanding the fluid mechanics for drops with thin necks. Viscous forces will eventually become important for these forms and a rigorous theory must account for their effect.

The fact that the asymptotic series formed from the expansion (VI.2.4) are the inner solutions to the regular expansion given in chapter V is easily seen by taking the appropriate limits of the amplitude function $A(T_{1/2})$ computed with $A(0) = +1$:

$$\lim_{\substack{\kappa \to \infty \\ k \to 0}} A(T_{1/2}) \sim \cos\left(4 - Q^{(0)^2}/4\pi\right)^{1/2} T_0,$$

$$\lim_{\substack{\kappa \to -\infty \\ k \to 0}} A(T_{1/2}) \sim \cosh\left(-4 + Q^{(0)^2}/4\pi\right)^{1/2} T_0 .$$

where κ and k are defined by equations (VI.2.2) and (VI.2.29), respectively. These forms agree with those of the outer expression as the Rayleigh limit is approached.

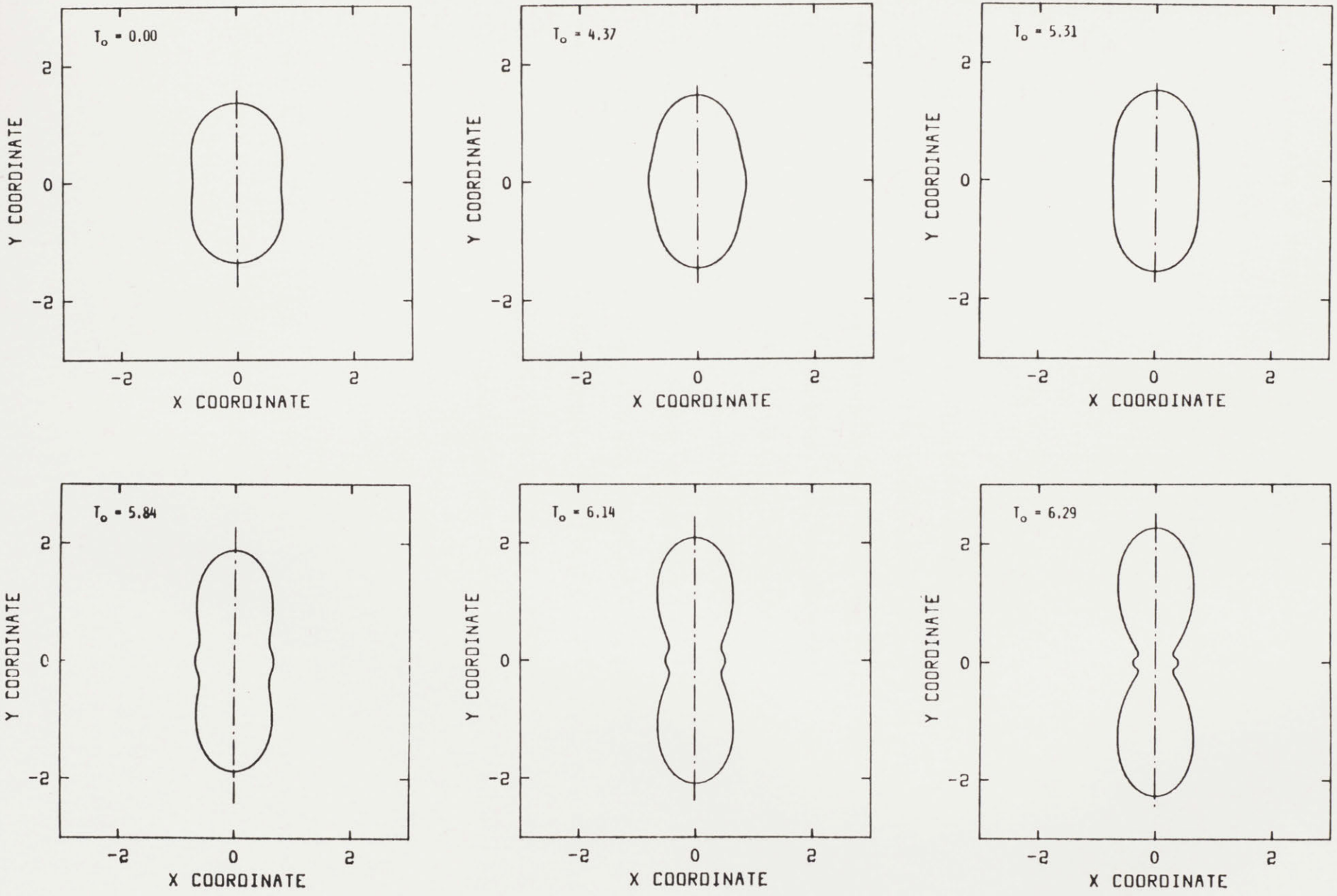

Figure VI.2.4 Evolution of unstable drop initially perturbed by a prolate perturbation with $\kappa = 3.4125$ and $\varepsilon = 0.3$.

VI.2b Dynamics of Drops with Nonzero Initial Velocity

The dominant terms as $\omega_2 \to 0$ in a regular perturbation solution for perturbations with nonzero initial velocity behave as

$$F(\theta) \sim 1 + \sum_{n=1}^{\infty} H_n \, \varepsilon^n \, P_2(\theta), \qquad \text{(VI.2.34a)}$$

$$\phi(\eta,\theta) \sim 1 + \sum_{n=1}^{\infty} G_n \, \varepsilon^n \, \eta^2 \, \omega_2 \, P_2(\theta), \qquad \text{(VI.2.34b)}$$

where the coefficients $\{H_n\}$ and $\{G_n\}$ scale as $O(\omega_n^{2-3n})$. This form suggests that the appropriate scaling for the frequency is $\omega_2 \sim \varepsilon^{1/3}$ or $\omega_2 = (\kappa\varepsilon)^{1/3}$, where $\kappa = O(1)$. The slow timescale for these initial conditions is $T_{1/3} = \varepsilon^{1/3} t$. This rescaling indicates that the nonlinear dynamics leading to breakup will take place in a shorter time, which is not a surprising result since the additional kinetic energy contained in the velocity perturbation is available to aid for the process.

The perturbation problems occuring in an analysis like the one described in section VI.2a will involve terms of orders $\varepsilon^{2/3}$, $\varepsilon^{4/3}$, etc., and result in a correction to the Rayleigh limit of the form $Q = 4\sqrt{\pi} + \varepsilon^{2/3} Q_1 + \ldots$. The initial conditions on the modulating amplitude $A(T_{1/3})$ are of the form

$$\frac{dA}{dT_{1/3}}(0) = g_1(\theta;\varepsilon) \neq 0, \qquad A(0) = 1, \qquad \text{(VI.2.35)}$$

where the initial fluid motion described by $g_1(\theta;\varepsilon)$ is irrotational. Apart from these changes, the analysis will be identical.

VI.3 FINITE ELEMENT ANALYSIS OF STATIC SHAPES

VI.3a Methodology

The region of validity of the perturbation results presented in the previous Section was established by comparing the static drop shapes predicted by equations (VI.2.33) to results of finite element calculations. The shape of electrostatic stationary drops and the electric potential in the outer medium described by the equation set (VI.1.5) - (VI.1.13) are calculated by the Galerkin finite element method. This method was originally developed by Ettouney and Brown (1983) for solving free-boundary problems and implemented by Beris et al. (1984) for the creeping flow of a sphere in a Bingham fluid and also by Adornato and Brown (1983) for the shape and stability of electrostatically levitated drops. In this approach, the equations governing the static shape and electrostatic potential are transformed to a fixed finite domain, where the finite element approximation to the potential is formulated. The far-field boundary condition (equation (VI.1.8)) is replaced with the approximation to the potential at a large radius R_∞ from the drop surface

$$V(R_\infty, \theta) = \frac{Q}{R_\infty} \quad , \tag{VI.3.1}$$

which slightly affects the static problem if the drop is not very deformed. The free-boundary problem defined on ($F(\theta) \leq r \leq R_\infty$, $0 \leq \theta \leq \pi$) is transformed using the mapping

$$\xi = [r - F(\theta)] \; / \; [R_\infty - F(\theta)] \; , \tag{VI.3.2}$$

to a fixed domain ($0 \leq \xi \leq 1$, $0 \leq \theta \leq \pi$) which is divided into quadrilateral

subdomains or elements. The potential $\hat{V}(\xi,\theta)=V(r,\theta)$ and the drop shape $F(\theta)$ are approximated in terms of Lagrangian biquadratic $\{\Psi_i(\xi,\theta)\}$ or quadratic $\{\Phi_i(\theta)\}$ basis functions, respectively. The details of these bases are given in Ettouney and Brown (1983) and in standard finite element texts, (Strang and Fix (1973)). The finite element representations are

$$\hat{V}(\xi,\theta) = \sum_{i=1}^{N_i} \alpha_i \Psi_i(\xi,\theta) + V_0 \sum_{i=1}^{N_S} \Psi_i(\xi,\theta) + \sum_{i=1}^{N_S} \alpha_i^0 \Psi_i(\xi,\theta), \quad \text{(VI.3.3a)}$$

$$F(\theta) = \sum_{i=1}^{N_S} \beta_i \Phi_i(\theta) \quad \text{(VI.3.3b)}$$

where the coefficients $\{\alpha_i\}$ and $\{\beta_i\}$ are to be determined and the $\{\alpha_i^0\}$ are the interpolated values of the far-field condition (VI.3.1). The total number of quadratic basis functions defined on each of the boundaries at $\xi=0$ and $\xi=1$ is N_S and the number of functions defined on the rest of the domain is N_i. The splitting of the expansion for $\hat{V}(\xi,\theta)$ used in (VI.3.3a) is a convenient method of accounting for the constant, but unknown potential V_0 and the boundary condition (VI.3.1). The normal stress balance (VI.1.5) is distinguished as the equation for determining the drop shape and the unknowns $\mathbf{X}^t = \{\boldsymbol{\alpha}, \boldsymbol{\beta}, V_0, \Delta P_0\}^t$ are determined by solving the nonlinear algebraic equations that result from the Gelerkin weighted residual equations of (VI.1.5) - (VI.1.13). These are

$$\int_v \nabla V \cdot \nabla \Psi_i \, dv = 0, \qquad i = 1,\ldots,N_i, \quad \text{(VI.3.4)}$$

$$\int_0^{\pi} \{[FF_\theta \Phi_{i,\theta} + \Phi_i(2F^2 + F_\theta^2)]/(F^2 + F_\theta^2)^{1/2} - F^2\Phi_i[\Delta P_0 + (\mathbf{n}\cdot\nabla\hat{V})^2/8\pi]\}$$

$$\sin(\theta)\, d\theta = 0, \qquad i = 1,\ldots,N_S, \quad \text{(VI.3.5)}$$

along with the integral constraints for volume (VI.1.6) and charge (VI.1.11)

through which the static pressure difference ΔP_0 and the constant drop potential V_0, respectively, are calculated. The symmetry around the axis and the vanishing of the N_i basis functions $\Psi_i(\xi,\theta)$ at $\xi=0$ and $\xi=1$ have been used in the derivation of (VI.3.4) and (VI.3.5). If a plane of symmetry exists, the computational domain can be cut in half ($0 \leqq \theta \leqq \pi/2$). Starting with a first approximation to the solution vector $\mathbf{X}^{(0)}$ these (N_i+N_s+2) algebraic equations, written in condensed form as $\mathbf{R}(\mathbf{X};\ Q)$, are solved by Newton's method, which converges iteratively according to the sequence

$$\mathbf{X}^{(i+1)} = \mathbf{X}^{(i)} + \boldsymbol{\delta}^{(i+1)} \quad , \tag{VI.3.6}$$

where $\boldsymbol{\delta}^{(i+1)}$ is the solution of

$$\mathbf{J}(\mathbf{X}^{(i)})\ \boldsymbol{\delta}^{(i+1)} = -\ \mathbf{R}(\mathbf{X}^{(i)};\ Q) \quad , \tag{VI.3.7}$$

and $\mathbf{J}$ is the Jacobian matrix, i.e. $J_{ij}=\partial R_i/\partial X_j$. Equation (VI.3.7) is solved by Gaussian elimination by implementing a so-called arrow routine (Ettouney and Brown). Newton's method has several advantages over the more simply formulated techniques for solving these equations. Besides the rapid convergence to a solution, the Jacobian matrix used in (VI.3.7) is the basis of computer implemented perturbation methods for tracking families of solutions and for detecting multiple solutions in terms of variations of in one or more parameters.

Intersections between two families of static shapes (simple bifurcation points) in the parameter space are signalled by a singular Jacobian matrix of the converged solution and are easily detected by checking the sign of the determinant of $\mathbf{J}$, which changes upon crossing a simple bifurcation

point. The methods used to force the finite element algorithm to converge to the new bifurcating solution family include the discretization of existing approximate solution and the null vector calculation close to the bifurcation point. The relative stability of multiple solutions is determined directly from the structure of the bifurcating families (Ioos and Joseph 1980). As described by Ungar and Brown (1982), changes in stability of the drop shapes can also occur at a limit point where a single family reverses direction in terms of a parameter. These points on the solution family are determined by the criteria for a vertical tangent ($\partial X_i/\partial Q$) of the field variables with respect to the surface charge. A new monotonically increasing parameter analogous to the arc-length of the solution curve is introduced. The vector of unknowns is augmented by the parameter being varied along a shape family (the net charge Q for this problem) and the equation set is augmented by adding the constraint

$$R_{N_i+N_s+3} = \|\mathbf{X} - \mathbf{X_0}\|^2 + (Q - Q_0)^2 - (S - S_0)^2 = 0 , \qquad \text{(VI.3.8)}$$

In this equation S_0 is an arbitrary reference value for the arc-length at a regular and close to the limit point solution ($\mathbf{X_0}$, Q_0). Keller (1977) has shown that the Jacobian matrix of the augmented equation set is regular in the vicinity of the limit point.

VI.3b Implementation and results

The location of the unknown boundary in the mathematical problem is moved to $R_\infty = 12$ in all the calculations presented here. Finite element meshes of 8 azimuthal and 20 radial Lagrangian biquadratic elements were used for the solution of the transformed field equations on the region

($0 \leq \xi \leq 1$; $0 \leq \theta \leq \pi/2$) for shapes in the two-lobed and four-lobed families. This discretization yielded a system of 682 nonlinear algebraic equations. The elements were graded radially toward the surface of the drop for better approximation to the potential gradients there. Shapes in the three-lobed family were computed using 16 elements distributed uniformly in the azimuthal direction ($0 \leq \theta \leq \pi$) and 1322 total equations.

The accuracy of the finite element approximations was determined by computing the values of Q for the lowest four bifurcation points between the family of spheres and multi-lobed static forms. The results are presented in Table VI.3.1 with the exact results from Rayleigh's analysis. The finite element results are in very good agreement, as have been the previous calculations of these critical points (Basaran and Scriven 1981; Adornato and Brown 1983).

The families of static shapes evolving from the first three bifurcation points are represented in figure VI.3.1 by the component of the corresponding bifurcating mode in the computed shape. In this projection, the transcritical bifurcation of the prolate and oblate shapes is approximated very well by the asymptotic analysis. The three-lobed forms bifurcate supercritically (to higher values of Q) from the spheres. The stability of the static shapes to small amplitude disturbances follows from elementary ideas about the connections between bifurcation and linear dynamical analyses. Since the spheres are stable for $Q < 4\sqrt{\pi}$, the oblate forms are stable and the prolate ones unstable as computed in the dynamical analysis above. The three- and four-lobed shapes are all unstable. All bifurcations of even-lobed shape families will be transcritical and all odd-lobed families will be either sub- or supercritical because of the mode coupling

Table VI.3.1 Comparison of critical values of charge computed by finite element analysis with exact solution to linear problem.

Bifurcating Shape Family	Exact Value of Q	Finite Element Calculation	Relative Error
Two-Lobed	7.090	7.095	0.0007
Three-Lobed	7.927	7.936	0.0011
Four-Lobed	8.683	8.697	0.0016
Five-Lobed	9.379	9.400	0.0022

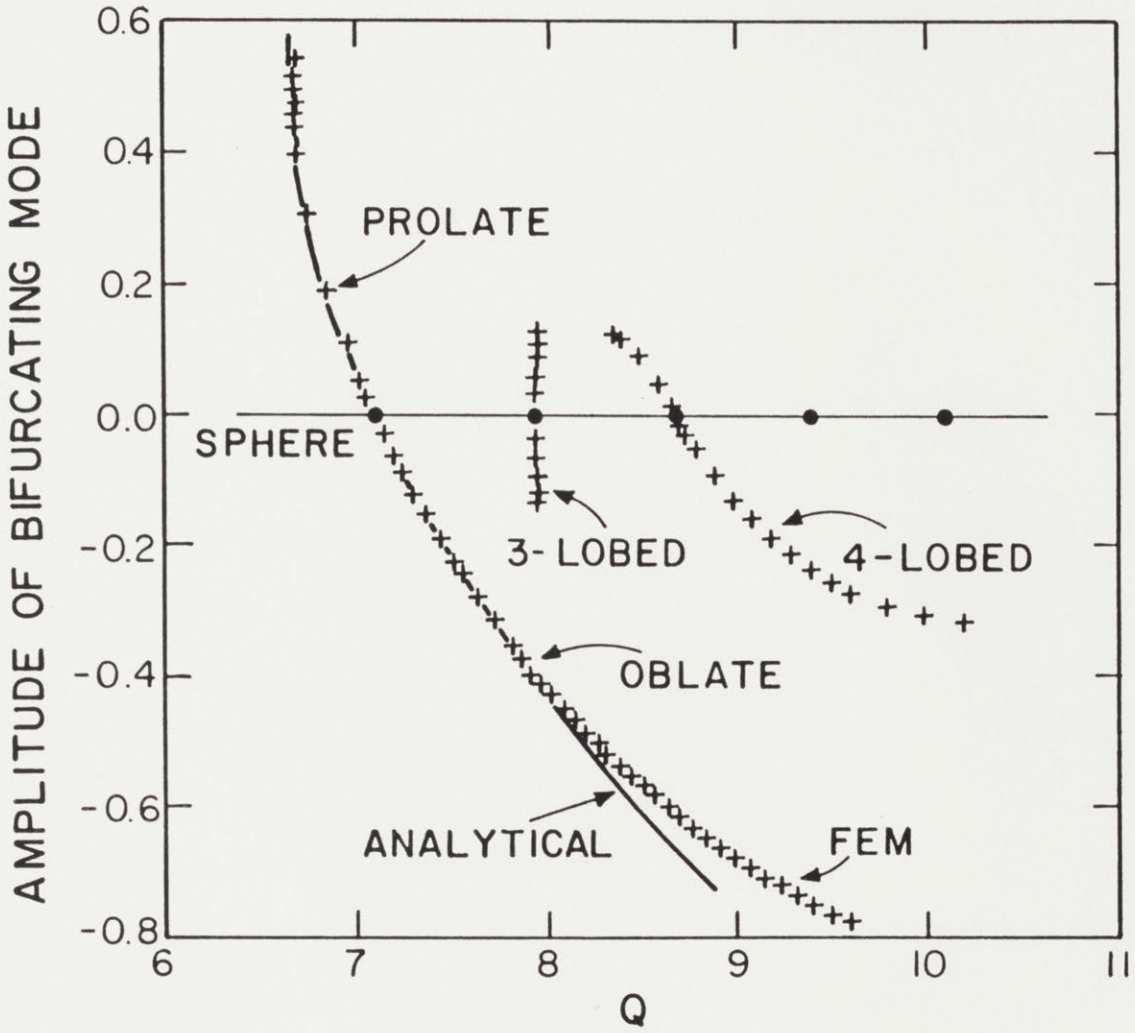

Figure VI.3.1 Families of two-, three-, and four-lobed static drop shapes computed by finite element analysis represented by the magnitude of the corresponding component of the shape. The perturbation solution eq. (VI.2.33c) is represented by the dashed curve.

of the spherical harmonics.

The family of prolate forms evolving from $Q = 4\sqrt{\pi}$ is the analog of the Bohr-Wheeler saddle shapes for a conducting drop and are expected to evolve to the uncharged configuration of two spheres just touching with Q=0. Both the finite element calculations and the asymptotic analysis of the bifurcating prolate shapes predict that this family passes through a limit point where it turns towards higher values of charge Q. The value of Q at the limit point Q_1 is predicted to be 6.6504 from equation (VI.2.33c) and 6.678 from the finite element calculations. We have been unsuccessful in numerically tracking the evolution of the prolate forms through a second limit point and back toward Q=0 because of incorrect interactions between the drop shape and the imposed boundary condition at $r = R_\infty = 12$. To accurately compute very deformed prolate shapes we would need either to increase R_∞ drastically, or to match the finite element approximation of the potential field near the drop to a perturbation solution valid far away, as done by Orr et al. (1977).

A limit point in the family of three-lobed shapes was found where the shapes evolved to lower values of Q. This is expected by analogy with the Bohr-Wheeler forms: the three-lobed shapes should terminate at Q=0 in a shape composed of three equal size spheres. Prolate and oblate drop shapes computed by finite element analyis are shown in figure VI.3.2 for several values of Q. Sample shapes in the three- and four-lobed families are shown in figure VI.3.3.

A quantitative comparison between these forms and the perturbation results, equation (VI.2.33) is made by decomposing the shapes in finite element representation into a Legendre-Fourier series

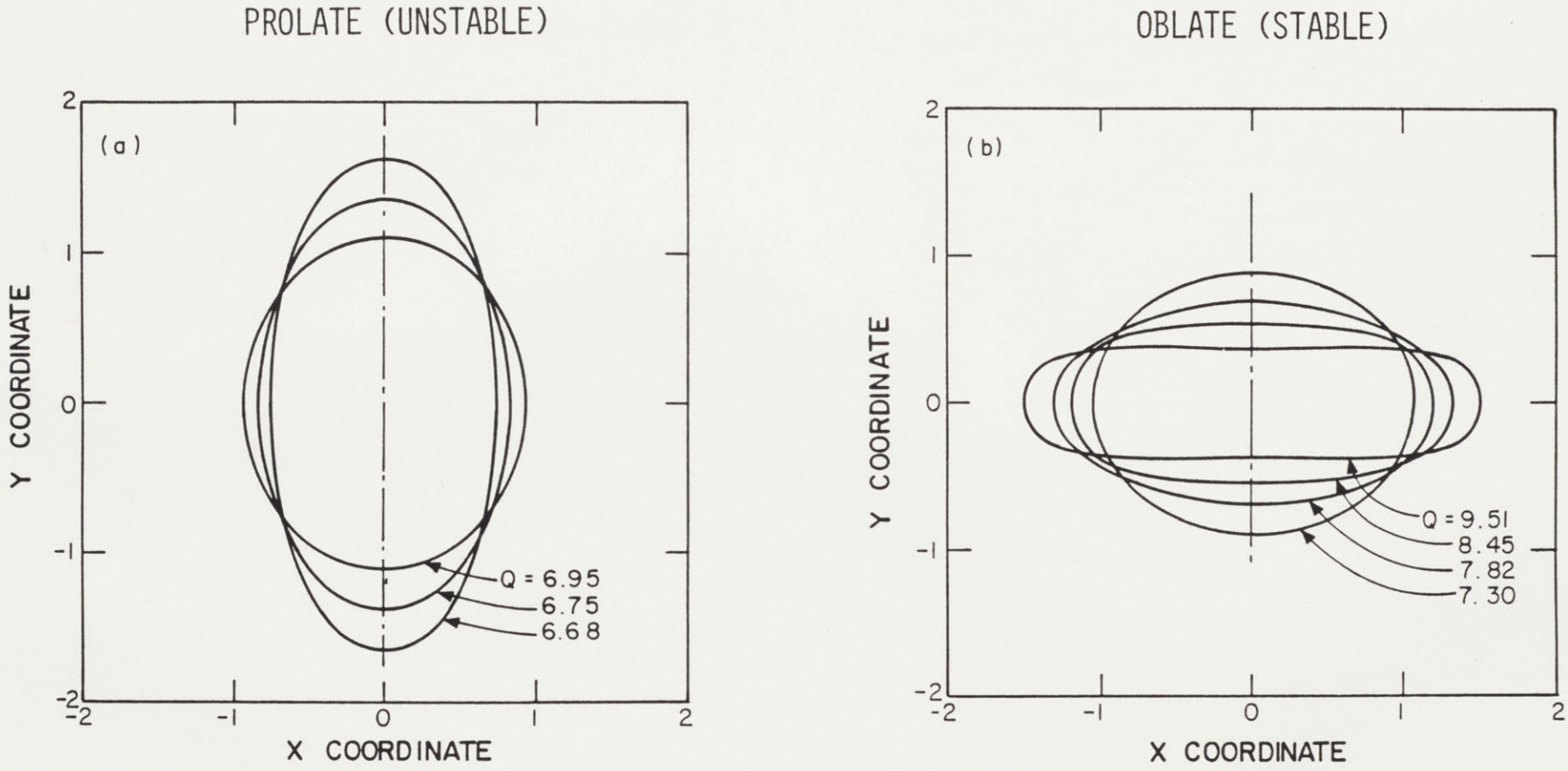

Figure VI.3.2 Sample drop prolate and oblate shapes in the family of two-lobed static forms for different values of charge.

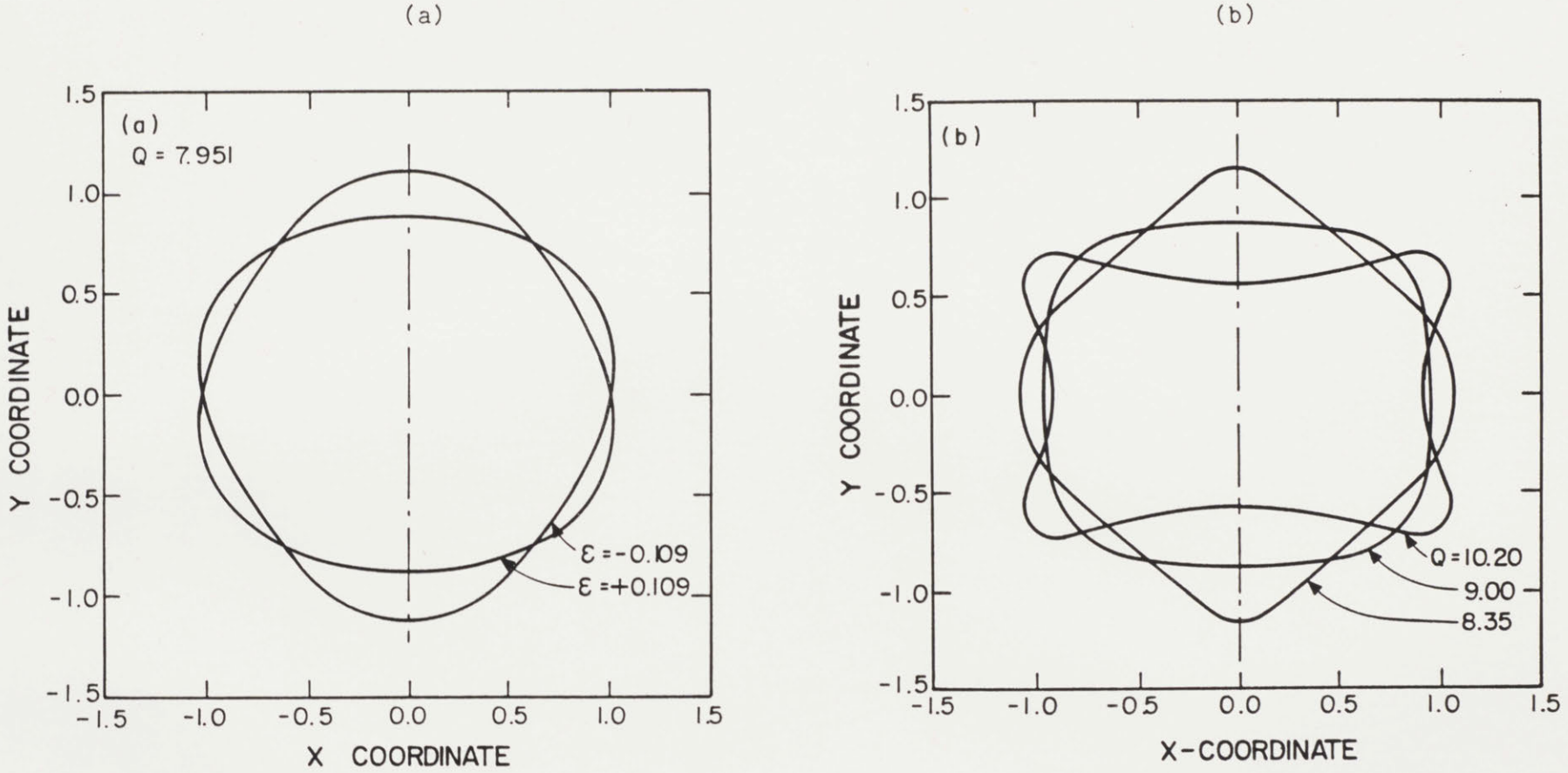

Figure VI.3.3 Sample shapes in the (a) three-lobed and (b) four-lobed shape families for different values of charge.

$$F(\theta) = \sum_{j=0}^{m} \hat{c}_j P_j(\theta), \qquad \text{(VI.3.9)}$$

where the coefficients are computed as

$$\hat{c}_n = \int_0^{\pi} f_n(\theta) \; P_n(\theta) \sin(\theta) \, d\theta \; . \qquad \text{(VI.3.10)}$$

The values of the first eight coefficients calculated from equation (VI.3.10) for the two-lobed shapes are given in Table VI.3.2 and compared to similar coefficients $\{c_j\}$ resulting from the perturbation solution at $O(\varepsilon^2)$. Drop shapes with the identical component c_2 are compared, so that the value of charge for the two forms may be different. The coefficients $c_{2n-1} = 0$, because of the plane of symmetry at $\theta = \pi/2$ for these shapes. Even for deformations as large as $\varepsilon = -0.5043$, the coefficients for the $P_4(\theta)$ component differed by less than 2 percent. The values of net charge used in the finite element calculations and computed from the formula (VI.2.33c) are also compared in Table VI.3.2 and agree to within 1 percent for the most extreme deformations listed. The analytical result, equation (VI.2.33c) is also plotted on figure VI.3.1 for comparison with the numerical results.

VI.4 CONCLUDING REMARKS

The asymptotic analysis presented here gives a complete description of the nonlinear dynamics of an inviscid, charged drop near the Rayleigh limit where an initially spherical drop breaks into fragments. The dynamics of drop breakup is expressed in terms of a slowly varying amplitude,

Table VI.3.2 Legendre-Fourier coefficients and net charge calculated from series expansion $\{c_i, Q\}$ and finite element results $\{\hat{c}_i, \hat{Q}\}$. Results are compared for the same value of the magnitude of the $P_2(\theta)$ component of the shape.

$\varepsilon = c_2 = \hat{c}_2$	c_0	$\hat{c}_0$	c_4	$\hat{c}_4$	$\hat{c}_6$	$\hat{c}_8$	Q	$\hat{Q}$
0.1049	0.9978	0.9978	0.0076	0.0076	0.0005	0	6.945	6.950
0.1924	0.9926	0.9923	0.0254	0.0260	0.0030	0.0003	6.846	6.850
0.3066	0.9812	0.9797	0.0645	0.0683	0.0131	0.0020	6.747	6.750
0.3935	0.9690	0.9649	0.1062	0.1163	0.0303	0.0065	6.695	6.700
0.4625	0.9572	0.9490	0.1467	0.1661	0.0536	0.0150	6.668	6.680
-0.1044	0.9978	0.9978	0.0075	0.0074	-0.0004	0	7.263	7.270
-0.1922	0.9926	0.9926	0.0253	0.0249	-0.0026	0.0002	7.430	7.440
-0.2992	0.9821	0.9819	0.0614	0.0607	-0.0099	0.0010	7.662	7.680
-0.4087	0.9666	0.9654	0.1145	0.1147	-0.0262	0.0041	7.930	7.970
-0.5043	0.9491	0.9454	0.1744	0.1781	-0.0519	0.0108	8.190	8.270

the initial shape deformation of the drop, and the net charge. Spheres with charge less than the Rayleigh limit are unstable only when the initial deformation is large enough to drive the motion beyond the separatrix that surrounds the stable center. This precise criterion for drop instability can be compared directly to the estimate used in the nuclear physics literature of determining the prolate or Bohr-Wheeler saddle shape with the same amount of charge as the "energy barrier" for fission of the drop. Our results predict that instability of the spherical drop is initiated by a shape deformation substantially smaller than predicted by using the unstable prolate form as the energy barrier. This conclusion is clear from the phase-plane diagram figure VI.2.1a. A perturbation to the spherical shape (0,0) can reach the separatrix with a smaller absolute deformation than required to reach the saddle point corresponding to the static prolate form. Then this initially oblate deformation will evolve toward the saddle point and eventually lead to drop breakup after a "long time". This type of secular instability is not accounted for in the "energy barrier" approach to nonlinear stability of the drop. Formally, deformation to the static prolate form is a sufficient, but not necessary, condition for drop instability with $Q < Q_c^{(2)}$.

Examining the stability of the oblate forms to non-axisymmetric forms is an extremely difficult task because of the complexity of the perturbation equations when dependence on the azimuthal angle ϕ is allowed. The linear analysis will follow closely the work reported by Wong and Tang (1974) for a volumetrically charged drop and show that the set of modes at $Q=4\sqrt{\pi}$ with zero frequency must be expanded to include all shape perturbations expressed in terms of general spherical harmonics as

$$F(\theta,\phi,t) = 1 + \varepsilon\, Y_{2m}(\theta,\phi),\ m = 0,1,2,$$

where $Y_{2m}(\theta,\phi)$ is a spherical harmonic function. The shapes with m=0 are the prolate and oblate axisymmetric forms discussed above. The other infinitesimal non-axisymmetric perturbations represent the same small amplitude, prolate and oblate shapes described in a spherical coordinate system rotated from the original one, and so are not unique configurations. Cohen and Siatecki (1962) realized this fact and stated, as do Businaro and Gallone (1955), that oblate forms with volumetrically distributed charge are unstable to non-axisymmetric perturbations. Neither author presents an analysis to support this claim. To do this requires examining the effect of threee-dimensional disturbances on the stability of the axisymmetric oblate shapes given approximately by equation (VI.2.33c).

Whether or not the oblate forms are physically realizable is of special significance in determining the effects of an applied electric field on the shape of a charged drop. Adornato and Brown (1983) correctly computed the shape of a charged drop in a uniform field and showed that the field acts as an imperfection, causing the shape family originating from a sphere to turn at a limit point to a value of charge below the Rayleigh limit. They did not compute the evolution of the separated solution family containing oblate shapes which will result from splitting the transcritical bifurcation described here. If the oblate forms are stable in the absence of an applied field, the shapes in this separated branch will also be stable when the applied field is present.

VII. OSCILLATIONS OF COMPOUND DROPS

Hollow spherosymmetric shells of metal or glass have been produced by centering a bubble inside a drop and solidifying the resulting shell or so-called compound drop (Hendricks 1976, 1977, 1981). The first step in this process is to manufacture these compound drops by breaking an annular liquid jet into hollow spheres through a Rayleigh-like instability. By doing so the compound drops have well defined gaseous and liquid content and are also spherosymmetric. The first characteristic is understood as a result of external forcing on the annular liquid jet that initiates the instability at a very short range of wave-lengths, the second is analysed in this chapter. In the compound drops of interest van der Waals forces that would tend to bring the two interfaces as far apart as possible are unimportant, since the distance between them is typically larger than 1000 Å. Also, surface tension forces are ineffective in positioning the bubble inside the drop, since all locations of the spherical bubble are energetically equivalent.

In spite of these preliminary thoughts, experiments by Lee et al. (1981) show that the centering force attainable by means of mode oscillations initiated during the breakup process is very strong. In addition, if surfactant is added to the liquid of the shell the frequency and amplitude of this oscillation is greatly diminished but still the final centering of the surfaces is equally good. Experiments performed by Saffren et al. (1981) on neutrally buoyant compound drops suspended in an immiscible liquid have confirmed the existence of two distinct oscillation frequencies which are predicted by the linear hydrodynamic theory for inviscid flows.

The "bubble" mode results when the two interfaces oscillate in phase and is characterized by a higher oscillation frequency, whereas the "sloshing" mode results when the two interfaces oscillate out of phase with lower frequency. Shapes of compound drops oscillating in these distinct modes are shown in figure VII.0.1.

The decomposition into normal modes of infinitesimal amplitude describes the motion of the trapped bubble about the center of the drop entirely by the first spherical harmonic $P_1(\cos\theta)$ (Morse and Feshbach 1953). These disturbances are calculated to be neutrally stable and induce no tendency for the bubble to move with respect of the drop, or equivalently, the linearization of the governing equations of fluid motion proves that the time constant associated with these disturbances is identically zero. As a result, the restoring forces responsible for centering of the bubble inside the drop can only be accounted for by considering nonlinear interactions between the fluid in the shells and the two interfaces. The normal mode analysis of Patzer and Homsy (1975) for small amplitude oscillations of a viscous liquid shell gives the same result for the decentering disturbance.

Lee and Wang (1984) attempted an analysis aimed at explaining the centering phenomenon. They assumed that the displacement of the bubble from the center of the liquid drop is small compared with the bubble radius, but large compared with the amplitude of the wave on the shell surface. This scaling argument allowed them to consider the motion of the system due to the core displacement alone and solve for the linearized equations of motion. However, they had to include nonlinear terms to calculate a nonzero force on the bubble in an ad hoc manner. According

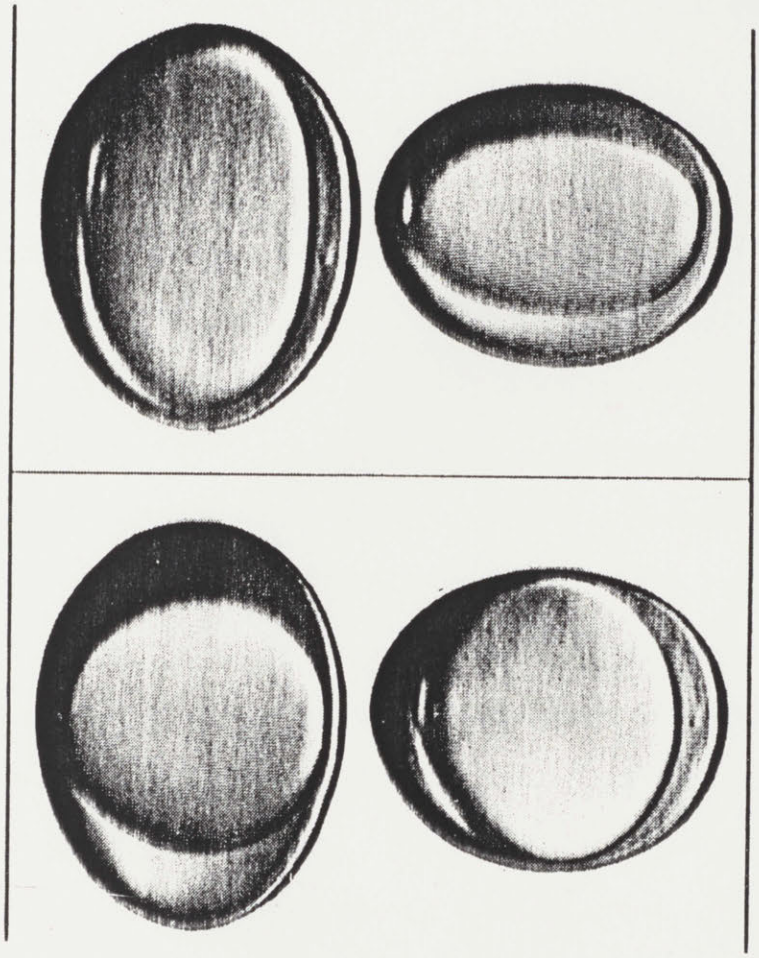

Figure VII.0.1 "Bubble" mode (top) and "sloshing" mode (bottom) oscillations of an oil-water-oil compound drop (Saffren et al. 1981).

to their results, the direction of the motion of the bubble center can be both towards or away from the liquid drop center, depending on the shell thickness and on the mode which was initially excited. This result is not confirmed by experiments which have always shown centering of the bubble inside the drop.

We undertake here the weakly nonlinear analysis of axisymmetric mode oscillations, of a compound inviscid drop which is initially eccentric. To avoid the physically unacceptable results associated with the inviscid liquid/liquid interfaces we limit our study to cases where both the fluid in the bubble and that of the surrounding medium are either a vacuum or a tenuous gas, so that its hydrodynamical effects can be neglected. The calculations are focused on predicting the conditions under which the centering of the bubble is enhanced, along with describing the effect of the finite amplitude of deformation on the oscillation frequency and shape of the compound drop. The present analysis is based on the method of multiple timescales as applied to approximating the time-periodic solutions of conservative systems. In section VII.1 the governing equations are given and their solution follows in section VII.2.

VII.1 FORMULATION

The irrotational and incompressible motion of a compound drop of total volume $\tilde{V}_2=4\pi R_2^3/3$ which contains a bubble of volume $\tilde{V}_1=4\pi R_1^3/3$ is considered. The density of the liquid in this shell is ρ and the surface tension of both gas/liquid interfaces is σ. The motion of the spherical shell in a tenuous medium is caused by initially introducing a small

axisymmetric deformation with the center of the inside bubble translated from the center of the drop along the axis of symmetry. The unperturbed radius of the outer surface, R_2, is used as a characteristic length of the system and is used to dimensionalize the outer and inner interfaces by describing them as $F_2(\theta,t)$ and $F_1(\theta,t)$ respectively, where θ is the meridional angle in spherical coordinates. The inner surface disturbance contains the first Legendre polynomial that describes the off-centered bubble with respect to the drop in addition to the appropriate oscillation mode. Scales based on the results of the linear theory are used to define the dimensional velocity potential $(\sigma R_2/\rho)^{1/2}\phi(r,\theta,t)$, pressure $(2\sigma/R_2)$ $P(r,\theta,t)$ and time $(\rho R_2^3/\sigma)^{1/2}t$ each in terms of its dimensionless counterpart. Then the equations governing the inviscid motion are

$$\nabla^2\phi = 0 \qquad (F_1(\theta,t)\leq r\leq F_2(\theta,t),\ 0\leq\theta\leq\pi), \qquad \text{(VII.1.1)}$$

$$\frac{\partial F_1}{\partial t} = \frac{\partial\phi}{\partial r} - \frac{1}{r^2}\frac{\partial\phi}{\partial\theta}\frac{\partial F_1}{\partial\theta} \qquad (r=F_1(\theta,t)), \qquad \text{(VII.1.2)}$$

$$\frac{\partial F_2}{\partial t} = \frac{\partial\phi}{\partial r} - \frac{1}{r^2}\frac{\partial\phi}{\partial\theta}\frac{\partial F_2}{\partial\theta} \qquad (r=F_2(\theta,t)), \qquad \text{(VII.1.3)}$$

$$\frac{\partial\phi}{\partial t} = -\frac{1}{2}\left[\left(\frac{\partial\phi}{\partial r}\right)^2 + \left(\frac{1}{r}\frac{\partial\phi}{\partial\theta}\right)^2\right] - 2P \qquad (F_1(\theta,t)\leq r\leq F_2(\theta,t),\ 0\leq\theta\leq\pi), \qquad \text{(VII.1.4)}$$

$$\Delta P_1 + 2P = -2H_1 \qquad (r=F_1(\theta,t),\ 0\leq\theta\leq\pi), \qquad \text{(VII.1.5)}$$

$$\Delta P_2 - 2P = -2H_2 \qquad (r=F_2(\theta,t),\ 0\leq\theta\leq\pi), \qquad \text{(VII.1.6)}$$

$$\int_0^\pi F_2^3(\theta,t)\sin(\theta)\,d\theta = \frac{1}{R^3}\int_0^\pi F_1^3(\theta,t)\sin(\theta)\,d\theta = 2\,. \qquad \text{(VII.1.7a,b)}$$

Equation (VII.1.1) is the Laplace equation governing the irrotational flow inside the shell; (VI.1.2,3) are the kinematic conditions in the

inner and the outer interface respectively; (VII.1.4) is Bernoulli's equation for the pressure everywhere in the shell. Equations (VII.1.5,6) are the balances of dynamic and capillary pressure across the inner and outer interface respectively, where the right-hand side is the negative of the local mean curvature of the inner (H_1), or outer (H_2) interface; (IV.1.7) are the constraints for constant volume of the liquid shell and the encapsulated bubble. The static pressure difference across the inner interface is ΔP_1 and across the outer ΔP_2 whereas the ratio of the inner to the outer static radius is R and provides the only new parameter in this problem.

The dynamical problem is solved for the velocity potential in the shell and the two interfaces for motions originating with an initial deformation of the compound drop. Initial deformations are used that satisfy conservation of mass (VII.1.7) and have no initial velocity, i.e.

$$\frac{\partial F_1}{\partial t}(\theta,0) = 0, \quad \frac{\partial F_2}{\partial t}(\theta,0) = 0 . \tag{VII.1.8}$$

The amplitude of the oscillation ε is defined in terms of the initial deformation of the outer surface as

$$F_2(\theta,0) = 1 + \varepsilon P_2(\theta) - \frac{1}{5}\varepsilon^2 + O(\varepsilon^3) , \tag{VII.1.9}$$

where $P_2(\theta)$ is the Legendre polynomial of the second order. The initial deformation of the bubble interface is of similar form but also includes the first Legendre polynomial to describe its off-centered position. The distance between the two centers is confined to be of order ε so that the analysis can be carried out on the simple reference domain of two concentric spheres, in which Laplace's equation is readily solvable.

Therefore

$$F_1(\theta,0) = R\{1 + \varepsilon[AP_1(\theta) + BP_2(\theta)] - \varepsilon^2[\frac{B^2}{5} + \frac{A^2}{3}] + O(\varepsilon^3)\}, \quad \text{(VII.1.10)}$$

where the initial distance between the two centers, A, is an arbitrary constant which is taken to be one for convenience and B is an unknown constant determined from the solution of the linear problem. The amplitude of deformation of the outer interface, ε, is taken to be the small parameter in the analysis that follows and is subject to the additional requirement that also εB is much smaller than one.

VII.1 PERTURBATION SOLUTION

The potential field $\phi(r,\theta,t)$ and compound drop shapes $F_1(\theta,t)$, $F_2(\theta,t)$ are determined for moderate-amplitude motions by constructing expansions in the initial disturbance of the outer interface ε. The asymptotic methods couple together the technique of multiple timescales for freely oscillating non-dissipative systems and the domain perturbation analysis outlined by Joseph (1973) and described in chapter IV of this thesis. Formally, we assume that the dependent variables are functions of three timescales related to the actual time as $T_0=t$, $T_1=\varepsilon t$ and $T_2=\varepsilon^2 t/2$. The different timescales are introduced into the field equations by expanding the partial derivative $\partial/\partial t$ as

$$\frac{\partial}{\partial t} \equiv \frac{\partial}{\partial T_0} + \varepsilon \frac{\partial}{\partial T_1} + \frac{\varepsilon^2}{2} \frac{\partial}{\partial T_2} + O(\varepsilon^3). \quad \text{(VII.2.1)}$$

The expansion for the domain shape is implemented by transforming the inner and outer interfaces to the surfaces of two concentric spheres

of radius R and 1 respectively, using the coordinate transformation

$$\eta = \frac{r - F_1}{F_2 - F_1} + R\,\frac{r - F_2}{F_1 - F_2} \quad , \tag{VII.2.2}$$

and expanding each dependent variable in a Taylor series

$$\begin{bmatrix} F_1(\theta,t;\varepsilon) \\ F_2(\theta,t;\varepsilon) \\ \phi(r,\theta,t;\varepsilon) \end{bmatrix} = \sum_{k=0}^{\infty} \frac{\varepsilon^k}{k!} \begin{bmatrix} F_1^{(k)}(\theta,T_0,T_1,T_2) \\ F_2^{(k)}(\theta,T_0,T_1,T_2) \\ \phi^{[k]}(\eta,\theta,T_0,T_1,T_2) \end{bmatrix} , \tag{VII.2.3}$$

where the superscript [k] denotes the kth total derivative of the quantity with respect to ε. As in chapter IV, each term in these expansions for the potential can be written as a sum of a contribution based on the domain between two concentric spheres ($R \leq \eta \leq 1$, $0 \leq \theta \leq \pi$) and terms that account for the deformation of the domain at each order of ε. The derivatives evaluated on this domain are denoted by $\phi^{(k)}(\eta,\theta,T_0,T_1,T_2) \equiv \partial^{(k)}\phi/\partial\varepsilon^{(k)}$. Because the compound drop shape is independent of the radial coordinate, $F^{[k]}(\theta,T_0,T_1,T_2) = F^{(k)}(\theta,T_0,T_1,T_2)$ for both interfaces. Expressions for the total derivatives of a potential up to $\phi^{[2]}$ are given by equation (IV.2.3) of chapter IV. We anticipate the form of the solution to the compound drop shape and expand it at each order as a series of Legendre polynomials

$$\begin{bmatrix} F_1^{(k)}(\theta,T_0,T_1,T_2) \\ F_2^{(k)}(\theta,T_0,T_1,T_2) \end{bmatrix} = \sum_{m=0}^{\infty} \begin{bmatrix} \alpha_{3m}^{(k)}(T_0,T_1,T_2) \\ \alpha_{4m}^{(k)}(T_0,T_1,T_2) \end{bmatrix} P_m(\theta). \tag{VII.2.4}$$

Using these forms for the corrections to the interfaces, the mean curvatures

H_1, H_2 are conveniently expanded in ε; the results valid up to $O(\varepsilon^3)$ are given in Appendix A.

Similarly the potential in the domain between two concentric spheres in each order has the form

$$\phi^{(k)}(\eta,\theta,T_0,T_1,T_2) = \sum_{m=0}^{\infty} [\alpha_{1m}^{(k)}(T_0,T_1,T_2)\ \eta^m + \alpha_{2m}^{(k)}(T_0,T_1,T_2)\ \eta^{-m-1}]\ P_m(\theta). \tag{VII.2.5}$$

The equations governing the zeroth-order contributions from the set (VII.1.1) - (VII.1.10) describe a static compound and concentric drop and have the solution

$$\begin{bmatrix} F_1^{(0)}(\theta,T_0) \\ F_2^{(0)}(\theta,T_0) \\ \phi^{(0)}(\eta,\theta,T_0) \end{bmatrix} = \begin{bmatrix} R \\ 1 \\ 0 \end{bmatrix}. \tag{VII.2.6}$$

The equation set that governs the first-order corrections to the potential and the interfaces ($\phi^{(1)}$, $F_1^{(1)}$, $F_2^{(1)}$) is

$$\nabla^2\phi^{(1)} = 0 \qquad (R\leqq\eta\leqq 1,\ 0\leqq\theta\leqq\pi), \tag{VII.2.7}$$

$$\frac{\partial F_1^{(1)}}{\partial T_0} = \frac{\partial\phi^{(1)}}{\partial\eta} \qquad (\eta=R,\ 0\leqq\theta\leqq\pi), \tag{VII.2.8}$$

$$\frac{\partial F_2^{(1)}}{\partial T_0} = \frac{\partial\phi^{(1)}}{\partial\eta} \qquad (\eta=1,\ 0\leqq\theta\leqq\pi), \tag{VII.2.9}$$

$$\frac{\partial\phi^{(1)}}{\partial T_0} = +\,(n-1)(n+2)F_1^{(1)}(\theta,t)/R^2 \qquad (\eta=R,\ 0\leqq\theta\leqq\pi), \tag{VII.2.10}$$

$$\frac{\partial\phi^{(1)}}{\partial T_0} = -\,(n-1)(n+2)F_2^{(1)}(\theta,t) \qquad (\eta=1,\ 0\leqq\theta\leqq\pi), \tag{VII.2.11}$$

$$\int_0^{\pi} F_1^{(1)}(\theta,t)\,\sin(\theta)\,d\theta = \int_0^{\pi} F_2^{(1)}(\theta,t)\,\sin(\theta)\,d\theta = 0, \quad \text{(VII.2.12a,b)}$$

$$F_1^{(1)}(\theta,0,0,0) = R\,[AP_1(\theta) + BP_2(\theta)], \quad \text{(VII.2.13)}$$

$$F_2^{(1)}(\theta,0,0,0) = P_2(\theta)\ , \quad \text{(VII.2.14)}$$

$$\frac{\partial F_1^{(1)}}{\partial T_0}(\theta,0,0,0) = \frac{\partial F_2^{(1)}}{\partial T_0}(\theta,0,0,0) = 0. \quad \text{(VII.2.15)}$$

The solutions to (VII.2.7) - (VII.2.12) describe the linear modes of oscillation calculated previously by Saffren et al. (1981). These are cast here in the framework of the multiple-scale expansion as

$$\begin{bmatrix} \alpha_{1n}^{(1)}(T_0,T_1,T_2) \\ \alpha_{2n}^{(1)}(T_0,T_1,T_2) \\ \alpha_{3n}^{(1)}(T_0,T_1,T_2) \\ \alpha_{4n}^{(1)}(T_0,T_1,T_2) \end{bmatrix} = \begin{bmatrix} \chi_{1n} \\ \chi_{2n} \\ \chi_{3n} \\ \chi_{4n} \end{bmatrix} D_n(T_1,T_2)\, e^{\omega T_0} + \text{c.c.}\ , \quad \text{(VII.2.16)}$$

where c.c. stands for the complex conjugate of the immediately preceding term and ω are the imaginary eigenvalues of the initial value problem defined by (VII.2.8) - (VII.2.11) and are given by

$$\omega^2 \equiv \omega_n^2 = \frac{(n-1)(n+2)}{2R^3(1-R^{2n+1})}\,[\,-(n+1)(1+R^{2n+4}) - n(R^3+R^{2n+1}) \pm \sqrt{S}\,], \quad \text{(VII.2.17a)}$$

with

$$S \equiv (n+1)^2R^{4n+8} - 2n(n+1)R^{4n+5} + n^2R^{4n+2}$$

$$+ 2n(n+1)R^{2n+7} + 2(6n^2+6n+1)R^{2n+4} + 2n(n+1)R^{2n+1}$$

$$+ n^2R^6 - 2n(n+1)R^3 + (n+1)^2 \ . \qquad \text{(VII.2.17b)}$$

The bubble mode corresponds to the negative sign in equation (VII.2.17a) and the sloshing mode corresponds to the positive sign. The variation of the in-phase and out-of-phase frequencies with the ratio of the inner to the outer radius, R, is shown in figure VII.2.1 for n=2,3,4. The the components of the eigenvectors of the same system of equations for only n=2, $\chi_{in} \equiv \chi_i$, are given below;

$$\chi_1 = \frac{4\omega^2R^3 + 48}{P}, \quad \chi_2 = -\frac{4\omega^2R^8 - 32R^5}{P}, \quad \chi_3 = \frac{20\omega R^4}{P}, \quad \chi_4 = 1, \qquad \text{(VII.2.18a)}$$

with

$$P \equiv (\omega^2R^8 - 8R^5 - \omega^2R^3 - 12)\omega \ . \qquad \text{(VII.2.18b)}$$

The constant B used in the initial condition given by equation (VII.1.10) is determined from the linear solution to be equal to χ_3. The ratio χ_3/χ_4 gives the relative displacement between the inner and the outer interfaces and is plotted in figure VII.2.2 as a function of R. In the case of the sloshing mode this relative displacement is O(1) for all values of R, whereas it becomes unbounded for low values of R for the bubble mode. Expansion in a Taylor series of this ratio for small values of R and for the bubble mode yields

$$\lim_{R \to 0} \frac{\chi_3}{\chi_4} = \frac{1}{5}\left[\frac{3}{R^4} - \frac{2}{R} + 2R + O(R^2)\right], \qquad \text{(VII.2.19a)}$$

whereas for the sloshing mode yields

$$\lim_{R \to 0} \frac{\chi_3}{\chi_4} = -\frac{5R^4}{3}\left[1 + \frac{2R^3}{3} + O(R^6)\right]. \qquad \text{(VII.2.19a)}$$

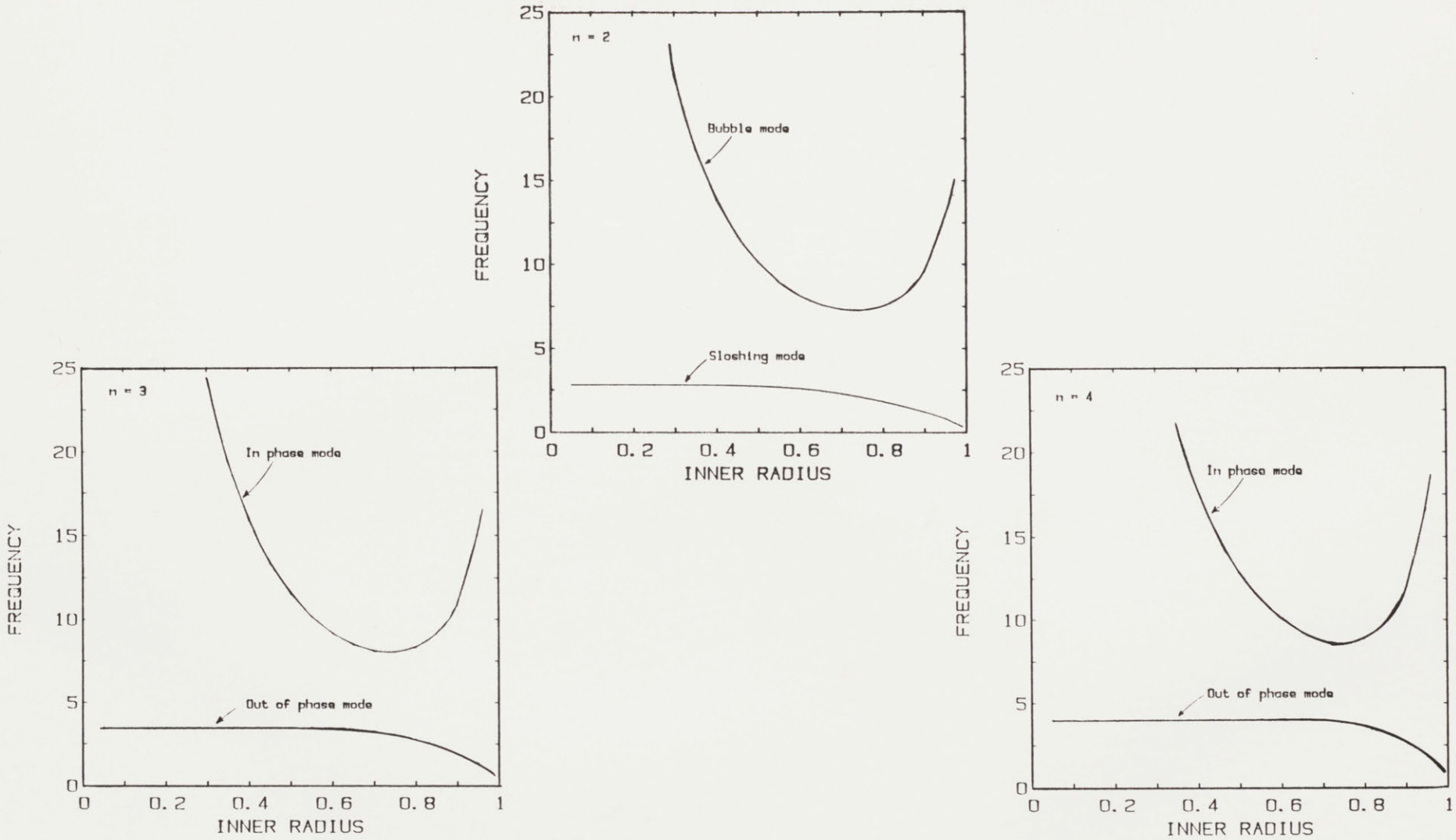

Figure VII.2.1 Variation of the in and out of phase frequencies for n=2,3,4 as a function of the ratio of the inner to the outer radius of the shell (R).

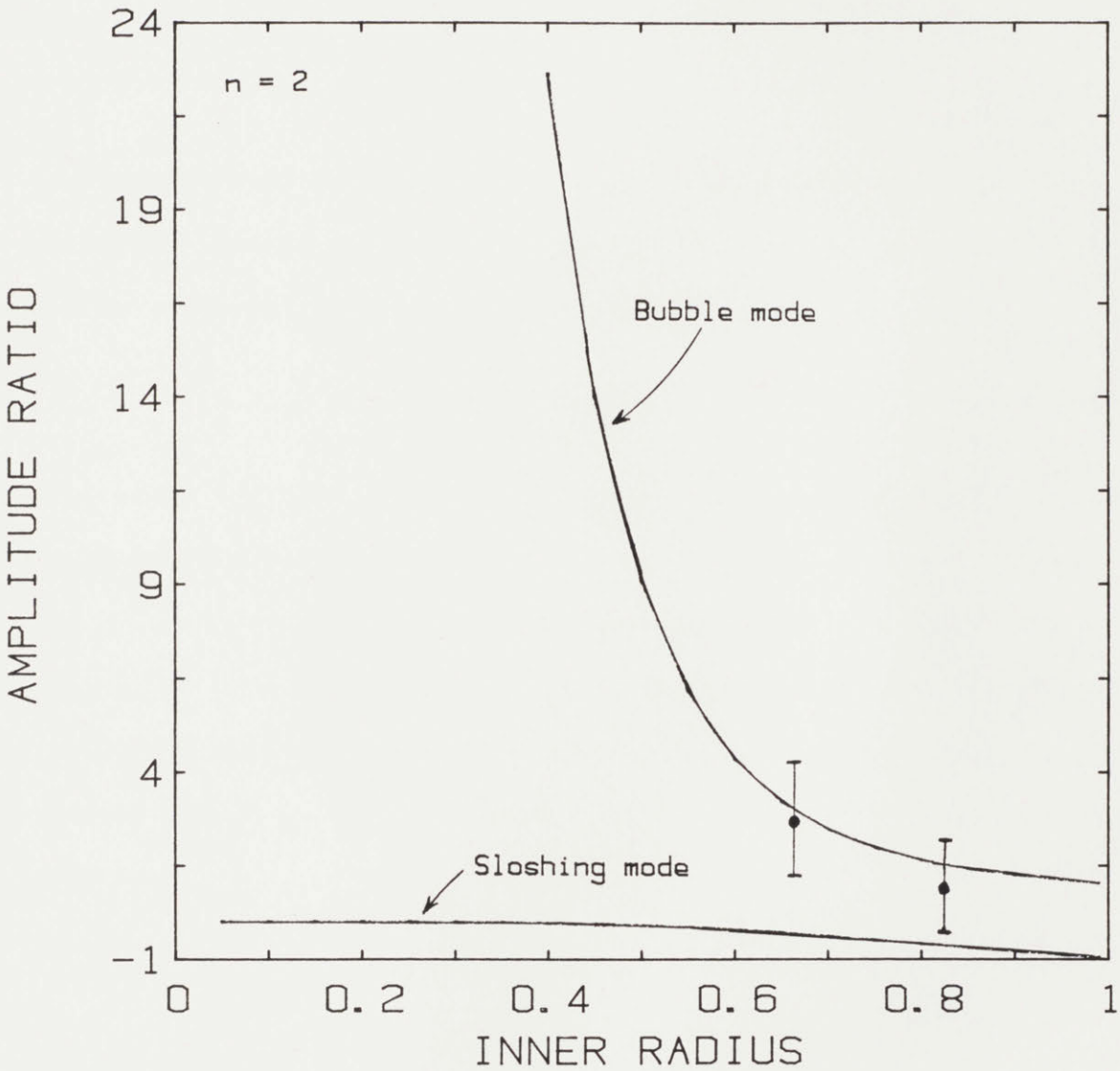

Figure VII.2.2 Relative displacement of the inner to the outer interface for the bubble and the sloshing modes as a function of the ratio of the inner to the outer radius of the shell (R). Experimental results of Saffren et al. (•) are shown.

The perturbation series defined by equation (VII.2.3) converges to a solution if the amplitude on either interface is much smaller than one. This result requires that for the bubble mode and as $R \to 0$ the perturbation parameter ε must satisfy

$$\varepsilon \ll R^4 \quad . \tag{VII.2.19c}$$

The complex functions $D_n(T_1,T_2)$ and their conjugates $D_n^*(T_1,T_2)$ depend on the slower timescales and are determined as part of the second- and third-order problems subject to the initial conditions

$$D_n(0,0) = D_n^*(0,0) = 1/2 \quad . \tag{VII.2.20}$$

They represent the modulation in the slow timescales of the amplitude and frequency of the oscillations.

Equation (VII.2.17) demonstrates the fact that the eigenfrequency is identically zero for n=1, which in turn means that the decentering mode is independent of time and no motion of the bubble relative to the drop occurs according to the linear theory. The linear solution for this mode is

$$\begin{bmatrix} \alpha_{11}^{(1)}(T_0,T_1,T_2) \\ \alpha_{21}^{(1)}(T_0,T_1,T_2) \\ \alpha_{31}^{(1)}(T_0,T_1,T_2) \\ \alpha_{41}^{(1)}(T_0,T_1,T_2) \end{bmatrix} = \begin{bmatrix} 0 \\ 0 \\ 1 \\ 0 \end{bmatrix} A(T_1,T_2) \quad , \tag{VII.2.21}$$

with the initial condition

$$A(0,0) = 1 \quad . \tag{VII.2.22}$$

The complete solution to the equation set (VII.2.7) - (VII.2.15) is the superposition of equations (VII.2.21) and (VII.2.16) evaluated for n=2. It is anticipated that the nonlinearities caused by inertia, capillarity, and the moving boundary will interact at higher order approximations to force the centering of the bubble relative to the drop.

The equation set for the second-order terms ($\phi^{(2)}$, $F_1^{(2)}$, $F_2^{(2)}$) in the expansion is cumbersome because of the multitude of non-homogeneous terms that are generated by the domain perturbation. This set is listed in Appendix E and is solved by expanding the potential $\phi^{(2)}$ and interface shapes ($F_1^{(2)}$, $F_2^{(2)}$) in series of Legendre polynomials and powers of η similar to those given by equations (VII.2.4) and (VII.2.5), which satisfy the field equations. Equations (E2) - (E5) are reduced to a sequence of non-homogeneous initial value problems by applying the orthogonality properties of Legendre polynomials. Their homogeneous solution is similar to equation (VII.2.16). The solvability condition for the equations (E2) - (E5) requires their inhomogeneous part to be orthogonal to the adjoint eigenvector of the first order problem for n=2 and also to the right-hand-side of equation (VII.2.21) which leads to two equations for the slowly varying amplitudes of the initial modes

$$\frac{\partial A}{\partial T_1} = \frac{\partial D}{\partial T_1} = \frac{\partial D^*}{\partial T_1} = 0. \qquad \text{(VII.2.23)}$$

This result indicates that the slowly varying functions D, D^* and A depend at best on T_2. The solutions to the second order problem, determined so that the initial conditions (E7) - (E10) and the integral constraints (E6) are satisfied, are written in the form of equations (VII.2.4) and (VII.2.5), where the numerical values for the coefficients are tabulated

in Appendix E. The form of this solution along with equation (VII.2.23) indicates that there is an induced oscillatory motion of the bubble with respect to the drop with the same frequency as the initial mode, but relative to the bubble center, not to the drop center. Obviously, this result does not provide a centering mechanism.

The dependence of the frequency and amplitude modulations on the slow timescale T_2 is computed from the solvability conditions of the third-order problem. The corrections to the shapes and the potential ($\phi^{(3)}$, $F_1^{(3)}$, $F_2^{(3)}$) are again expanded in Legendre series, and a set of ordinary differential equations is derived by the same procedure used to solve the second-order problem. The solvability condition for this $O(\varepsilon^3)$ problem is nontrivial and results in two first-order ordinary differential equations for the amplitude of the centering mode $A(T_2)$ and the complex amplitudes of the excited mode $D(T_2)$, $D^*(T_2)$

$$\frac{dA}{dT_2} = \beta A \,, \qquad \text{(VII.2.24)}$$

$$\frac{dD}{dT_2} = i\gamma_1 D^* D^2 + i\gamma_2 A^2 D + i\gamma_3 D \,, \qquad \text{(VII.2.25a)}$$

$$\frac{dD^*}{dT_2} = -i\gamma_1 D^{*2} D - i\gamma_2 A^2 D^* - i\gamma_3 D^* \,, \qquad \text{(VII.2.25b)}$$

where all amplitudes are functions of the slow timescale $T_2 \equiv \varepsilon^2 t/2$, and the real constants γ_1, γ_2, γ_3 are functions of the radius of bubble, R. For the sloshing mode, β is given by

$$\beta \equiv [\, 5(2R^{10}\chi_1^2 + 3\chi_2^2 + 4R^5\chi_3^2) + 2\omega(2R^9\chi_1 - 3R^4\chi_2)\chi_3] \,/\, (5R^9), \qquad \text{(VII.2.26)}$$

and is negative for all R, as shown in figure VII.2.3.

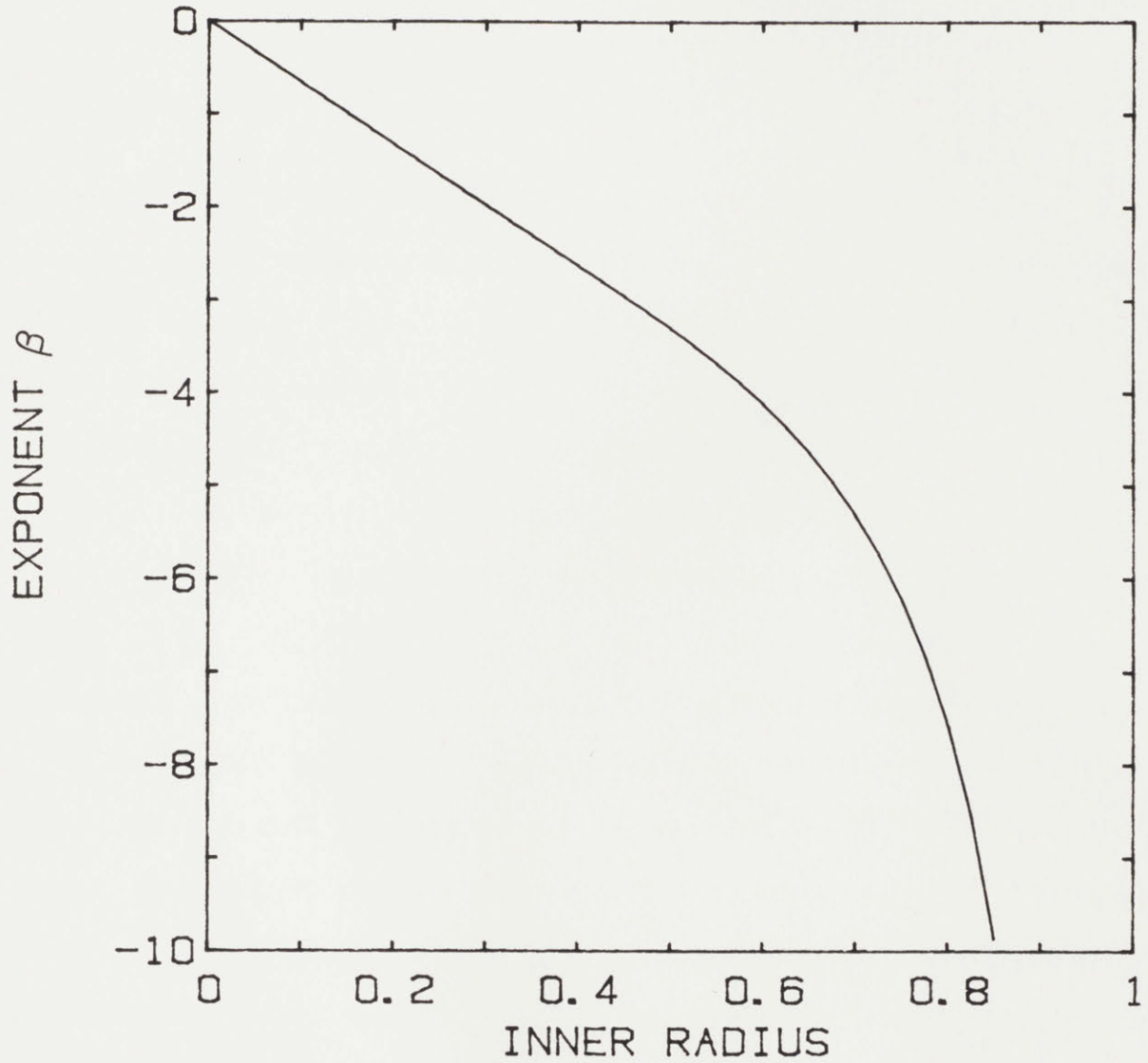

Figure VII.2.3 Dependence of the damping exponent of the distance between the two centers, on the ratio of the inner to the outer radius of the shell (R).

The asymptotic forms of β for small and large values of R are given below

$$\lim_{R \to 1-} \beta = \frac{4}{5} \left[\frac{2}{R-1} + 3 + 16(R-1) + O((R-1)^2) \right], \quad \text{(VII.2.27a)}$$

$$\lim_{R \to 0} \beta = -\frac{20R}{3} \left[1 - \frac{R^3}{3} + O(R^6) \right], \quad \text{(VII.2.27b)}$$

On the contrary, β is identically zero for the bubble mode.

As a result, when the compound drop oscillates in the sloshing mode centering occurs on a slow timescale and the distance between the two centers diminishes exponentially, whereas when the compound drop oscillates in the bubble mode alone, no centering is observed up to this order of analysis. The centering mechanism is most effective in a thin shell when the nonlinear interaction of the two interfaces is most prominent, whereas it is less effective for a small bubble contained in a drop. This result is also demonstrated by comparing figures VII.2.4a and VII.2.4b. In the first one there is an exponential decay of the distance between the two centers with the induced oscillation and in the second only the undamped oscillation exists. The long-time distance between the bubble and drop centers is slightly negative because of the second-order homogeneous term in equation (E11a). Higher-order approximations will offset this result and will lead to a concentric configuration.

The second of the amplitude equations (VII.2.25a) and its complex conjugate (VII.2.25b) are readily solved using the transformation

$$D(T_2) = r(T_2)\, e^{i\theta(T_2)}, \quad \text{(VII.2.28a)}$$

$$D(T_2)^* = r(T_2)\, e^{-i\theta(T_2)}, \quad \text{(VII.2.28b)}$$

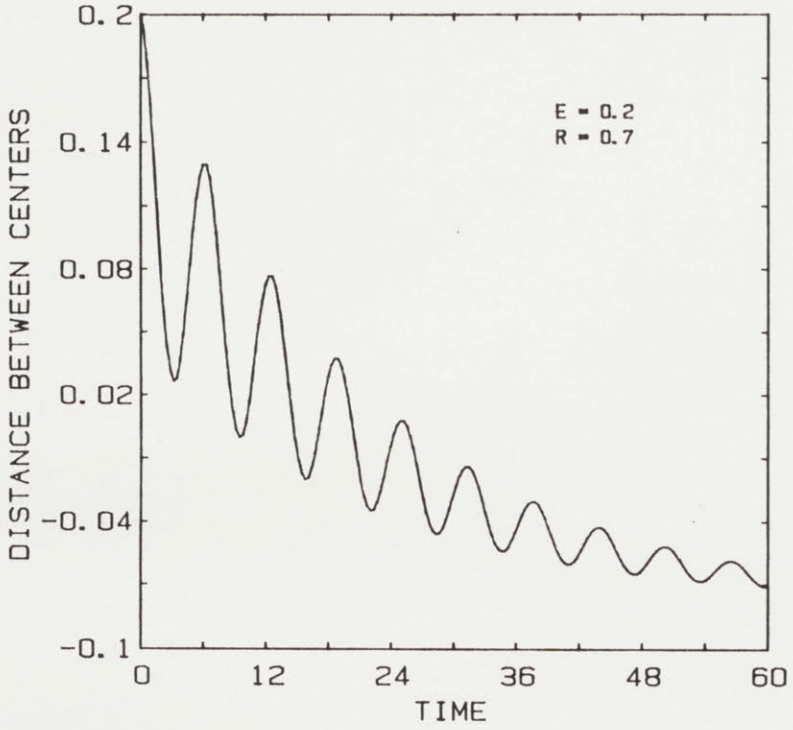

(a)

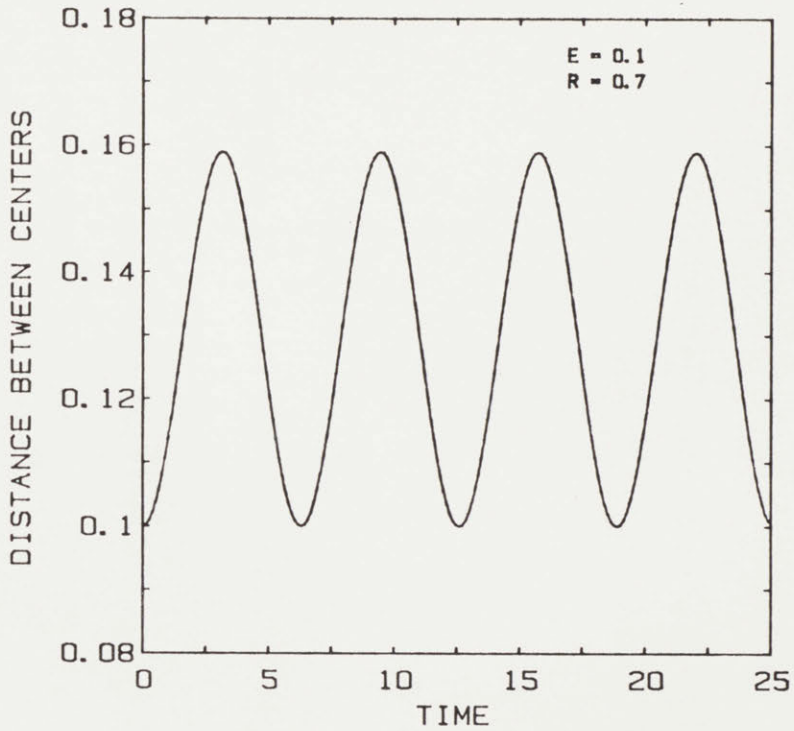

(b)

Figure VII.2.4 Evolution of the distance between the two centers for (a) sloshing mode and (b) bubble mode. Time has been dimensionalized with the corresponding inverse frequency.

where r, θ are the real amplitude and phase modulations. Introducing equations (VII.2.28) into (VII.2.25) and separating real from imaginary parts yields

$$\frac{dr}{dT_2} = 0 \quad , \tag{VII.2.29a}$$

$$\frac{d\theta}{dT_2} = \gamma_1 r^2 + \gamma_2 A + \gamma_3 \quad . \tag{VII.2.29b}$$

Thus according to equation (VII.2.29a) no amplitude modulation or energy exchange occurs between the modes. There is no deformation or kinetic energy associated with the centering mode and the total energy of the system remains constant, as expected for a conservative system. Equation (VII.2.29b) shows a slow frequency decrease that is proportional to the square of the amplitude of the motion and depends on the ratio of radii, R and on the instantaneous distance between the two centers. This is the same result derived previously for the oscillations of a simple drop. Because there can be no dependence of the frequency modulation on any odd powers of the amplitude, the result (V.2.29b) is accurate up to $\mathbf{O}(\varepsilon^4)$.

VII.3 RESULTS AND CONCLUSIONS

Representative shapes of compound drops correct up to $\mathbf{O}(\varepsilon^2)$ are shown for the sloshing mode with ε=0.2 on figure VII.3.1 and for the bubble mode with ε=0.1 on figure VII.3.2. In both cases the ratio of the inner to the outer radius is set to be equal to 0.7 and time is dimensionalized with the inverse frequency of the corresponding primary mode. A lower value of the perturbation parameter ε is used in the representations of the bubble mode since the deformation of the inner interface is signific-

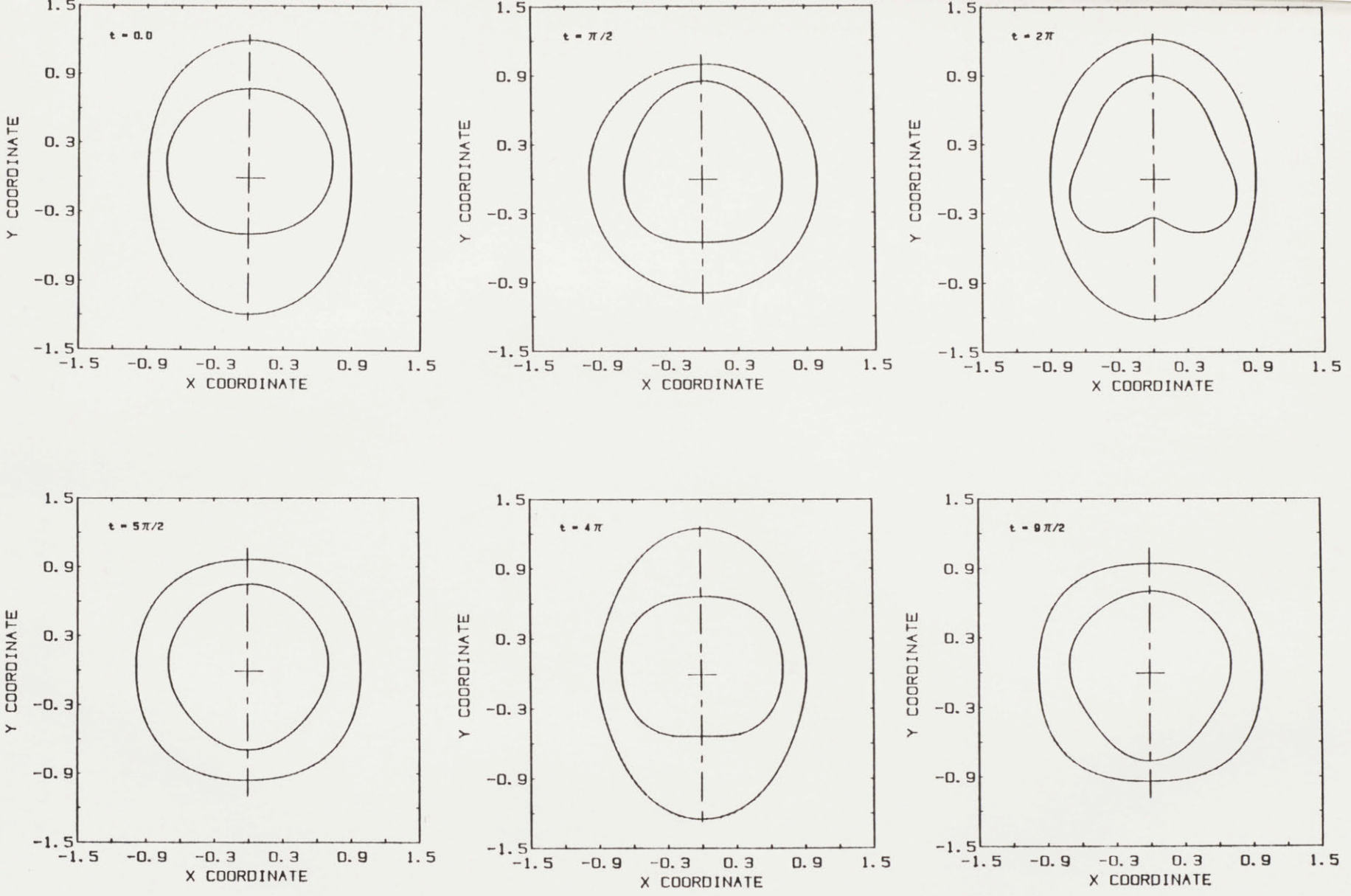

Figure VII.3.1 Shapes of oscillating compound drops in the sloshing mode with R=0.7 and ε=0.2. Time has been dimensionalized with the inverse frequency of the sloshing mode.

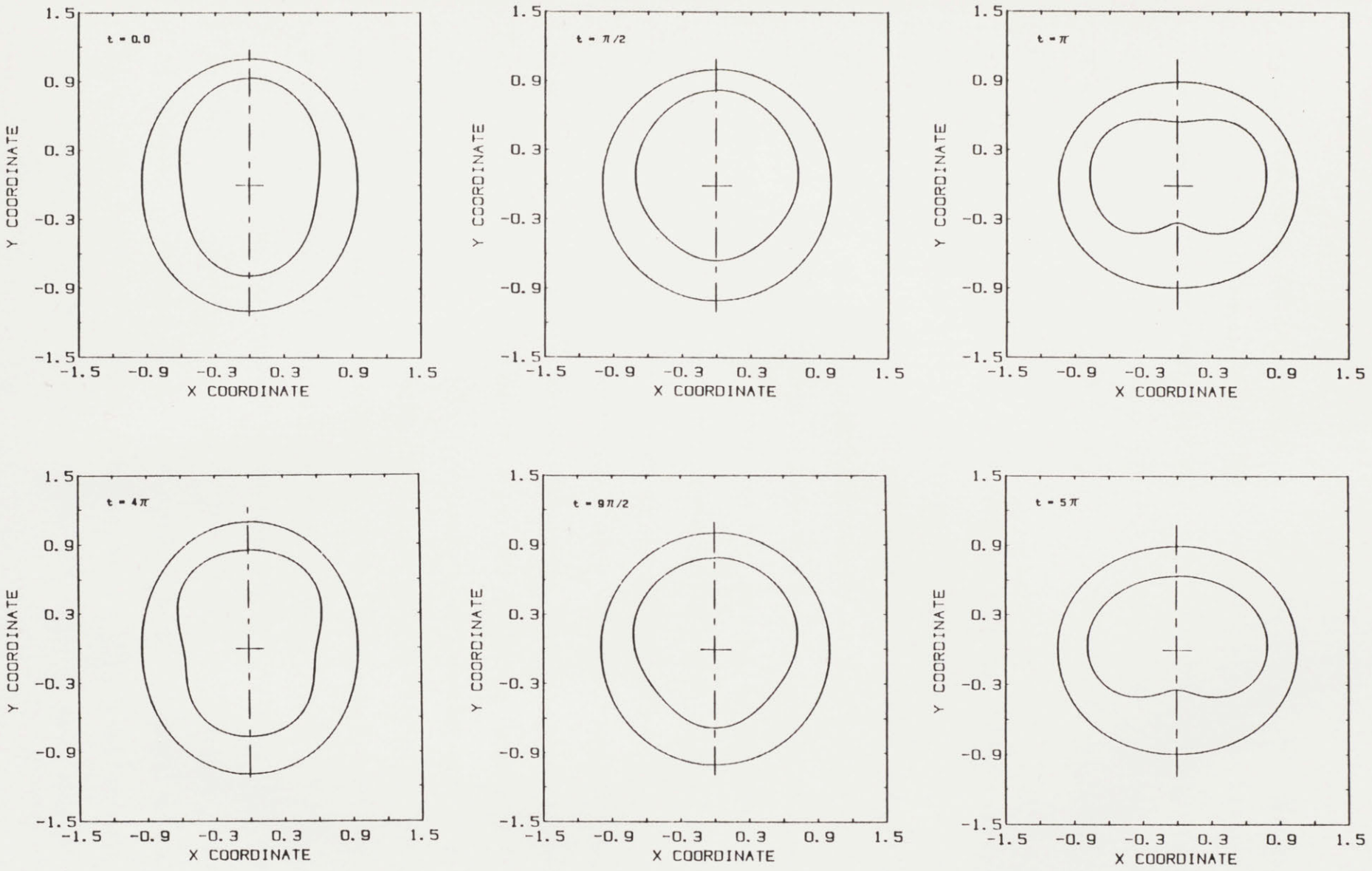

Figure VII.3.2 Shapes of oscillating compound drops in the bubble mode with R=0.7 and ε=0.1. Time has been dimensionalized with the inverse frequency of the bubble mode.

antly larger than that of the outer and may lead to failure of the expansion series. In both cases the representation of the outer surface up to this order of approximation involves only the zeroth, second and fourth Legendre polynomials, whereas the representation of the inner involves also the first and third polynomials, as required by the orthogonality properties of the spherical harmonics.

In order to satisfy the initial conditions (equations (VII.1.8) - (VII.1.10)) to this order, the homogeneous solution had to be included in the interface representation resulting in a periodic motion with a period equal to the least common multiplier of the frequncies involved and not 2π. The sloshing mode is shown at the initial form after a quarter of a period and also after one and two periods of the primary mode. THe bubble mode is shown at the initial disturbance after a quarter and half a period and after two periods of the promary mode.

The experiments by Lee et al. (1981) and by Saffren et al. (1981) where mostly qualitative and do not report initial eccentricities or approximate time intervals in which the centering mechanism occured. They simply verify the linear frequencies of oscillation and give the two experimental points shown in figure VII.2.2 for the ratio of the disturbance on the inner versus that of the outer interface. In an experimental situation the breakup of the annular jet leads into a compound drop the external surface of which has a prolate shape, and the inner surface is rather undetermined. The ensuing oscillations could then be expanded in Fourier series that include both the sloshing and bubble mode. The nonlinear dynamic interactions in the sloshing mode result in a concentric shell. Finally, harmonic resonance (see chapter V) may

occur between higher harmonics and the oscillating fundamental for specific values of R, but energy cannot be transmitted to the centering mode in this fashion in order to accelerate the uncovered centering mechanism.

VIII. POSTSCRIPT

A rigorous mathematical framework has been developed for studying the nonlinear dynamics of simple and compound drops and bubbles and has been applied to several of the outstanding problems in drop dynamics. A combination of domain perturbation and multiple timescales methods have been used to systematically compute the evolution of axisymmetric and inviscid simple and compound drops. The complexity of the nonlinear equations is reduced by using the symbolic manipulator MACSYMA.

Moderate-amplitude oscillations of simple and compound drops display an array of nonlinear dynamic phenomena. Figure VIII.1 summarizes the nonlinear effects for a single drop with elecrtical charge. The results of Rayleigh's linear theory and the quadratic decrease of the frequency of the oscillation as the net charge increases appear in the plane $\varepsilon=0$. The frequency becomes zero according to linear theory at the Rayleigh limit ($Q=Q_c=4\sqrt{\pi}$), where the capillary force is exactly balanced by the electrostatic repulsion. The decrease of the eigenfrequencies is proportional to the square of the amplitude as shown in any plane of constant charge Q ($0\leq Q\leq Q_c$). This last result is caused by the fluid inertia and has been verified experimentally for uncharged drops (Trinh and Wang 1982). At specific values of the dimensionless charge, $Q\equiv Q_r$, harmonic resonance is induced by the nonlinear interaction between the primary oscillation mode and one of its harmonics. For purely four-lobed initial oscillations with $Q_r=\sqrt{(32\pi/3)}<Q_c$ the drop assumes an almost six-lobed shape within two periods of the primary oscillation. Initial disturbances with combinations of four- and six-lobed shapes lead to a continuous exchange of energy

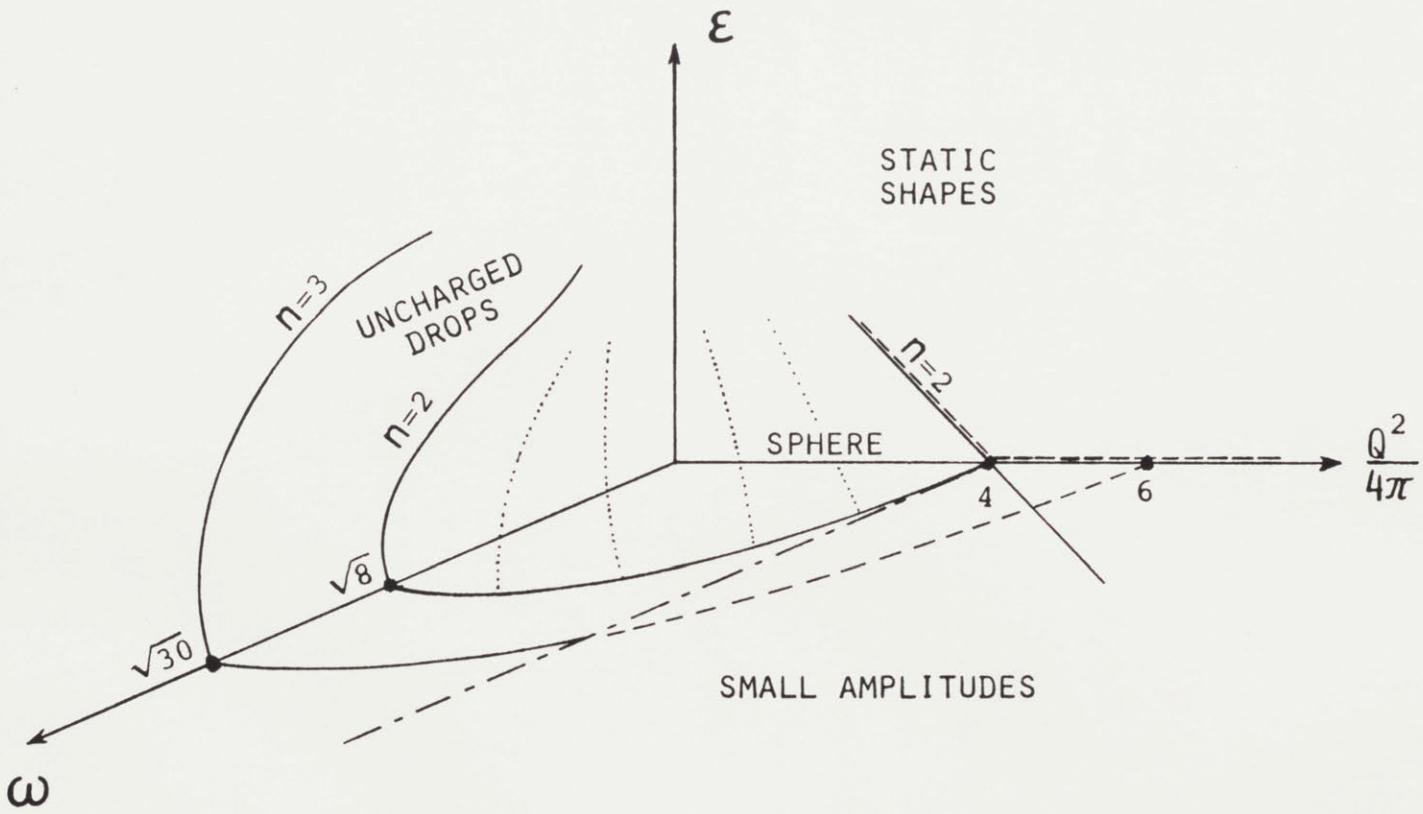

Figure VIII.1 Dependence of dynamics and statics of a charged drop on amplitude of disturbance and net charge.

between these two modes. In general, the shape evolution in these cases is highly dependent on the initial shape perturbation. This effect is shown in figure VIII.1 as a deviation from the quadratic decrease of the frequency for high enough values of the initial disturbance.

The evolution of the drop shape for charge values close to the Rayleigh stability limit is shown in the plane of static shapes (ω=0) as a trans-critical bifurcation point between the families of static spherical shapes and oblate (ε<0) and prolate (ε>0) axisymmetric forms. Prolate forms exist for lower values of charge and are unstable to small amplitude perturbations. Finite amplitude oscillations destabilize the spherical drops at values of charge below Q_c, with a decrease proportional to the amplitude of the initial disturbance. Oblate static shapes exist for $Q > Q_c$ and are stable to small axisymmetric perturbations, but unstable to disturbancies large enough to move the dynamics outside the separatrix of the motion.

The dynamics of the compound drop are also characterized by the quadratic decrease of the oscillation frequency with the amplitude of the initial disturbance. In addition, an initially eccentric compound drop becomes concentric if excited to oscillate in the sloshing mode, where the motion of the bubble and drop are out of phase. This is a direct effect of the nonlinear dynamics of the compound drop and has been observed experimentally (Saffren et al. 1981).

An important extension to the present studies is to determine the effects of viscous forces on the nonlinear interactions described above. For gas/liquid interfaces the effect of viscosity on the frequency of oscillation and the shape of the drop is small when the product $(\sigma R/\nu^2\rho)^{1/2}$

is large, where ν is the kinematic viscosity. Then the timescale for viscous dissipation, or equivalently of vorticity diffusion from the interface, is much longer than the characteristic time for the inviscid oscillation. This condition is satisfied for water drops, but not for higher viscosity fluids of interest in materials processing. For two fluids of comparable density the inviscid analysis leads to a discontinuity between the components of tangential velocity on the two phases, which is avoided by introducing a viscous boundary layer on both sides of the interface.

Finally, the stability of the oblate shapes to non-axisymmetric disturbances close to the Rayleigh limit is an interesting but extremely difficult problem because of the complexity of the perturbation equations when azimuthal variation is allowed.

IX. REFERENCES

Abramowitz, M. and Stegun, I.A. 1964 Handbook of Mathematical Functions, chaps 16 and 17. National Bureau of Standards, Washington D.C.

Adornato, P.M. and Brown, R.A. 1983 Shape and stability of electrostatically levitated drops. Proc. R. Soc. Lond. A 389, 101-117.

Akylas, T.R. and Benney, D.J., 1980 Direct resonance in nonlinear wave systems. Stud. Appl. Math. 63, 209-226.

Aris, R., 1962 Vectors, Tensors and the basic equations of Fluid Mechanics, Prentice Hall.

Alonso, C.T. 1974 The dynamics of colliding oscillating drops. In Proc. Int. Colloq on Drops and Bubbles. (Ed. D. J. Collins, M. S. Plesset and M. M. Saffren). Jet Propulsion Laboratory.

Annamalai, R.S., Subramanian, R.S. and Cole, R., 1980 Rotation as a centering mechanism for microballoon fusion targets. Presented at Topical Conference on Inertial Confinement Fusion, San Diego.

Barthes-Biesel, D. and Acrivos, A. 1973 Deformation and burst of a liquid droplet freely suspended in a linear shear field. J. Fluid Mech. 61, 1-21.

Basaran, O.A., Amudson, K.R., Patzek, T.W. and Scriven, L.E. 1982 Deformation, Oscillation and Break-up of Charged Drops in Electric Field. Bull. Amer. Phys. Soc. 27, 1168.

Basaran, O.A. and Scriven, L.E. 1981 Profiles of electrified drops and bubbles. In Proc. second Int. Colloq. Drops Bubbles, (ed. D.H. Le Croissette) Pasadena, California: Jet Propulsion Laboratory.

Bender, C.M. and Orszag, S.A., 1978 Advanced Mathematical Methods for Scientists and Engineers, McGraw-Hill.

Benner, R.E. 1983 Equilibria, stability, and bifurcations in fluid physics. Ph.D. Thesis in Chemical Engineering University of Minnesota.

Benney, D.J 1962 Non-linear gravity wave interactions. J. Fluid Mech. 14, 577-584.

Beris, A.N., Tsamopoulos, J.T., Armstrong, R.C. and Brown, R.A. 1984 Creeping motion of a sphere through a Bingham plastic. J. Fluid Mech. (Accepted).

Bertsch, G.F. 1983 Vibrations of the Atomic Nucleus. Sci. Am. 248, 62-73.

Blake, J.R. and Gibson, D.C. 1981 Growth and collapse of a vapour cavity

near a free surface. J. Fluid Mech. 111, 123-140.

Bohr, N. and Wheeler, J.A. 1939 The Mechanism of nuclear fission Phys. Rev. 56, 426-450.

Bohr, A. and Mottelson B.R. 1975 Nuclear Structure Vol. II Ch. 6 W. A. Benjamin, Boston.

Brazier-Smith, P.R., Brook, M., Latham, J., Saunders, C.P.R. and Smith, M.H. 1971 The vibration of electrified drops. Proc. Roy. Soc. Lond. A322, 523-534.

Bretherton, F.P. 1964 Resonant interactions between waves. The case of discrete oscillations. J. Fluid Mech. 20, 457-479.

Brink, D.M. and Satchler, G.R. 1968 Angular Momentum, 2nd ed. Clarendon.

Brook, M. and Latham, D.J. 1968 Fluctuating radar echo: Modulation by vibrating drops J. Geophys. Res. 73, 7137-7144.

Brown, R.A., Orr, F.M. and Scriven, L.E., 1980 Static drop on an inclined plate: Analysis by the Finite Element Method. J. Colloid Interface Sci. 73, 76-87.

Brown, R.A. and Scriven, L.E. 1980a The shape and stability of rotating liquid drops. Proc. Roy. Soc. Lond. A 371, 331-357.

Brown, R.A. and Scriven, L.E. 1980b New class of asymmetric shapes of rotating liquid drops. Physical Review Letters 45, 180-183.

Brown, R.A. and Scriven, L.E. 1980c On the multiple equilibrium shapes and stability of an interface pinned on a slot. J. Colloid Interface Sci. 78, 528-542.

Bupara, S.S., 1965 Spontaneous movements of small round bodies in viscous fluids. Ph. D. Thesis in Chemical Engineering University of Minnesota.

Businaro, U.L. and Gallone, S. 1955 On the interpretation of fission asymmetry according to the liquid drop model. Il Nuovo Cimento 1, 629-643.

Calliger, R.J., Turnbull, R.J. and Hendricks, C.D. 1977 Hollow drop production by injection of gas bubbles in a liquid jet. Rev. Sci. Instrum. 48, 846-851.

Carruthers, J.R. 1974 The application of drops and bubbles to the science of space processing of materials. In Proc. Int. Colloq. on Drops and Bubbles (Ed. by D.J. Collins, M.S. Plesset and M.M. Saffren) Jet Propulsion Laboratory, 161-193.

Chandrasekhar, S. 1961 Hydrodynamic and Hydromagnetic Stability. Oxford University Press.

Chandrasekhar, S. 1965 The stability of a rotating liquid drop. Proc. R. Soc. Lond. A286, 1-26.

Chandrasekhar, S. 1969 Ellipsoidal figures of equilibrium. Yale Univ. Press.

Chang, C.J. and Brown, R.A. 1984 Natural convection in steady solidification: Finite element analysis of a two-phase Rayleigh-Bernard problem. J. Comput. Phys. 53, 1-27.

Chi, B.K. 1979 The growth of Sphero-symmetric Microballoons. S.B. Thesis in Chemical Engineering, M.I.T.

Ciliberto, S. and Gollub, J.P. 1984 Pattern Competition Leads to Chaos. Phys. Rev. Lett. 52, 922-925.

Cohen, S., Plasil, R., and Swiatecki, W.J. 1974 Equilibrium configurations of gravitating liquid masses with surface tension. Ann. Phys. 82, 557-596.

Cohen, S. and Swiatecki, W.J., 1962 The deformation energy of a charged drop. IV: Evidence for discontinuity in the conventional family of saddle point shapes. Ann. of Phys. 19, 67-164.

Cohen, S. and Swiatecki, W.J., 1963 The deformation energy of a charged drop. V: Results of electronic computer studies. Ann. of Phys. 22, 406-437.

Concus, P. 1962 Standing capillary-gravity waves of finite amplitude. J. Fluid Mech. 14, 568-576.

Crane, J.S. and Pohl, M.A. 1968 A Study of Living and Dead Yeast Cells using Dielectrophoresis. J. Electrochem. Soc. 115, 584-586.

Daly, B.J., 1969 A technique for including surface tension effects in hydrodynamic calculations. J. Comp. Phys. 4, 97-117.

Davis, E.I. and Ray, A.K., 1980 Single aerosol particle size and mass measurements using an electrodynamic balance. J. Colloid Interface Sci. 75, 566-576.

Davis, R.E and Acrivos, A. 1967 The stability of oscillatory internal waves. J. Fluid Mech. 30, 723-736.

Eliassen, J.D., 1963 Interfacial Mechanics. Ph. D. Thesis in Chemical Engineering University of Minnesota.

Elliott, C.M. and Ockendon, J.R., 1982 Weak and variational methods for moving boundary problems. Pitman, Boston.

Ettouney, H.M. and Brown R.A. 1983 Finite element methods for steady solidification problems. J. Comput. Phys. 49, 118-150.

Fenton, J.D. and Rienecker, M.M., 1982 A Fourier method for solving nonlinear water-wave problems: application to solitary wave interactions. J. Fluid Mech. 118, 411-443.

Fornberg, B. and Whitham, G.B., 1978 A numerical and theoretical study of certain nonlinear wave behaviour. Phil. Trans. R. Soc. Lond. A 289, 373-404.

Foote, G.B., 1973 A numerical method for studying simple drop behavior: simple oscillation. J. Comp. Phys. 11, 507-530.

Gear, W.C., 1971 Numerical Initial Value Problems in Ordinary Differential Equations. Prentice Hall, Englenwood Cliffs.

Greenspan, H.P., 1981 Fluid model and simulations of biological cell phenomena. In Proc. of the 2nd Int. Colloq. on Drops and Bubbles (ed. D. H. Le Croissette). Jet Propulsion Laboratory

Hall, P. and Seminara, G. 1980 Nonlinear oscillations of non-spherical cavitation bubbles in acoustic fields. J. Fluid Mech. 101, 423-444.

Harlow, F.H. and Welch, J.E., 1965 Numerical calculation of time-dependent viscous incompressible flow of fluid with free surface. Phys. Fluids 8, 2182-2189.

Harper, E.Y., Grube, G.W. and Chang I., 1972 On the breakup of accelerating liquid drops. J. Fluid Mech. 52, 565-591.

Hasse, R.W. 1975 Inertia, friction and angular momentum of an oscillating viscous charged liquid drop under surface tension Ann. Of Phys. 93, 68-87.

Hendricks, C.D. 1962 Charged droplet experiments. J. Colloid Sci. 17, 249-259.

Hendricks, C.D. 1976 Target fabrication: Overview. Laser Program, Annual Report Lawrence Livermore Laboratory, UCRL-50021-76, 4.122-4.136.

Hendricks, C.D. 1977 Target fabrication: Overview. Laser Program, Annual Report Lawrence Livermore Laboratory, UCRL-50021-77, 5.1-5.5.

Hendricks, C.D. 1981 Inertial confinement fusion targets. In Proc. of the 2nd Int. Colloq. on Drops and Bubbles (Ed. by D. H. Le Croissette). Jet Propulsion Laboratory, 88-93.

Hendricks, C.D. and Johnson, W.L. 1977 Production of power-plant inertial confinment fusion targets. Laser Program, Annual Report Lawrence Livermore Laboratory, UCRL-50021-77, 5.42-5.50.

Hendricks, C.D. and Schneider, J.M. 1963 Stability of a conducting droplet under the influence of surface tension and electrostatic forces. Am.

J. Phys. 31, 450-453.

Hetsroni, G. and Haber, S. 1978 Low reynolds number motion of two drops submerged in an unbounded arbitrary velocity field. Int. J. Mult. Flow 4, 1.

Hill, D.H. and Wheeler, J.A. 1953 Nuclear constitution and the interpretation of fission phenomena. Phys. Rev. 89 1102-1145.

Ioos, G. and Joseph, D.D 1980 Elementary Stability and Bifurcation Theory Springer-Verlag, New York.

Jacobi, N., Croonquist, A.P., Elleman, D.D. and Wang, T.G. 1981 Acoustically induced oscillation and rotation of a large drop in space. In Proc. of 2nd Int. Colloq. on Drops and Bubbles (Ed. by D.H. Le Croissette). Jet Propulsion Laboratory.

Joseph, D. D., 1973 Domain perturbations: The higher order theory of infinitesimal water waves. Arch. Rat. Mech. Anal. 51, 295-303.

Kammash, T., 1975 Fusion Reactor Physics. Ann Arbor Sciences, Ann Arbor.

Keller H.B. and Rabinowitz P.H. (ed.) 1977 Applications of Bifurcation theory, Academic Press, New York.

Kendall, J.M., 1980 Fluid dynamic studies relating to production of large fusion targets. Presented at Topical Meeting On Inertial Confinement Fusion, San Diego.

Kendall, J.M. 1981 Hydrodynamic Performance of an annular liquid jet: production of liquid shells. In Proc. of the 2nd Int. Colloq. on Drops and Bubbles (Ed. by D. H. Le Croissette). Jet Propulsion Laboratory, 79-87.

Kiang, R.L. 1969 Nonlinear theory of inviscid Taylor instability near the cutoff wavenumber. Phys. Fluids 12, 1333-1339.

Lamb, H. 1932 Hydrodynamics, 6th Edition. Cambridge University Press.

Landau, L., 1944 On the problem of turbulence. Doklady Acad. Sci. URSS XLIV, 311-314.

Lauterborn, W. and Bolle, H. 1975 Experimental investigations of cavitation-bubble collapse in the neighbourhood of a solid boundary. J. Fluid Mech. 72, 391-399.

Lebovitz, N.R., 1982 Perturbation expansions on perturbed domain. SIAM Review 24, 381-400.

Lee, M.C., Feng, I., Elleman, D.D., Wang, T.G. and Young, A.T. 1981 Generation of a strong centering force in a submillimeter compound droplet system. In Proc. of the 2nd Inter. Colloq. on Drops and Bubbles

(Ed. by D. H. Le Croissette). Jet Propulsion Laboratory, 107-111.

Lee, C.P. and Wang, T.G. 1984 The core-centering force in a compound drop system - inviscid theory. Submitted for publication.

Li, N.N. 1971 Permeation through liquid surfactant membranes. J. AICHE 17, 459-463.

Longuet-Higgins, M.S. 1983 Bubbles, breaking waves and hyperbolic jets at a free surface. J. Fluid Mech. 127, 103-121.

Longuet-Higgins, M.S. and Cokelet, E.D., 1976 The deformation of steep surface waves on water I. A numerical method of computation. Proc. Roy. Soc. Lond. A 350, 1-26.

MACSYMA 1977 Reference Manual. Laboratory of Computer Science, Massachusetts Institute of Technology.

Marston, P.L. 1980 Shape oscillation and static deformation of drops and bubbles driven by modulated radiation stresses: theory. J. Acoust. Soc. Am. 67, 15-26.

Marston, P.L. and Apfel, R.E. 1979 Acoustically forced shape oscillation of hydrocarbon drops levitated in water. J. Colloid Interface Sci. 68, 280-286.

Marston, P.L. and Apfel, R.E, 1980 Quadrapole resonance of drops driven by modulated acoustic radiation pressure: experimental properties. J. Acoust. Soc. Am. 67, 27-37.

Martin, T.P. and Davies, G.A. 1976 The extraction of copper from dilute aqueous solutions using a liquid membrane process. J. Hydrometallurgy 2, 315.

McGoldrick, L.F. 1965 Resonant interactions among capillary-gravity waves. J. Fluid Mech. 21, 305-331.

McGoldrick, L.F. 1970a An experiment on second-order capillary-gravity resonant interactions. J. Fluid Mech. 40, 251-271.

McGoldrick, L.F. 1970b On Wilton's ripples: a special case of resonant interactions. J. Fluid Mech. 42, 193-200.

McGoldrick, L.F. 1972 On the rippling of small waves: a harmonic nonlinear nearly resonant interaction. J. Fluid Mech. 52, 725-751.

McGoldrick, L.F., Phillips, O.M., Hung, N.E. and Hodgson, T.H. 1966 Measurements of third-order resonant wave interactions. J. Fluid Mech. 25, 437-456.

Miller, C.A. and Scriven, L.E. 1968 The oscillations of a fluid droplet immersed in another fluid. J. Fluid Mech. 32, 417-435.

Moeckel, G.P. 1975 Thermodynamics of an interface. Arch. Rat. Mech. Anal. 57, 255-280.

Morse, P.M. and Feshbach, H. 1953 Methods of theoretical Physics. McGraw-Hill Co. Vol. 1.

Multer, R.H. 1973 Exact nonlinear model of wave generator. J. Hyd. Div. A.S.C.E. 99, 31-46.

Nayfeh, A.H. 1970 Nonlinear stability of a liquid jet. Phys. Fluids 13, 841-847.

Nayfeh, A.H. 1971 Third-harmonic resonance in the interaction of capillary and gravity waves. J. Fluid Mech. 48, 385-395.

Nayfeh, A.H. and Mook, D.T. 1979 Nonlinear Oscillations, Wiley-Interscience.

Nix, J.R. 1972 Calculation of fission barriers for heavy and superheavy nuclei. Ann. Rev. Nucl. Sci. 22, 65-120.

Nuckolls, J., Wood, L., Thiessen, A. and Ziemmerman, G., 1972 Laser compression of matter to super-high densities: thermonuclear application. Nature 239, 139-142.

O'Konski, C.T. and Thacker, H.C. 1953 The distortion of aerosol droplets by an electric field. J. Phys. Chem. 57, 955-958.

Orr, F.M., Brown, R.A., and Scriven, L.E. 1977 Tree dimensional menisci: numerical simulation by finite elements. J. Colloid Interface Sci. 60, 137-147.

Patzek, T.W., Benner, R.E. and Scriven, L.E. 1982 Nonlinear Oscillations of inviscid free drops. Bull. Amer. Phys. Soc. 27, 1168.

Patzer, J.F., II, and Homsy, G.M., 1975 Hydrodynamic stability of thin spherically concentric fluid shells. J. Colloid Interface Science 51, 499-508.

Pavelle, R., Rothstein, M. and Fitch, J 1981 Computer algebra. Sci. Am. 245, 136-152.

Pfeifer, R.J. and Hendricks, C.D., 1967. Charge-to-mass relationships for electrohydrodynamically sprayed liquid droplets. Physics of Fluids 10, 2149-2154.

Philip, M.A., Gelbard, F. and Arnold, S. 1983 An absolute method for aerosol particle mass and charge measurement. J. of Colloid Interface Sci 91, 507-515.

Phillips, O.M., 1981 Wave interactions - the evolution of an idea. J. Fluid Mech. 106, 215-227.

Pimbley, G.H., Jr. 1976 Stationary solutions of the problem of Rayleigh-Taylor instability. J. math. Anal. Appl. 55, 170-206.

Plateau, J.A.F. 1873 Statique Experimentale et Theoritique des liquides soumis aux seules forces moleculaires. Gauthier-Villars.

Princen, H.M., Zia, I.Y.Z. and Mason, S.C., 1967 Measurement of interfacial tension from the shape of a rotating drop. J. Colloid Interface Sci. 23, 99-107.

Prosperetti, A. 1974 On the oscillations of drops and bubbles in viscous liquids. In Proc. Int. Colloq. on Drops and Bubbles. (Ed. D.J. Collins, M.S. Plesset and M.M. Saffren). Jet Propulsion Laboratory.

Prosperetti, A. 1980a Free oscillations of drops and bubbles: the initial-value problem. J. Fluid Mech. 100, 333-347.

Prosperetti, A. 1980b Normal-mode analysis for the oscillations of a viscous liquid drop in an immiscible liquid. J. de Mecanique 19, 149-182.

Rallison, J.M. 1984 The deformation of small viscous drops and bubbles in shear flows. Ann. Rev. Fluid Mech. 16, 45-66.

Rayleigh, J.W.S., 1879 On the capillary phenomena of jets. Proc. Poy. Soc. XXIX, 71-97.

Rayleigh, J.W.S., 1882 On the equilibrium of liquid conducting masses charged with electricity. Phil. Mag. 14, 184-186.

Reid, W.H. 1960 The oscillations of a viscous liquid drop. Q. Appl. Math. 18, 86-89.

Rienecker, M.M. and Fenton, J.D., 1981 A Fourier approximation method for steady water waves. J. Fluid Mech. 104, 119-137.

Rosencwaig, A. and Hendricks, C.D., 1977 Production of hollow glass microspheres. Laser Program, Annual Report. Lawrence Livermore Laboratory, UCRL-50021-77, 5.5-5.12.

Rotenberg, M., Bivins, R., Metropolis, N. and Wooten, J.K. 1959 The 3j and 6j Symbols. M.I.T. Technology Press.

Saffren, M., Elleman, D.D. and Rhim, W.K., 1981 Normal modes of a compound drop. In Proc. of the 2nd Int. Colloq. on Drops and Bubbles (Ed. by D. H. Le Croissette). Jet Propulsion Laboratory, 7-14.

Saito, H.L. and Scriven, L.E., 1981 Study of coating flow by finite element simulation. J. Comp. Phys., 42, 53-76.

Sample, S.B., Raghupathy, B. and Hendricks, C.D. 1970 Quiescent distortion

and resonant oscillations of a liquid drop in an electric field. Int. J. Engng Sci. 8, 97-109.

Sartor, J.D. 1961 Calculations of cloud electrification based on a general charge-separation mechanism J.Geophys. Res. 66, 831-838.

Saunders, C.P.R. 1974 Water drop interactions. In Proc. Int. Colloq. on Drops and Bubbles (ed. D.J. Collins, M.S. Plesset and Saffren). Jet Propulsion Laboratory, 487-505.

Savart, F. 1833 Memoire sur la constitution des veines liquides lancees par des orifices circulaires en mince paroi. Ann. de Chim. 53, 337-386.

Saville, D.A. 1974 Electrohydrodynamic oscillation and stability of a charged drop. Phys. Fluids 17, 54-60.

Silliman, W.J. and Scriven, L.E., 1980 Separating flow near a static contact line. J. Comp. Phys. 34, 287-313.

Stoker, J.J., 1957 Water Waves, Interscience, New York.

Strang, G. and Fix, G.J., 1973 An Analysis of the Finite Element Method. Prentice Hall, Englewood Cliffs.

Stratton, J.A. 1941 Electrohydrodynamic Theory. McGraw-Hill, New York.

Stuart, J.T., 1971 Nonlinear stability theory. Ann. Rev. Fluid Mech. 3, 347-371.

Swiatecki, W.J. 1956 Deformation energy of a charged drop. I. Qualitative features. Phys. Rev. 101, 651-654.

Swiatecki, W.J. 1956 Deformation energy of a charged drop. II. Symmetric saddle point shapes. Phys. Rev. 104, 993-1005.

Swiatecki, W.J. 1974 The rotating, charged or gravitating liquid drop, and problems in nuclear physics and astronomy. In Proc. Int. Colloq. on Drops and Bubbles (Ed. by D.J. Collins, M.S. Plesset and M.M. Saffren) Jet Propulsion Laboratory, 52-78.

Tadjbakhsh, I. and Keller, J.B. 1960 Standing surface waves of finite amplitude. J. Fluid Mech. 115, 453-474.

Takamatsu, T., Yamaguchi, M. and Katayama, T. 1982 Formation of single charged drops in liquid media under a uniform electric field. J. Chem. Eng. Japan 15, 349-355.

Tang, H.H.K. and Wong, C.Y. 1974 Vibration of a viscous liquid sphere. J. Phys. A: Math., Nucl. Gen. 7, 1038-1050.

Taylor, G.I. 1964 Disintegration of water drops in an electric field. Proc. Roy. Soc. Lond. A 280, 383-397.

Torza, S., Cox, R.G. and Mason, S.G 1972 Particle motions in sheared suspensions. XXVII. Transient and steady deformation and burst of liquid drops. J. Colloid Interface Sci. 38, 395-411.

Trinh, E., and Wang, T.G. 1982 Large-amplitude free and driven drop-shape oscillations: experimental observations. J. Fluid Mech. 122, 315-338.

Trinh, E., Zwern, A. and Wang, T.G. 1982 An experimental study of small-amplitude drop oscillations in immiscible liquid systems. J. Fluid Mech. 115, 453-474.

Tsamopoulos, J.A., Akylas, T.R. and Brown, R.A 1984 Dynamics of charged drop breakup. Proc. Roy. Soc. Lond. (submitted).

Tsamopoulos, J.A. and Brown, R.A. 1983 Nonlinear oscillations of inviscid drops and bubbles. J. Fluid Mech. 127, 519-537.

Tsamopoulos, J.A. and Brown, R.A. 1984 Resonant oscillations of inviscid drops. J. Fluid Mech. 147, 373-395.

Tsamopoulos, J.A. and Brown, R.A. 1985 The centering mechanism of a bubble inside a drop. Phys. Fluids (to be submitted)

Tsang, C.F., 1974 Similarities and differencies between volumecharged (nuclear) drops and charged conducting (rain) drops. In Proc. Int. Colloq. on Drops and Bubbles (ed. D.J. Collins, M.S. Plesset and M.M. Saffren). Jet Propulsion Laboratory, 85-105.

Ungar, L.H. and Brown, R.A. 1982 The dependence of the shape and stability of captive rotating drops on multiple parameters. Phil. Trans. R. Soc. Lond. A 306, 347-370.

Van Wijngaarden, L. 1976 Hydrodynamic interaction between gas bubbles in liquid. J. Fluid Mech. 77, 27-44.

Vrij, A. 1966 Possible mechanism for the spontaneous rupture of thin, free liquid films. Disc. Faraday Soc. 42, 23-33.

Vrij, A. and Overbeek, J.Th.G., 1968 Rupture of thin films due to spontaneous fluctuations in thickness. J. Amer. Chem. Soc. 90, 3074-3078.

Welch, J.E., Harlow, F.H., Shannon, J.P. and Daly, B.J., 1966 The MAC method, Los Alamos Scientific Laboratory Report LA-3425.

Williams, A. 1973 Combustion of droplets of fluid fuels: A Review. Combust. Flame 21, 1-31.

Wilton, J.R. 1915 On ripples. Phil. Mag. 29, 688-700.

Woerner, R.L., Draper, V.F., Koo, J.C. and Hendricks, C.D., 1980 Fabrication of glass spheres for laser fusion targets. Presented at Topical

Conference on Inertial Confinement Fusion, San Diego.

Wong, C.Y. and Tang, H.H.K. 1974 Vibrational frequency of non-conducting charged liquid drop. In Proc. second Int. Colloq. Drops Bubbles, (ed. D.H. Le Croissette) Pasadena, California: Jet Propulsion Laboratory.

Yonas, G., 1978 Fusion power with particle beams. Sci. Amer. 239, 50-61.

Zwick, S.A. and Plesset, M.S. 1955 On the dynamics of small vapor bubbles in liquids. J. Math. Phys. 33, 308-330.

X.1 APPENDIX A

The mean curvature $2\mathbf{H}$ and the normal, $\mathbf{n}$ and tangent, $\mathbf{t}$ vectors are expanded in ε as follows

$$
\begin{aligned}
-2\mathbf{H} = 2 &+ \varepsilon \sum_{i=2}^{\infty} (i-1)(i+2)\, F_i^{(1)} \\
&+ \frac{\varepsilon^2}{2} \Big\{ \sum_{j=0}^{\infty} (j-1)(j+2) F_j^{(2)} - 4 \sum_{i=2}^{\infty} (i^2+i-1)(F_i^{(1)})^2 \\
&+ \frac{\varepsilon^3}{6} \Big\{ \sum_{l=0}^{\infty} (l-1)(l+2) F_l^{(3)} + 18 \sum_{i=2}^{\infty} (i^2+i-\tfrac{2}{3})(F_i^{(1)})^3 \\
&\quad - 6 \sum_{i=2}^{\infty} \sum_{j=0}^{\infty} (i^2+i+j^2+j-2)\, F_i^{(1)} F_j^{(2)} \\
&\quad + 3 \sum_{i=2}^{\infty} (F_{i,\theta}^{(1)})^2 (3F_{i,\theta\theta}^{(1)} + \cot(\theta) F_{i,\theta}^{(1)}) \Big\} \Big\} , \qquad \text{(A1)}
\end{aligned}
$$

$$
\begin{aligned}
\mathbf{n} = \mathbf{e}_r &\{1 - \frac{\varepsilon^2}{2} (F_\theta^{(1)})^2 - \frac{\varepsilon^3}{6} [3F_\theta^{(1)} F_\theta^{(2)} - 6F^{(1)} (F_\theta^{(1)})^2]\} \\
&- \mathbf{e}_\theta \{\varepsilon F_\theta^{(1)} + \frac{\varepsilon^2}{2} [F_\theta^{(2)} - 2F^{(1)} F_\theta^{(1)}] \\
&+ \frac{\varepsilon^3}{6} [F_\theta^{(3)} - 3F^{(1)} F_\theta^{(2)} - 3(F_\theta^{(1)})^3 - 3F^{(2)} F_\theta^{(1)} + 6(F^{(1)})^2 F_\theta^{(1)}]\}, \qquad \text{(A2)}
\end{aligned}
$$

$$
\begin{aligned}
\mathbf{t} = \mathbf{e}_r &\{\varepsilon F_\theta^{(1)} + \frac{\varepsilon^2}{2} [F_\theta^{(2)} - 2F^{(1)} F_\theta^{(1)}] + \\
&\frac{\varepsilon^3}{6} [F_\theta^{(3)} - 3F^{(1)} F_\theta^{(2)} - 3(F_\theta^{(1)})^3 - 3F^{(2)} F_\theta^{(1)} + 6(F^{(1)})^2 F_\theta^{(1)}]\} \\
&+ \mathbf{e}_\theta \{1 - \frac{\varepsilon^2}{2} (F_\theta^{(1)})^2 - \frac{\varepsilon^3}{6} [3F_\theta^{(1)} F_\theta^{(2)} - 6F^{(1)} (F_\theta^{(1)})^2]\} . \qquad \text{(A3)}
\end{aligned}
$$

X.2 APPENDIX B

The equations that govern the second-order corrections are

$$\nabla^2\phi^{(2)} = 0 \qquad (0\leqq\eta\leqq 1,\ 0\leqq\theta\leqq\pi), \tag{B1}$$

$$\phi_\eta^{(2)} = 0 \qquad (\eta=0,\ 0\leqq\theta\leqq\pi), \tag{B2}$$

$$\phi_\eta^{(2)} - F_{T_0}^{(2)} = 2F_{T_1}^{(1)} - 2F^{(1)}\phi_{\eta\eta}^{(1)} + 2F_\theta^{(1)}\phi_\theta^{(1)} \qquad (\eta = 1,\ 0\leqq\theta\leqq\pi), \tag{B3}$$

$$\phi_{T_0}^{(2)} + 2F^{(1)}\phi_{T_0\eta}^{(1)} + 2\phi_{T_1}^{(1)} + (\phi_\eta^{(1)})^2 + (\phi_\theta^{(1)})^2 - \frac{1}{4\pi}[V_\eta^{(1)} + F^{(1)}V_{\eta\eta}^{(0)}]^2$$

$$- \frac{1}{4\pi}V_\eta^{(0)}[V_\eta^{(2)} - (F_\theta^{(1)})^2 V_\eta^{(0)} + 2F^{(1)}V_{\eta\eta}^{(1)} + F^{(2)}V_{\eta\eta}^{(0)} + (F^{(1)})^2 V_{\eta\eta\eta}^{(0)}$$

$$- 2F_\theta^{(1)}V_\theta^{(1)}] = -\sum_{m=2}^{\infty}(m-1)(m+2)F^{(2)} + 4(F^{(1)})^2(n^2 + n - 1)$$

$$(\eta=1,\ 0\leqq\theta\leqq\pi), \tag{B4}$$

$$\int_0^\pi \{2F^{(1)2} + F^{(2)}\}\sin(\theta)\,d\theta = 0, \tag{B5}$$

$$\nabla^2 V^{(2)} = 0 \qquad (1\leqq\eta\leqq\infty,\ 0\leqq\theta\leqq\pi), \tag{B6}$$

$$V^{(2)} \to 0 \qquad (\eta\to\infty,\ 0\leqq\theta\leqq\pi), \tag{B7}$$

$$\int_0^\pi [V_\eta^{(2)} + F^{(2)}V_{\eta\eta}^{(0)} + 2F^{(1)}V_{\eta\eta}^{(1)} + (F^{(1)})^2 V_{\eta\eta\eta}^{(0)} - (F_\theta^{(1)})^2 V_\eta^{(0)}$$

$$- 2F_\theta^{(1)}V_\theta^{(1)} + 4F^{(1)}(V_\eta^{(1)} + F^{(1)}V_{\eta\eta}^{(0)})]\sin(\theta)\,d\theta$$

$$- Q^{(0)}\int_0^\pi [2F^{(2)} + 2(F^{(1)})^2 + (F_\theta^{(1)})^2]\sin(\theta)\,d\theta = 0 \quad (\eta=1), \tag{B8}$$

$$V_\theta^{(2)} + 2F^{(1)}(V_{\theta\eta}^{(1)} - V_\theta^{(1)}) + V_\eta^{(0)}(F_\theta^{(2)} - 2F^{(1)}F_\theta^{(1)}) +$$

$$2F_{\theta}^{(1)}(V_{\eta}^{(1)} + F^{(1)}V_{\eta\eta}^{(0)}) = 0 \qquad (\eta=1,\ 0\leq\theta\leq\pi), \tag{B9}$$

$$F^{(2)}(\theta,0,0,0) = \begin{bmatrix} -\frac{2}{5}, & (n=2) \\ -\frac{2}{7}, & (n=3) \\ -\frac{2}{9}, & (n=4) \end{bmatrix}, \tag{B10}$$

$$2F_{T_1}^{(1)} + F_{T_0}^{(2)} = 0 \qquad (T_0 = T_1 = T_2 = 0), \tag{B11}$$

The coefficients in the second-order correction (equation (V.2.21)) to the drop shape are

$$\begin{aligned}
L_{220} &= -\frac{2}{5}\cos^2(\Psi_2) \\
L_{222} &= -G_2\cos(\omega_2 T_0) + \frac{1}{21}[G_{21}\cos(2\Psi_2) + G_{22}] \\
L_{224} &= -\frac{G_4}{3}\cos(\omega_4 T_0) + \frac{48}{35}[G_{41}\cos(2\Psi_2) + G_{42}] \\
L_{230} &= -\frac{2}{7}\cos^2(\Psi_3) \\
L_{232} &= -H_2\cos(\omega_2 T_0) + \frac{8}{21}[H_{21}\cos(2\Psi_3) + H_{22}] \\
L_{234} &= -\frac{H_4}{3}\cos(\omega_4 T_0) + \frac{144}{77}[H_{41}\cos(2\Psi_3) + H_{42}] \\
L_{236} &= -\frac{H_6}{5}\cos(\omega_6 T_0) + \frac{600}{77}[H_{61}\cos(2\Psi_3) + H_{62}] \\
L_{240} &= -\frac{2}{9}\cos^2(\Psi_4)
\end{aligned} \tag{B12}$$

$$L_{242} = - I_2 \cos(\omega_2 T_0) + \frac{50}{693} [I_{21} \cos(2\Psi_4) + I_{22}]$$

$$L_{244} = - \frac{I_4}{3} \cos(\omega_4 T_0) + \frac{54}{1001} [I_{41} \cos(2\Psi_4) + I_{42}]$$

$$L_{246} = - \frac{I_6}{5} \cos(\omega_6 T_0) + \frac{40}{33} [I_{61} \cos(2\Psi_4) + I_{62}]$$

$$L_{248} = - \frac{I_8}{7} \cos(\omega_8 T_0) + \frac{15680}{1287} [I_{81} \cos(2\Psi_4) + I_{82}]$$

The coefficients in the second-order correction to the velocity potential are

$$M_{220} = \frac{S_{20}}{\omega_2} \sin(2\Psi_2)$$

$$M_{222} = \frac{G_2 \omega_2}{2} \sin(\omega_2 T_0) + \frac{S_{22}}{\omega_2} \sin(2\Psi_2)$$

$$M_{224} = \frac{G_4 \omega_4}{12} \sin(\omega_4 T_0) + S_{24} \omega_2 \sin(2\Psi_2)$$

$$M_{230} = \frac{S_{30}}{\omega_3} \sin(2\Psi_3)$$

$$M_{232} = \frac{H_2 \omega_2}{2} \sin(\omega_2 T_0) + S_{32} \omega_3 \sin(2\Psi_3)$$

$$M_{234} = \frac{H_4 \omega_4}{12} \sin(\omega_4 T_0) + S_{34} \omega_3 \sin(2\Psi_3)$$

$$M_{236} = \frac{H_6 \omega_6}{30} \sin(\omega_6 T_0) + S_{36} \omega_3 \sin(2\Psi_3) \qquad \text{(B13)}$$

$$M_{240} = \frac{S_{40}}{\omega_4} \sin(2\Psi_4)$$

$$M_{242} = \frac{I_2 \omega_2}{2} \sin(\omega_2 T_0) + S_{42} \omega_4 \sin(2\Psi_4)$$

$$M_{244} = \frac{I_4\ \omega_4}{12} \sin(\omega_4 T_0) + S_{44}\ \omega_4 \sin(2\Psi_4)$$

$$M_{246} = \frac{I_6\ \omega_6}{30} \sin(\omega_6 T_0) + S_{46}\ \omega_4 \sin(2\Psi_4)$$

$$M_{248} = \frac{I_8\ \omega_8}{56} \sin(\omega_8 T_0) + S_{48}\ \omega_4 \sin(2\Psi_4)$$

The coefficients in the second-order correction to the electric potential are

$$N_{220} = 0$$

$$N_{222} = Q\ (L_{222} - \frac{20}{7} L_{220})$$

$$N_{224} = Q\ (L_{224} - \frac{36}{7} L_{220})$$

$$N_{230} = 0$$

$$N_{232} = Q\ (L_{232} - 4\ L_{230})$$

$$N_{234} = Q\ (L_{234} - \frac{54}{11} L_{230})$$

$$N_{236} = Q\ (L_{236} - \frac{100}{11} L_{230}) \qquad \text{(B14)}$$

$$N_{240} = 0$$

$$N_{242} = Q\ (L_{242} - \frac{400}{77} L_{240})$$

$$N_{244} = Q\ (L_{244} - \frac{5832}{1001} L_{240})$$

$$N_{246} = Q\ (L_{246} - \frac{80}{11} L_{240})$$

$$N_{248} = Q\ (L_{248} - \frac{1960}{143} L_{240})$$

where

$$G_{21} = \frac{23\hat{Q} - 116}{\omega_2^2} \qquad G_{22} = \frac{-15\hat{Q} + 132}{\omega_2^2} \qquad G_2 = \frac{1}{21}(G_{21} + G_{22})$$

$$G_{41} = \frac{-9\hat{Q}^2 - 54\hat{Q} + 648}{(\omega_4^2 - 4\omega_2^2)\,\omega_4^2} \qquad G_{42} = \frac{15\hat{Q}^2 - 258\hat{Q} + 1080}{(\omega_4^2 - 4\omega_2^2)\,\omega_4^2} \qquad G_4 = \frac{144}{35}(G_{41} + G_{42})$$

$$H_{21} = \frac{39\hat{Q}^2 - 380\hat{Q} + 896}{(\omega_2^2 - 4\omega_3^2)\,\omega_2^2} \qquad H_{22} = \frac{-33\hat{Q}^2 + 652\hat{Q} - 2464}{(\omega_2^2 - 4\omega_3^2)\,\omega_2^2} \qquad H_2 = \frac{8}{21}(H_{21} + H_{22})$$

$$H_{41} = \frac{28\hat{Q}^2 - 470\hat{Q} + 1812}{(\omega_4^2 - 4\omega_3^2)\,\omega_4^2} \qquad H_{42} = \frac{-8\hat{Q}^2 + 234\hat{Q} - 808}{(\omega_4^2 - 4\omega_3^2)\,\omega_4^2} \qquad H_4 = \frac{432}{77}(H_{41} + H_{42})$$

$$H_{61} = \frac{-55\hat{Q}^2 + 420\hat{Q} + 160}{(\omega_6^2 - 4\omega_3^2)\,\omega_6^2} \qquad H_{62} = \frac{9\hat{Q}^2 - 284\hat{Q} + 2080}{(\omega_6^2 - 4\omega_3^2)\,\omega_6^2} \qquad H_6 = \frac{3000}{77}(H_{61} + H_{62})$$

$$I_{21} = \frac{331\hat{Q}^2 - 3518\hat{Q} + 8776}{(\omega_2^2 - 4\omega_4^2)\,\omega_2^2} \qquad I_{22} = \frac{-299\hat{Q}^2 + 8398\hat{Q} - 40040}{(\omega_2^2 - 4\omega_4^2)\,\omega_2^2} \qquad I_2 = \frac{50}{693}(I_{21} + I_{22})$$

$$I_{41} = \frac{65\hat{Q} - 602}{\omega_4^2} \qquad I_{42} = \frac{3\hat{Q} + 618}{\omega_4^2} \qquad I_4 = \frac{162}{1001}(I_{41} + I_{42})$$

$$I_{61} = \frac{-15\hat{Q}^2 - 2510\hat{Q} + 21040}{(\omega_6^2 - 4\omega_4^2)\,\omega_6^2} \qquad I_{62} = \frac{-33\hat{Q}^2 + 1918\hat{Q} - 4880}{(\omega_6^2 - 4\omega_4^2)\,\omega_6^2} \qquad I_4 = \frac{200}{33}(I_{61} + I_{62})$$

$$I_{81} = \frac{-203\hat{Q}^2 + 2254\hat{Q} - 2240}{(\omega_8^2 - 4\omega_4^2)\,\omega_8^2} \qquad I_{82} = \frac{13\hat{Q}^2 - 662\hat{Q} + 7480}{(\omega_8^2 - 4\omega_4^2)\,\omega_8^2} \qquad I_8 = \frac{109760}{1287}(I_{81} + I_{82})$$

and

$$S_{20} = \frac{-3\hat{Q} + 13}{10} \qquad S_{22} = \frac{4(-5\hat{Q} + 26)}{21} \qquad S_{24} = \frac{36(-2\hat{Q} + 9)}{35(\omega_4^2 - 4\omega_2^2)}$$

$$S_{30} = \frac{-20\hat{Q} + 85}{14} \qquad S_{32} = \frac{16(\hat{Q} - 6)}{3(\omega_2^2 - 4\omega_3^2)}$$

$$S_{34} = \frac{60(4\hat{Q} - 35)}{77(\omega_4^2 - 4\omega_3^2)} \qquad S_{36} = \frac{1600(-\hat{Q} + 6)}{231(\omega_6^2 - 4\omega_3^2)}$$

$$S_{40} = \frac{-72\hat{Q} + 378}{36} \qquad S_{42} = \frac{50(12\hat{Q} - 83)}{77(\omega_2^2 - 4\omega_4^2)} \qquad S_{44} = \frac{54(-37\hat{Q} + 328)}{1001\omega_4^2}$$

$$S_{46} = \frac{10(2\hat{Q} - 35)}{11(\omega_6^2 - 4\omega_4^2)} \qquad S_{48} = \frac{980(-2\hat{Q} + 15)}{143(\omega_8^2 - 4\omega_4^2)}$$

where $\hat{Q} \equiv \frac{Q^2}{4\pi}$

X.3 APPENDIX C

The equations that govern the third-order problem are

$$\nabla^2\phi^{(3)} = 0 \qquad (0\leqq\eta\leqq1,\ 0\leqq\theta\leqq\pi), \tag{C1}$$

$$\phi^{(3)}_{\eta} = 0 \qquad (\eta=0,\ 0\leqq\theta\leqq\pi), \tag{C2}$$

$$\phi^{(3)}_{\eta} - F^{(3)}_{T_0} = 3F^{(2)}_{T_1} + 3F^{(1)}_{T_2} - 3F^{(2)}\phi^{(1)}_{\eta\eta} - 3F^{(1)}\phi^{(2)}_{\eta\eta} - 3(F^{(1)})^2\phi^{(1)}_{\eta\eta\eta}$$

$$+ 3F^{(2)}_{\theta}\phi^{(1)}_{\theta} + 3F^{(1)}_{\theta}(\phi^{(2)}_{\theta} + 2F^{(1)}\phi^{(1)}_{\eta\theta} - 4F^{(1)}\phi^{(1)}_{\theta}) \quad (\eta=1, 0\leqq\theta\leqq\pi), \tag{C3}$$

$$\phi^{(3)}_{T_0} + 3F^{(2)}\phi^{(1)}_{T_0\eta} + 3\phi^{(2)}_{T_1} + 3\phi^{(1)}_{T_2} + 3F^{(1)}(\phi^{(2)}_{T_0\eta} + F^{(1)}\phi^{(1)}_{T_0\eta\eta} + 2\phi^{(1)}_{T_1\eta})$$

$$+ 3\phi^{(1)}_{\eta}(\phi^{(2)}_{\eta} + 2F^{(1)}\phi^{(1)}_{\eta\eta}) + 3\phi^{(1)}_{\theta}(\phi^{(2)}_{\theta} + 2F^{(1)}\phi^{(1)}_{\theta\eta}) - 6F^{(1)}(\phi^{(1)}_{\theta})^2$$

$$- \frac{3}{4\pi}(V^{(1)}_{\eta} + F^{(1)}V^{(0)}_{\eta\eta})[(F^{(1)})^2 V^{(0)}_{\eta\eta\eta} + 2F^{(1)}V^{(1)}_{\eta\eta} - (F^{(1)}_{\theta})^2 V^{(0)}_{\eta}$$

$$+ F^{(2)}V^{(0)}_{\eta\eta} + V^{(2)}_{\eta} - 2F^{(1)}_{\theta}V^{(1)}_{\theta}]$$

$$- \frac{1}{4\pi}V^{(0)}_{\eta}\{3V^{(0)}_{\eta}[2F^{(1)}(F^{(1)}_{\theta})^2 - F^{(1)}_{\theta}F^{(2)}_{\theta}] - 3V^{(1)}_{\eta}(F^{(1)}_{\theta})^2$$

$$+ (F^{(1)})^2[3V^{(1)}_{\eta\eta\eta} + F^{(1)}V^{(0)}_{\eta\eta\eta\eta}] + 3F^{(1)}[V^{(2)}_{\eta\eta} + F^{(2)}V^{(0)}_{\eta\eta\eta}$$

$$- V^{(0)}_{\eta\eta}(F^{(1)}_{\theta})^2] + F^{(3)}V^{(0)}_{\eta\eta} + V^{(3)}_{\eta} + 3F^{(2)}V^{(1)}_{\eta\eta} - 3V^{(1)}_{\theta}F^{(2)}_{\theta}$$

$$+ 12F^{(1)}F^{(1)}_{\theta}V^{(1)}_{\theta} - 3F^{(1)}_{\theta}(V^{(2)}_{\theta} + 2F^{(1)}V^{(1)}_{\theta\eta})\} = (2\mathbf{H})^{(3)}$$
$$(\eta=1,\ 0\leqq\theta\leqq\pi), \tag{C4}$$

$$\int_0^{\pi} \{2(F^{(1)})^3 + F^{(3)} + 6F^{(1)}F^{(2)}\} \sin(\theta)\, d\theta = 0, \qquad (C5)$$

$$\nabla^2 V^{(3)} = 0 \qquad (1 \leqq \eta \leqq \infty,\ 0 \leqq \theta \leqq \pi), \qquad (C6)$$

$$V^{(3)} \to 0 \qquad (\eta \to \infty,\ 0 \leqq \theta \leqq \pi), \qquad (C7)$$

$$\int_0^{\pi} [V_{\eta}^{(3)} + 3F^{(2)}V_{\eta\eta}^{(1)} + F^{(3)}V_{\eta\eta}^{(0)} + (F^{(1)})^2(3V_{\eta\eta\eta}^{(1)} + F_{\theta}^{(1)}V_{\eta\eta\eta}^{(0)})$$

$$- 3F_{\theta}^{(1)}(V_{\theta}^{(2)} + 2F^{(1)}V_{\theta\eta}^{(1)}) + 3V_{\theta}^{(1)}(4F^{(1)}F_{\theta}^{(1)} - F_{\theta}^{(2)})$$

$$+ 3V_{\eta}^{(0)}F_{\theta}^{(1)}(2F^{(1)}F_{\theta}^{(1)} - F_{\theta}^{(2)}) - 3(F_{\theta}^{(1)})^2V_{\eta}^{(1)}$$

$$+ 3F^{(1)}[V_{\eta\eta}^{(2)} + F^{(2)}V_{\eta\eta\eta}^{(0)} - (F_{\theta}^{(1)})^2V_{\eta\eta}^{(0)}] \sin(\theta)\, d\theta$$

$$+ 6\int_0^{\pi} F^{(1)}[V_{\eta}^{(2)} + F^{(2)}V_{\eta\eta}^{(0)} + F^{(1)}(2V_{\eta\eta}^{(1)} + F^{(1)}V_{\eta\eta\eta}^{(0)})$$

$$- F_{\theta}^{(1)}(2V_{\theta}^{(1)} + F_{\theta}^{(1)}V_{\eta}^{(0)})] \sin(\theta)\, d\theta$$

$$+ 3\int_0^{\pi} (V_{\eta}^{(1)} + F^{(1)}V_{\eta\eta}^{(0)})[2F^{(2)} + 2(F^{(1)})^2 + (F_{\theta}^{(1)})^2] \sin(\theta)\, d\theta$$

$$- Q^{(0)}\int_0^{\pi} [2F^{(3)} + 6F^{(1)}F^{(2)} + 3F_{\theta}^{(1)}F_{\theta}^{(2)}] \sin(\theta)\, d\theta = 0 \ (\eta=1), \qquad (C8)$$

$$V_{\theta}^{(3)} + 3F^{(2)}V_{\theta\eta}^{(1)} + 3F^{(1)}(V_{\theta\eta}^{(2)} + F^{(1)}V_{\theta\eta\eta}^{(1)}) - 3F^{(1)}(V_{\theta}^{(2)} + 2F^{(1)}V_{\theta\eta}^{(1)})$$

$$- 3V_{\theta}^{(1)}[F^{(2)} - 2(F^{(1)})^2 + (F_{\theta}^{(1)})^2] + 3F_{\theta}^{(1)}(F^{(2)}V_{\eta\eta}^{(0)} + V_{\eta}^{(2)})$$

$$+ V_{\eta}^{(0)}[3F^{(1)}(2F^{(1)}F_{\theta}^{(1)} - F_{\theta}^{(2)}) - 3F_{\theta}^{(1)}(F^{(2)} + (F_{\theta}^{(1)})^2) + F_{\theta}^{(3)}]$$

$$+ 3V_{\eta}^{(1)}(F_{\theta}^{(2)} - 2F^{(1)}F_{\theta}^{(1)}) + 3(F^{(1)})^2F_{\theta}^{(1)}(V_{\eta\eta\eta}^{(0)} - 2V_{\eta\eta}^{(0)})$$

$$+ 3F^{(1)}(F_{\theta}^{(2)}V_{\eta\eta}^{(0)} + 2F_{\theta}^{(1)}V_{\eta\eta}^{(1)}) = 0 \qquad (\eta=1, \quad 0\leqq\theta\leqq\pi), \tag{C9}$$

$$F^{(3)}(\theta,0,0,0) = \begin{bmatrix} -\frac{4}{35}, & (n=2) \\ 0, & (n=3) \\ -\frac{36}{1001}, & (n=4) \end{bmatrix}, \tag{C10}$$

$$3F_{T_2}^{(1)} + 3F_{T_1}^{(2)} + F_{T_0}^{(3)} = 0 \qquad (T_0 = T_1 = T_2 = 0), \tag{C11}$$

X.4 APPENDIX D

Integrals of products of Legendre polynomials and their derivatives are conveniently written in terms of the 3j and 6j symbols (Rotenberg et al. 1959; Brink & Satcher 1968). Several integrals used in the analysis presented here are

$$I_1 \equiv \int_0^\pi P_n(\theta)\, P_m(\theta)\, P_l(\theta)\, \sin(\theta)\, d\theta = 2 \begin{bmatrix} n & m & l \\ 0 & 0 & 0 \end{bmatrix}^2 , \tag{D1}$$

$$I_2 \equiv \int_0^\pi P_n'(\theta)\, P_m'(\theta)\, P_l'(\theta)\, \sin(\theta)\, d\theta = -2[n(n+1)m(m+1)]^{1/2} \begin{bmatrix} n & m & l \\ 1 & -1 & 0 \end{bmatrix} \begin{bmatrix} n & m & l \\ 0 & 0 & 0 \end{bmatrix} \tag{D2}$$

$$I_3 \equiv \int_0^\pi P_n(\theta)\, P_m(\theta)\, P_l(\theta)\, P_k(\theta)\, \sin(\theta)\, d\theta = 2 \sum_{j=|n-m|}^{n+m} (2j+1) \begin{bmatrix} n & m & j \\ 0 & 0 & 0 \end{bmatrix}^2 \begin{bmatrix} l & k & j \\ 0 & 0 & 0 \end{bmatrix}^2 , \tag{D3}$$

$$I_4 \equiv \int_0^\pi P_n'(\theta)\, P_m'(\theta)\, P_l(\theta)\, P_k(\theta)\, \sin(\theta)\, d\theta = -2[n(n+1)m(m+1)]^{1/2} \sum_{j=|n-m|}^{n+m} (2j+1) \begin{bmatrix} n & m & j \\ 1 & -1 & 0 \end{bmatrix} \begin{bmatrix} n & m & j \\ 0 & 0 & 0 \end{bmatrix} \begin{bmatrix} l & k & j \\ 0 & 0 & 0 \end{bmatrix}^2 . \tag{D4}$$

Properties of the symbol $\begin{bmatrix} n & m & l \\ a & b & c \end{bmatrix}$ cause it to be zero whenever the triangle inequality ($|l-m| \leq n \leq l+m$) is not satisfied between the integers of the first row. It is this property that terminates the expansions (e.g. (IV.2.4) and (IV.2.23) for the drop shapes and potentials. This symbol is also identically zero when $a+b+c \neq 0$, or when $a=b=c=0$ and simultaneously $n+m+l=2\lambda+1$, where $\lambda=0,1,2,\ldots$. It is this last property that eliminates the odd-order Legendre polynomials from the second-order approximation.

X.5 APPENDIX E

The equations that govern the second-order corrections are

$$\nabla^2 \phi^{(2)} = 0 \qquad (R \leqq \eta \leqq 1,\ 0 \leqq \theta \leqq \pi), \tag{E1}$$

$$F^{(2)}_{1T_0} = \phi^{(2)}_{\eta} - 2F^{(1)}_{1T_1} + 2F^{(1)}_{1}\phi^{(1)}_{\eta\eta} - 2F^{(1)}_{1\theta}\phi^{(1)}_{\theta} \qquad (\eta = R,\ 0 \leqq \theta \leqq \pi), \tag{E2}$$

$$F^{(2)}_{2T_0} = \phi^{(2)}_{\eta} - 2F^{(1)}_{2T_1} + 2F^{(1)}_{2}\phi^{(1)}_{\eta\eta} - 2F^{(1)}_{2\theta}\phi^{(1)}_{\theta} \qquad (\eta = 1,\ 0 \leqq \theta \leqq \pi), \tag{E3}$$

$$\phi^{(2)}_{T_0} = -2F^{(1)}_{1}\phi^{(1)}_{T_0\eta} - 2\phi^{(1)}_{T_1} - [(\phi^{(1)}_{\eta})^2 + (\tfrac{1}{r}\,\phi^{(1)}_{\theta})^2]$$

$$+ \sum_{m=2}^{\infty} (m-1)(m+2)F^{(2)}_{1}/R^2 - 4F^{(1)}_{1}[F^{(1)}_{1} + F^{(1)}_{1}(n-1)(n+2)]/R^3$$

$$(\eta = R,\ 0 \leqq \theta \leqq \pi), \tag{E4}$$

$$\phi^{(2)}_{T_0} = -2F^{(1)}_{2}\phi^{(1)}_{T_0\eta} - 2\phi^{(1)}_{T_1} - [(\phi^{(1)}_{\eta})^2 + (\tfrac{1}{r}\,\phi^{(1)}_{\theta})^2]$$

$$- \sum_{m=2}^{\infty} (m-1)(m+2)F^{(2)}_{2} + 4F^{(1)}_{2}[F^{(1)}_{2} + F^{(1)}_{2}(n-1)(n+2)]$$

$$(\eta = 1,\ 0 \leqq \theta \leqq \pi), \tag{E5}$$

$$\int_0^{\pi} \{2F^{(1)2}_{1,2} + F^{(2)}_{1,2}\} \sin(\theta)\, d\theta = 0, \tag{E6a,b}$$

$$F^{(2)}_{1}(\theta,0,0,0) = -\frac{2}{5}B^2 - \frac{2}{3}A(t=0)^2 \quad , \tag{E7}$$

$$F^{(2)}_{2}(\theta,0,0,0) = -\frac{2}{5} \quad , \tag{E8}$$

$$2F^{(1)}_{1T_1} + F^{(2)}_{1T_0} = 0 \qquad (T_0 = T_1 = T_2 = 0)\ , \tag{E9}$$

$$2F^{(1)}_{2T_1} + F^{(2)}_{2T_0} = 0 \qquad (T_0 = T_1 = T_2 = 0)\ , \tag{E10}$$

The coefficients in the second-order correction to the coefficients $\alpha_{ij}^{(2)}$ are

$$\alpha_{10}^{(2)} = (D^2 R_{10} e^{2\omega T_0} + c.c.) + HR_{10} ,$$

$$\alpha_{20}^{(2)} = (D^2 R_{20} e^{2\omega T_0} + c.c.) + HR_{20} ,$$

$$\alpha_{30}^{(2)} = (D^2 R_{30} e^{2\omega T_0} + c.c.) + HR_{30} , \qquad \text{(E11)}$$

$$\alpha_{40}^{(2)} = (D^2 R_{40} e^{2\omega T_0} + c.c.) + HR_{40} ,$$

$$\alpha_{11}^{(2)} = A(D R_{11} e^{\omega T_0} + c.c.) + HR_{11} ,$$

$$\alpha_{21}^{(2)} = - \alpha_{11}^{(2)} ,$$

$$\alpha_{31}^{(2)} = A(D R_{21} e^{\omega T_0} + c.c.) + HR_{21} , \qquad \text{(E12)}$$

$$\alpha_{41}^{(2)} = 0 ,$$

$$\alpha_{12}^{(2)} = (D^2 R_{12} e^{2\omega T_0} + c.c.) + (HR_{12} e^{\omega T_0} + c.c.) ,$$

$$\alpha_{22}^{(2)} = (D^2 R_{22} e^{2\omega T_0} + c.c.) + (HR_{22} e^{\omega T_0} + c.c.) ,$$

$$\alpha_{32}^{(2)} = (D^2 R_{32} e^{2\omega T_0} + c.c.) + (HR_{32} e^{\omega T_0} + c.c.) , \qquad \text{(E13)}$$

$$\alpha_{42}^{(2)} = (D^2 R_{42} e^{2\omega T_0} + c.c.) + (HR_{42} e^{\omega T_0} + c.c.) ,$$

$$\alpha_{13}^{(2)} = A(D R_{13} e^{\omega T_0} + c.c.) + (HR_{13} e^{\omega_3 T_0} + c.c.) ,$$

$$\alpha_{23}^{(2)} = -\alpha_{13}^{(2)} \quad ,$$

$$\alpha_{33}^{(2)} = A(D\,R_{23}\,e^{\omega T_0} + c.c.) + (HR_{33}\,e^{\omega_3 T_0} + c.c.) \quad , \tag{E14}$$

$$\alpha_{43}^{(2)} = 0 \quad ,$$

$$\alpha_{14}^{(2)} = (D^2\,R_{14}\,e^{2\omega T_0} + c.c.) + (HR_{14}\,e^{\omega_4 T_0} + c.c.) \quad ,$$

$$\alpha_{24}^{(2)} = (D^2\,R_{24}\,e^{2\omega T_0} + c.c.) + (HR_{24}\,e^{\omega_4 T_0} + c.c.) \quad ,$$

$$\alpha_{34}^{(2)} = (D^2\,R_{34}\,e^{2\omega T_0} + c.c.) + (HR_{34}\,e^{\omega_4 T_0} + c.c.) \quad , \tag{E15}$$

$$\alpha_{44}^{(2)} = (D^2\,R_{44}\,e^{2\omega T_0} + c.c.) + (HR_{44}\,e^{\omega_4 T_0} + c.c.) \quad .$$

where $\omega \equiv \omega_2$, $A \equiv A(T_2)$, $D \equiv D(T_2)$ and the coefficients R_{ij} are given below

$$R_{10} = -\{[60R^5(R^2 + \chi_3^2) + 45\chi_2^2(1 - R^7) + 30R^7\chi_1^2(R^3 - 1)] / (2\omega)$$
$$+ 3R^7(3\chi_2 - 2\chi_1) + 3R^4(2\chi_1 R^5 - 3\chi_2)\chi_3] / [15R^7(R - 1)] \quad ,$$

$$HR_{10} = [5(4 - 2\chi_1^2 - 3\chi_2^2) + 2\omega(3\chi_2 - 2\chi_1)] / 10 \quad ,$$

$$R_{20} = \{[60R^5(R^3 + \chi_3^2) + 45\chi_2^2(1 - R^8) + 30R^8\chi_1^2(R^2 - 1)] / (2\omega)$$
$$+ 3R^8(3\chi_2 - 2\chi_1) + 3R^4(2\chi_1 R^5 - 3\chi_2)\chi_3] / [15R^7(R - 1)] \quad , \tag{E16}$$

$$HR_{20} = -[5(2R^{10}\chi_1^2 + 3\chi_2^2 + 4R^5\chi_3^2) + 2\omega(2R^9\chi_1 - 3R^4\chi_2)\chi_3] / (10R^6) \quad ,$$

$$R_{30} = -[6(R^2 - 2)\chi_2 + 2R^5(3R^2 - 1)\chi_1]\chi_3 / (5\omega R^5) \quad ,$$

$$HR_{30} = -\frac{2}{3} - \frac{2}{5}\chi_3^2 - \frac{R_{30}}{2} \quad ,$$

$$R_{40} = 2(3\chi_2 - 2\chi_1) / (5\omega) \quad ,$$

$$HR_{40} = -\frac{2}{5} - \frac{R_{40}}{2} \quad ,$$

$$R_{11} = -4[12R\chi_3/\omega + (-3\chi_2 + 2\chi_1 R^5)] / [5R(R^3 - 1)] \quad ,$$

$$HR_{11} = [24R\chi_3 - 2\omega(3\chi_2 - 2R^5\chi_1)] / 15R^3 \quad ,$$

$$R_{21} = -4[3R^2 - 12)\chi_2 + R^5(3R^2 - 2)\chi_1] / (5\omega R^4) \quad , \qquad \text{(E17)}$$

$$HR_{21} = -R_{21} \quad ,$$

$$R_{12} = -\{[60R^5(1 + \chi_3^2) + 21R^5(R^5 - 1)\chi_1^2 + 36(1 - R^5)\chi_2^2] / \omega$$

$$+ 6R^5(3\chi_2 - 2\chi_1) + 6R^4(2R^5\chi_1 - 3\chi_2)\chi_3\} / [21R^5(R^5 - 1)] \quad ,$$

$$HR_{12} = \{20R^4(1 + R\chi_3^2) + 12\chi_2^2(1 - R^4) + 6\chi_1\chi_2R^4(1 - R) + 7\chi_1^2R^4(R^6 - 1)$$

$$+ 2\omega R^4[2\chi_1(R^5\chi_3 - 1) + 3\chi_2(1 - \chi_3)]\} / (14R^4(R^5 - 1)] \quad ,$$

$$R_{22} = \{[60R^5(R^5 + \chi_3^2) + 18R^5(R^5 - 1)\chi_1\chi_2 + 36(1 - R^{10})\chi_2^2] / \omega$$

$$+ 6R^{10}(3\chi_2 - 2\chi_1) + 6R^4(2R^5\chi_1 - 3\chi_2)\chi_3\} / [21R^5(R^5 - 1)] \quad , \qquad \text{(E18)}$$

$$HR_{22} = \{40(\chi_3^2 + R^5) + 24\chi_2^2(1 - R^9) + 12\chi_1\chi_2R^5(R^4 - 1) + 14\chi_1^2R^9(R - 1)$$

$$+ 4\omega[2\chi_1R^9(\chi_3 - 1) + 3\chi_2(R^9 - \chi_3R^4)]\} / [42R^4(R^5 - 1)] \quad ,$$

$$R_{32} = -[6(R^2 - 4)\chi_2 + 2R^5(3R^2 - 2)\chi_1]\chi_3 / (7\omega R^5) \quad ,$$

$$HR_{32} = -\frac{R_{32}}{4} \quad ,$$

$$R_{42} = 2(9\chi_2 - \chi_1) / (7\omega) \quad ,$$

$$HR_{42} = -\frac{R_{42}}{4} \quad ,$$

$$R_{13} = -6[12R^2\chi_3/\omega + (-3R\chi_2 + 2R^6\chi_1)] / [5(R^7 - 1)] \quad ,$$

$$HR_{13} = [36R\chi_3 - 3\omega(3\chi_2 - 2\chi_1)] / (35R^3) \quad ,$$

$$R_{23} = 12[(R^2 + 6)\chi_2 + R^5(R^2 + 1)\chi_1] / (5\omega R^4) \quad , \qquad \text{(E19)}$$

$$HR_{23} = -\frac{R_{23}}{2} \quad ,$$

$$R_{14} = -\{[180R^3(1 + R^2\chi_3^2) + 45(1 - R^3)\chi_2^2 + 180R^3(1 - R^2)\chi_1\chi_2] / \omega$$
$$+ 18R^3(3\chi_2 - 2\chi_1) + 18R^4(2\chi_1R^5 - 3\chi_2)\chi_3\} / [35R^3(R^9 - 1)] \quad ,$$

$$HR_{14} = \{180(R^5\chi_3^2 + R^2) + 45\chi_2^2(1 - R^2) + 180\chi_1\chi_2R^2(1 - R^3) +$$
$$18\omega[(3\chi_2 - 2\chi_1)R^2 + (2R^9\chi_1 - 3\chi_2R^4)\chi_3]\} / [140R^2(R^9 - 1)],$$

$$R_{24} = \{[180R^5(R^7 + \chi_3^2) + 45(1 - R^{12})\chi_2^2 + 180R^5(R^7 - 1)\chi_1\chi_2] / \omega$$
$$+ 18R^{12}(3\chi_2 - 2\chi_1) + 18R^4(2\chi_1R^5 - 3\chi_2)\chi_3\} / [35R^3(R^9 - 1)] \quad ,$$

$$HR_{24} = \{[180R^5(R^6 + \chi_3^2) + 45\chi_2^2(1 - R^5) + 180\chi_1\chi_2R^5(R^6 - 1) + \qquad \text{(E20)}$$
$$18\omega[3\chi_2 - 2\chi_1)R^{11} + (2R^5\chi_1 - 3\chi_2)R^4\chi_3]\} / [175R^6(R^9 - 1)] \quad ,$$

$$R_{34} = [72(R^2 + 3)\chi_2 + 36R^5(2R^2 + 1)\chi_1] / (35\omega R^5) \quad ,$$

$$HR_{34} = -\frac{R_{34}}{4} \quad ,$$

$$R_{44} = 36(8\chi_2 + 3\chi_1) / (35\omega) \quad ,$$

$$HR_{44} = -\frac{R_{44}}{4} \quad .$$